EXPOSURE TO ON-ROAD PARTICULATE AIR POLLUTION DURING ACTIVE TRAVEL

A Dissertation
SUBMITTED TO THE FACULTY OF THE
UNIVERSITY OF MINNESOTA
BY

Steven Conrad Hankey Jr.

IN PARTIAL FULFILLMENT OF THE REQUIREMENTS
FOR THE DEGREE OF
DOCTOR OF PHILOSOPHY

Adviser: Julian D. Marshall

August 2014

Acknowledgements

A big thanks to all those who helped along the way. Mom and Dad, your support never waivers; whenever the family gets together I'll always wonder how you pulled off raising three great guys. Pete and Sam, you two are a great pair of brothers to figure out this life thing with. Thanks to Julian for guiding me through a research world that felt like a foreign country to me at first; and, also thanks for the support to send me to actual foreign countries to do research! Greg, watching you in action let me know it's possible to be a professor and be cool, well done. Matt and Bill, thanks for always having an open door regardless of how randomly I used it. To the rest of Julian's research group (Chris, Lara, Maninder, Matt, Nam, Srinidhi), how did we actually make working 6 floors below ground fun? To all my good friends who've gone through this process: (1) look at me like I'm crazy as I rant about bikes, air pollution models, or some other nerdy thing, (2) shake your head, and (3) offer to buy me a beer – you're right, I am crazy, you all keep my feet on the ground. Lastly, I owe a big thank you to all the bikers in Minneapolis. I never finished a sampling route without at least a few of you riding along for a few miles to chat about what I was doing with this trailer full of blinking lights and tubes. Hopefully, the maps I made are interesting.

Abstract

Increasing active travel is a commonly cited strategy to improve public health and reduce the environmental impact of transportation. Active travel has a number of benefits to both the individual (e.g., physical activity) and to society (e.g., reduced emissions, shifting trips off the motor-vehicle network); however, how cyclists and pedestrians are exposed to hazards during active travel is understudied. One such risk factor is exposure to on-road particulate air pollution. My dissertation explores how people are exposed to particulate air pollution during active travel and how spatial patterns of cycling and walking traffic may impact exposure.

I measured real-time particulate air pollution (particle number, black carbon, $PM_{2.5}$, and particle size) while cycling in Minneapolis, MN. I then use those measurements to explore exposure to particulate air pollution during active travel including: (1) assessing whether measures of particulates are correlated with each other, with motor-vehicle traffic counts, and with traffic mix (i.e., truck, bus, or passenger vehicle), (2) developing land use regression (LUR) models to determine correlates of particulate air pollution and to extrapolate estimates to locations without measurements, and (3) comparing the spatial patterns of modeled particulate air pollution with the spatial patterns of bicycle and pedestrian traffic.

I collected 129 hrs of measurements (886 miles) on streets and off-street trails during 42 sampling runs in year-2012. Mobile bicycle-based sampling was completed using a bicycle trailer, modified to safely carry air pollution equipment and to allow for an elevated air intake that samples at heights close to the breathing zone of cyclists and

pedestrians. I carried air pollution instrumentation that measures four aspects of particulate air pollution: (1) TSI CPC 3007 (particle number concentration), (2) AethLabs AE-51 micro-aethalometer (black carbon mass concentration), (3) TSI DustTrak 8530 ($PM_{2.5}$ mass concentration), and (4) TSI NanoScan (particle size distribution). A GPS and temperature and relative humidity sensor were included on the sampling platform to geo-locate and adjust air pollution measurements for meteorological variables. Two video cameras were included to assess the impact of traffic volume and mix on exposure concentrations.

In Chapter 3, I explore trends in measured on-road concentrations associated with traffic dynamics (i.e., volume and mix), between-pollutant correlations, and how concentrations vary by street characteristics. I developed a set of underwrite functions to control for day-to-day variability in background concentrations, and I used the background-adjusted dataset for all spatial comparisons of concentrations. (Analyses here that are not focused on spatial patterns do not use this adjustment). I found that black carbon and particle number (two traffic-related pollutants) were the most correlated among the pollutants measured (R^2: 0.39 and 0.61, respectively, for 1- and 30-minute averages). Correlations among all pollutant pairs increased with averaging time. Particle size was modestly correlated with particle number (negative correlation) and with black carbon (positive correlation). In regression models that control for meteorological parameters, median particle size on-road is more correlated with background concentration of black carbon and particle number than on-road concentration (ratio of background to on-road model β for black carbon [particle number]: 5.3 [8.3]). Traffic

counts (assessed from the video footage) were correlated with particulate concentrations; the presence of a truck in the video frame (from a camera mounted on the handlebars) was correlated with a 30,600 pt/cc [1.6 μg/m^3] increase in particle number [black carbon] concentration compared to a 2,300 pt/cc [0.26 μg/m^3] increase for buses and a 240 pt/cc [0.02 μg/m^3] increase for passenger-vehicles. Concentrations were associated with street functional class and decreased with distance from a major road; presence of a bike facility had little impact on concentrations.

In Chapter 4, I describe an approach for developing land use regression (LUR) models from the mobile measurements to estimate concentrations at locations where measurements are not available. I aggregated measurements at various spatial resolutions and tested model performance using a number of different averaging times. Models were developed using 215 candidate independent variables and a stepwise regression approach that selects the variables most correlated with concentrations from those candidate variables. In total 1,224 LUR models were generated; 8 models were chosen to extrapolate concentration estimates to the entire City of Minneapolis. Variables that were most commonly selected in the models either described separation from emission sources (e.g., distance from a major road, area of open space, or length of local [low-traffic] road) or proximity to or density of emissions (e.g., length of major road or freeway, industrial area, or traffic intensity). In general model goodness-of-fit statistics were modest; morning [afternoon] adjusted R^2 were 0.50 [0.48] for particle number, 0.28 [0.42] for black carbon, 0.30 [0.49] for $PM_{2.5}$, and 0.29 [0.20] for particle size. Models generally underestimated the highest concentration locations; analysis of spatial autocorrelation of

model residuals suggests this may be owing to measurements at highly congested street segments during rush-hour. Since data were not available on real-time congestion my models do not capture this relationship.

In Chapter 5, I present a sample application of the LUR models by comparing spatial patterns of particulate air pollution to those of bicycle and pedestrian traffic. I estimated bicycle and pedestrian traffic volumes for every street segment in Minneapolis using regression models based on peak-hour bicycle and pedestrian traffic counts. I then used the LUR models developed in Chapter 4 to estimate concentrations for the same street segments. I overlaid the estimates of these two factors to assess spatial patterns of population exposure during active travel. Few neighborhoods in Minneapolis were classified as "healthy" (i.e., high rates of active travel and low particulate concentrations). Bicycle and pedestrian traffic is highest on arterial and collector streets where estimated concentrations are also highest; moving one block away from major roads reduces morning [afternoon] exposure concentrations by 21% [12%] for particle number, 15% [20%] for black carbon, and 7% [3%] for $PM_{2.5}$. Non-motorized traffic increased for areas with greater land use mix while air pollution concentrations were unchanged; non-motorized traffic and particulate concentrations were not well correlated with population density. Finally, the burden of exposure during active travel appears to occur in neighborhoods that are low-income and have the highest proportion of non-whites (i.e., low-income, non-white neighborhoods were associated with high rates of active travel and increased particulate concentrations). People exposed in those locations may be residents or visitors (e.g., in downtown Minneapolis where job density is high).

This dissertation presents work to describe the spatial patterns of exposure to particulate air pollution during active travel in Minneapolis. The analyses herein provide evidence that mobile measurements of air pollution concentrations can yield insight into how and where cyclists and pedestrians are exposed. The results presented here may be of interest to planners and policy-makers interested in designing clean, healthy cities.

Table of Contents

List of Tables

List of Figures

Chapter 1 Introduction and literature review

Summary of dissertation objectives

In the past 10 years, multiple US federal agencies have launched programs aimed at promoting healthy, sustainable communities (CDC, 2012; HUD, 2012). One commonly cited strategy is to encourage active travel (i.e., walking and cycling). Active travel can have numerous benefits both to the individual (e.g., increased physical activity [de Hartog et al., 2010; Rojas-Rueda et al., 2011; Andersen et al., 2000; Hamer and Chida, 2008], mental health [Barton and Pretty, 2010; Sugiyama et al., 2008; Unger, 1995]) and to society (e.g., reduced emissions [Grabow et al., 2011; Woodcock et al., 2009], increased social capital [Leyden, 2003; Lund, 2002; McNeill et al., 2006], shifting demand from the vehicle network [Ewing and Cervero, 2001; FHWA, 1998; Handy, 2005], economic activity [Krizek, 2007; Lankford et al., 2011; Weigand, 2008]). However, planners and policy-makers have little guidance or evidence-based examples of how best to design bicycle and pedestrian networks (Porter and Suhrbier, 1999). One area which warrants further investigation is how best to design networks that minimize exposure to hazards, for example, crashes, air pollution, noise, or crime. This dissertation aims to explore spatial patterns of exposure for one such risk factor: on-road particulate air pollution.

Exposure to air pollution is an important risk factor in urban areas (WHO, 2009); exposure during transport (especially during active travel) is an important exposure pathway (Dons et al., 2011, 2012; Reyes and Serre, 2014). A little studied aspect of

exposure is how within-city spatial patterns of active travel compare to those of air pollution. Readily available information on ambient air pollution concentrations are typically focused on either regulatory enforcement (e.g., the Environmental Protection Agency's criteria pollutant monitoring network), modeling concentrations at relatively large spatial scales based on changes in meteorology or emissions (e.g., mechanistic models), or idealized models of plume dispersion from a steady-state point source (e.g., Gaussian plume models). Since many traffic-related pollutants (e.g., NO, CO, black carbon, ultrafines) vary on small spatial scales (see discussion of within-city variability of air pollution below) assessing spatial patterns of pedestrians' and cyclists' exposure to air pollution requires estimating pollutant concentrations at a fine-scale spatial resolution. This requirement necessitates methods other than the tools which are currently available (e.g., spatial interpolation of ambient regulatory monitors or large-scale mechanistic modeling).

This dissertation describes an approach I developed to measure and model particulate air pollution at a fine-scale spatial resolution to overlay on spatial estimates of bicycle and pedestrian traffic volumes in Minneapolis, MN. The general approach for my work includes collecting and assembling data on particulate air pollution concentrations and non-motorized traffic volumes to build statistical models that give estimates of both factors (rates of active travel; air pollution concentrations) at ~100 meter spatial resolution. Specifically, this document focuses on three sets of analyses:

1. A description of a mobile, bicycle-based air pollution measurement campaign. A custom sampling platform was developed (Chapter 2) to measure real-time

particulate air pollution on prescribed sampling routes to explore small-scale variability of particulate air pollution concentrations in an urban environment (Chapter 3).

2. Development of land use regression models (Chapter 4) for multiple measures of particulate air pollution (particle number, black carbon, $PM_{2.5}$, and particle size) using mobile measurements rather than traditional methods (i.e., fixed-site measurements).
3. Use of a longitudinal bicycle and pedestrian traffic count dataset to develop a statistical model that estimates bicycle and pedestrian traffic on all roads in Minneapolis, MN to overlay onto the particulate air pollution estimates generated by the LUR model (Chapter 5).

In the first chapter I give a brief summary of the health effects of air pollution as it relates to spatial patterns within cities. I then introduce the concept of land use regression (LUR) and describe how my method of exposure assessment (i.e., using mobile measurements of air pollution to characterize spatial patterns and develop LURs) may in some cases be a more efficient approach than using a traditional LUR approach (i.e., fixed-site air pollution measurements). Finally, I apply the LUR models to compare spatial patterns of air pollution to estimates of bicycle and pedestrian traffic for all roads and off-street trails in Minneapolis, MN.

Health effects of air pollution: "Between-city" analyses

Quantifying exposure to air pollution is a challenge because of many factors including: (1) concentrations vary in space and time and (2) exposure is determined not

only by ambient concentrations but also by a person's daily activities and the location of those activities. A variety of pollutants have been associated with adverse health effects including carbon monoxide (Mott et al., 2002; Ritz et al., 2002), oxides of nitrogen (Nafstad et al., 2004; Nyberg et al., 2000; Jerrett et al., 2009), ozone (Bell et al., 2005; Ruidavets et al., 2005), and various measures of particulates (e.g., $PM_{2.5}$ [Krewski et al., 2009; Pope et al., 2002], PM_{10} [Daniels et al., 2000; Stieb et al., 2002]); health endpoints that have been associated with poor air quality include: mortality (Bell et al., 2005; Krewski et al., 2009), cardiovascular disease (Laden et al., 2006; Miller et al., 2007), respiratory disease (Beelen et al., 2008; Bell et al., 2004), lung cancer (Nyberg et al., 2000; Pope et al., 2002), and asthma (Chauhan et al., 2003; Friedman et al., 2001) among others. Since the burden of disease that is related to urban air quality has largely been attributed to premature mortality as a result of $PM_{2.5}$ exposure (WHO, 2009), I focus my discussion of the health effects of air pollution on that pollutant with some references to urban air quality in general.

Studies that aim to explain the health effects of exposure to $PM_{2.5}$ focus on both acute and chronic effects (Brunekreef and Holgate, 2002; Pope and Dockery, 2006). Acute health effects of air pollution have been widely studied (Dominici et al., 2006; Hoek et al., 2001; Pope et al., 2006; Stieb et al., 2002). Historically, the first evidence of the health impacts of air pollution came during extreme air pollution episodes in London, England (year-1952 [Bell et al., 2004]), Donora, Pennsylvania (year-1948 [Snyder, 1994]), and Meuse Valley, Belgium (year-1930 [Nemery et al., 2001]). In response to increased awareness of poor air quality in the US, the Clean Air Act was passed in 1970

(and subsequently amended in 1990) which established regulatory rules for ambient air pollution levels. Since the Clean Air Act, a relatively small number of high-impact studies have focused on long-term, chronic exposures to $PM_{2.5}$ (Dockery et al., 1993; Jerrett et al., 2009; Pope et al., 2002, 2004) and have contributed to strengthening regulatory standards (Krewski et al., 2009; EPA, 2013). Furthermore, available evidence suggests there is not a threshold where health benefits diminish from decreasing $PM_{2.5}$ concentrations (Crouse et al., 2012; Pope et al., 2009a; Schwartz et al., 2002) and that reducing ambient $PM_{2.5}$ concentrations increases life expectancy (Pope et al., 2009b; Correia et al., 2013).

A few key studies (Jerrett et al., 2005; Krewski et al., 2009; Laden et al., 2000, 2006; Pope et al., 2004) have been very influential in guiding regulation including setting ambient concentration limits (i.e., National Ambient Air Quality Standards [NAAQS]) enforced by the Environmental Protection Agency (EPA). These studies are all long-term cohort studies that require following a group of people over time to assess health impacts of the risk factor of interest; a key aspect of this type of study is assigning exposure values to individuals during the study period. The EPA monitoring network was originally deployed to capture "ambient" concentrations to enforce the NAAQS. As such, the monitor network was developed to capture trends over time for specific urban areas not spatial variability within cities. Since for many years characterizing small-scale variability was not feasible, these long-term health effects studies typically assigned uniform exposure values for all people living in the same city (Cohen et al., 2009; Laden et al., 2000; Pope et al., 2004). Between-city variability was large enough to assess the

impact of long-term exposure; these studies estimate the effect of living in a polluted vs. clean city but do not take into account spatial variability of air pollution concentrations within a city or the activities of people within a city.

Health effects of air pollution: "Within-city" analyses

A key question for urban planners and policy makers is whether the spatial gradients of air pollution within an urban area are relevant to health or if mitigation strategies should be considered only on larger scales (i.e., do local decisions matter?). Multiple studies report adverse health effects associated with within-urban $PM_{2.5}$ concentration gradients (Jerrett et al., 2005; Miller et al., 2007) and that urban air quality is correlated with certain urban form variables (Bechle et al., 2011; Clark et al., 2011; Hankey et al., 2012; Stone, 2008). Furthermore, within-city health studies of $PM_{2.5}$ and mortality (see Table 1.1) report similar differences in risk as the larger, between-city cohort studies that have guided policy on ambient air pollution (Dockery et al., 1993; Pope et al., 2009b). These findings suggest that where one lives in a given urban area could matter just as much as choosing to live in a clean or polluted urban area. If that's true, then it may also be the case that policy makers in local government can potentially have a meaningful impact on residents' exposure to air pollution. Table 1.1 summarizes results from key studies of long-term exposure to $PM_{2.5}$. Risk estimates are of similar magnitude for within-cities as compared to between-cities.

Table 1.1 Summary of long-term health effects studies of $PM_{2.5}$

Within-city studies			
Study	**Health endpoint**	**Study details**	**Hazard Ratio (HR) or Relative Risk (RR) and 95% CI per 10 $\mu g/m^3$ of $PM_{2.5}$[a]**
Jerrett et al., 2005	Ischemic heart disease mortality	Los Angeles, CA; subset of ACS[b] cohort (n=22,905)	RR: 1.25 (0.99-1.59)
Miller et al., 2007	Cardiovascular disease mortality	Women aged 50-75 years (n=65,893); 36 US cities	HR: 2.28 (1.10-4.75)
Between-city studies			
Study	**Health endpoint**	**Study details**	**Hazard Ratio (HR) or Relative Risk (RR) and 95% CI per 10 $\mu g/m^3$ of $PM_{2.5}$[a]**
Pope et al., 2004	Ischemic heart disease mortality	ACS[b] cohort (n=319,000); 51 US cities	RR: 1.18 (1.14-1.23)
Laden et al., 2006	Cardiovascular disease mortality	"Six cities" cohort (n=8,096); 6 US cities	RR: 1.28 (1.13-1.44)
Miller et al., 2007	Cardiovascular disease mortality	Women aged 50-75 years (n=65,893); 36 US cities	HR: 1.63 (1.10-2.40)

[a]HR and RR are different measures of risk (i.e., ratios of risk in exposed vs. unexposed populations). RR is estimated by averaging events over a specific time period; HR is estimated using survival curves and gives instantaneous estimates.
[b]ACS = American Cancer Society.

There is evidence that traffic-related pollutants (including some pollutants not currently regulated by the EPA [e.g., ultrafines and black carbon]) may play a significant role in the within-city health disparities related to air pollution (Carr et al., 2002; Gauderman et al., 2007; Henderson et al., 2007; Jerrett et al., 2009; Peters et al., 2004; Wilhem and Ritz, 2004). Ultrafines and black carbon are two pollutants that (1) are highly variable within cities (Hoek et al., 2008; 2011) and (2) have been associated with adverse health effects (Knibbs et al., 2011; Politis et al., 2008; Vinzents et al., 2005; Wilker et al., 2010). Exposure to ultrafines and black carbon are associated with automobile traffic (Fruin et al., 2008; HEI, 2009) and thus are good candidates for developing models which aim to explore gradients of on-road pollutant concentrations.

Multiple epidemiological studies have explored using distance to a major road instead of pollutant concentration estimates as an exposure variable (Brauer et al., 2008; Brugge et al., 2007; Gilbert et al., 2003); those studies found that risk estimates were similar to studies that used air pollution concentration estimates generated by measurements or models. For example, Hoek et al. (2002) estimated relative risks (RR) for cardiopulmonary mortality for a cohort in the Netherlands using central monitors for black smoke (RR=1.71[1.10-2.67 CI] per 10 $\mu g/m^3$); however, when proximity to a major road was added to the models the black smoke variable was not statistically significant and living near a major road was (RR=1.95 [1.09-3.51 CI]; within 50 meters of a major road). A challenge with characterizing the spatial patterns of traffic-related pollutants (e.g., ultrafines or black carbon) is that there often is greater spatial and temporal variability for those pollutants than other particulate air pollutants monitored by the EPA (e.g., PM_{10} and $PM_{2.5}$ [Harrison and Jones, 2005; Puustinen et al., 2007; Wang et al., 2012; Zhou and Levy, 2007]). New methods that do not require costly fixed-site monitoring networks may be helpful for characterizing the spatial patterns of traffic-related particulate air pollution.

Health effects of air pollution: Evidence during active travel

To better plan for bicycle and pedestrian transportation networks, and to design infrastructure that avoids undue exposures to walkers and bikers, planners need information on how air pollution varies on a small spatial scale. For some pollutants, exposure during transport is an important component of personal air pollution exposure. For example, a recent exposure assessment for 62 people in Flanders, Belgium found that

the ~6% of people's time spent in transport accounted for an average of 30% of the total inhaled black carbon (Dons et al., 2012). An earlier study estimated in-vehicle exposure to diesel particulate matter accounted for 28-55% of total exposure in California (Fruin et al., 2004). Multiple studies have investigated exposure during various modes of transport and concluded that typically, walking and cycling are among the modes most exposed to traffic-related pollution when accounting for breathing rates (Bigazzi and Figliozzi, 2014; Briggs et al., 2008; Dons et al., 2012; Int Panis et al., 2010; Quiros et al., 2013). Additionally, exposure to ultrafines and black carbon during active travel has been found to impact lung function, exacerbate asthma, and change heart rate variability (McCreanor et al., 2007; Strak et al., 2010; Weichenthal et al., 2011). Researchers have characterized concentration gradients of certain pollutants near roadways and shown that during daytime hours concentrations decrease rapidly as distance from the roadway increases (Zhang et al., 2002; Zhu et al., 2002a; 2002b). Concentrations may decrease less rapidly during nighttime hours (Hu et al., 2009).

Land use regression (LUR) models: Fixed-site measurements of air pollution

LUR has been developed over the past 15 years as an alternative modeling approach to dispersion models or spatial interpolation for urban air pollution (Brauer et al., 2003; Briggs et al., 2000; Briggs, 2005; Cyrys et al., 2005). LUR models typically can provide air pollution concentrations at higher spatial resolution than other models (i.e., spatial interpolation or dispersion modeling [Jerrett et al., 2005; Marshall et al., 2008]). The typical LUR approach is to perform air pollution measurements representative of long-term averages at many locations throughout a study area; then, a

number of land use related variables are assembled for varying buffer sizes around each measurement location. These land use variables are used to build a regression model that can estimate air pollution concentrations at a small spatial scale throughout the study area. This approach is typically used at the urban scale (Beelen et al., 2007; de Hoogh et al., 2013) though more recently it has been developed at the national scale in North America (Beckerman et al., 2013; Hystad et al., 2011; Novotny et al., 2011; Sampson et al., 2013) and Europe (Gulliver et al., 2001, 2013; Vienneau et al., 2013). Urban scale models have been developed in many global cities including those in North America (Jerrett et al., 2007; Ross et al., 2007; Sahsuvaroglu et al., 2006), Europe (Beelen et al., 2013; Eeftens et al., 2012; Rosenlund et al., 2008), South Asia (Saraswat et al., 2013), East Asia (Kashima et al., 2009), and Australia (Rose et al., 2011).

A number of urban scale land use variables have been shown to be significant in LUR models. Variables employed in LURs generally fall into one of four categories: (1) traffic/road characteristics, (2) physical geography, (3) land use, or (4) population dynamics. A number of review papers summarize LUR model performance and validation as well as give summaries of significant variables in various study areas (Ryan and LeMasters, 2007; Hoek et al., 2008). Table 1.2, adapted from Hoek et al. (2008), shows the most commonly cited significant variables in the 25 LUR models included in that review paper. Traffic-related variables are the most commonly cited variables indicating that the LUR approach may be useful for modeling traffic-related pollutants such as ultrafines or black carbon. That same result (that traffic-related variables are very

common in published LURs) may also partially reflect researcher focus on traffic-related pollutants and on traffic-driven spatial patterns.

Table 1.2 Frequency of independent variables cited in LUR models (adapted from Hoek et al., 2008; out of a total n=25 models/journal articles)

Variable type	Variable	n
Traffic	Intensity	16
Traffic	Road length	13
Physical Geography	Altitude	9
Traffic	Distance	7
Population	Housing	7
Population	Population	6
Land use	Composite	4
Land use	Industry	4
Land use	Urban/rural	3
Physical Geography	Region	3
Physical Geography	Distance to water	3
Land use	Open space	2

A limitation of LUR is that input requirements are typically large (Kanaroglou et al., 2005; Kumar, 2009); for example, Hoek et al. (2008) suggest that measurements be collected for at least 40-80 locations to properly specify an urban scale model. As such, most LUR models have been limited to pollutants for which inexpensive sampling is possible (most commonly NO or NO_2) or else suffer from too few measurement sites for pollutants where sampling equipment is expensive (e.g., ultrafines, black carbon [Abernathy et al., 2013; Hoek et al., 2011]). These limitations have prevented LUR from being deployed widely or used for pollutants that necessitate expensive measurement devices. New sampling methods, such as the mobile monitoring approach described next, are needed to expand the utility of the LUR approach.

Land use regression models: Mobile measurements of air pollution

A potential alternative to traditional LUR sampling campaigns is to develop a mobile monitoring scheme which aims to describe spatial patterns of air pollution for specific time periods (e.g., during peak-hour traffic). My dissertation describes a mobile monitoring campaign designed to explore correlates of particulate air pollution and to develop a LUR which estimates rush-hour (7-9am; 4-6pm) particulate air pollution concentrations on all roads and off-street trails in Minneapolis, MN. The trade-off between using mobile vs. fixed-site monitoring is that mobile monitoring allows for wide deployment and modeling of pollutants which are expensive to detect, but that specific time periods must be chosen to control for hourly and daily variability in concentrations. A key advantage to mobile monitoring is that it allows for developing land use regression models for pollutants that would otherwise be cost and labor prohibitive. For example, for a typical (i.e., fixed-site) land use regression of ~100 monitoring sites, if one sought to model particle number concentrations, 100 monitoring devices would be needed (~$8,000 per unit [TSI CPC 3007]) and each unit would need to be visited every 6 hours to re-wet the condensation wick – a nearly impossible (and costly: $800,000 just in equipment) task.

A limited number of exploratory studies have used mobile monitoring to build LUR models. Few studies have designed mobile measurement campaigns specifically for extrapolating estimates from LUR models (all are for woodsmoke [Larson et al., 2007; 2009, Su et al., 2013]; other studies include real-time counts of traffic at measurement locations precluding the ability to extrapolate estimates to places without counts (Li et al.,

2014; Zwak et al., 2011) and are disproportionately for measurements on or near freeways (Aggarwal et al., 2012; Patton et al., 2014). Some exploratory studies have measured air pollution on various bicycle routes in urban areas with the goal of investigating spatial variability (Hatzopoulou et al., 2013; Hong and Bae, 2012; Van Poppel, 2013; Zuurbier et al., 2010). In the bicycle-based studies some regression models were developed to assess the impact of traffic levels and mix, but complete LUR models were not developed. Fundamental questions remain on how best to design mobile monitoring campaigns with the goal of extrapolating spatial estimates; for example, how best to determine the spatial scale for aggregating and analyzing mobile measurements (Lightowlers et al., 2008).

Models of bicycle and pedestrian traffic

Researchers have worked on methods to estimate non-motorized traffic for many years, but accepted methods and protocols for estimating traffic have not been established. Two of the earliest examples from the 1970s are: (1) use of aerial photography to count pedestrians and develop regression models to estimate pedestrian traffic as a function of built environment variables (Pushkarev and Zupan, 1971) and (2) estimating pedestrian traffic per hour for blocks in Milwaukee, Wisconsin as a function of land use and other variables (Behnam and Patel, 1977). More than 20 years after these exploratory studies, Hunter and Huang (1995) completed a comprehensive review of reports on the use of bicycle lanes and off-street trails and found wide variation in the level of detail and quality.

Best practices for counting non-motorized traffic have yet to be developed (Porter et al., 1999). Designing effective count campaigns is an active area of research; recent additions to the literature include information on three key issues in non-motorized traffic monitoring: (1) the length of short-duration counts needed to minimize error in extrapolation, (2) the identification of factor groups based on hourly traffic patterns, and (3) the development of adjustment factors for bicycle traffic (Nordback et al., 2013; Miranda-Moreno et al., 2013; El Esaway et al., 2013). The National Bicycle and Pedestrian Documentation Project (Jones, 2009), cited by Handy et al. (2009) as a "promising beginning", is designed to establish consistent count and survey methodologies, create a national database of counts, and support analyses of factors that influence non-motorized traffic.

Although the scope of studies remains insufficient, researchers have added new insights in several key areas thought to impact non-motorized travel: Built environment characteristics (Dill, 2009; Guo, 2007; Haynes and Andrezejewski, 2010; Jones et al., 2010), infrastructure design characteristics (Lindsey et al, 2006; 2007; 2008; Reynolds et al., 2007), neighborhood socio-economics (Adams, 2010), and weather (Aultman-Hall et al., 2009). Furthermore, incremental steps have been made towards developing traditional traffic models (e.g., gravity models) for non-motorized travel by developing impedance functions for cycling and walking (Iacono et al., 2010), modeling mode share near bicycle facilities (Krizek et al., 2009), and building route-choice models (Hood et al., 2011).

Primary outcomes of this dissertation

The aim of my dissertation is to explore spatial aspects of exposure to particulate air pollution during active travel. Because the methods I develop required extensive field measurements, I focused my efforts on my home location: Minneapolis, MN. Key outcomes from my dissertation include the following:

1. Developed and field-tested a mobile, bicycle-based platform to sample particulate air pollution. The platform samples particulates in real-time allowing for assessment of small-scale spatial variability of on-road particulate air pollution concentrations.
2. Developed a method to build LUR models from mobile measurements of air pollution. This method represents a cost-effective alternative to fixed-site measurements.
3. Developed a sample application of the mobile measurement based LUR approach for exposure assessment. I used publicly available bicycle and pedestrian traffic counts to build a statistical model that estimates bicycle and pedestrian traffic volumes (Hankey et al., 2012) and compares the estimates to the results of the particulate air pollution LUR models.

The research described in this dissertation makes contributions by offering a unique approach to modeling spatial patterns of air pollution and adds to our understanding of how cyclists and pedestrians are exposed to air pollution in urban environments. Specifically, I present a method (i.e., using mobile measurements as an input to LUR models) that allows for spatial modeling of pollutants for which prior

methods would be cost and labor prohibitive (particle number, black carbon, and particle size). Lastly, I show how combining spatially resolved estimates of air pollution and rates of active travel can shed light on population level exposure to air pollution during active travel and how that information may be used in certain urban planning contexts.

Chapter 2 Mobile, bicycle-based air pollution sampling platform, sampling protocol, and data assembly

To measure on-road concentrations of particulate air pollution I developed a custom, mobile sampling platform. Since the focus of my work is to assess air pollution exposure during active travel I chose to build the mobile sampling platform using a bicycle and a modified bicycle trailer. The bicycle-based sampling platform has two distinct advantages: (1) it is zero emissions, eliminating the potential for self-pollution (i.e., emissions from the sampling vehicle) and (2) it is a mode of transport that is a focus of my exposure assessment (i.e., comparing spatial patterns of particulate air pollution to those of bicycle and pedestrian traffic volumes). This chapter gives details on: (1) the customization and assembly of the mobile sampling platform and a description of the air pollution instrumentation used, (2) planning of the mobile sampling protocol including route selection, and (3) a MatLab based script developed for assembling and post-processing of all sampling data.

Description of air pollution instrumentation

I modified a commercial bicycle trailer (Burley Nomad Cargo trailer) to carry air pollution instrumentation that measures four aspects of particulate air pollution: (1) TSI CPC 3007 (particle number concentration), (2) AethLabs AE-51 micro-aethalometer (black carbon mass concentration), (3) TSI DustTrak 8530 ($PM_{2.5}$ mass concentration), and (4) TSI NanoScan (particle size distribution). Each instrument logs measurements in real-time, i.e., 1-second intervals (except the NanoScan [1-minute scans]). Measuring

particulates in real-time gives information on small-scale changes in concentrations (both in space and time) attributable to acute exposure events such as vehicles passing in close proximity, crossing over a busy freeway, or waiting at a stoplight in traffic.

The bicycle and trailer were also equipped with a GPS device, odometer, rear- and forward-facing video cameras, and a temperature and relative humidity data logger. These supplementary devices served different purposes including geo-locating the air pollution measurements (GPS), recording bicycle speed and distance traveled (odometer), recording video of the traffic dynamics and volume near the sampling platform (video cameras), and recording instantaneous weather data (temperature and relative humidity) needed to correct measurements of $PM_{2.5}$. Since GPS measurements can become unreliable in urban-canyons (Borriello et al., 2005) the odometer was included to adjust unreliable GPS data if needed.

A unique aspect of the sampling platform is that video footage was collected to explore possible sources of emissions. Certain types or numbers of vehicles might impact each measure of particulate air pollution in different ways; the video footage allowed for investigation of associations between vehicle mix and traffic volumes with each parameter of particulate matter measured by the mobile sampling platform. Video footage was collected for only a subset (~5%) of the sampling campaign to explore these relationships. I was able to capture video for this purpose using low-quality equipment: a "point and shoot" digital camera with video option (Nikon CoolPix S570 [year-2010]) and a high-definition FlipCam (F460 HD [year-2008]). Table 2.1 gives technical specifications of all instrumentation in the mobile sampling platform.

Table 2.1 Summary of instrumentation affixed to mobile, bicycle-based sampling platform

Device	Manufacturer	Measurement	Sampling interval	Instrument flow rate	Instrument range	Instrument accuracy/resolution	Corrections needed
Condensation particle counter 3007	TSI, Inc.	Particle number concentration	1 second	Sample: 100 ml/min Total: 700 ml/min	0-100,000 pt/cc[a]	Size range: 10nm to >1µm	Particle coincidence at >100,000 pt/cc
Micro-aethalometer AE-51	AethLabs	Black carbon mass concentration	1 second	150 ml/min (50, 100 ml/min optional)	0-1 mg/m^3	Resolution: 0.001 µg/m^3 Accuracy: ± 0.1 µg/m^3, 1 min avg., 150 ml/min flow rate	Censor vibration errors; particle loading factor
DustTrak 8530	TSI, Inc.	$PM_{2.5}$ mass concentration	1 second	1.4-4.0 L/min	0.001-100 mg/m^3	Resolution: 0.001 mg/m^3 Accuracy: ±0.001 mg/m^3 or ±0.1% of reading Size range: 0.1-10 µm	Adjust for co-located filter measurements
NanoScan	TSI, Inc.	Particle size distribution	60 second	Total: 750 ml/min Sample: 250 ml/min	100-1,000,000 pt/cc	Size range: 10-420 nm Size channels: 13	None
GPS 62s	Garmin	Latitude/Longitude	1 second	-	-	Accuracy: <10 m for 95% of measurements	None (potential for corrections using odometer)
CS 600x	Polar	Speed	1 second	-	-	Resolution: 0.1 mph Accuracy: ±1%	None
Video cameras	FlipCam; Nikon	Video	Continuous	-	-	-	None
Nomad OM-73	Omega	Temperature, relative humidity, dew point	1 second	-	Temp: -40 to 70 °C RH: 9 to 99%	Resolution: Temp: 0.1 °C; RH: 0.05% Accuracy: Temp: ±0.5 °C; RH: ±0.05%	None

[a]Device functions above 100,000 pt/cc but accuracy declines and empirical corrections are needed.

Building and customizing the mobile sampling platform

Mobile monitoring with air pollution instrumentation presents several challenges. For example, some instruments (i.e., CPC 3007 and NanoScan) use a saturation chamber (isopropyl alcohol) to grow the size of particles; this design requires that the instruments are not tilted in orientation or else the optics of the device can be damaged. Additionally, some instruments are sensitive to vibrations (e.g., micro-aethalometer AE-51). All instruments should be shielded from the sun, and none of the instruments should be operated during rain events. Because of those limitations, I needed to modify both the bicycle trailer and some of the instruments themselves (i.e., CPC 3007) to avoid as many of these potential challenges as possible.

Installation of the padded mounting system

Since the floor of the bicycle trailer was not level I first needed to ensure that the instruments would sit on a level surface during the sampling runs. To do this, I inserted a thin piece of plywood (leveled using styrofoam blocks) to create a level baseboard. The baseboard was then attached to the trailer using nylon rope. I drilled holes in the baseboard which were later used to attach straps to secure the air pollution instruments.

To reduce the potential for spurious measurements owing to mechanical shock I cut a 4" piece of sofa cushion rubber foam to sit on top of the baseboard. Insets were cut from the rubber foam to secure the air pollution devices. Each strap ran through the rubber foam and beneath the baseboard (using the drilled holes) to secure the instrument and foam pad to the trailer. Instruments were attached using a parachute buckle that allowed for tightening of the straps to minimize vibration and absorb any potential shock

from on-road measurements (potholes, bumps, etc.). Figure 2.1 shows stages of installation of the padded mounting system.

Figure 2.1 Three stages of installation of the padded mounting system for the Burley Nomad Cargo trailer.

Creating an elevated air intake

I aimed to collect air pollution measurements that are representative of concentrations in the breathing zone of cyclists and pedestrians. To do this I elevated the air intake of the air pollution instruments by mounting a 3/8” stainless steel pipe (as well as supplementary sampling tubes) to the frame of the bicycle trailer resulting in an air intake ~5 feet above ground level. During preliminary testing, simply mounting the steel pipe to the trailer frame resulted in vibrations that eventually led to shearing of the brackets used to mount the sampling tube (where the screws attached the bracket to the frame). To fix this problem I used a welded steel brace to attach the sampling tubes to the bicycle trailer frame.

For preliminary trials the elevated intake was split into four separate flows using ¼” junctions mounted below the bicycle support bar (to avoid pinching intake tubing when the cover was placed on the trailer). Each instrument was then connected to the intake using conductive tubing. During early tests it was evident that the combined flow rate of the instruments was too large for the 3/8” diameter steel pipe resulting in “low flow rate” errors from the micro-aethalometer (and automatic shutdown of some devices). To address this issue, the DustTrak and micro-aethalometer were connected to separate sampling lines (using conductive tubing) and the inlets were oriented adjacent to the stainless steel sampling tube. Since the NanoScan and CPC 3007 both sample particle number concentration those instruments drew air from the same intake (i.e., stainless steel pipe). Figure 2.2 shows both the steel brace and elevated intake.

Figure 2.2 Attaching the elevated sampling air intake.

Description of final sampling platform configuration

Figure 2.3 shows the final bicycle-based sampling platform. The cover was placed on top of the trailer to protect the instrumentation from sun and rain exposure. A hole was cut in two places to allow for the elevated sampling intake and the NanoScan conductive tubing to be unaffected by the cover. A GPS antenna was attached to the top of the elevated intake for two reasons: (1) to geo-locate measurements at the exact intake location and (2) to give the GPS the best opportunity to have unobstructed access to satellite signal. The temperature and relative humidity data logger was attached to the steel brace to log instantaneous, ambient weather conditions. The speed sensor was placed on the front wheel of the bicycle and speed data was logged on a data logger attached to the handlebars. Video cameras were placed on the handlebars (forward-facing footage) and on the steel brace (backward-facing footage). Timestamps were synced for all instruments prior to each sampling run. Data were loaded into a spreadsheet template to plot and visually check for errors after each sampling run.

Figure 2.3 Final mobile sampling bicycle trailer configuration.

Equipment modification, flow and zero checks, and adjusting for time delay

Disabling the CPC tilt alarm

The CPC 3007 factory default hardware includes a tilt alarm that automatically shuts down the instrument if it is tilted from a level position for more than 10 seconds. This setting is problematic for mobile monitoring when the unit might be tilted for short amounts of time (e.g., while biking up an incline). To sample continuously, I followed a recommendation from the manufacturer to disarm the tilt alarm during the sampling runs. The risk from tilting the 3007 is that if the wick is oversaturated with isopropyl alcohol, a tilted instrument might leak alcohol on the instrument optics. The sampling protocol used during this sampling campaign mitigated this risk in two ways: (1) before inserting the wick into the 3007 the wick was held vertically and "flicked" to remove excess drips of alcohol and (2) the unit was run for 30 minutes before each sampling run (to record reference site measurements) ensuring any remaining excess alcohol (i.e., not contained in the wicking material) evaporated.

Figure 2.4 shows the CPC 3007 board and indicates the location of the tilt alarm switch. The board was accessed by unscrewing the instrument's protective shell and removing the board from its mount. The tilt alarm was disabled by soldering a small piece of copper wire between the two tilt switch leads (opposite side of the board as shown in the photo) creating a short-circuit that disarms the tilt alarm while not impacting the device's performance. This procedure was completed using guidance from Mr. Maynard Havlicek at TSI, Inc.

Figure 2.4 CPC 3007 board and tilt switch.

Flow rate checks and zero checks

Flow rate checks and zero checks were performed prior to the first sampling run of each day. All pollution instruments (those listed in the first four rows in Table 2.1) were turned on prior to the 30 minute reference site measurements and a zero check (HEPA zero filter included with CPC 3007) and flow rate check (BGI, Inc. RM65 Rotameter) were performed on each pollution instrument. During the sampling campaign flow rates remained constant and zero checks did not indicate any errors with the instrumentation.

Laboratory check of NanoScan and CPC 3007 against reference CPC 3776

The NanoScan used in this study was one of the first off the production line at TSI, Inc. Both the NanoScan and CPC 3007 were checked against a laboratory-based reference CPC (Ultrafine Condensation Particle Counter 3776 located in a TSI lab) to ensure the results from the field measurements would be comparable and consistent during the sampling campaign. The goal of the laboratory checks was to ensure there was

not drift in the field-based instruments as compared to the laboratory instrument during the sampling campaign. Figure 2.5 shows comparison curves for the field-based instruments to the reference CPC before and after the sampling campaign. There was little change in these curves over time.

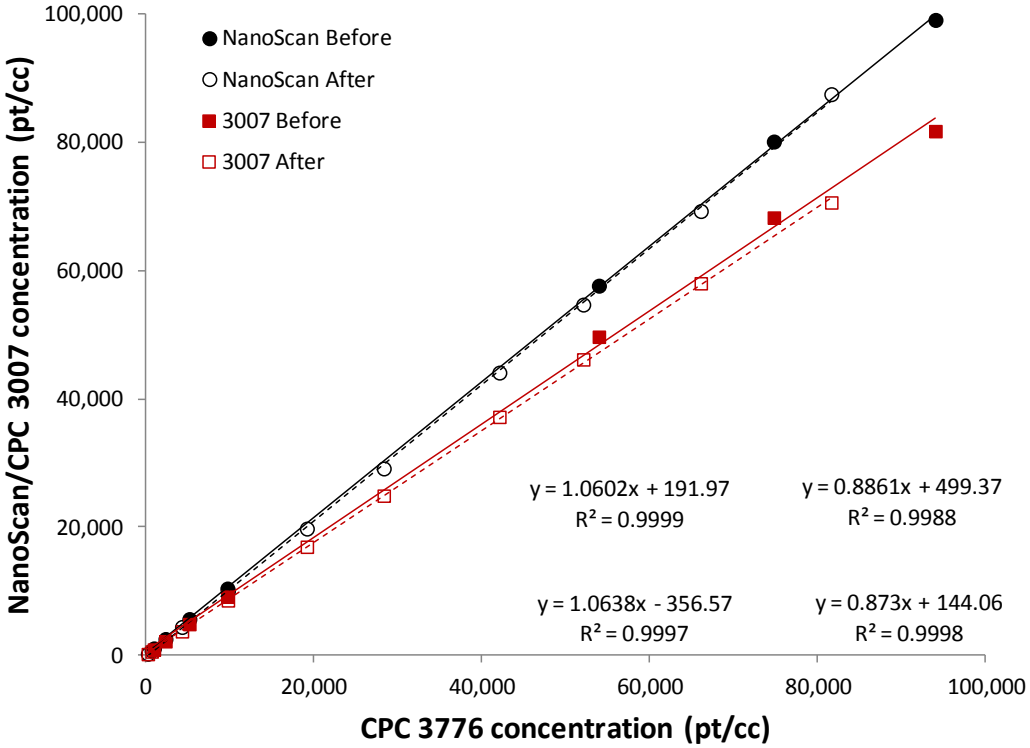

Figure 2.5 Comparison of laboratory (3776) and field-based CPCs (NanoScan, 3007).

For the laboratory tests nebulized NaCl particles were generated with a geometric mean diameter of 69.5 nm and a geometric standard deviation of 1.58. Particles were generated at multiple concentrations; measurements were collected at each concentration for ~5 minutes and average concentrations were compared for each instrument. The size ranges for each instrument are different (NanoScan: 10-420nm; 3007: 10nm-1µm; 3776: 2.5nm-1µm) and thus a 1:1 relationship for concentrations between instruments is not expected. The NanoScan factory default setting adjusts measurements by a factor of 1.2

to match the 3776 concentrations; the coefficients on the laboratory check of 1.06 (see trendlines for the NanoScan in Figure 2.5) are within acceptable limits as defined by TSI. The 3007 measurements are unadjusted and the trendline coefficients of 0.87 and 0.89 are consistent with the smaller size range of the 3007.

Estimating instrument delay times

Instrument response time can be delayed (relative to the GPS data) owing to two factors: (1) the time required for air to flow through the intake tube and (2) internal instrument processing delay. I adjusted each instrument measurement using an estimated, instrument specific lag time. I estimated lag times as follows: First, I created a polluted indoor environment by burning a small amount of bacon in a frying pan. Then, with the instruments running, the bicycle trailer was moved between the (polluted) indoor and the (comparatively clean) outdoor environments at timed intervals. The lag times were then calculated based on the observed step function from the large difference in concentrations. This process was repeated 5 times and average lag times were estimated for each instrument. All measurements for the sampling campaign were then adjusted by the instrument specific lag times. For the NanoScan, I applied the CPC 3007 lag time because (1) those instruments used the same sampling line, (2) had similar flow rates, and (3) since a full scan takes 60 seconds it was impossible to accurately determine the actual lag time. In Figure 2.6 (below) it appears the instrument has a longer lag time; this effect is due to the way this data is plotted (i.e., scan start times are used in the plot for the x-axis). During spatial analysis I applied the values reported by the NanoScan (every 60s) to each 1s GPS point that corresponded to that scan. Therefore for the purpose of

applying lag times I used the value estimated for the CPC 3007 for all 1s NanoScan data points. Figure 2.6 shows the experimental step functions; Table 2.2 gives the estimated lag time for each instrument.

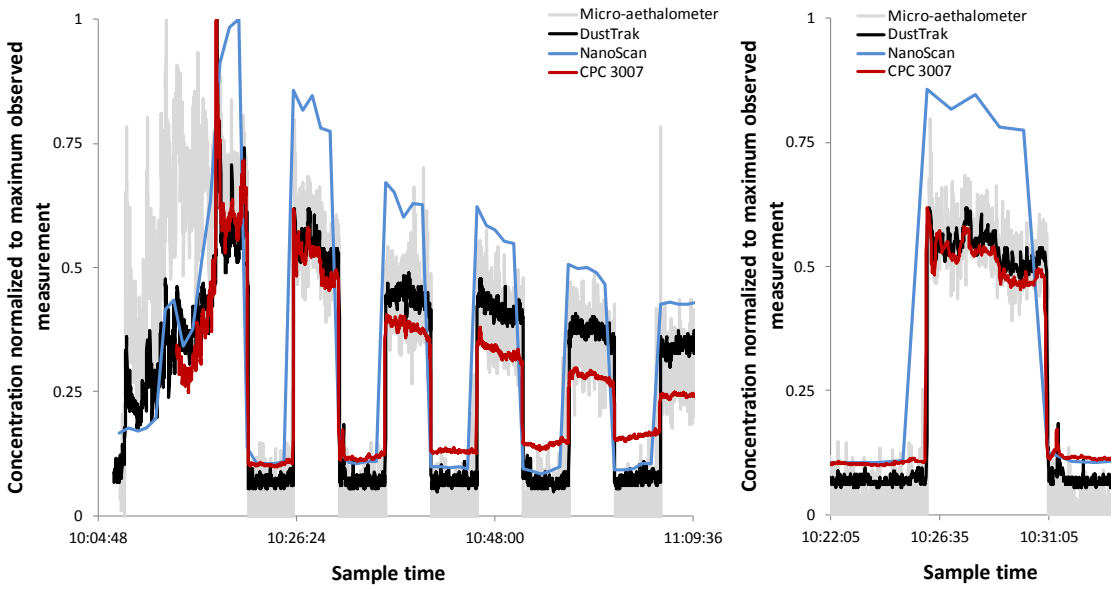

Figure 2.6 Step function used to calculate instrument delay time. Transitions from indoor to outdoor were used to estimate response time (n=5). Multiple transitions (left-panel); zoom in for one transition (right-panel).

Table 2.2 Delay time estimates for each air pollution instrument

Instrument	**Delay time**	
	Mean (s)	Standard deviation (s)
CPC 3007	2	1
NanoScan	2	1
DustTrak	5	1
Micro-aethalometer	8	2

Route selection and sampling protocol

I established 3 sampling routes that aim to be representative of the variability in traffic-related air pollutants in Minneapolis, MN. Routes were chosen based mainly on two goals: (1) street segment selection was stratified by street classification (motorized vehicle traffic [and presumably emissions] is correlated road type) and (2) areas with high non-motorized traffic were oversampled (based on the statistical models and traffic counts presented in Chapter 5). In addition to those two main goals I aimed to include a variety of land uses (e.g., industrial areas, open space/parks, retail corridors, etc.) and include each road type at varying distances from major emission sources (i.e., major highways and the central business district).

I strived to cover as many neighborhoods as possible in the sampling routes. Since my study design included sampling only during specific periods of day (rush-hours) and since I needed to return to the same location for reference measurements my sampling runs were limited to 2 hours (see text below for details). Thus, I could only travel to a limited number of places in the City. My routes had mostly good spatial coverage of neighborhoods in Minneapolis; I was unable to sample in the far north and south of the City because those locations were too far from the city-center to travel to during the 2 hours available in each sampling run. Table 2.3 gives details of the sampling routes by road type. The land uses that I aimed to include as variables in the LUR models (Chapter 4) had good representation along the sampling routes; for example, land uses within 25 meters of the route included: retail (35%), industrial (16%), railway (3%; there are few rail lines in the City), and open space (34%).

Table 2.3 Sampling routes by road (trail) type compared to the entire City of Minneapolis

	Entire City					
	Local	Collector	Arterial	Principal	Off-street	Total
Total miles	761.9	162.0	166.1	9.7	87.4	1,187
with facility	16.4	25.7	38.7	0.0	87.4	168 (80.6 on-street)
without facility	745.5	136.2	127.4	9.7	0.0	1,019
% with facility	2%	16%	23%	0%	100%	14% (7% of on-street)
% by road type	64%	14%	14%	1%	7%	-
	All sampling routes					
	Local	Collector	Arterial	Principal	Off-street	Total
Total miles	13.5	13.8	24.2	-	21.0	73.6
with facility	4.4	3.5	9.7	-	21.0	39.7 (17.6 on-street)
without facility	9.1	10.3	14.5	-	-	34.9
% with facility	32%	26%	40%	-	100%	53% (24% of on-street)
% by road type	19%	19%	33%	-	29%	-
	Route 1					
	Local	Collector	Arterial	Principal	Off-street	Total
Total miles	4.5	3.0	8.4	-	4.1	20.0
with facility	1.4	1.1	2.0	-	4.1	8.7 (4.5 on-street)
without facility	3.1	1.8	6.4	-	-	11.3
% with facility	32%	38%	24%	-	100%	44% (23% of on-street)
% by road type	23%	15%	42%	-	21%	-
	Route 2					
	Local	Collector	Arterial	Principal	Off-street	Total
Total miles	3.4	6.2	8.1	-	5.3	23.0
with facility	0.9	2.3	3.5	-	5.3	12.0 (6.7 on-street)
without facility	2.5	3.9	4.6	-	-	11.0
% with facility	26%	37%	43%	-	100%	52% (29% of on-street)
% by road type	15%	27%	35%	-	23%	-
	Route 3					
	Local	Collector	Arterial	Principal	Off-street	Total
Total miles	5.5	4.7	7.8	-	11.6	29.6
with facility	2.1	0.1	4.2	-	11.6	18.0 (6.4 on-street)
without facility	3.5	4.6	3.5	-	-	11.6
% with facility	37%	2%	55%	-	100%	61% (22% of on-street)
% by road type	19%	16%	26%	-	39%	-

Table 2.3 shows the length of each sampling route by road type as compared to the City of Minneapolis as a whole. The length of each route for mobile sampling was 19-22 miles. Routes were sampled in both forward and reverse directions (alternating each sampling run) in an attempt to mitigate potential hour-of-day patterns in traffic during rush-hours; as such, routes were adjusted slightly for one-way streets (depending

on direction) resulting in a total mileage of road sampled (as reported in Table 3) that is slightly longer (20-30 miles) than the actual sampling length for each sampling run. In general, "forward" refers to sampling routes in a counter clockwise direction and "reverse" in a clockwise direction (routes may cross themselves; rules here refer to the general directions of sampling). Figures 2.8-2.10 show the routes with directions for the "forward" alignment ("reverse" are the same but in the opposite direction and sometimes using alternate one-way streets shown with dashed lines). Table 2.4 gives the day and direction each route was sampled.

The final routes are distributed more equally among road types (i.e., arterial, collector, local, and off-street trails) than the City as a whole. Since principal arterials represent a small amount of road in the City and since non-motorized traffic volumes are small on those corridors I did not sample on principal arterials. However, I did sample ~2,600 meters on one off-street trail which is aligned adjacent to a principal arterial (Hiawatha Trail; State Highway 55). I selected routes so that 53% of the total mileage is on a bicycle facility (i.e., off-street trail or on-street lane, sharrow, etc.).

Since the goal of the mobile monitoring campaign was to describe the spatial patterns of traffic-related air pollution, it was necessary to sample during a consistent time of day to control for hourly variability in traffic patterns and emissions. Routes were sampled on a rotating basis during morning (7-9am; n=12 days) and afternoon (4-6pm; n=30 days) rush-hours on weekdays (8/14/12 – 10/16/2012). As such, the measurements and models presented in this dissertation are representative of rush-hour concentrations during late summer and fall. During each sampling run a specific location (Boom Island

Park) was used as a reference site to monitor daily background concentrations. The reference site is located near the Mississippi River in a park area ~300 meters from the nearest major roadway. Measurements at the reference site were for 30 minutes at the beginning and end of each sampling run. The reference concentrations were then used to adjust on-route measurements for between-day fluctuations in background concentrations (see the next section for more details and a description of the reference site).

I strived to complete the on-road measurement component of each sampling run within the 2-hour rush-hour period. This was not always possible but all sampling runs ended within 15 minutes of the targeted sampling period. All traffic laws were followed while cycling each route. When possible, bicycle facilities (e.g., lanes, advisory lanes, etc.) were used; if no facility was present then I cycled on the right-hand side of the right lane to ensure consistency of location on the roadway among sampling runs. Figure 2.7 shows each sampling route; Figures 2.8-2.10 show maps of each sampling route with surrounding land uses.

Table 2.4 shows sampling dates for: (1) morning mobile runs, (2) afternoon mobile runs, and (3) fixed-site DustTrak calibration samples. Afternoon sampling runs composed the bulk of the sampling days. For the first portion of the sampling campaign only afternoon sampling runs were performed to test and verify the procedure. Then, morning sampling runs were commenced for the rest of the campaign. DustTrak calibration samples required at least a 24-hour runtime at a fixed-site location (more detail on DustTrak calibration is given below). Since there was only one DustTrak available (and it was carried on the bicycle trailer during sampling runs), calibration

samples could only be collected on days when no mobile sampling occurred. To collect enough calibration samples, DustTrak samples were also collected after the end of the mobile sampling campaign.

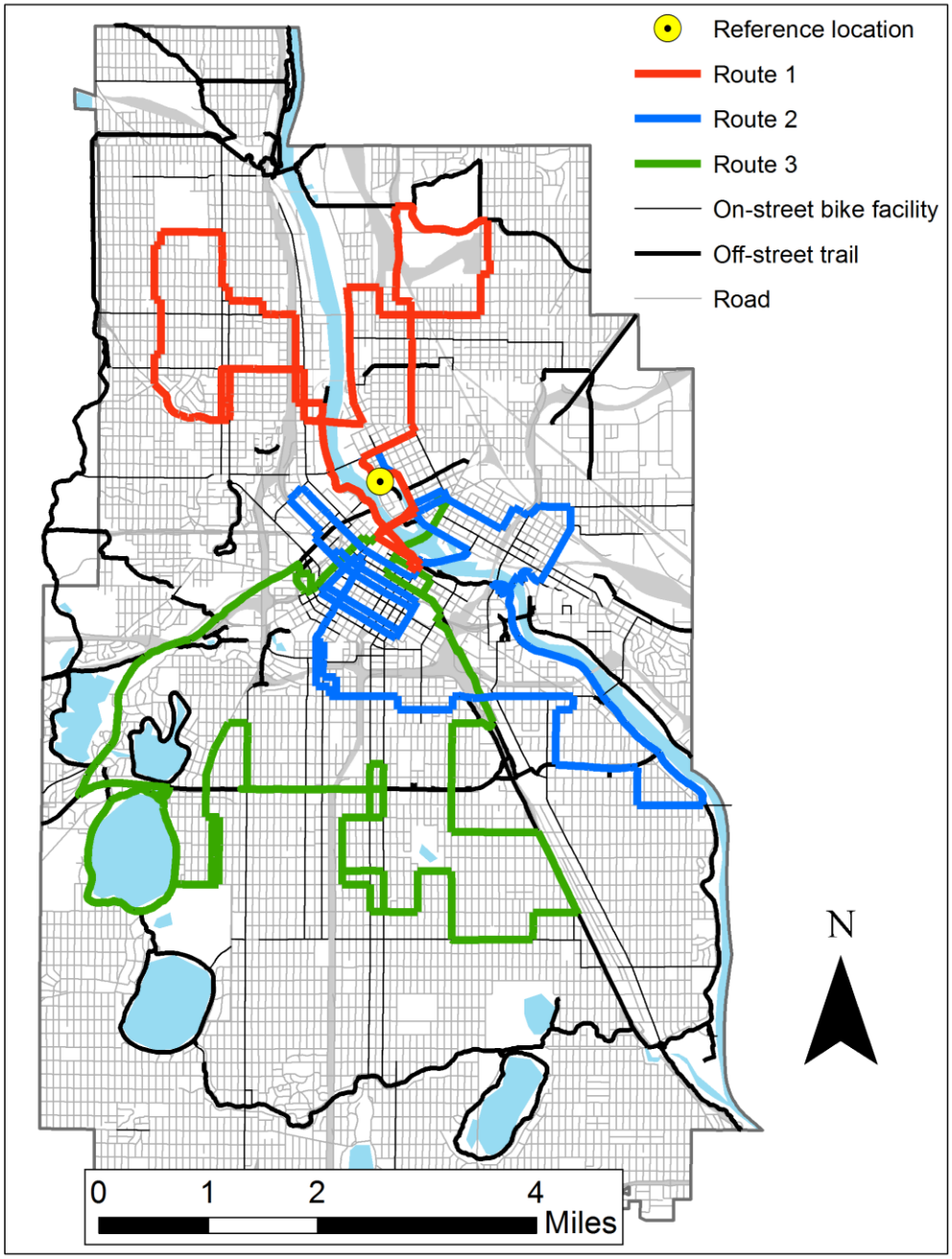

Figure 2.7 Three sampling routes used to collect mobile measurements of particulate air pollution.

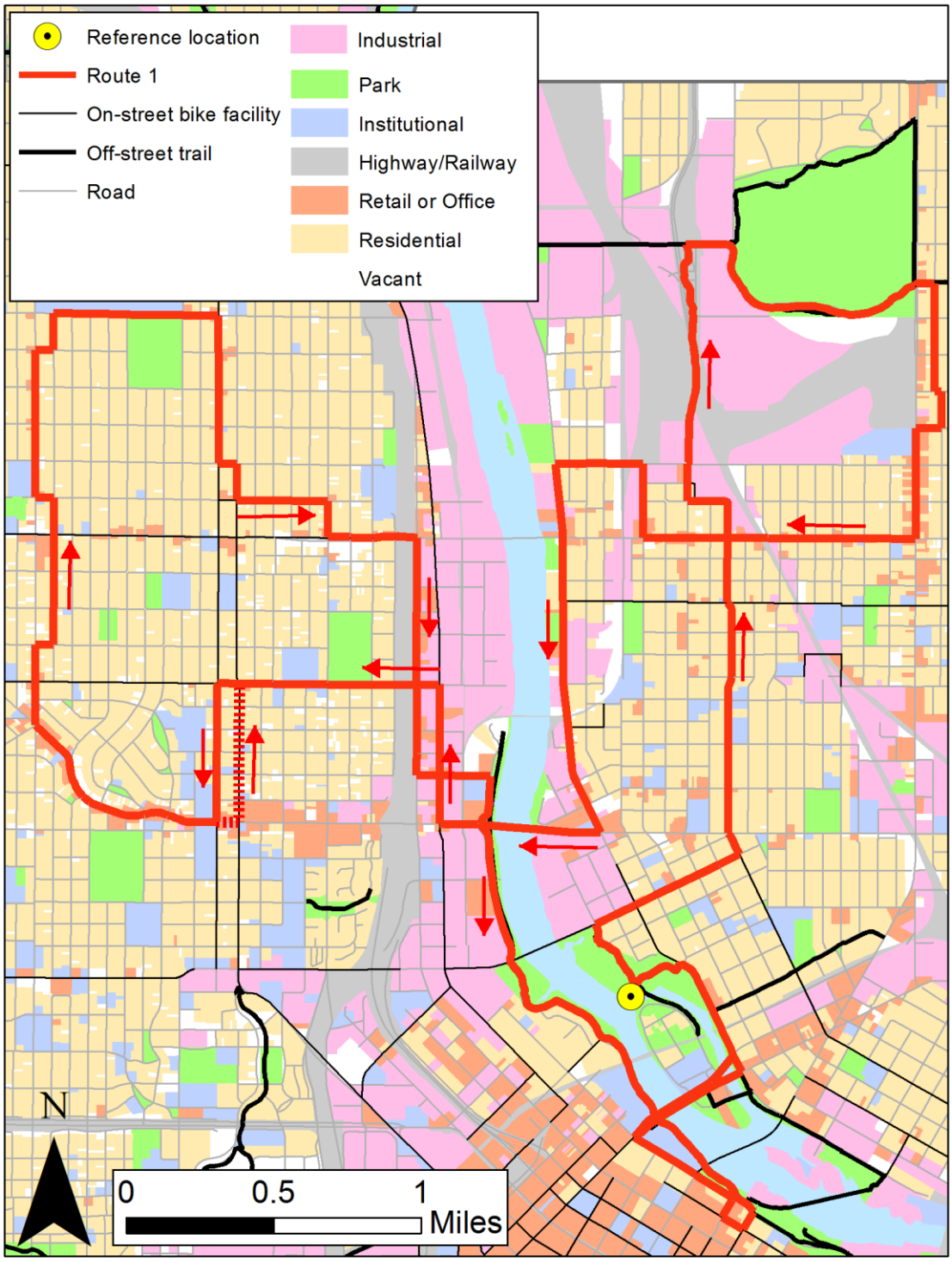

Figure 2.8 Route 1 with surrounding land use. Route run forward is counterclockwise direction (solid lines); backward clockwise (dashed line where needed for one ways). Arrows indicate direction of route where needed.

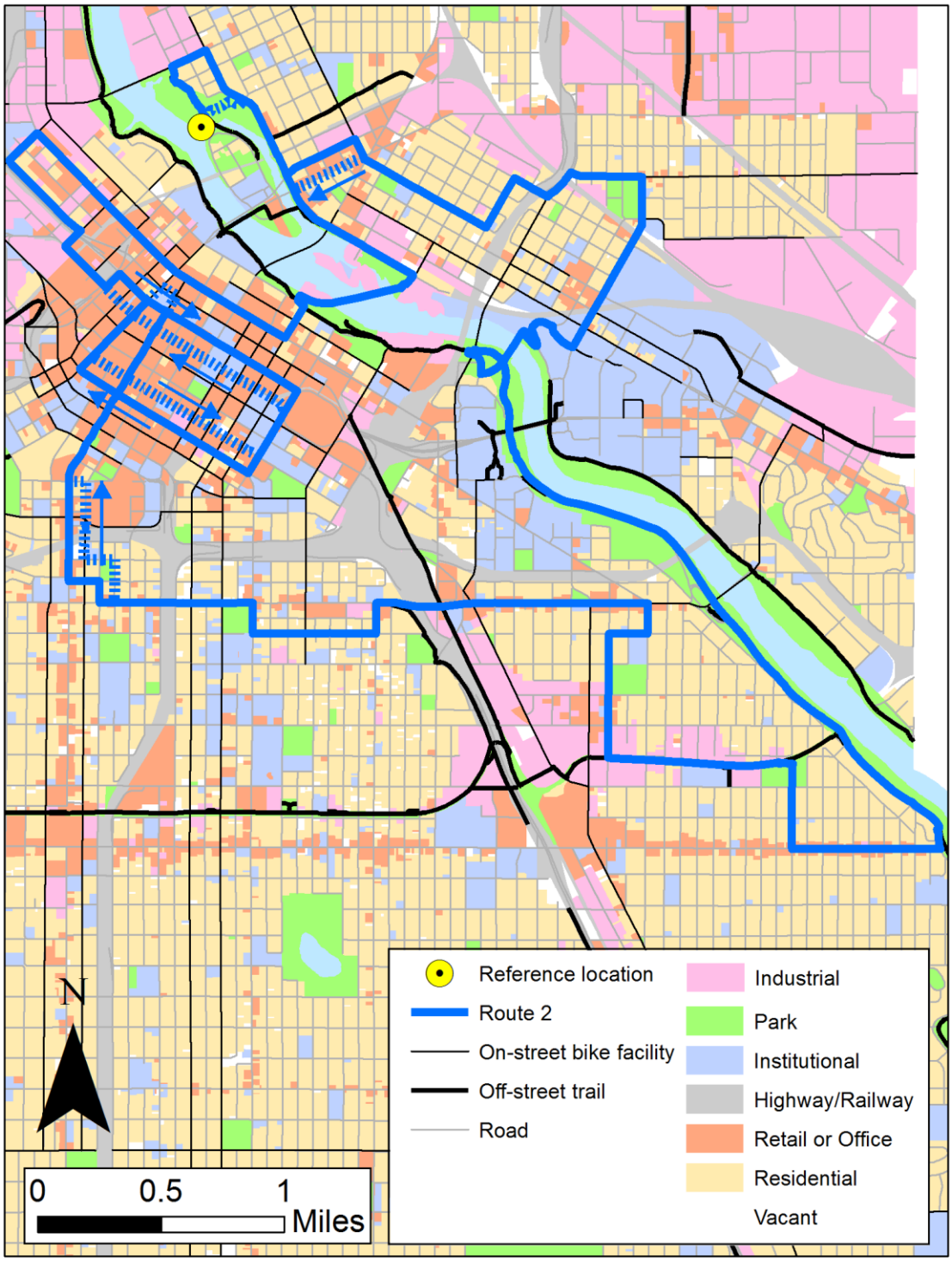

Figure 2.9 Route 2 with surrounding land use. Route run forward is counterclockwise direction (solid lines); backward clockwise (dashed line where needed for one ways). Arrows indicate direction of route where needed.

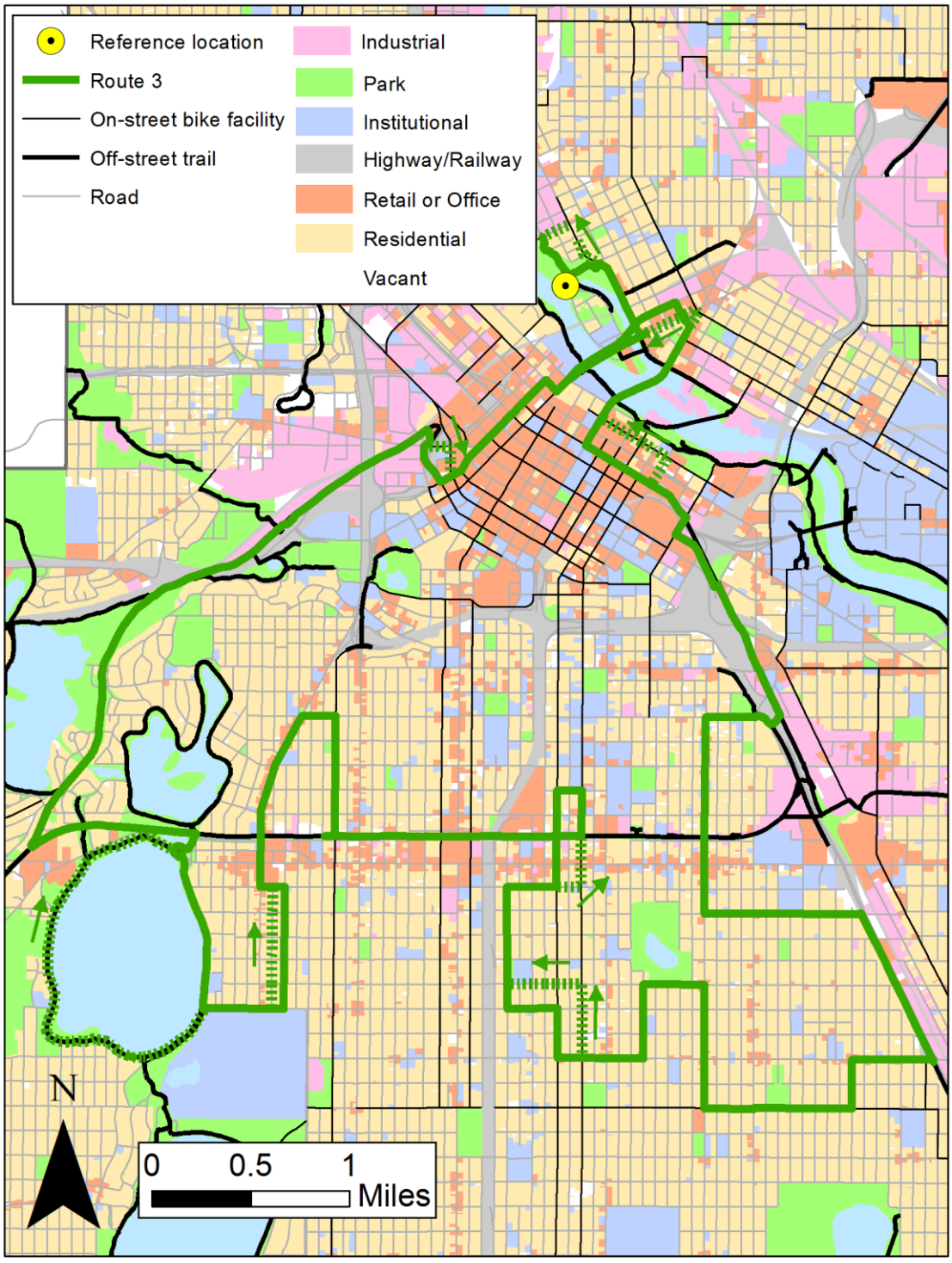

Figure 2.10 Route 3 with surrounding land use. Route run forward is counterclockwise direction (solid lines); backward clockwise (dashed line where needed for one ways). Arrows indicate direction of route where needed.

Table 2.4 Sampling schedule for morning and afternoon mobile measurements as well as DustTrak calibration measurements[a]

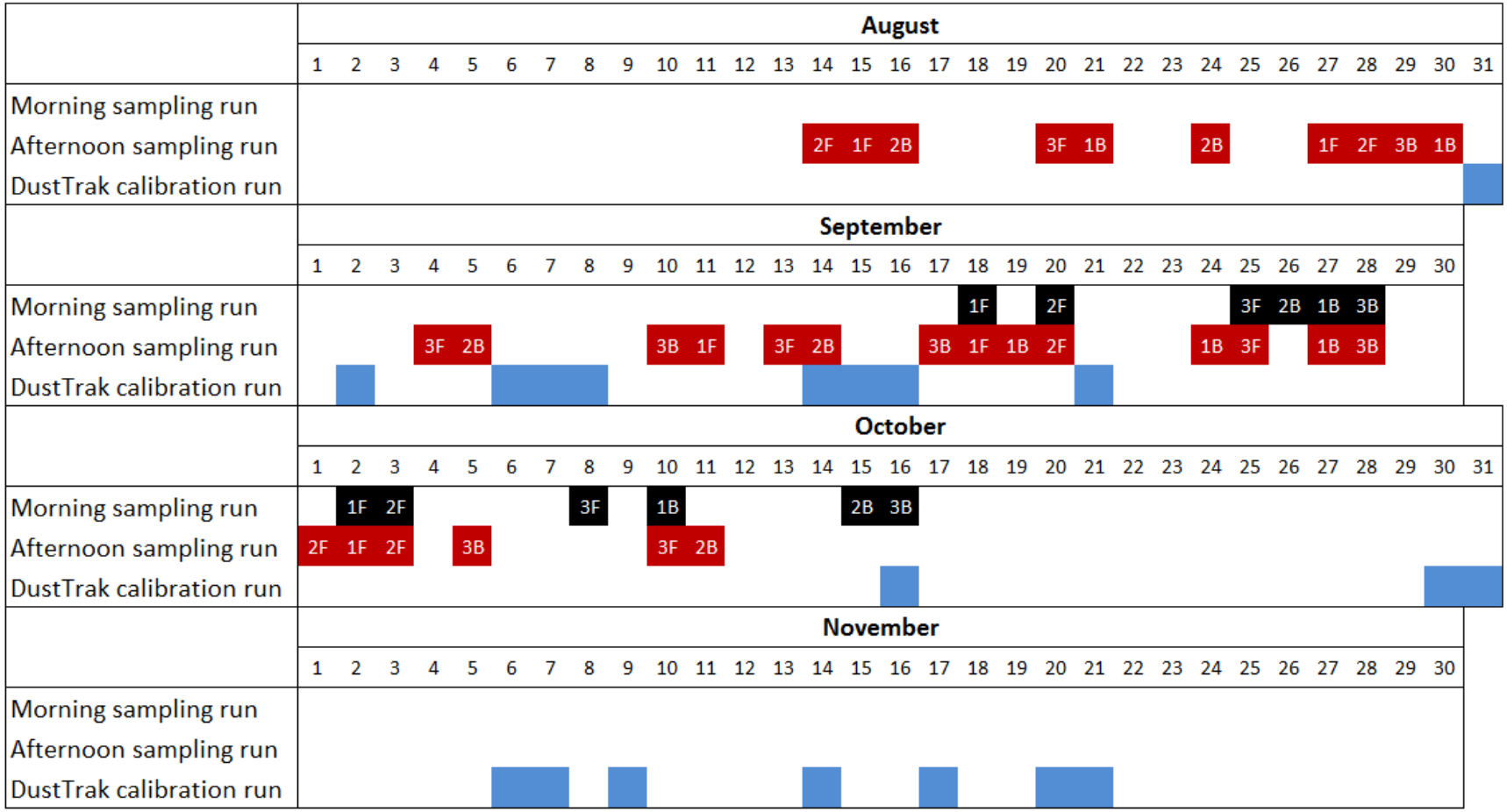

[a]Route numbers shown for each sampling day as well as direction of travel: forward ("F") and backward ("B").

Reference site measurements and site description

A potential issue that arises with collecting mobile samples on different days is that background concentrations vary from day-to-day; failing to account for those daily differences will reduce the reliability of the spatial estimates. Since only one set of monitoring equipment was available it was impossible to keep a continuous reference site running during the entire sampling campaign (to later adjust all mobile measurements). Instead an alternate approach was developed; namely, to adjust for the day-to-day differences in background concentrations I collected measurements at a reference site (see Figure 2.11) for 30 minutes before and after each sampling run to estimate the background concentration for that day.

The reference site was in a 36 acre park on the Mississippi River ~300m from the nearest major road (there is a small local road ~100m away on the island across from the reference site [Nicollet Island] that has very low traffic volumes). I used the reference site measurements to adjust for daily variability. Specifically, for each sampling run, I subtracted "background" concentrations for on-road measurements using various methods: (1) calculating an average reference site concentration for each day, (2) making a linear interpolation from the mean reference site concentration before and after the run for each pollutant, (3) developing an underwrite function that estimates a reference concentration based on the measurements made during the sampling run. More details on the approach used to adjust on-road measurements for reference site measurements are given in Chapter 3. In general, this approach allowed for aggregation of all sampling days

into one dataset with the aim of describing spatial patterns in concentrations, yet accounting for day-to-day variations in background pollution levels.

Figure 2.11 Reference site location in Boom Island Park.

Mobile sampling data post-processing

The measurements collected using the mobile sampling platform required significant post-processing. Instrument-specific artifacts of sampling have been documented in the literature. To account for those artifacts, I applied previously developed adjustment equations for each pollutant. Two scripts were used in MatLab to post-process all mobile, on-road measurements:

1. A script that corrects measurements from the micro-aethalometer. The script identifies spurious spikes due to vibration errors and corrects estimates for particle loading on the disposable filter. This script was originally developed by Josh Apte (Apte et al., 2011) and modified superficially to display plots of the process data to ensure the program worked correctly for the measurements described here.
2. A script that applies correction factors for all other instruments and joins the measurements from each instrument in one dataset. The script applies correction factors for the CPC 3007 and DustTrak as well as adjusts all timestamps for the estimated, instrument-specific delay time. All measurements are then joined based on timestamp and assembled in one dataset.

Corrections applied to measurements from each instrument are described below (micro-aethalometer, DustTrak 8530, CPC 3007). The NanoScan did not require adjustments; instead this instrument was checked against a laboratory-based reference instrument at TSI, Inc. as described above.

Corrections to micro-aethalometer measurements

I measured black carbon with a micro-aethalometer (Aethlabs; model: AE-51). Black carbon measurements were logged at 1s intervals and a flow rate of 150 mL/min. Raw data from the AE-51 were corrected in two ways: (1) removing spurious spikes due to mechanical shock and (2) correcting measurements for particle loading on the disposable filter.

The micro-aethalometer reports large spurious spikes when the unit experiences even mild mechanical shock (Apte et al., 2011). In brief, vibration errors generate spurious concentration spikes that usually follow a characteristic pattern, i.e., a large spike up in concentration followed by a negative spike in concentration (typically 1-3s after the initial spike). The spurious spike events usually do not average to zero introducing a bias to smoothed (i.e., time-averaged) AE-51 datasets. Apte et al. (2011) developed an algorithm that searches for high relative deviance in concentrations that follow this characteristic spurious spike signature. I implemented the algorithm developed by Apte et al. (2011) to identify and remove measurements that were the result of vibration or mechanical shock; using that approach, 2.1% (0.8%) of the afternoon (morning) on-road measurements were censored.

The micro-aethalometer estimates black carbon by measuring changes in light attenuation (λ = 880 nm) as particles are deposited on a disposable filter. Others have observed that as particle loading on the filter increases, the instrument underestimates black carbon concentrations (Kirchstetter and Novakov, 2007). Kirchstetter and Novakov (2007) developed an empirical correction equation for this effect; I used their equation to adjust all black carbon measurements:

$$BC = BC_o(0.88Tr + 0.12)^{-1}\,; TR = \exp\left(-\frac{ATN}{100}\right) \quad (2.1)$$

where *BC* is the adjusted black carbon measurement, BC_o is the black carbon estimate reported by the instrument, *TR* is the micro-aethalometer filter transmission, and *ATN* is the attenuation coefficient reported by the instrument.

Corrections to DustTrak 8530 measurements

I measured $PM_{2.5}$ using a DustTrak 8530 with the appropriate manufacturer impactor. Measurements were collected at 1s intervals and at a flow rate of 4.0 L/min. DustTrak measurements were corrected in two ways: (1) an instantaneous relative humidity (RH) correction and (2) a calibration using mass-based filter measurements to correct for bias related to regional differences in particulate matter composition.

$PM_{2.5}$ mass concentrations measured using a light scattering device typically overestimate concentrations at higher relative humidity due to increased condensational growth of the aerosol (McMurry et al., 1996). When RH changes during a sampling run, instantaneous (rather than time-average) RH correction is necessary for use of real-time concentration data (see Both et al., 2011). I collected 1s measurements of RH and $PM_{2.5}$ and used an empirical correction equation to adjust for the effect of RH:

$$PM2.5_{RH} = \frac{PM2.5_{DustTrak}}{CF} \; ; CF = 1 + \frac{0.25 * RH^2}{1 - RH} \qquad (2.2)$$

where $PM2.5_{RH}$ is the RH adjusted $PM_{2.5}$ measurement, $PM2.5_{DustTrak}$ is the raw DustTrak measurement, *CF* is the RH correction factor, and *RH* is the instantaneous relative humidity. In prior research, this correction approach was employed in southern California and Minneapolis, MN (Ramachandran et al., 2003; Chakrabarti et al., 2004). After correcting for RH I also created a mass calibration using filter measurements to correct for the specific particle size distribution at the study site. I co-located the DustTrak and pump/cyclone/filter system (Casella Apex Pro pump, BGI cyclone, PTFE filters with pore size of 2.0 µm) to develop a mass calibration curve for the on-road measurements. The fixed-site measurements were collected outdoors at my apartment, which is on

Nicollet Island very near (~500m) the reference site. The two units were co-located for 18 separate 24-hour periods during or soon after the on-road sampling period. The DustTrak (filter-based) 24-hour average concentration range was 3 – 43 µg/m^3 (1.6 – 24 µg/m^3). I carried field blanks to adjust all calibration measurements for changes in laboratory and field conditions during the sampling period. Blanks were weighed periodically throughout the study period and adjustments to calibration filter measurements were made according to the observed changes over time in the field blanks. Table 2.5 shows the blank masses for each date sample filters were weighed. Among all fixed-site measurements, the mean absolute filter mass adjustment to account for field blanks was 4.4 µg or about 10%. I chose a linear correction equation based on goodness-of-fit (R^2 = 0.82; Figure 12, equation 3).

$$PM2.5_{filter} = 0.459 * PM2.5_{RH} + 1.361 \quad (2.3)$$

where $PM2.5_{filter}$ is the filter-based $PM_{2.5}$ measurement and $PM2.5_{RH}$ is the RH-corrected DustTrak measurement of $PM_{2.5}$. The filter-based measurements used to create the adjustment equation (as well as each candidate correction function) are shown in Figure 2.12.

Table 2.5 Mass change in field and laboratory blanks

Date	Mass (mg)	
	Lab blank	**Field blank**
8/31/2012	204.833	201.642
9/6/2012	204.835	201.647
9/14/2012	204.835	201.647
9/21/2012	204.838	201.649
10/30/2012	204.846	201.662
11/6/2012	204.854	201.670
11/13/2012	204.854	201.671
11/19/2012	204.859	201.670
11/27/2012	204.874	201.678
Mass change	0.040	0.036

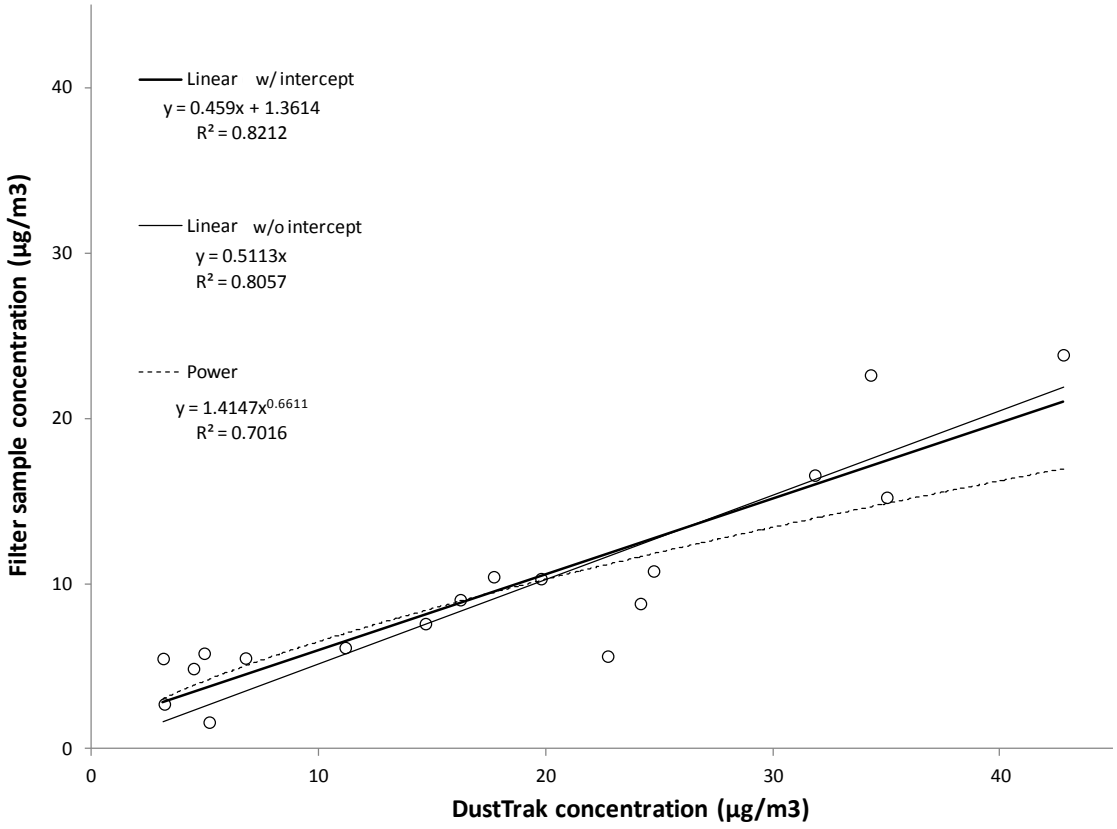

Figure 2.12 Fixed-site measurement data used to create the filter-based correction equation.

Corrections to CPC 3007 measurements

I measured particle number concentration using a condensation particle counter (TSI CPC 3007). Particle number measurements were logged at 1s intervals at a flow rate of 700 mL/min. Westerdahl et al. (2005) observed that the 3007 underestimates particle number (as compared to the laboratory standard: CPC 3022) at concentrations >100,000 pt/cc owing to particle coincidence (i.e., particles passing the light sensor side-by-side). I observed concentrations >100,000 pt/cc for 1.2% of the on-road measurements. For those data I used the following correction equation (Westerdahl et al., 2005) to adjust the measurements:

$$PNC_{corr} = 38456 * \exp\left(PNC_{raw} * 0.00001\right) \quad (2.4)$$

Where PNC_{corr} is the corrected particle number measurement and PNC_{raw} is the instrument-reported particle number measurement. Among the 1.2% of data that required correcting, the average correction factor employed was 1.22 (i.e., on average, values over 100,000 pt/cc were adjusted up by ~22%). The remaining 98.8% of the data were <100,000 pt/cc and so did not require correction.

Assessing NanoScan error flags

During the sampling runs the NanoScan occasionally reported error messages related to the instrument being tilted. Since the NanoScan used in this study was one of the first off of the production line, TSI, Inc. was consulted to discuss the possible causes of these errors. After discussions with TSI, Inc. it was determined that these errors were not serious and were likely due to unimportant tilt of the instrument (similar to with the CPC 3007) or very short breaks in power supply from the batteries moving during mechanical shock. The panel used to secure the batteries had a small gap between the battery and panel allowing for the battery to move out of place when the trailer hit a large bump; to mitigate this I used the remaining scraps of foam rubber to fill the space between the panel and battery and secure the battery and not disturb the power flow to the instrument. TSI, Inc. used this information to modify the instrument design to include a more robust battery mounting technique in new NanoScan devices.

I explored whether the reported errors impacted the particle size estimates reported by the NanoScan. Table 2.6 shows descriptive statistics for the distributions of two datasets: (1) all NanoScan measurements and (2) a dataset where data associated

with reported errors was censored. Figure 2.13 shows cumulative distribution plots for the two datasets (both concentrations and particle size). Since there are only minor differences in the distributions between the full and censored dataset, results reported in this dissertation include all measurements. Analyses reported in subsequent chapters were tested using both datasets to test the sensitivity of the reported particle size estimates to this choice.

Table 2.6 Descriptive statistics of the full dataset and a dataset with flagged data removed

Pollutant	**n**	**Arith. Mean**	**Geo. Mean**	**Std. Dev.**	**Geo. Std. Dev.**	**P10**	**P25**	**P50**	**P75**	**P90**
Morning sampling runs (n=12)										
Concentration (pt/cc) for all data	86,983	26,831	18,217	48,423	2.2	7,125	9,876	18,037	30,707	48,672
Conc. (pt/cc) for data w/o errors	61,859	26,520	18,020	43,945	2.2	7,154	9,683	17,558	29,523	47,751
Size (nm) for all data	86,983	42.1	41.2	9.1	1.2	33.9	37	40.2	45.4	52.3
Size (nm) for data w/o errors	61,859	41.9	41	8.9	1.2	33.9	36.9	40	45.2	51.4
Afternoon sampling runs (n=30)										
Concentration (pt/cc) for all data	213,687	14,215	10,545	22,301	2.1	4,179	7,150	10,591	16,367	24,323
Conc. (pt/cc) for data w/o errors	150,139	14,620	10,734	25,155	2.1	4,484	7,314	10,505	16,554	25,398
Size (nm) for all data	213,687	39.1	37.9	10.5	1.3	29.3	33.1	37.4	42.5	49.6
Size (nm) for data w/o errors	150,139	38.8	37.8	9.9	1.3	29.3	33.2	37.4	42.5	49.1

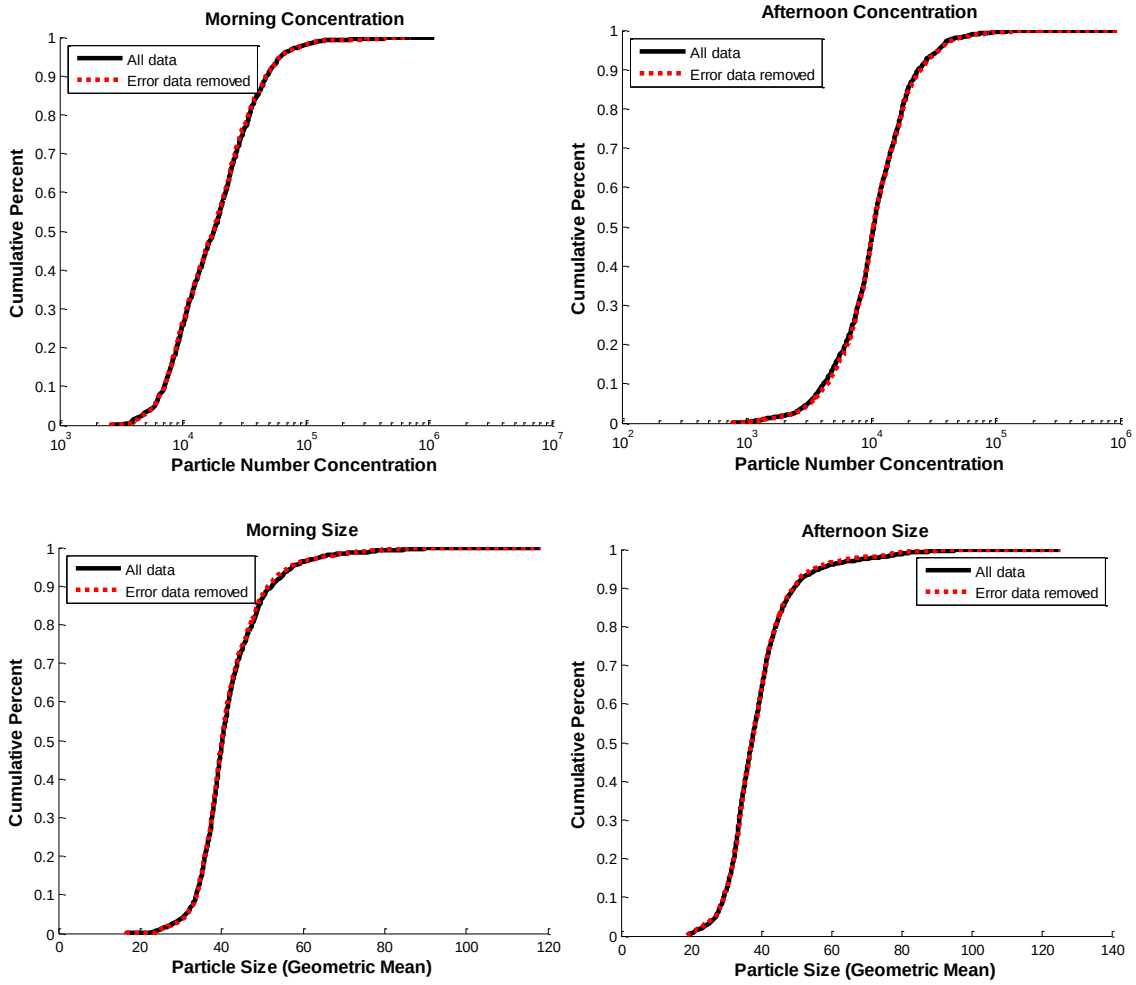

Figure 2.13 Cumulative distribution plots for the full and censored NanoScan datasets.

Chapter Conclusions

This chapter described work to develop a method for acquiring measurements of on-road particulate air pollution concentrations using a mobile sampling platform. Core outcomes from this chapter include the following:

1. It was possible to modify instrumentation and customize a bicycle trailer to measure particulates in real-time using a mobile, bicycle-based platform.

2. Sampling routes were determined using a selection process that stratified roads by street classification with a focus on oversampling areas with high rates of active travel and passing through a diverse set of land uses.
3. A reference site was located and measurements were collected to test methods for adjusting the mobile on-road measurements for day-to-day differences in background concentrations.
4. Matlab scripts were developed to apply instrument-specific corrections to the particulate air pollution measurements to adjust for known artifacts of sampling.

Chapter 3 Mobile, on-road measurements of particle number, black carbon, $PM_{2.5}$, and particle size

I completed 42 sampling runs during morning (7-9am; n=12) and afternoon (4-6pm; n=30) rush-hours in Minneapolis, MN (8/14/2012 – 10/16/2012). I collected a total of 129.3 hours of measurements (on-road: 87.3 hours; reference site: 42 hours), covering a total of 886 miles. The average cycling speed during the sampling runs was 10.2 mph; this speed represents a balance between ensuring air pollution instrumentation was not exposed to excess vibration during the sampling run and maximizing the distance traveled to improve spatial coverage. During morning sampling runs mean (interquartile range [IQR]) weather parameters were: 46.9 °F (42.8 – 51.4 °F), 69.6% (63.3 – 76.9%) relative humidity, and 5.6 mph (3.0 – 7.0 mph) wind speed; during afternoon sampling runs weather parameters were: 76.3 °F (68.3 – 86.8 °F), 31.2% (25.0 – 35.6%) relative humidity, and 9.2 mph (6.0 – 13.0 mph) wind speed. Measurements were processed and adjusted as described in Chapter 2. This chapter provides analyses of the measurements, including the following:

1. Development of a underwrite functions to control for non-linear changes in background concentrations.
2. Descriptive statistics of datasets with and without adjustments for background concentrations.
3. An analysis of pollutant correlations as a function of averaging time and estimation of the share of exposure related to in-traffic emissions.

4. A summary of particulate measurements stratified by aspects of the road network; these results may be of interest for planning bicycle and pedestrian networks.
5. Analysis of correlations among particle number, black carbon concentrations, and particle size.
6. Analysis of how traffic mix and traffic volume impact particle concentrations; this investigation focuses on the subset of sampling data that has video footage.

Underwrite functions to estimate "background" concentrations

I used reference site measurements before and after each sampling run to estimate daily background concentrations for each pollutant. However, background concentrations were not always constant during the two-hour on-road sampling period (i.e., average concentrations at the reference site before and after the sampling run were not equal). A first attempt to estimate changes in background concentrations during the on-road sampling runs was based on a linear interpolation between mean concentrations of the "before" and "after" reference site measurements. This method was problematic because during some sampling runs the changes in background concentrations did not appear to follow a linear pattern (e.g., in some cases, all instruments experienced a sharp drop in concentrations during a sampling run, presumably related to a meteorological event such as an inversion lifting).

To account for non-linear changes in background concentrations during sampling runs, instrument-specific underwrite functions were developed to estimate background concentrations. Underwriting functions have been applied in air pollution research as a technique to calculate the share of concentrations measured at a fixed-site attributable to

middle-, neighborhood-, and urban-scale emission sources (Watson and Chow, 2001); Watson and Chow (2001) used an urban and rural monitor as well as a successive moving average subtraction method to divide concentrations into the three spatial scale categories; Both et al., (2011) used alternative methods (i.e., moving 1.5 percentile) in addition to the successive moving average subtraction method and suggest that the method presented by Watson and Chow (2001) may underestimate local contributions.

The goal of the underwrite function is to capture baseline trends in the time-series data; usually this approach involves some sort of moving parameter (minimum value, specific percentile) calculated over some time period. I experimented with multiple iterations of underwrite functions including varying the time resolution of the input data, parameter of interest (in this case estimates of the lower end of the distribution), and the search window to calculate that parameter. The underwrite functions were applied to each sampling run's time-series data individually before aggregating the dataset. There is an important difference in generating functions that predict baseline estimates for particle size; unlike for the other three pollutants which are measured by concentration (i.e., underwrite functions estimate the lowest values of the distribution), baseline particle size is represented by a central tendency of the measurements since particle size can spike up or down during the sampling run depending on the local conditions. As such, for particle size I aimed to generate an "underwrite" function for a central tendency of size rather than a lower bound. To maintain consistency with the other pollutants I will refer to this as an "underwrite" function for particle size in this document; however, strictly speaking, a typical underwrite function does not attempt to characterize central tendencies.

Table 3.1 gives underwrite function parameters I used for each instrument. I strived to keep the smallest time resolution possible while keeping other parameters consistent. For three of the instruments I was able to apply the underwrite functions at the smallest time intervals possible (CPC: 1s, DustTrak: 1s, NanoScan: 60s); since the black carbon data has significant noise I needed to smooth those data before applying the underwrite function to ensure mostly positive values when concentrations were near zero. For black carbon, I tried data smoothing the measurements using 60, 120, and 180 seconds. I chose 180 seconds as the final input since that was the smallest time average where <10% of underwrite estimates were <0 (smoothing at 60s [27.7%],120s [16.8%], and 180s [7.6%]); for the 180s case the average value for the underwrite estimates that were <0 was -0.15 μg m^{-3}. Since I developed a dataset (for spatial analyses) that added a "typical" background concentration to the local component estimated by the underwrite, this approach resulted in no negative black carbon values in the final adjusted dataset (see description of developing the dataset for spatial analysis below) All underwrite functions are moving 1st percentiles with a 30 minute search window except for the particle size data (60 minute window; moving median). Figure 3.1 shows plots of on-road measurements and the associated under-write function for a morning sampling run.

Table 3.1 Parameters used to generate underwrite functions

Instrument	Time resolution	Moving parameter	Search window
CPC 3007	1 second	1st percentile	30 minute
DustTrak	1 second	1st percentile	30 minute
NanoScan (concentration)	60 second	1st percentile	30 minute
NanoScan (particle size)	60 second	median	60 minute
Micro-aethalometer	180 second	1st percentile	30 minute

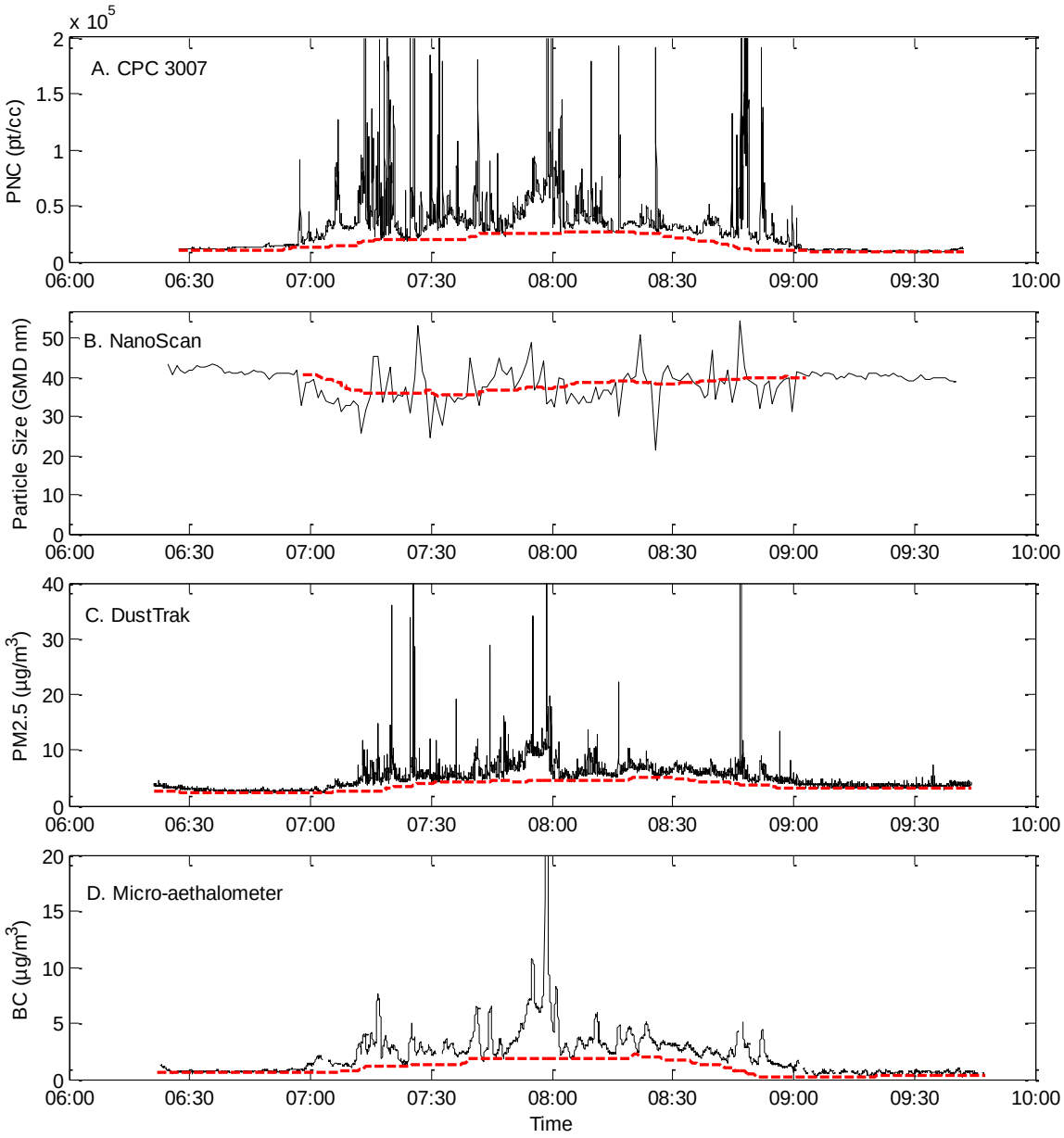

Figure 3.1 Example of underwrite functions for a morning sampling run. Solid lines are on-road measurements; dashed lines are the underwrite function.

To assess the accuracy of the underwrite function's estimates of background concentrations, I compared underwrite estimates to the instrument measurements from the reference site for each sampling run and to the on-road measurements. Figure 3.2 shows box plots of trip averaged concentrations from the reference site measurements,

underwrite function background estimates, and on-road measurements. In order to confirm that the underwrite function is reliably estimating background concentrations the estimates should be relatively similar to the reference site measurements.

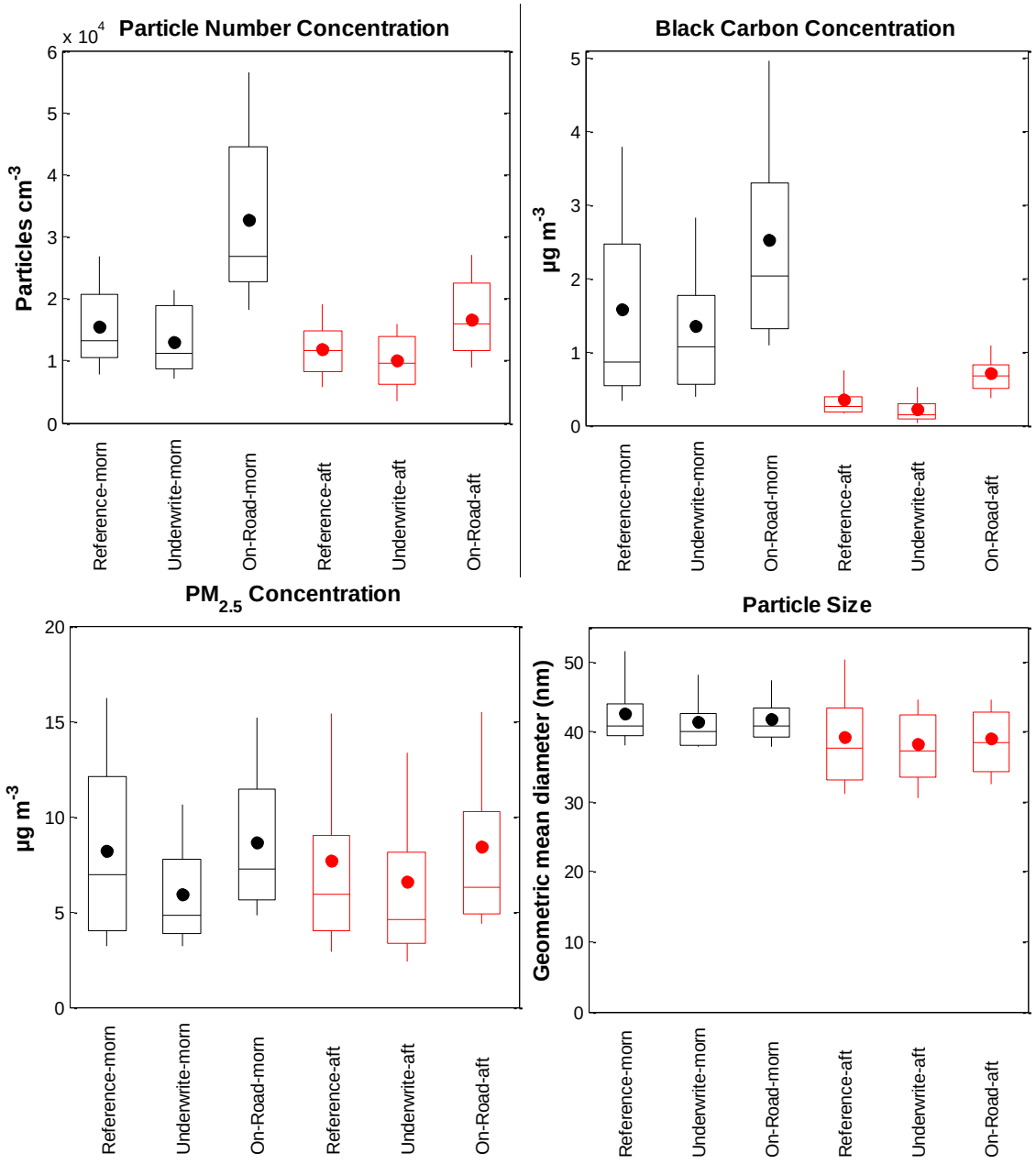

Figure 3.2 Trip averaged reference site measurements, underwrite function estimates, and on-road concentrations.

In general, the central tendencies of the underwrite function estimates are similar to those of the reference site measurements. The variability in reference site measurements was sometimes larger than for the underwrite function estimates; this difference was more pronounced for the morning than the afternoon sampling runs indicating that this difference could potentially be due to the relatively smaller sample size in the morning (n=12) than in the afternoon (n=30). For all measurements of particulates (except particle size) on-road concentrations were higher than both the reference site measurements and underwrite function estimates. On-road concentrations during morning sampling runs were higher than concentrations during afternoon sampling runs. Particle size underwrite estimates and instrument measurements (both reference and on-road) were similar in magnitude; this was expected since the underwrite function for particle size aims to capture central tendencies rather than relatively lower "background" concentrations.

Development of datasets with and without adjusting for background concentrations

Since background concentrations vary on a day-to-day basis, it is important to account for these differences when making spatial comparisons of measurements collected on different days. I used a combination of the reference site measurements and underwrite function estimates to create a dataset adjusted for differences in daily background concentrations. An important clarification regarding my approach is that my reference site measurements (and underwrite estimates) may not be representative of true background concentrations in the region. The reference site measurements capture day-to-day variability in background concentrations; however, the absolute value of the

estimated baseline concentrations may be slightly higher than true background. Nevertheless, in this document I will refer to the adjusted dataset as one that is adjusted for "background" concentrations.

For the remainder of the analyses presented in this chapter two datasets will be used: (1) a dataset of instrument reported measurements that are not adjusted for background concentrations and (2) a dataset adjusted for background concentrations using the underwrite functions and reference site measurements described above. The unadjusted dataset is used to explore the relationship between the different measures of particulate matter (e.g., between-pollutant correlations, effect of time averaging). The background adjusted dataset is used to describe spatial patterns in concentrations where it is desirable to remove the effect of day-to-day differences in background concentrations (e.g., concentrations by road type, bicycle facility type, or distance from major road).

To create the dataset that is adjusted for background concentrations a three step process was carried out. First, the underwrite function was generated for each time-series (i.e., sampling run) of particulate concentrations. Second, for each instrument-reported data point the corresponding underwrite concentration estimate was subtracted from the instrument-reported measurement. Third, a "typical" background concentration was calculated by averaging reference site measurements among all runs; this value was then added to all underwrite adjusted measurements from the second step. This process was repeated separately for afternoon and morning sampling runs (since background concentrations are higher in mornings than in afternoons). Table 3.2 gives descriptive statistics for datasets that are adjusted and unadjusted for background concentrations.

Table 3.2 Descriptive statistics for sampling runs with and without adjusting for background concentrations

Morning sampling runs (n=12)										
Pollutant	n	Arith. Mean	Geo. Mean	Std. Dev.	Geo. Std. Dev.	P10	P25	P50	P75	P90
PNC (pt/cc)	86,983	32,549	24,364	39,059	2.0	10,428	14,918	23,685	37,207	57,916
BC ($\mu g/m^3$)	86,951	2.5	1.9	2.1	2.2	0.7	1.1	1.9	3.1	5.6
$PM_{2.5}$ ($\mu g/m^3$)	86,983	8.7	7.4	6.3	1.7	3.8	5.0	7.1	10.7	15.5
Size (nm)	86,983	42.1	41.2	9.1	1.2	33.9	37	40.2	45.4	52.3
Morning sampling runs with reference site adjustment										
Pollutant	n	Arith. Mean	Geo. Mean	Std. Dev.	Geo. Std. Dev.	P10	P25	P50	P75	P90
PNC (pt/cc)	86,983	35,003	28,924	37,677	1.7	17,252	19,801	25,347	37,068	56,318
BC ($\mu g/m^3$)	86,951	2.7	2.5	1.4	1.4	1.7	1.9	2.3	3.0	4.0
$PM_{2.5}$ ($\mu g/m^3$)	86,983	10.9	10.5	4.8	1.3	8.6	9.0	9.8	11.4	14.2
Size (nm)	86,983	43.2	42.6	8.0	1.2	35.8	39.9	42.6	45.4	50.4
Afternoon sampling runs (n=30)										
Pollutant	n	Arith. Mean	Geo. Mean	Std. Dev.	Geo. Std. Dev.	P10	P25	P50	P75	P90
PNC (pt/cc)	220,097	16,592	12,902	17,783	2.0	5,284	8,961	13,461	18,995	28,778
BC ($\mu g/m^3$)	147,681	0.7	0.5	0.6	2.2	0.2	0.3	0.5	0.9	1.4
$PM_{2.5}$ ($\mu g/m^3$)	211,234	8.3	6.6	8.4	1.9	3.1	4.3	5.9	9.6	17.1
Size (nm)	213,687	39.1	37.9	10.5	1.3	29.3	33.1	37.4	42.5	49.6
Afternoon sampling runs with reference site adjustment										
Pollutant	n	Arith. Mean	Geo. Mean	Std. Dev.	Geo. Std. Dev.	P10	P25	P50	P75	P90
PNC (pt/cc)	220,097	18,401	16,534	16,374	1.4	12,458	13,141	14,678	17,961	25,318
BC ($\mu g/m^3$)	147,681	0.8	0.7	0.6	1.6	0.4	0.5	0.7	0.9	1.4
$PM_{2.5}$ ($\mu g/m^3$)	211,234	9.4	9.1	6.3	1.2	8.1	8.1	8.6	9.5	10.4
Size (nm)	213,687	40.1	39.5	7.6	1.2	34.5	37.7	39.3	41.1	45.6

Pollutant correlations, averaging time, and in-traffic exposure

Particulate matter varies in shape, size, and composition. I measured various parameters of particulate matter that may behave differently according to the type of emission source, transport and transformation in the atmosphere, and proximity to and density of emission sources. I used the data from my mobile measurements to address three questions that may arise from measuring different parameters of particulate matter:

1. How well correlated are the measured parameters of particulate air pollution?
2. Does increasing the time-series averaging time (i.e., smoothing the data) impact the between-parameter correlations?
3. What share of each parameter can be attributed to near-source (i.e., traffic) vs. regional emissions?

Correlations of particulate concentrations as a function of averaging time

To explore the first two questions, I smoothed the time-series data from the mobile on-road measurements using two methods: (1) applying a moving average to each time-series for various possible averaging times (sample size remains the same) and (2) calculating interval averages for each averaging time (reduces the sample size by a factor equal to the averaging time in seconds) to partially mitigate temporal correlation in the measurements. Trends of between-pollutant correlations were similar using both methods but were clearer using the moving average method; thus, those results are presented here. Correlations between the measures of particulate air pollution as a function of averaging time are shown in Figure 3.3.

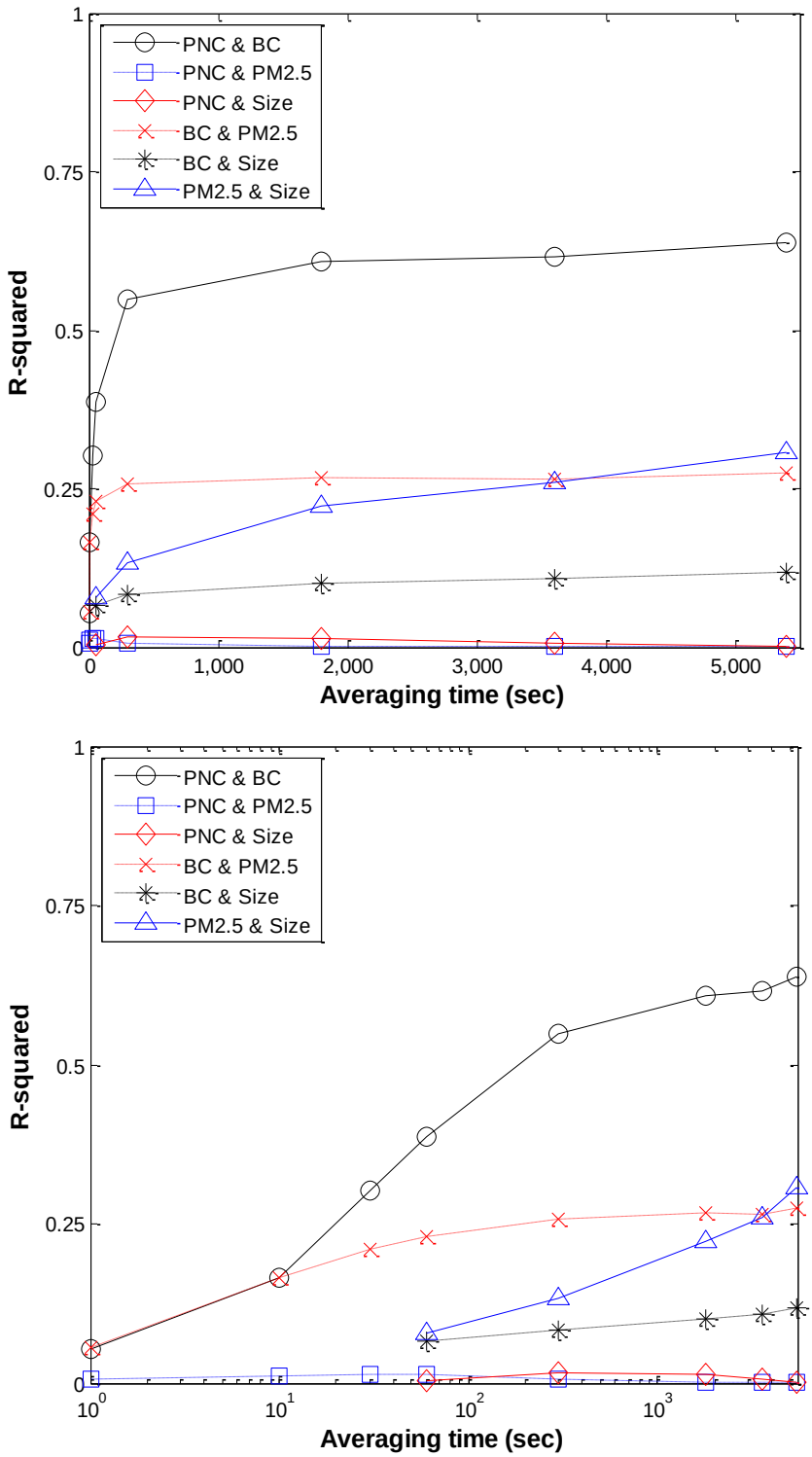

Figure 3.3 Correlations (R^2) of measured particulate matter parameters as a function of averaging time.

Overall, the strongest correlation was between particle number and black carbon concentration. This outcome is likely because particle number and black carbon are indicators of traffic-related air pollution and thus are elevated when I was near traffic emissions. Black carbon was also moderately correlated with $PM_{2.5}$ and particle size; $PM_{2.5}$ and particle size showed moderate correlation as averaging time increased. Particle number concentration was not correlated with either particle size or $PM_{2.5}$.

In general, between-parameter correlations increased with averaging time, until about 1-5 minutes; for averaging times greater than 5 minutes, correlations do not noticeably increase (exception: moderate increases between particle size and $PM_{2.5}$ concentration). This finding suggests that smoothing the time-series data to greater than 1-5 minutes will not yield better insight into how these parameters interact, yet would sacrifice temporal and spatial resolution. As such, data used to describe spatial patterns were not smoothed at more than 5 minutes.

Estimating share of exposure due to near-traffic emission sources

One way commonly used to characterize in-transport related exposure concentrations is the ratio of "in-vehicle" to ambient concentrations (Marshall et al., 2003). Another way to describe this relationship is to calculate the share of the instrument-reported concentration that is attributable to near-roadway emissions (as compared to ambient sources); following Apte et al. (2011), that parameter is represented here as φ ("phi").

$$\varphi = (C_{onroad} - C_{ambient})/C_{onroad} \quad (3.1)$$

where C_{onroad} is the instrument reported on-road mobile measurement and $C_{ambient}$ is the estimate of background concentration. I calculated φ using trip-averaged concentration values for both ways of estimating background concentrations: (1) reference site measurements and (2) underwrite function estimates of ambient concentrations. Figure 3.4 shows the distribution of φ values using box plots for each pollutant and for both morning and afternoon sampling runs.

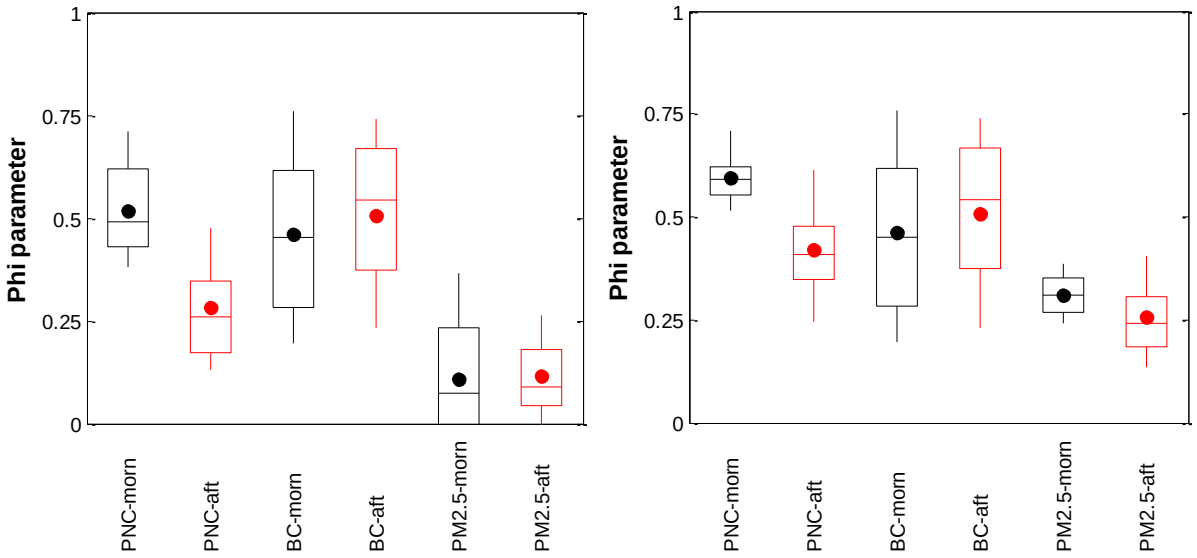

Figure 3.4 Share of measured concentrations attributable to near-traffic emissions. Left panel: Using reference site measurements; Right panel: Using underwrite function.

Central tendencies for the φ parameter were similar using both methods to estimate background concentrations for black carbon; φ estimates were slightly higher for particle number and for $PM_{2.5}$ when using the underwrite function than when not using it. There were a relatively small number of days that reported negative φ values for $PM_{2.5}$ using the reference site measurements for background concentrations; negative values occurred on days when background concentrations were highly non-linear (e.g., when the "before" reference site measurements were very high and quickly dropped during the

start of the sampling run causing an inflated estimate of average background concentration using only the reference site measurements) and thus estimates of background concentrations are likely over-estimated for times during the sampling run. The φ estimates calculated using the underwrite functions better handle this type of non-linear behavior and do not give estimates below zero; thus, I expect that those estimates (i.e., calculated using the underwrite functions; right panel of Figure 3.4) are a more robust representation of φ.

As expected, φ is higher for the traffic-related pollutants (black carbon and particle number) than for $PM_{2.5}$. That finding is consistent with Apte et al. (2011), who studied in-traffic exposure concentrations while riding in auto-rickshaws in Delhi, India. Particle number and $PM_{2.5}$ had lower φ values in the afternoon than in the morning; this result is presumably attributable to the increased dilution that occurs in the afternoons as the mixing height of the atmosphere increases, thus more rapidly diluting on-road emissions. However, black carbon shows the opposite effect (i.e., φ was higher in the afternoon than in the morning). This result is perhaps explained by the difference in background concentrations of black carbon during the course of the day as compared to the other pollutants. $PM_{2.5}$ and particle number background concentrations decreased modestly over the course of the day ($PM_{2.5}$: 8 μg m^{-3} [morning], 7.8 μg m^{-3} [afternoon]); particle number: 15,000 particles cm^{-3} [morning], 12,000 particles cm^{-3} [afternoon]). Black carbon showed a more drastic decrease in background concentration (1.5 μg m^{-3} [morning], 0.3 μg m^{-3} [afternoon]). Since black carbon background concentrations approached zero during the afternoon, almost all of the instrument reported

concentrations would be attributed to near-traffic emissions thus increasing the value of φ.

Particulate concentrations and street characteristics

As highlighted in Chapter 1, there is growing interest in designing cities that promote active transportation. One issue that may need to be considered is how best to design transportation networks that allow for active travel while addressing (i.e., reducing) exposure to air pollution. A strategy that may help with this goal is to locate bicycle facilities (e.g., bike lanes or shared spaces) where air pollution concentrations are relatively low. To explore this topic I summarize here my on-road measurements by different characteristics of the road network: (1) street functional class, (2) distance from a major (i.e., high-traffic) road, and (3) by bicycle facility type.

Summary data shown in Figures 3.5-3.7 were generated using the dataset that adjusts for background concentrations using the underwrite functions. This dataset was chosen since the goal of this analysis is to explore differences by road characteristics (i.e., a spatial aspect of the measurements) without the effect of day-to-day variability in background concentrations. Data were smoothed using a 60 second moving average for particle number, $PM_{2.5}$, and particle size; black carbon data was smoothed using a 180 second moving average since this was the time interval necessary to apply the underwrite function for those data.

Concentrations by street functional class

Road networks are designed in a hierarchal fashion to group streets into classes or systems according to their desired service. Typically, this involves classifying streets by

expected motor-vehicle traffic volumes. In Minneapolis, streets are classified into 4 groups for the purpose of motor-vehicle traffic: Principal arterial, arterial, collector, and local streets. When considering non-motorized travel this classification scheme changes slightly: specifically, principal arterials need not be considered since they are typically high-traffic highways without bicycling or walking; also, an additional group exists (off-street trails) that is for use only by cyclists and pedestrians. For that reason, I focused on measuring air pollution (and describing results) for four groups of streets: Arterial, collector, local streets, and off-street trails.

Transportation networks typically route the majority of vehicular traffic on arterial and collector streets; local streets typically have relatively less traffic, off-street trails have no vehicular traffic. As such, the expected result would be to find relatively higher concentrations on major roads (i.e., arterials and collectors) and relatively lower concentrations on local roads and off-street trails. Figure 3.5 shows my mobile, on-road measurements stratified by street functional class for both the morning and afternoon sampling runs and for all four measured parameters of particulate air pollution.

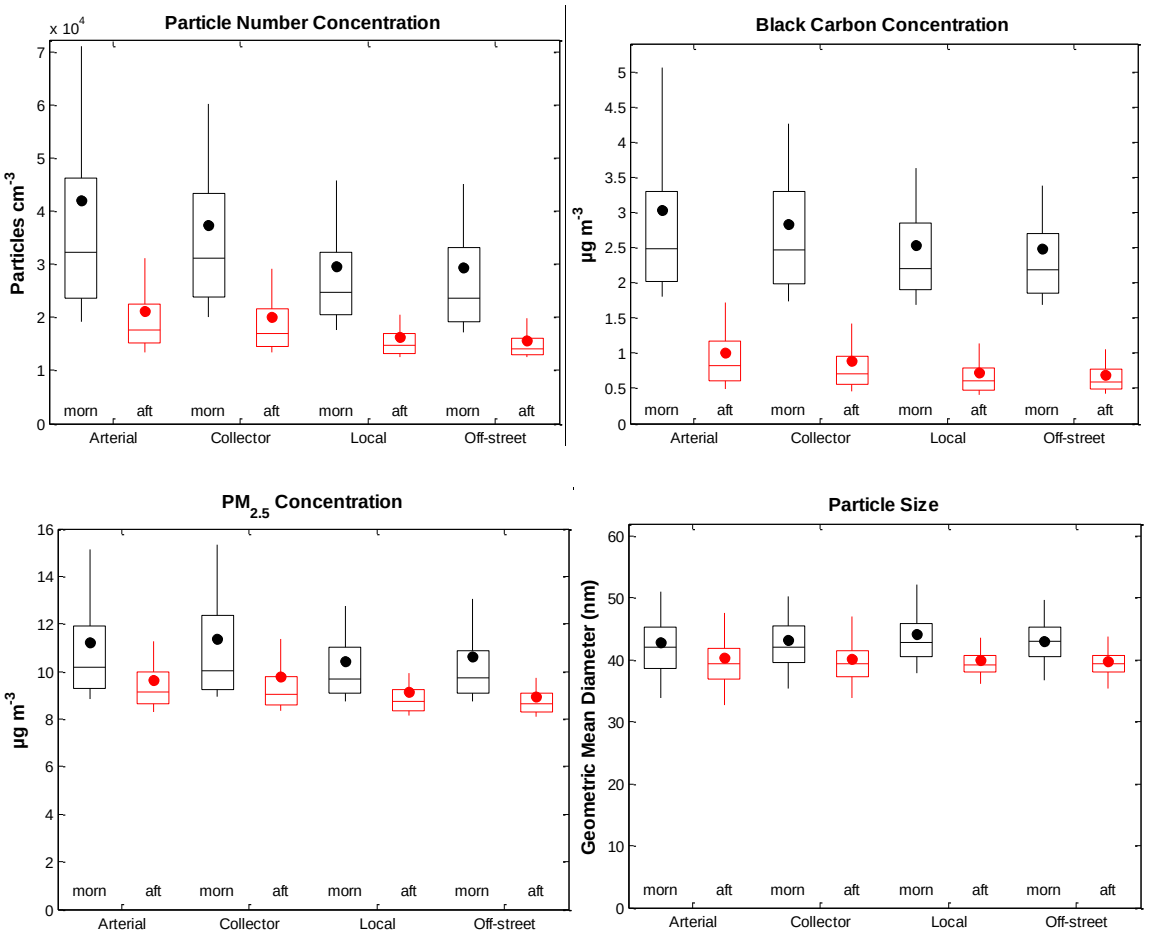

Figure 3.5 Concentrations by street functional class.

As shown in Figure 3.5 particle number and black carbon concentrations were modestly elevated on arterials and collectors as compared to local streets and off-street trails. Particle size and $PM_{2.5}$ did not vary much by street classification. In general, concentrations were much higher in mornings than in afternoons for the traffic-related pollutants; the between-road type difference in concentrations was slightly more pronounced during mornings than afternoons for particle number (morning [afternoon] arterial to local median ratio: 1.31 [1.20]) but the opposite for black carbon (morning [afternoon] arterial to local median ratio: 1.13 [1.36]). Furthermore, the upper ends of the

distributions (i.e., 75th and 90th percentiles) typically showed larger differences between road types than central tendencies (i.e., mean and median) suggesting that short-duration exposures to elevated concentrations are more likely to occur on major roads.

Concentrations by distance from a major road

Since concentrations (for traffic-related pollutants) are moderately elevated on major roads (i.e., arterials and collectors), a logical approach to building a network for non-motorized traffic that protects against air pollution exposure might be to locate routes (i.e., bicycle facilities such as bike lanes or sharrows) on local streets instead of arterials or collectors. However, utilitarian cyclists and pedestrians (like motor vehicles) are typically traveling to get to a destination and usually the road network is designed so that the most efficient route (i.e., shortest distance) is on major roads. A logical question follows: how much is air pollution exposure reduced by moving short distances from major roads (i.e., does moving over one block, from an arterial road to a parallel adjacent local road, reduce exposure)? Figure 3.6 shows particulate concentrations for two categories of roads: (1) all major roads (both arterials and collectors) and (2) local roads adjacent to major roads (at varying distances). The local roads are separated into 4 bins with increasing distances from the nearest major road.

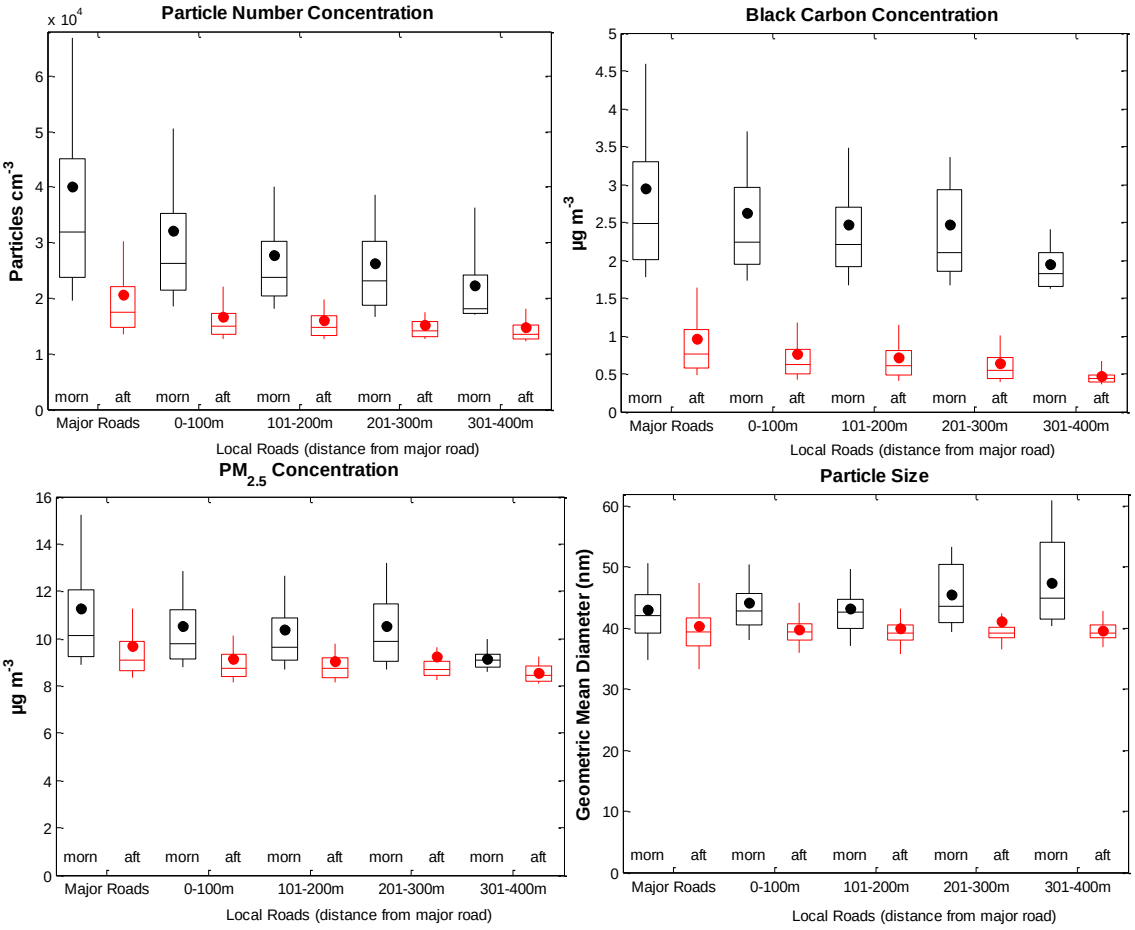

Figure 3.6 Particulate concentrations for major roads and local roads by distance from the nearest major road.

Particle number and black carbon concentrations on local streets decreased with increasing distance from a major road; $PM_{2.5}$ and particle size showed only small changes as distance from a major road increased. Similar to the stratification for street functional class these patterns were slightly more pronounced for mornings than for afternoons for particle number (morning [afternoon] median major road to local road [101-200m] ratio: 1.34 [1.18]) and the opposite for black carbon (morning [afternoon] median major road to local road [101-200m] ratio: 1.15 [1.28]). Again, concentration differences were larger for the upper ends of the distributions than for central tendencies.

Reductions in exposure by moving over one block could be significant for particle number and black carbon concentrations. For example, a typical block in Minneapolis is about 150 meters; using that distance as a basis, and based on average conditions shown in Figure 3.6, mean exposure during morning rush-hours would be reduced by 31% (16%) for particle number (black carbon) and 90th percentile exposure would be reduced by 40% (24%) upon moving from an arterial to a non-arterial parallel road. This finding suggests that moving over one block may be a relatively minor spatial shift in the bicycle network infrastructure that could yield noteworthy reductions in air pollution exposure during active travel.

Although there was little change in the geometric mean particle size, there does appear to be a slight trend (for the morning sampling runs) of increasing particle size as distance from a major road increases. This trend is consistent with expectations. Fresh emissions are typically associated with smaller particle sizes (Ripamonti et al., 2013; Zhu et al., 2002b); small (i.e., ultrafine) particles can be removed by coagulation, evaporation, or deposition on surfaces as emissions are diluted. Field studies have observed a decrease in particle number as distance from high-traffic freeways increases (Zhu et al., 2002a; 2002b). The factor most likely responsible for the decrease in particle number concentrations is dilution from the emission source; however, the other mechanisms (coagulation, evaporation, deposition to surfaces) could also play a role in the observed particle number gradient as well as the increase in geometric mean particle size.

Concentrations by bicycle facility type

The last aspect of designing streets for active travel that is considered here is the type of bicycle facility (if any) that is present. There exist multiple types of bicycle facilities, including separate off-street trails, striped bicycle lanes on-road, and shared spaces such as marked bicycle boulevards or sharrows. I stratified my measurements of particulate concentrations by the three most common bicycle facility types in Minneapolis (off-street trails, bicycle lanes, and bicycle boulevards) and compared to roads with no bicycle facility (Figure 3.7).

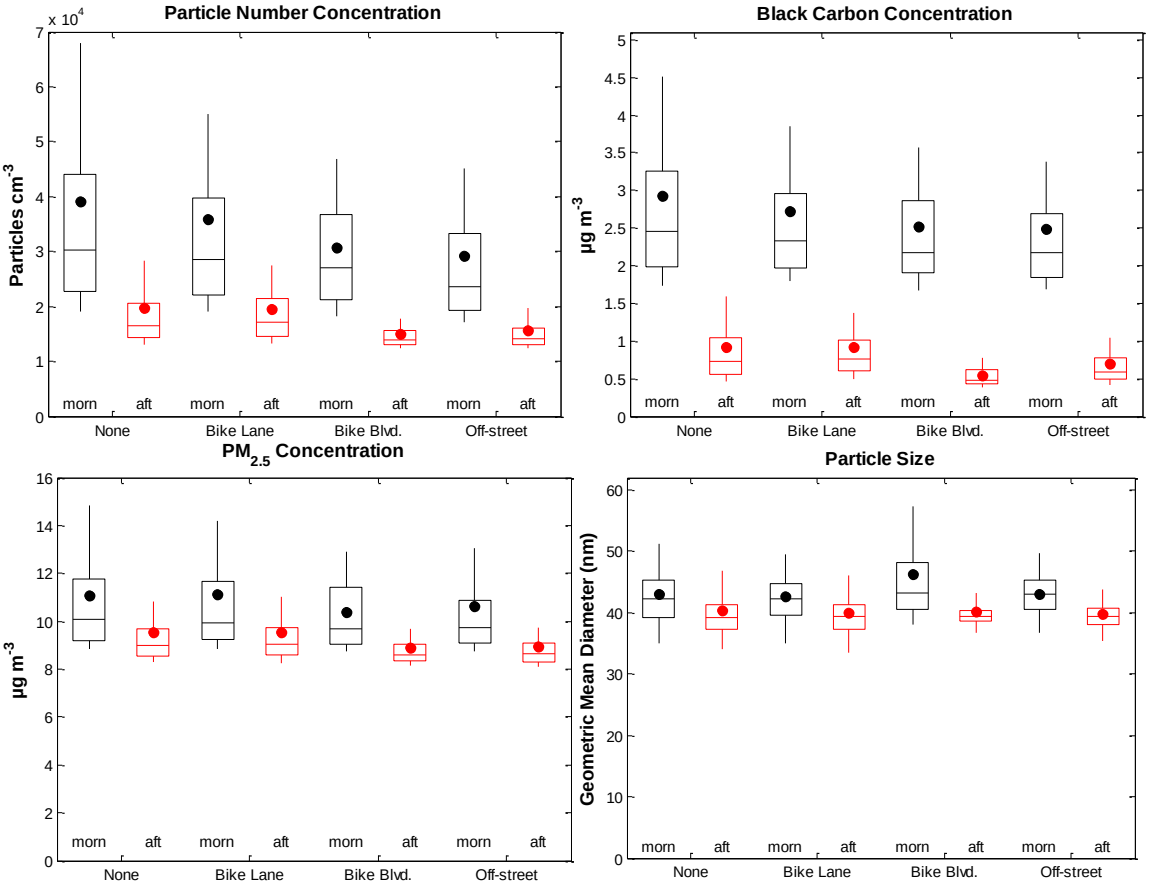

Figure 3.7 Particulate concentrations by bicycle facility type.

Similar to trends for street functional class and distance from a major road, differences by type of bicycle facility were most evident for particle number and black carbon concentrations (again, $PM_{2.5}$ and particle size did not change much by bicycle facility type). Roads without a bicycle facility had the highest concentrations followed by roads with bicycle lanes, bicycle boulevards, and off-street trails. There was almost no change in central tendencies (e.g., morning [afternoon] mean differences for no facility vs. a bike lane were -4.9% [1.7%] for particle number and -6.8% [0.06%] for black carbon) with slight differences for the upper ends (i.e., 75^{th} and 90^{th} percentiles) of the distributions e.g., morning [afternoon] 90^{th} percentile differences for no facility vs. a bike lane were -11.4% [-2.7%] for particle number and -14.7% [-13.5%] for black carbon.

An important caveat to stratifying by bicycle facility type is that these treatments are not always installed on similar types of roads. For example, bicycle lanes are most frequently used on high-traffic (e.g., arterial) roads and bicycle boulevards are used almost exclusively on local roads. Therefore, summary statistics shown here may be both a function of street classification, location of the road/facility in the City, and the type of bicycle facility. Sample sizes were not sufficient to stratify by all of these potential confounding factors.

Correlations of particle number and black carbon concentrations with particle size

There are many factors that could influence in-traffic measurements of particle size. For example, mean particle size would likely decrease near to traffic or other combustion emissions. Another factor is that particle size may vary in different ways depending on the type of vehicle emissions (e.g., diesel vs. gasoline engines). The mobile

measurements I collected include proxies for some of these factors: particle number concentration (indicating fresh emissions from combustion sources) and black carbon concentration (indicating diesel emissions or other incomplete combustion from fossil fuels). I used measurements from the condensation particle counter and micro-aethalometer to explore whether geometric mean particle size (from the 1-minute NanoScan particle size distribution scans) is correlated with particle number or black carbon concentrations.

I first pooled all data from morning and afternoon sampling runs (including the instrument-reported measurements and underwrite function estimates) at various averaging times. I calculated the median geometric mean particle diameter among all scans (39.2 nm) and then defined 7 total bins of particle size (including 3 bins above and below the bin that included the median particle size). I used the 60-second time averaged particle number and black carbon data (to directly compare to the 1-minute NanoScan scan time) and plotted distributions of those concentrations within each of the particle size bins (Figure 3.8).

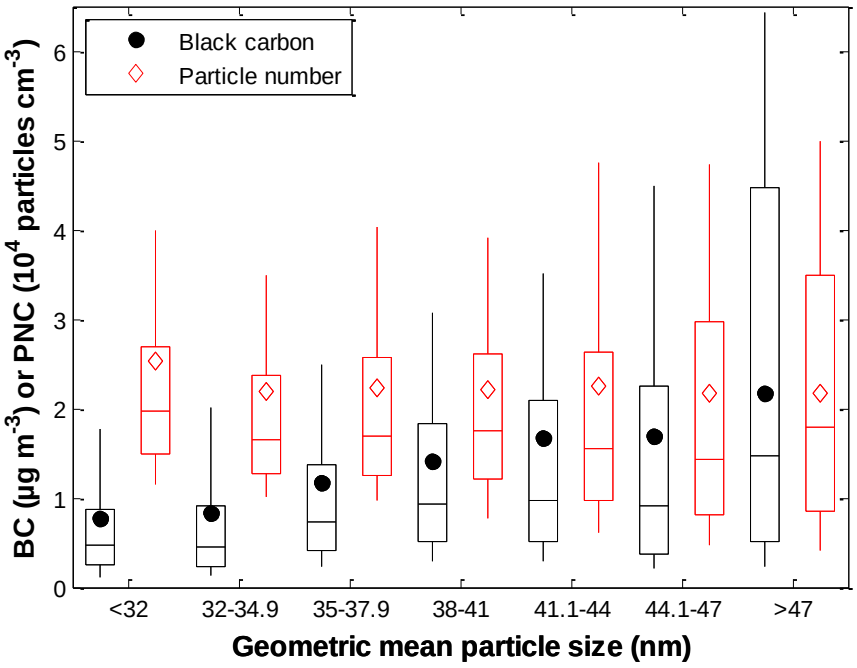

Figure 3.8 Particle number and black carbon concentrations by geometric mean particle diameter.

As shown in Figure 3.8, black carbon concentrations increased with larger particle sizes; however, central tendencies of particle number concentrations were relatively consistent among all particle size bins. The highest particle number concentration was for the smallest particle size bin and variability in particle number was greatest for larger particle size bins. The fact that the lower end (i.e., 10^{th} and 25^{th} percentile) of the distribution for particle number decreased as particle size bins increased indicates there may be some impact of increasing particle number concentrations on decreasing particle size; however, this relationship remains ambiguous since spikes in black carbon concentrations also are correlated with increased particle number counts.

To better understand this relationship I ran a series of regressions to infer the relationship between particle number and black carbon concentrations and particle size, while controlling for potential confounding variables (weather). Regressions included

data for a number of different time averages (1, 60, 300, 1800, 3600, and 5400 seconds) and a variety of different independent variables (instrument-reported concentrations, separate background and on-road concentrations, and weather related parameters). Data was averaged for specific intervals for each time average (i.e., not a moving average) to lessen the effects of possible temporal correlation in the measurements; this approach resulted in a smaller sample size as the time average interval increased.

Three categories of independent variables were used in the regression models: (1) instrument-reported concentrations, (2) concentrations separated into an on-road component and a background component, and (3) separated on-road/background concentrations with additional weather related variables. A regression was performed for each set of variables and each time averaging interval for comparison.

On-road concentrations were calculated by subtracting the underwrite estimate from the instrument reported measurement. Background concentrations were assumed to be the estimate from the underwrite function. Separating concentrations into an on-road and background component allowed for the exploration of whether small time-scale spikes in particle number and black carbon concentrations (likely due to micro-plumes from passing vehicles) or background concentrations had were more correlated with 1-minute particle size scans. Weather variables were introduced into the final regression to control for potential temperature, wind, or humidity impacts on the relationship between the pollutant concentrations and particle size. Table 3.3 shows regression results for each set of independent variables and for each averaging time interval.

Table 3.3 Regression results for each category of independent variables[a]

Instrument measurements						
Averaging time	1s	60s	300s	1,800s	3,600s	5,400s
PNC	-0.0000066 ***	-0.00012 ***	-0.00021 ***	-0.00028 ***	-0.00034 ***	-0.00018
BC	0.42 ***	2.14 ***	3.20 ***	4.09 ***	4.60 ***	3.37 ***
Constant	39.0 ***	39.3 ***	39.7 ***	39.9 ***	40.8 ***	38.6 ***
n	230,957	3,412	779	119	54	33
Model R^2	0.03	0.17	0.25	0.40	0.41	0.29
Onroad/underwrite separate						
Averaging time	1s	60s	300s	1,800s	3,600s	5,400s
PNC onroad	-0.0000081 ***	-0.000067 ***	-0.0001 ***	-0.000087	0.000021	0.000056
PNC under	-0.00055 ***	-0.00054 ***	-0.00049 ***	-0.00051 ***	-0.00058 ***	-0.00036 *
BC onroad	0.17 ***	-0.92 ***	1.32 ***	2.015 *	-0.64	3.13
BC under	5.06 ***	5.06 ***	4.69 ***	4.50 ***	5.14 ***	2.41
Constant	43.4 ***	43.2 ***	41.9 ***	41.5 ***	42.7 ***	39.1 ***
n	230,957	3,412	779	119	54	33
Model R^2	0.20	0.32	0.33	0.47	0.49	0.34
Onroad/underwrite separate with weather variables						
Averaging time	1s	60s	300s	1,800s	3,600s	5,400s
PNC onroad	-0.00001 ***	-0.00007 ***	-0.00012 ***	-0.00013 *	-0.000017	0.00030
PNC under	-0.0006 ***	-0.00058 ***	-0.00046 ***	-0.00048 ***	-0.00055 ***	0.00021
BC onroad	0.16 ***	0.83 ***	1.33 ***	1.95	-1.06	3.07
BC under	4.39 ***	4.42 ***	4.06 ***	3.93 ***	4.17 ***	2.01
Temp	0.121 ***	0.111 ***	0.006	0.023	0.065	0.096
RH	0.093 ***	0.087 ***	0.049 **	0.054	0.095	0.110
Wind	-0.079 ***	-0.089 ***	0.008	-0.024	-0.095	0.262
Constant	33.4 ***	34.3 ***	39.8 **	38.5 ***	36.4 ***	10.1 ***
n	230,957	3,412	779	119	54	33
Model R^2	0.22	0.34	0.35	0.49	0.51	0.36

[a] *** denotes p-value <0.01; ** denotes p-value < 0.05; * denotes p-value < 0.10.

In general the models showed the expected direction of effect for both particle number (decreases particle size with increasing concentration) and black carbon (increases particle size with increasing concentration). Separating concentrations into a background and on-road component increased model R^2, especially at smaller time averaging intervals (i.e., 1 and 60 seconds), and the coefficients for particulate

concentrations were typically larger for the underwrite estimate (or background) component than the on-road component. This finding suggests that particle size is more correlated with background concentrations than small time-scale spikes in concentrations from local sources. A limitation of this analysis is that the NanoScan's smallest time resolution is 1-minute. Changes in particle size can occur rapidly (e.g., via coagulation, deposition, or evaporation) during dilution from the emission source; it is possible that the on-road component may become more significant in the regression models if instruments with faster scan times were available.

Adding weather-related variables to the model (i.e., temperature, relative humidity, wind speed) resulted in small improvements in model performance. In general, the direction and magnitude of the particle number and black carbon coefficients were similar in models with the weather variables as those without; this result suggests that relationships between particle size and the pollutant concentrations described here are robust to changes in weather-related parameters. Models for each category of independent variables improved with increased averaging time (Figure 3.9). The largest time interval (5,400 seconds) is not included in subsequent plots since R^2 decreased significantly for each model using that time interval. It is likely that the reduced sample size for the 5,400 second time interval (n=33) impacted the results of those models (e.g., since there are likely too many independent variables in those models for the number of observations).

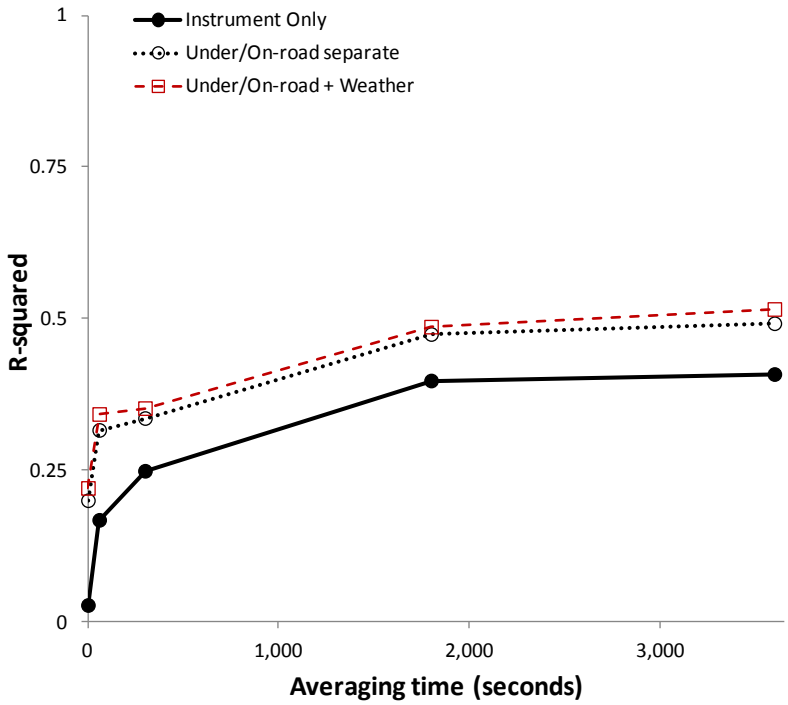

Figure 3.9 Model R^2 as a function of averaging time for regressions including 3 sets of independent variables.

As mentioned previously, model coefficients for the background concentration component were typically larger than for the on-road component. However, the magnitude of the model coefficients alone is not sufficient criteria to conclude that the background component truly is the most related to changes in particle size in these models. For example, another way to interpret these results is to multiply the model coefficient by some measure of the range of values used for that variable in the model. It could be possible that the range of values for the background concentrations was small and thus minimally affecting particle size despite the relatively larger coefficient for those variables; conversely the range of the on-road concentrations could be large making the relatively smaller model coefficient for on-road concentrations more important for particle size estimates. I calculated the product of the model coefficients and the

interquartile range (IQR) for each variable in the final model (model with weather variables) to explore how each variable is correlated with particle size. Results for each time average interval are shown in Figure 3.10.

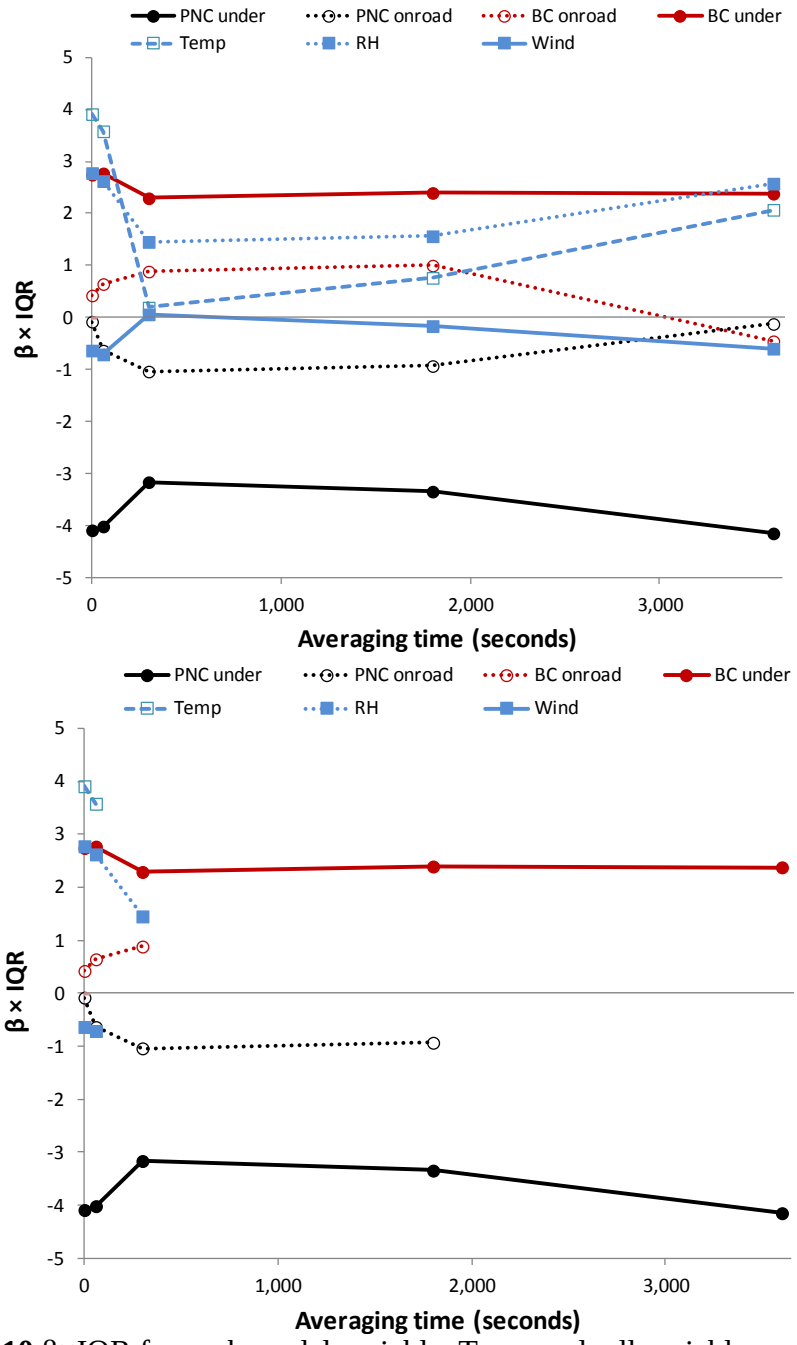

Figure 3.10 β×IQR for each model variable. Top panel: all variables and averaging times. Bottom panel: β coefficients are statistically significant in the model ($p < 0.1$).

In Figure 3.10 values that are farthest from zero (regardless of direction) have the strongest impact in the regression model. After controlling for the effect of the variable range (by multiplying the each variable's model coefficient and IQR) the background component variables are still the strongest variables in the regression models; on-road concentrations are relatively weaker. Temperature and relative humidity are correlated with particle size for smaller time intervals (i.e., 1 and 60 seconds) but are not statistically significant for larger time intervals. The background component variables were the only variables that were statistically significant for all averaging times highlighting the correlation these variables have with particle size.

The regressions described above used the instrument reported geometric mean particle size from the 1-minute scans as the dependent variable; another way to explore this relationship is to use an alternate dependent variable in the regression models: the difference between the instrument reported geometric mean particle size and the background particle size estimate (i.e., the moving median function referred to as an "underwrite" function above). Using the difference of the instrument-reported particle size from the estimated background particle size as the dependent variable essentially removes changes in particle size due to changes in overall background particulate concentrations. The regression models using the alternate dependent variable focus on exploration of any correlations owing to acute changes in on-road concentrations and particle size. Table 3.4 shows regression results using the alternate dependent variable; a 60 second time average interval was used to match the 1-minute particle size scans.

Table 3.4 Regression models using difference in geometric mean particle size from underwrite function as the dependent variable

Variable	Model coefficients		
	Model 1	Model 2	Model 3
PNC	-0.000073 ***	-	-
BC	0.499 ***	-	-
PNC onroad	-	-0.000082 ***	-0.000084 ***
PNC under	-	-0.000015	0.0000038
BC onroad	-	0.888 ***	0.871 ***
BC under	-	-0.288 *	-0.377 *
Temp	-	-	-0.038 **
RH	-	-	-0.012
Wind	-	-	0.009
Constant	1.64 ***	1.08 ***	3.73 ***
n	3,412	3,412	3,299
Model R^2	0.024	0.034	0.036

[a] *** denotes p-value <0.01; ** denotes p-value < 0.05; * denotes p-value < 0.10.

Model R^2 were low using the alternate dependent variable. One difference between the models is that the coefficient for the on-road component is larger in magnitude than for the background component. This finding is consistent with previous regression models in that it shows when background concentrations are controlled for (i.e., using the difference between instrument reported particle size and background estimate) that small time-scale spikes in on-road concentrations of particle number and black carbon concentrations contribute the most to changes in particle size. The small R^2 values indicate that this effect is likely small for particle size distribution scans of 1-minute.

I also performed regression analysis for a subset of the data that represents extreme spikes up or down in particle size. Using the difference between instrument-reported particle size and background estimates as a basis I pulled values below the 10th

percentile (extreme spikes down in size) and values above the 90th percentile (extreme spikes up in size). I then re-estimated regressions based on this subset of the data using both dependent variables (i.e., instrument-reported geometric mean particle size and the difference between particle size and background estimate). Again, I used 60 second time averages to directly compare to the 1-minute NanoScan scans. Overall, models performed poorly using the extreme spike subset of the data as compared to the full dataset. Model R^2 was lower when using the geometric mean particle size as the dependent variable; model R^2 was slightly higher using the difference from background as the dependent variable but many model coefficients did not follow the expected direction. Table 3.5 shows regression results for each model using the extreme spike subset of data.

Table 3.5 Regression results using a subset of the data for extreme spikes up and down in particle size

Variable	**Model coefficients**					
	Dependent variable: Geometric mean particle size			Dependent variable: Difference from underwrite		
	Model 1	Model 2	Model 3	Model 4	Model 5	Model 6
PNC	-0.00012 ***	-	-	-0.0015 ***	-	-
BC	1.54 ***	-	-	0.65 **	-	-
PNC onroad	-	-0.00011 ***	-0.00011 ***	-	-0.00017 ***	-0.0017 ***
PNC under	-	-0.00037 ***	-0.00041 ***	-	0.00031 **	0.00034 **
BC onroad	-	0.732 ***	0.686 ***	-	1.39 ***	1.4 ***
BC under	-	3.88 ***	3.99 ***	-	-2.32 ***	-1.32
Temp	-	-	0.057	-	-	-0.229 ***
RH	-	-	0.007	-	-	-0.186 ***
Wind	-	-	-0.089	-	-	0.024
Constant	43.8 ***	45.5 ***	42.9 ***	5.7 ***	2.7 **	23.8 ***
n	622	622	613	622	622	613
Model R^2	0.12	0.18	0.19	0.05	0.09	0.10

[a] *** denotes p-value <0.01; ** denotes p-value < 0.05; * denotes p-value < 0.10.

I performed a number of regression models to explore correlation of black carbon and particle number concentrations with particle size. The main finding from these regression models is that background concentrations (here estimated using the underwrite functions) seemed to be the most correlated with particle size. Evidence here suggests that background concentrations are more important to particle size than small time-scale spikes in other pollutants and that those findings are robust to weather parameters. A limitation is that the instrument used to estimate particle size had a minimum time resolution of 1 minute. At my average biking speed (~10 mph) this represents averaging measurements over approximately 270 meters. If instruments that measured particle size at a smaller time resolution were available it's possible that small time-scale spikes in particle number and black carbon concentrations could become more correlated with particle size.

Traffic mix, traffic volume, and changes in particulate concentrations

Description of video-based traffic counts at randomly selected locations

A total of 4.5 hours of video (5.3% of the total on-road sampling time) was collected by each of the two cameras (forward-, rear-facing). The video was collected during four sampling runs (2 morning [10/10/2014 & 10/15/2014] and 2 afternoon [10/10/2012 & 10/11/2014]). The battery life of the cameras did not allow for a full sampling run to be recorded; thus the each sampling run was partially recorded for each of the dates listed above.

I used the video to assess how traffic volume and vehicle type were correlated with the measured parameters of particulate matter. To do this I used a randomly selected

portion of the data with video footage to build regression models of particulate concentrations based on instantaneous traffic volumes for three types of vehicles: passenger vehicles, trucks, and buses. For this analysis, measurements that were candidates to be selected were restricted to those collected during on-street portions of the routes only (i.e., all measurements on off-street trails were removed from the dataset). Since there were not vehicles in close proximity to many of the off-street trail locations, those data were not candidates for random selection to assess the impact of vehicle types and volumes on particulate concentrations.

After removing the measurements on off-street trails there were 11,810 1-second measurements (i.e., measurement locations) available for selection with video footage; I randomly selected 118 of those measurement locations (approximately 1% of the available video data). For each of the randomly selected locations the corresponding video was assessed and a screenshot of the video at that timestamp was saved and archived. Then, vehicles were counted within those screenshots. Counts were tallied separately for passenger vehicles, trucks, and buses. To be counted vehicles must be moving (parked vehicles were not counted) and be located within one city block of the location of the bicycle at the randomly selected measurement location. The vehicle counts for each measurement location were then used for regression analysis.

The idea to use video cameras during the sampling runs was not in the original sampling plan. After many sampling runs it became apparent that it would be useful to have some information regarding the types and volumes of vehicles in close proximity to the sampling platform. As such, I only collected video footage towards the end of the

sampling campaign (i.e., for portions of the final 4 sampling runs). The video and vehicle counts described here were derived from a forward-facing camera on the handlebars of the bicycle. A rear-facing camera was also mounted on the bicycle trailer; however, data from that camera are not presented here due to 3 limitations: (1) the camera mount was prone to bending and thus the image during a significant amount of the sampling time did not capture vehicles behind the bicycle, (2) the memory capacity of the camera used was smaller than the forward-facing camera, causing gaps in video collection, (3) the resolution of the rear-facing camera was worse than the forward-facing camera which made it difficult to count vehicles in (semi-dark) morning hours. The sum of these limitations resulted in a much smaller amount of video available for use for the rear-facing camera. Since the subset of data available for this analysis was already small compared to the full dataset, I chose to limit my analysis of vehicle counts to the forward-facing camera only.

At some high traffic locations it was difficult to count vehicles from the instantaneous screenshot of the video alone due to various obstructions. For example, sometimes a bus in close proximity to the video camera blocked the view of the video in an adjacent lane at the timestamp of the randomly selected measurement location. For those locations an alternate approach was used to count vehicles. Namely, video footage for times near the randomly selected location timestamp (approximately ±10 seconds) were used to estimate the number of vehicles that would be in the screenshot had the view not been obstructed. For example, there were multiple locations where a bus pulled up adjacent to the bicycle in the neighboring lane blocking the view of the opposite

direction of traffic. In this case, video footage from near the measurement timestamp was used to count vehicles before the bus arrived in the shot. This approach potentially introduces some uncertainty to these estimates (i.e., it is impossible to know what is exactly behind the bus in the example above); however, this approach likely gives a better overall estimate of traffic levels in these high-traffic areas. Figure 3.11 shows an example of a screenshot at a low- and high- traffic location.

Table 3.6 shows summary statistics for vehicle counts at the 118 locations. Mean passenger-vehicle counts (4.8 vehicles) were the largest of the three categories of vehicles. Overall, trucks were only counted at a small amount of locations (n=7) resulting in a very small mean truck count (0.1). Buses averaged just under 1 bus per location (0.7); however, there were some locations with a relatively high number of buses counted (5 [1 location], 4 [2 locations], 3 [9 locations]). Passenger vehicles had the largest range of counts followed by buses and trucks. As expected, passenger vehicle counts were correlated with street functional class with the highest counts on arterials (7.1) followed by collectors (3.7) and local roads (1.2).

Figure 3.11 Examples of low vehicle count (top panel; Marshall Avenue and 5th Avenue NE) and high vehicle count (bottom panel; Lake Street & West River Parkway) locations.

Table 3.6 Summary statistics for the vehicle counts at the 118 randomly selected measurement locations

	Vehicle count			
	Passenger vehicle	Truck	Bus	Total
Total (n=118)				
Mean	4.8	0.1	0.7	5.6
Median	3	0	0	4
IQR	1-7	0-0	0-1	1-8
Arterial (n=59)				
Mean	7.1	0.1	0.8	8.0
Median	5	0	0	7
IQR	2-10	0-0	0-1	3-11
Collector (n=33)				
Mean	3.7	0.1	0.6	4.4
Median	3	0	0	4
IQR	1-5	0-0	0-1	2-6
Local (n=26)				
Mean	1.2	0	0.4	1.5
Median	0	0	0	1
IQR	0-2	0-0	0-0	0-3

The random selection of measurement locations was well distributed spatially among the potential selection locations (Figure 3.12). The candidate selection locations covered much of the total sampling routes; areas that were on sampling routes, but did not have video, included portions of routes in Northeast Minneapolis, near the University of Minnesota, and residential areas in South Minneapolis. Total vehicle counts demonstrated a spatial pattern consistent with expectations: counts were largest on arterial streets that are popular commuting routes and were generally elevated in the downtown area, and were lowest on local roads, several of which in this case are from the North Minneapolis route section.

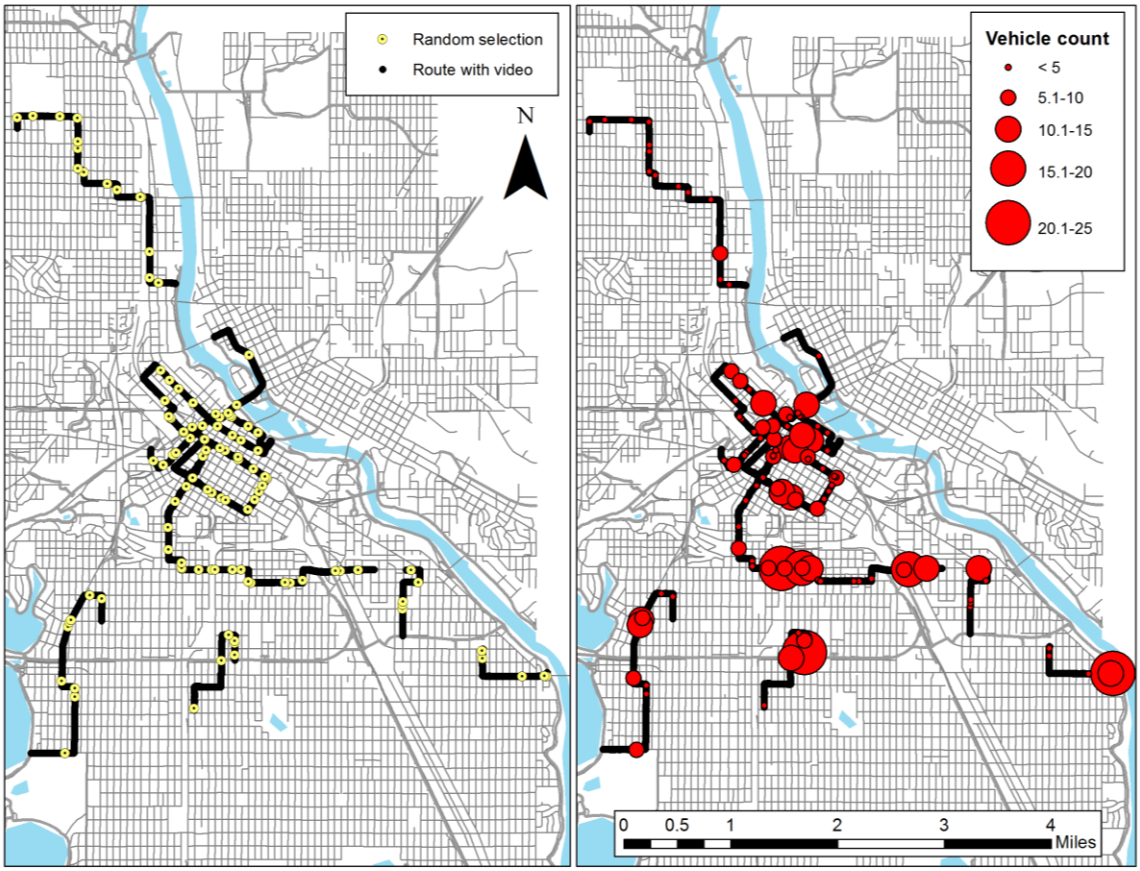

Figure 3.12 Randomly selected measurement locations for regression analysis (n=118). Left panel: Selected and candidate locations; right panel: Total vehicle count at locations.

Regression analysis of particulate concentrations and vehicle counts

Regressions were performed using the "on-road" (i.e., instrument-reported minus "background" [underwrite] estimates) pollutant concentrations and mean particle size as the dependent variables. Since measurements were pooled from mornings and afternoons (and among 3 different sampling days) I aimed to remove the effect of differences in background concentrations from this analysis. As a sensitivity analysis I tried using instrument-reported values as the dependent variables; results were similar for the traffic-

related pollutants (particle number and black carbon) but regressions performed poorly for particle size and $PM_{2.5}$. For those reasons, I report results for the on-road component of pollutant concentrations; as such the regressions presented below should be interpreted as models of the "local" or on-road component of the concentrations (see discussion of the φ parameter above). Since particle number and black carbon had higher φ values the models are explaining a larger proportion of the total concentrations for those pollutants than for $PM_{2.5}$.

Counts of each vehicle type (i.e., passenger vehicles, trucks, buses) were used as independent variables; alternate approaches for creating independent variables for the models were performed to test the impact of this choice on regression results: (1) combining buses and trucks into a single heavy-duty vehicle variable and (2) combining all vehicle types into a total vehicle count variable. Regression performance was similar regardless of the input variable specifications; for that reason I chose to use the disaggregate vehicle counts to assess the impact of each vehicle type on pollutant concentrations.

Since the vehicle counts collected here are instantaneous counts it is expected that smaller time averages (e.g., 1 to 60 seconds) of air pollution concentrations will perform better in regression analysis than longer time averages. To explore this relationship I ran regression models for various time averages (i.e., 1 to 1,800 seconds) for each pollutant as the dependent variable. I then explored both model performance and the impact of each independent variable by pollutant averaging time.

Table 3.7 shows regression results for each pollutant and averaging time (Figure 3.13 shows model R^2 for each pollutant as a function of averaging time). Results varied depending on the pollutant. In general, independent variables were statistically significant at smaller time averages and lost significance for larger time averages. As expected, coefficients for vehicle-counts are positive, i.e., more vehicles correlate with higher concentrations. For particle number concentrations, coefficients with the largest magnitude were for trucks (trucks were highly significant in each model); the magnitude of coefficients were moderate for buses and relatively small (and mostly insignificant) for passenger vehicles. Black carbon concentrations showed a similar relationship among independent variables with the largest magnitude coefficient for trucks (statistically significant in most models) followed by buses and then passenger vehicles. Regression results for $PM_{2.5}$ were again similar to particle number and black carbon; however, passenger vehicles were statistically significant in that model for smaller time averages. Results for particle size were weak and in the opposite direction as expected (i.e., increased particle size with traffic) which could be a result of the relatively larger time resolution of the NanoScan (i.e., quickest scan was 60 seconds); that time resolution may be too large to capture the instantaneous impact of a specific, short-duration traffic event such as vehicles overtaking the cyclist or passing over a high traffic road (e.g., overpass over a freeway).

Table 3.7 Regression results[a] for the randomly selected measurement locations with video derived vehicle counts

Particle number						
Averaging time	1s	10s	30s	60s	300s	1,800s
Passenger vehicle	317 *	304	243	420	-144	-264 **
Truck	16,726 ***	19,927 ***	30,607 ***	27,340 ***	16,244 ***	5,062 **
Bus	2,254 **	2,378 **	2,284 *	2,234 *	1,323	-287
Constant	5,026 ***	5,753 ***	7,520 ***	7,799 ***	11,526 ***	12,202 ***
n	118	118	118	118	118	118
R^2	0.25	0.27	0.27	0.25	0.17	0.09
$PM_{2.5}$						
Averaging time	1s	10s	30s	60s	300s	1,800s
Passenger vehicle	0.05	0.06 **	0.06 ***	0.04 **	0.01	0.00
Truck	0.29	0.48	0.99 **	0.59 *	0.22	0.07
Bus	0.35 *	0.28 *	0.21 *	0.21 **	0.15 **	0.06
Constant	1.35 ***	1.19 ***	1.19 ***	1.30 ***	1.40 ***	1.43 ***
n	118	118	118	118	118	118
R^2	0.04	0.07	0.14	0.10	0.07	0.02
Particle size						
Averaging time	1s	10s	30s	60s	300s	1,800s
Passenger vehicle	-	-	-	0.31 **	0.18 ***	0.05 *
Truck	-	-	-	8.13 ***	-1.94	-0.59
Bus	-	-	-	-0.28	0.17	0.07
Constant	-	-	-	-0.01	1.03 *	0.98 ***
n	-	-	-	118	118	118
R^2	-	-	-	0.13	0.08	0.04
Black carbon						
Averaging time	1s	10s	30s	60s	300s	1,800s
Passenger vehicle	0.03	0.02	0.02	0.01	-0.01	-0.01
Truck	1.62 *	2.48 ***	1.57 ***	0.99 ***	0.41 *	0.21
Bus	0.36	0.41 **	0.26 ***	0.25 ***	0.11 *	0.04
Constant	0.55	0.62 **	0.62 ***	0.69 ***	0.71 ***	0.67 ***
n	116	114	108	101	115	118
R^2	0.05	0.17	0.23	0.19	0.08	0.05

[a] *** denotes p-value <0.01; ** denotes p-value < 0.05; * denotes p-value < 0.10.

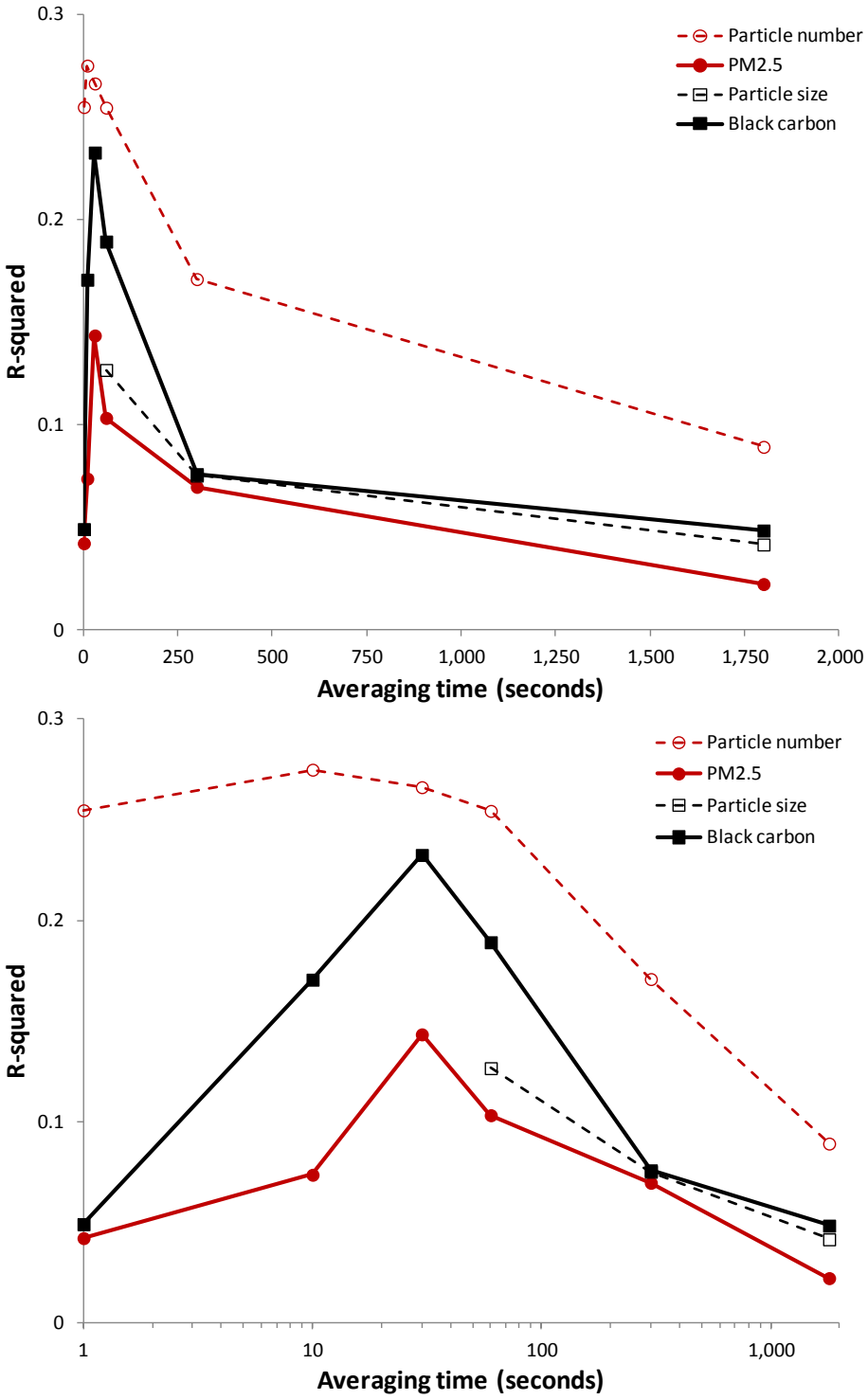

Figure 3.13 R^2 as a funcion of averaging time (top: normal scale; bottom: log scale).

Figure 3.13 shows model R^2 for each pollutant and averaging time. As expected model performance was best for the smaller time averages: Particle number (10 seconds), $PM_{2.5}$ (30 seconds), particle size (60 seconds [minimum time available]), and black carbon (30 seconds). For averaging times larger than 60 seconds, model R^2 dropped rapidly. In all cases, small time averages (e.g., 10-30 seconds) performed better than 1-second measurements. This result is likely because the instantaneous air pollution measurement (associated with the video-based vehicle counts) may or may not include the time when most of the vehicles in the video image are passing the sampling platform (e.g., the bicycle may pass through the micro-plumes of the vehicles in the image 10-30 seconds before or after the image was recorded). For this reason it seems appropriate to use slight temporal smoothing of the data (e.g., 30-second average) in this analysis to capture dynamics of traffic.

To better assess the impact of each independent variable on the regression models I multiplied the model coefficient by the difference between the variable 95^{th} and 5^{th} percentile for each pollutant and averaging time. Since truck counts were infrequent it was necessary to use the difference between the 95^{th} and 5^{th} percentile rather than a smaller range (e.g., interquartile range) to include all independent variables in this analysis. (The truck counts IQR is 0; see Table 3.6.) Figure 3.14 shows plots of this parameter ($\beta \times 5^{th}/95^{th}$ percentile difference) as a function of averaging time. Averaging times of 1, 10, 30, 60, and 300 seconds are shown; for longer averaging times (1,800s) model performance was poor (see Table 3.7).

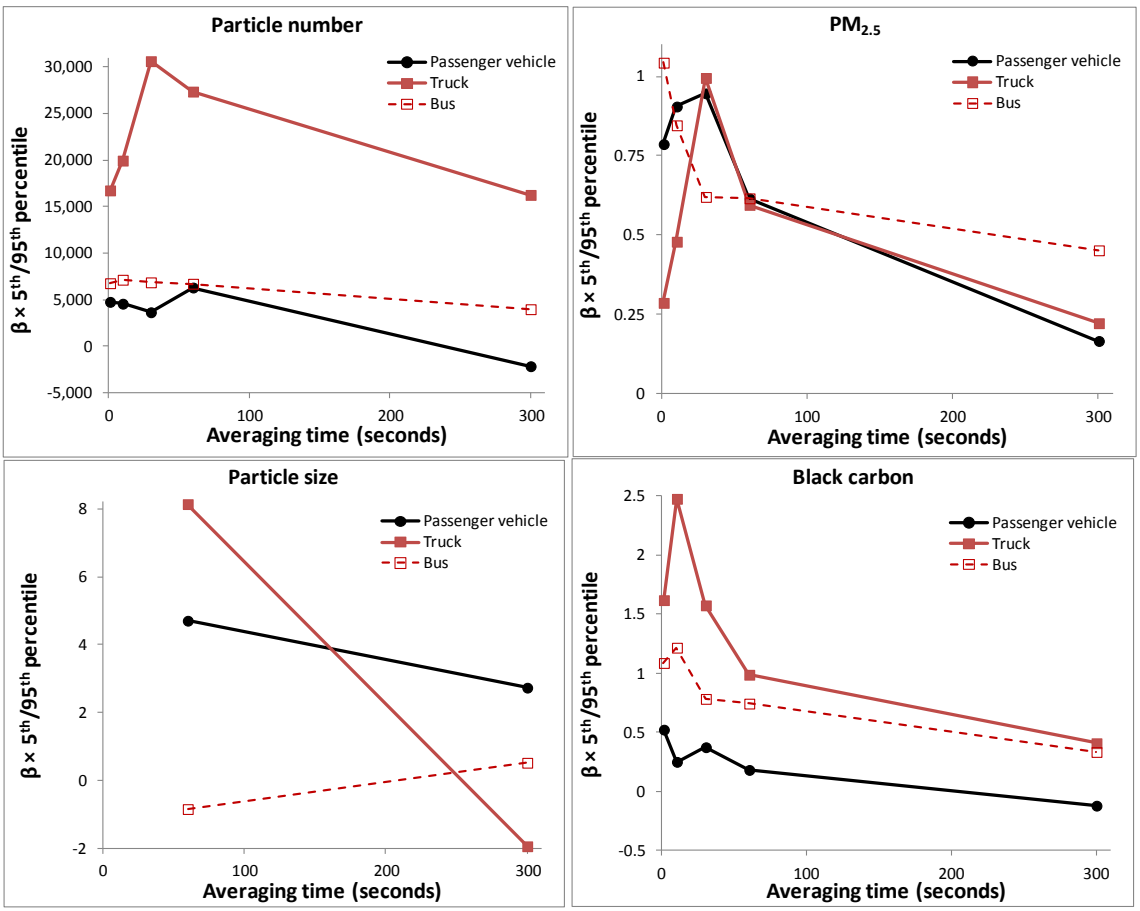

Figure 3.14 Impact of variables in regression models shown as the product of the model β and the difference between the 95th and 5th percentile for each variable. Each panel shows results for separate pollutants.

Several interesting results are shown in Figure 3.14. First, trucks (although infrequent) seem to have a large impact on particle number and black carbon concentrations. Trucks were the most important variable in the models for those pollutants for all averaging times. In both the particle number and black carbon models, buses had the second highest impact with passenger vehicles having the smallest impact. For $PM_{2.5}$ concentrations all vehicle types had a similar influence in the regression;

results for particle size are difficult to interpret since averaging times smaller than 60 seconds were not available.

One additional approach to compare model results among pollutants is to fully normalize the coefficients in the regression models. The model βs have units of dependent variable over independent variable (i.e., concentration/vehicle count). In order to compare among models I multiplied each β by this factor: difference between 95th and 5th percentile vehicle counts / difference between 95th and 5th percentile concentration. I performed this normalization for the 30 second time average regression model since those models performed best (particle size is not included since data was not available for that time resolution). Results are presented in Table 3.8.

Table 3.8 Fully normalized β for the 30 second time average regression models

	Model β	**95th/5th Independent variable**	**95th/5th Dependent variable**	**Fully normalized β**
Particle number				
Passenger	243	15	50,848	0.07
Truck	30,607	1	50,848	0.60
Bus	2,284	3	50,848	0.13
$PM_{2.5}$				
Passenger	0.06	15	4.13	0.23
Truck	0.99	1	4.13	0.24
Bus	0.21	3	4.13	0.15
Black carbon				
Passenger	0.02	15	3.79	0.10
Truck	1.57	1	3.79	0.42
Bus	0.26	3	3.79	0.21

Results from these regression analyses suggest that trucks (and to a lesser degree buses) are likely associated with acute exposure to highly elevated concentrations of traffic-related pollutants (i.e., particle number and black carbon concentrations), despite trucks being infrequent on the roads. The fully normalized βs are 8.5 (particle number)

and 4.2 (black carbon) times higher for trucks than for passenger vehicles; normalized βs for buses are 1.9 (particle number) and 2.1 (black carbon) times higher than for passenger vehicles. It is possible that the results presented here could be confounded by other factors. For example, it could be that the likelihood of passing a truck on a street is correlated with passing through an industrial area of the city; in that case, this variable (likelihood of seeing a truck) would be capturing both emissions from the trucks as well as surrounding (industry-related) emission sources. Similarly, it could also be that the liklihood of passing a truck is correlated with higher vehicle volumes (bus and passenger vehicles) in general. Despite these possiblities, larger vehicles (e.g., buses and trucks) are heavier emitters than smaller passenger vehicles and are certainly responsible for at least a portion of the eleveated concentrations.

To test whether I passed trucks more often in high traffic areas or industrial areas I divided the randomly selcted measuremets into two groups: locations with and without trucks. I then calculated the industrial area within a 50 meter buffer of each location. Table 3.9 shows mean industrial area, passenger vehicle counts, and bus counts for each location type (i.e., with and without trucks). There was no statistically significant difference in vehicle traffic between location types; however, truck traffic was more likely to be located in industrial areas according to this dataset.

Table 3.9 Comparison of locations with and without trucks present in video

	Trucks	**No trucks**	**t-test (p-value)**
Number of locations	7	111	-
Mean (IQR) industrial area within 50m (m^2)	1,641 (0-2,770)	326 (0-0)	<0.01
Mean (IQR) passenger vehicle count	5 (2-9)	4.8 (1-7)	0.94
Mean (IQR) bus count	1.1 (0-2)	0.6 (0-1)	0.22

Chapter conclusions

Results in this chapter focused on the interaction between different measures of particulate air pollution, how street design is correlated with concentrations, and how traffic dynamics influence on-road particulate concentrations. I also applied methods for adjusting mobile measurements for background concentrations and averaging times. Main findings from this chapter include the following:

Methodological findings

1. Underwrite functions better describe non-linear changes in background concentrations than linear interpolation of reference site measurements.
2. Developing time-series data sets that are adjusted for background concentrations allows for better analysis of spatial patterns of concentrations.
3. Exploring various averaging times of time-series data allows for insight into whether background or regional trends (e.g., correlation of particle size with black carbon and particle number) or small time scale (e.g., instantaneous vehicle counts) events better explain concentrations.

Empirical findings

1. Based on values for the φ parameter, near-traffic emissions were responsible for on average ~50% of the on-road concentrations for particle number and black carbon (~26% for $PM_{2.5}$).
2. Concentrations of traffic-related pollutants (i.e., black carbon and particle number) were associated with attributes of streets such as functional class and distance from a major road.

3. Geometric mean particle size was modestly correlated with particle number (decreased particle size) and black carbon (increased particle size) concentrations; correlations were strongest for background concentrations.
4. Traffic-related pollutants (i.e., black carbon and particle number) were most correlated with each other among the pollution parameters I measured. All correlations increased with increasing averaging time.
5. Counts of vehicles from video footage were associated with short time-scale spikes in particulate concentrations. Trucks, and to a lesser extent buses, had the largest impact. Trucks were associated with being in an industrial area.

Chapter 4 Land use regression models for concentrations of particle number, black carbon, $PM_{2.5}$ and particle size

A core goal of my dissertation is to use mobile measurements of particulate air pollution to develop land use regression (LUR) models to estimate concentrations at locations across Minneapolis without measurements. Few studies offer precedent on how best to aggregate and model mobile measurements using LUR (Lightowlers et al., 2008). My approach is based on aggregating measurements at equal interval distances along the sampling routes. Then, I use estimates of concentrations from pooled data at each aggregation location to build LUR models for each pollutant. I aimed to select one base-case model for each pollutant and time of day (i.e., morning and afternoon rush-hour) to extrapolate estimates to all street segments in Minneapolis; I explored varying three key model building parameters to inform my choice of final models:

1. Distance between aggregation locations. I aggregated counts at varying distances (i.e., 200m, 100m, 50m) along the sampling routes to test how the choice of spatial resolution impacts model performance. I describe tradeoffs between spatial resolution and measurement sample size at each aggregation location resultant from this choice.
2. Modeling different characteristics of the measurement distributions at aggregation locations. My goal is to develop models for "typical" on-road exposure concentrations in Minneapolis during morning and afternoon rush-hours; as such, my core models use estimates of central tendencies (i.e., mean and median) of the

measurement distributions at each aggregation location. I also explored modeling other parameters of the distributions which could be used to describe spatial patterns of "acute" (i.e., 75^{th} and 90^{th} percentiles) and "baseline" (i.e., 10^{th} and 25^{th} percentile) exposure concentrations.

3. Temporal smoothing of mobile measurement time series data. I also checked for differences in LUR model performance using various averaging times for the time-series particulate concentration measurements (i.e., 1s, 10s, 30s, 60s, 300s) and discuss how temporal smoothing of mobile measurements may also dampen spatial variability.

This chapter describes my approach to build LUR models from mobile measurements including: (1) method of measurement aggregation, (1) assembly of independent variables, (3) model building protocol, and (4) model validation. I performed a series of sensitivity analyses to explore how the three parameters listed above impact model performance. In total, I developed 1,224 separate LUR models (see description of model building below); I explored trends in model performance by spatial resolution, aggregation location measurement distribution characteristics, and pollutant averaging time. Then, I discuss choosing base-case models for "typical" exposure concentrations for all four pollutants (particle number, black carbon, $PM_{2.5}$, particle size) and for each time of day (morning and afternoon rush-hour) to compare to models of bicycle and pedestrian traffic volumes (Chapter 5). Lastly, I describe a set of validation exercises used to assess the base-case model performance.

Spatial aggregation of mobile measurements

A key decision when using mobile measurements for LUR is how best to aggregate data both spatially and across sampling days. My approach involves aggregating measurements at specific, equal interval points along the sampling routes. I used the mobile measurement dataset adjusted for background concentrations using underwrite functions (as described in Chapter 3) to control for day-to-day differences in background concentrations. I relaxed the requirement for a 180s averaging time for the black carbon underwrite function (see discussion of developing underwrite functions in Chapter 3); instead I used a 60s time average to develop an underwrite function to apply to the relatively smaller time averages (1-300s) used for model building. I then created 3 versions of aggregation locations to summarize the mobile measurements for model inputs; the only difference between each version of aggregation was the distance between each location along the route (200m, 100m, 50m). These distances represent spatial resolutions that are >1 city block (200m), ~1 block (100m), and <1 block (50m). Since my estimates of bicycle and pedestrian traffic volumes are for each city block (see Chapter 5) I chose to use the 100m aggregation approach as my base-case; I then use the other two distances as a sensitivity analysis.

As the distance between each aggregation location decreases, the spatial resolution of the aggregate air pollution concentration estimate increases; however, the concentration estimate is also based on fewer data points (e.g., aggregating at 50m includes fewer mobile measurements per aggregation location than at 200m) and so might yield less-robust models. As such, it may not be possible to accurately describe all

characteristics of the distribution at each aggregation location (e.g., 10th and 90th percentiles). Figure 4.1 shows a ~6 block portion of the sampling routes with the mobile measurements colored by aggregation location for each spatial resolution (this example is for the morning sampling runs). The 200m spatial resolution corresponds with aggregating mobile measurements over approximately 2 blocks; aggregation at a 100m distance covers about 1 block. Using 50m as an aggregating distance results in multiple aggregation locations per block.

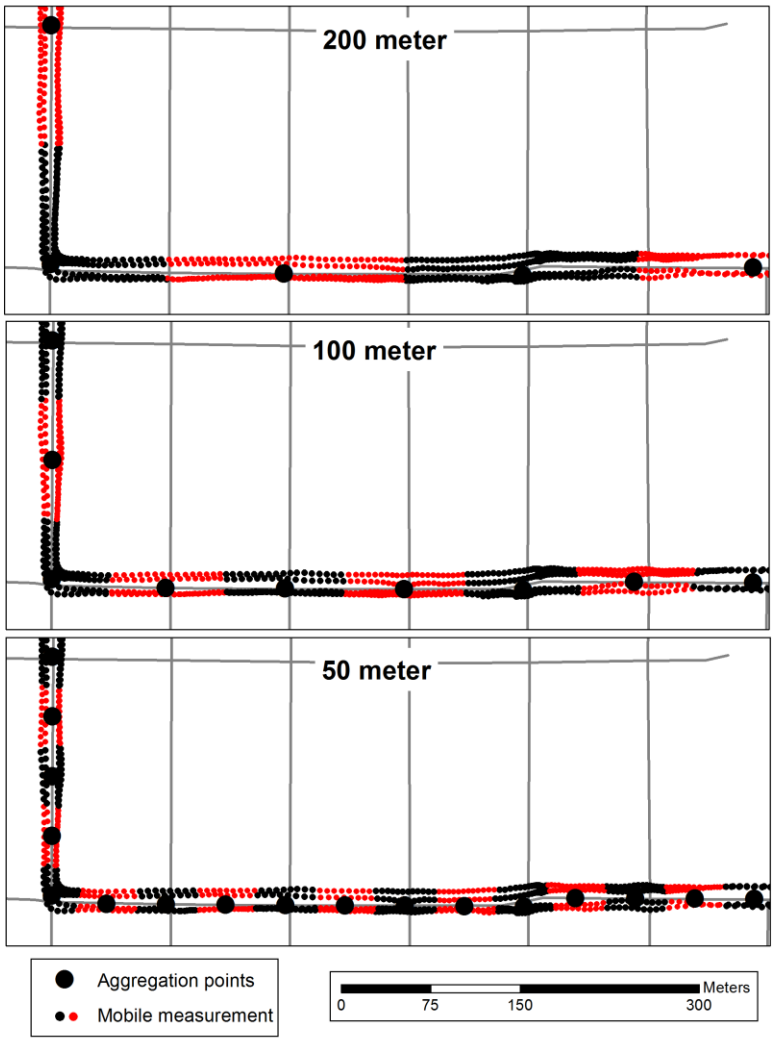

Figure 4.1 Example of aggregating mobile measurements at varying spatial resolutions for the morning sampling runs.

Reducing the distance between aggregation locations also minimizes the frequency with which measurements are aggregated across multiple blocks near intersections. For example, in Figure 4.1, where the sampling route turns from an east-west alignment to a north-south alignment there is potential for averaging across different types of traffic environments (i.e., the north-south street is a busy arterial; the east-west street is a local road). For the 200m case measurements are combined from ~1/2 of the high-traffic (north-south) block and the entire low-traffic (east-west) block. Aggregating across different blocks could become problematic when the streets are of different functional classification, for example, arterial (high-traffic) vs. local (low-traffic) streets or otherwise differ in traffic dynamics. This effect is diminished as the spatial resolution increases (and distance between aggregation locations decreases).

Figures 4.2 and 4.3 show box plots of the number of measurements assigned to aggregation locations for each of the 3 spatial resolutions (200m, 100m, 50m). In general, the number of mobile measurements per aggregation location is lower in the morning than in the afternoon (since more sampling runs were conducted during afternoon [n=30] than morning [n=12] rush-hour). Some aggregation locations had sample sizes that may be too small to characterize high- and low- ends of the distribution (i.e., for the high spatial resolution cases). For example, for the morning sampling runs and 50m spatial resolution median measurements per aggregation location were 36; the 10^{th} percentile was 18 measurements per aggregation location. Those sample sizes represent a small number of measurements to specify parameters of the distribution other than central tendencies; this suggests that using the 100m or 200m aggregating approach may be

necessary to model distributional parameters such as the 10th and 90th percentile concentrations at each aggregation location. As shown in Figures 4.2 and 4.3, some aggregation locations have relatively large numbers of measurements (for each of the spatial resolutions); those locations were typically near the beginning and end of the sampling routes where all 3 routes converged along the same street or trail.

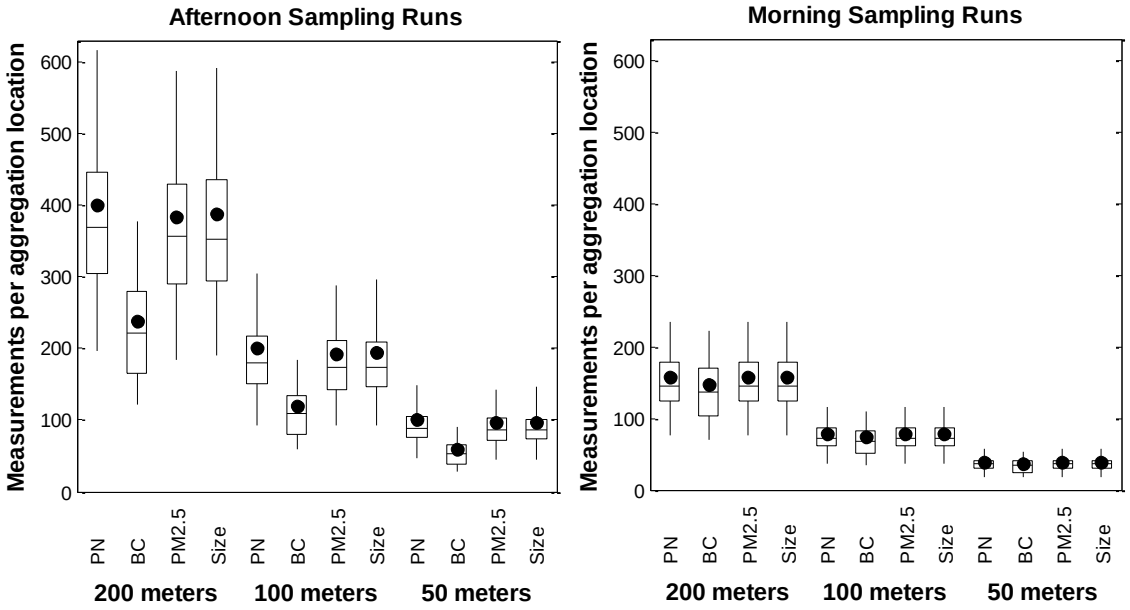

Figure 4.2 Number of air pollution measurements per aggregation location for each of the aggregation resolutions, each pollutant, and morning vs. afternoons.

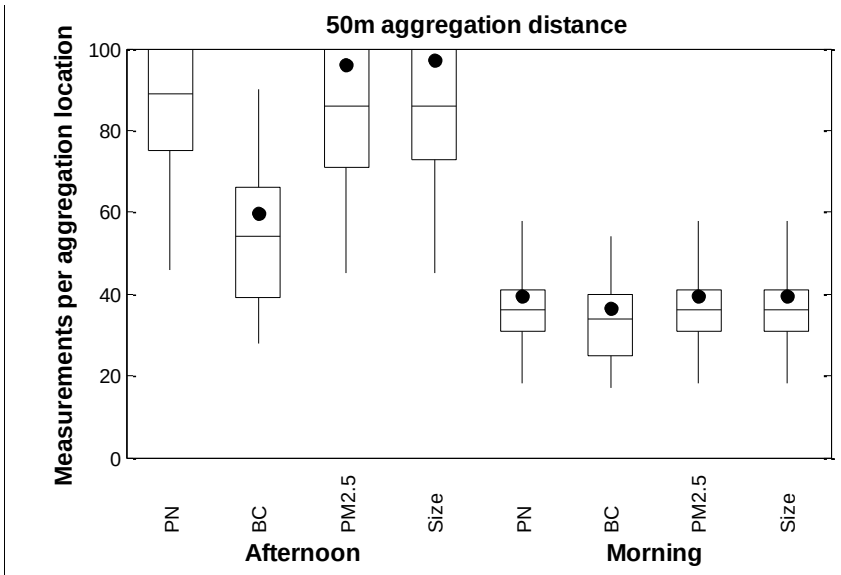

Figure 4.3 Zoomed in boxplot with the 50m aggregation locations (smallest number of measurements per location.

Another issue that arose when aggregating data at various spatial resolutions was misclassification of measurements across blocks. For example, typical block lengths in Minneapolis are 100-200m; when performing the 200m based aggregation some mobile measurements were classified as being on the wrong block. As the aggregating distance decreased (i.e., as spatial resolution increased) this problem was diminished. Figure 4.3 shows an example of this effect for a location where a sampling route ran along a street and off-street trail in close proximity. For the 200m aggregation there is significant misclassification between the street and trail. For the 100m aggregation there is a small amount of misclassification and nearly zero misclassification for the 50m aggregation.

The proximity of the two portions of the sampling route illustrated in Figure 4.4 is not typical across the sampling routes as a whole. Thus, the example in Figure 4.4 represents a strict criterion for designing the aggregation protocol. This issue was mostly resolved using the 100m aggregation; the minor misclassification shown in Figure 4.4 at

that distance only occurred in a few locations (~7 aggregation locations). One potential solution to this issue would be to record the distance traveled along each route and only allow points to be aggregated that are similar distances; since there was a small number of locations where misclassification occurred I did not further refine the aggregation approach.

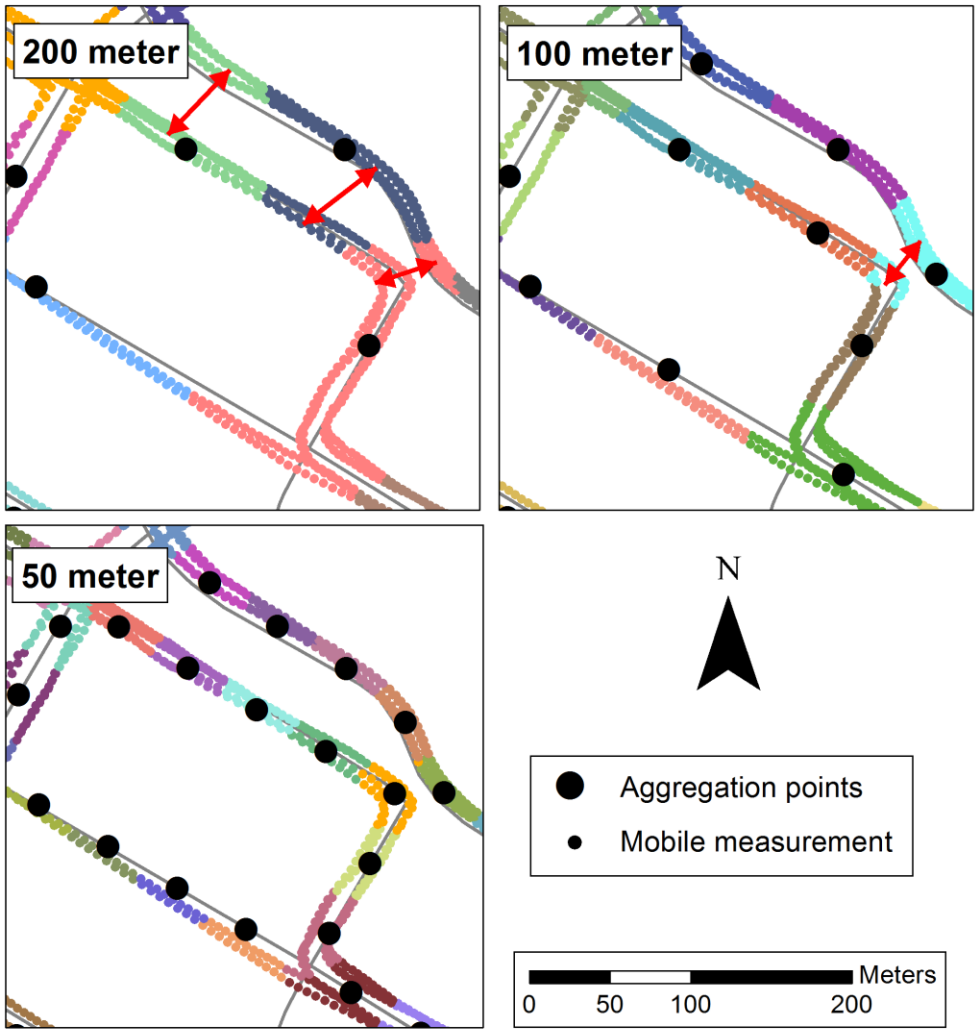

Figure 4.4 Maps showing mobile measurements aggregated at different spatial resolutions in a location where misclassification occurred. Misclassification was reduced as the aggregation distance decreased.

Description of land use regression model dependent variables

I varied a number of parameters associated with the dependent variable in the LUR models (i.e., pollutant concentrations) to aid in choosing base-case models for extrapolating estimates of particulate concentrations to the entire City of Minneapolis. The parameters used to specify the dependent variable in the LUR models are listed in Table 4.1. I focused on primarily 3 factors when selecting core models: (1) type of pollutant, (2) time of day (i.e., morning and afternoon rush-hour), and (3) measure of central tendency of the measurements at each aggregation location. Models varying other parameters were used to test the sensitivity of the core models to other choices such as averaging time, spatial resolution, and modeling aspects other than central tendencies. Results for 612 separate LUR models are reported in this chapter (i.e., 4 pollutants × 2 times of day × 6 distributional concentration estimates × 5 averaging times × 3 spatial resolutions = 720 potential LUR models; since fewer averaging times (n=2) were available for the NanoScan the total number of actual LUR models was 612).

Table 4.1 Parameters used to generate various iterations of LUR models

Parameter	**Values for core model**	**Values for sensitivity analysis**
Pollutant	Particle number, black carbon, $PM_{2.5}$, particle size	(same)
Time of day	Morning, afternoon	(same)
Statistical summary of concentrations measured at each aggregation location	Mean, median	P10, P25, P75, P90
Averaging time	Lowest time average with sufficient model performance	1s, 10s, 30s, 60s, 300s
Spatial resolution	100 meters	50 meters, 200 meters
Are concentrations (dependent variable) log-transformed?	Yes	No

Input pollutant concentrations mostly did not follow a normal distribution. I inspected histograms and Q-Q plots for both the normal and log-transformed dataset for each pollutant. I found that the concentration estimates more closely represented a log-normal distribution. As such, the results presented in this chapter all used the log-transformed concentrations as the dependent variable in LUR models. To ensure the appropriateness of this choice I re-ran all 612 LUR models using the untransformed dataset to compare to model results using the log-transformed dataset. Overall, model performance was consistently improved using the log-transformed dataset and thus those results are presented here. In total, this resulted in the previously reported 1,224 separate LUR models.

I designed my analysis to choose 8 final models (one for each pollutant and time of day) for extrapolation to all locations in Minneapolis. Candidate independent variables were the same for all models; thus, differences in models are based on how the pollutant concentrations were processed and used as dependent variables in the models. I varied the supplementary parameters described above (i.e., averaging time, concentration estimates at aggregation locations, and spatial resolution) to choose which models would be most appropriate for final selection. Much of the text in this chapter describes observed trends in model performance when varying these parameters. Final model selection was based both on model performance and ensuring concentration estimates would be appropriate for comparison to the estimates of bicycle and pedestrian traffic described in Chapter 5.

Varying the spatial resolution of the aggregation locations and the averaging time of the mobile measurements represents smoothing the data in both space and time. In

general, smoothing the data should improve model performance metrics (such as R^2) but may or may not be appropriate depending on the context. For example, if exposure concentrations change on small time scales (i.e., seconds) it may not be appropriate to use large averaging times or aggregation distances. Furthermore, these two types of smoothing are not mutually exclusive; for example, applying an averaging time to the time-series data is not only smoothing the data temporally but also spatially since the measurements were collected using a mobile method. I strived to vary these parameters and observe trends in model performance to inform my choice of final models.

Description of land use regression model independent variables

I assembled data in four main categories as candidate independent variables in the LUR models: (1) traffic, (2) land use, (3) population dynamics, and (4) physical geography. Variables were either point estimates at a specific spatial location or (more commonly) based on radial buffers around a measurement location. Buffer variables are calculated as some measure (e.g., length of road or area of a certain land use) within a specific distance around a measurement location. I calculated buffer variables at various lengths since the scale at which each variable may impact the model could differ. Table 4.2 lists variables included as candidates for selection in the models; in total I included 14 buffer variables (at 15 buffer lengths) and 5 point variables resulting in a total of 215 variables available for selection in each model.

Table 4.2 Independent variables included in model building

Variable	Unit	Buffer/ Point	Data Source
Traffic			
Length of all roads	Meters	Buffer	Metropolitan Council
Length of freeways	Meters	Buffer	Metropolitan Council
Length of major roads	Meters	Buffer	Metropolitan Council
Length of local roads	Meters	Buffer	Metropolitan Council
Count of intersections	Number	Buffer	Calculated from road network file
Length of bus routes	Meters	Buffer	Metropolitan Council
Count of bus stops	Number	Buffer	Metropolitan Council
Traffic intensity	AADT m^{-2}	Point	Minnesota Pollution Control Agency
Distance to freeway	Meters	Point	Calculated from road network file
Distance to major road	Meters	Point	Calculated from road network file
Land use			
Industrial land use area	Square meters	Buffer	Metropolitan Council
Retail land use area	Square meters	Buffer	Metropolitan Council
Railway land use area	Square meters	Buffer	Metropolitan Council
Open space land use area[a]	Square meters	Buffer	Metropolitan Council
Population			
Population density	People km^{-2}	Buffer	NHGIS
Housing unit density	House km^{-2}	Buffer	NHGIS
Median HH income	USD	Buffer	NHGIS
Physical geography			
Elevation	Meters	Point	USGS
Slope	Grade (%)	Point	Calculated from elevation file
Buffers (m): 25, 50, 75, 100, 150, 200, 250, 300, 400, 500, 750, 1000, 1500, 2000, 3000, 5000			

[a] Includes: parks, water, golf courses, and cemeteries.

Since a significant emission source of particulate air pollution is motor vehicle traffic the largest category of independent variables were traffic-related. The lengths of road from various street functional classes were calculated as buffer variables. Length of freeways, major roads (i.e., arterials and collectors), and local roads were calculated separately in addition to the length of all roads. Distance to the nearest freeway and major road were also included as point estimates. Intersection counts within a buffer were

included as a proxy for the potential of increased motor vehicle acceleration (and increased road density in general). A traffic intensity raster created by the Minnesota Pollution Control Agency gave point estimates of traffic density derived from available information on motor vehicle annual average daily traffic on the road network. Characteristics of the bus network including length of bus route and number of bus stops within buffers were also included.

The areas of four types of land use were calculated within each buffer. Industrial area was included both as a potential emission source as well as a proxy for increased truck traffic (see regression models of vehicle counts and concentrations in Chapter 3). Retail area was included since locations with high retail area likely have increased vehicle traffic activity and are typically located along high-traffic transportation corridors. Railway area included both tracks and railyards and is assumed to be a source of significant diesel emissions (both from the trains and the equipment used to load/unload cargo). Open space area included all parks, water, golf courses, and cemeteries (there were 4 large cemeteries in Minneapolis that were coded in separately). Open space area was included as a variable where there are likely no emissions, and thus unlike the other land use variables a negative coefficient is expected in the LUR models.

Population and housing density were included as an indicator of the density of activities by residents; presumably, as more people live in a given area the density of trips in that area increases. Median household income was also included since lower income populations often are located in areas near emission sources. Income may also be a proxy for the types of vehicles in those neighborhoods (i.e., lower income neighborhoods may

have, on average, older and higher emission vehicles). Lastly, elevation and slope were also included as point variables; elevation is a variable that has been significant in a number of previous LUR models and steep slopes may indicate areas where vehicles need to accelerate more than average.

The LUR models reported here are unique in multiple ways. My study area (the City of Minneapolis) is smaller in geographic scope than many LURs (usually for an entire urban area). Furthermore, aggregating the mobile measurements at the spatial resolutions described above resulted in a large number of measurement locations used for modeling (i.e., n=550 – 2,202) compared to previous LUR models (n~50 – 100). The geographic scale of my study area and resolution of my concentration estimates allowed for two notable differences in how I assembled independent variables. First, I included buffer sizes (25-100 meters) that are smaller than is typical for previous LUR models. The relatively smaller buffer sizes allowed for investigation of small-scale changes in land use that may impact on-road concentrations such as being in close proximity to an intersection or bus stop. Second, since my study area is for only one municipality I was able to assemble GIS data that has more detail than is typically available at larger scales (e.g., regional or national level models). For example, I was able to use better information on street classification (freeway, arterial, collector, local) than is available from state or national databases (federal, state, municipal roads).

I calculated all buffer variables using a freely available set of tools for ArcGIS developed by Dr. Yasuyuki Akita at the University of North Carolina-Chapel Hill (http://www.unc.edu/~akita/lurtools/). The tools are available for download on the ESRI

website as an ArcGIS toolbox. A key limitation of the standard tools for ArcGIS used to calculate buffer variables is that they do not allow for calculation of statistics within overlapping buffers. Dr. Akita developed tools for ArcGIS that are designed specifically for LUR modeling and do not have this issue. Since I calculated buffer variables at many locations (n=550 – 2,202) significant processing time was necessary to complete the buffer calculations (e.g., 1 variable at 15 buffers took ~15 hours for each iteration of the spatial aggregation); the ArcGIS LUR toolbox developed by Dr. Akita helped by automating this process.

Description of land use regression model building approach

I followed the stepwise regression technique developed by Su et al. (2009) to build LUR models. Namely, all 215 potential independent variables are checked for strength of correlation with the dependent variable (pollutant concentrations); then, the independent variable most correlated with the dependent variable is added to the model. The regression is performed on the included variable and the remaining candidate variables are then tested for correlation with the model residuals; again, the most correlated variable is added to the model. This process repeats until the last added variable is either not significant in the model (i.e., $p>0.05$) or has a Variance Inflation Factor (VIF; a check for multicollinearity with other independent variables) of greater than 5. If a variable was selected at one buffer length I allowed the model to again select that variable at another buffer length (as long as the same criteria for inclusion in the model were satisfied).

VIF is a check for multicollinearity among the independent variables in an ordinary least squares regression. Multicollinearity is when two or more independent variables in a linear regression model are highly correlated. Although multicollinearity may not reduce the prediction power of the model within the range of the sample data, it can lead to overfitting of the model itself as well as make interpretation of each variable coefficient in the model difficult. A robust regression model has independent variables that correlate well with the dependent variable but are not correlated amongst themselves. VIF is used in my models as a check and filter for multicollinearity; the threshold value of 5 has been used in previous LUR models (e.g., Novotny et al., 2011).

LUR models represent a hybrid of theoretical and empirical approaches. The independent variables included in the model all have a theoretical a priori impact on particulate air pollution concentrations; for example, more high traffic roads or bus routes in close proximity to the measurement locations should theoretically be correlated with increased concentrations. However, the stepwise regression approach (coupled with the numerous buffer sizes) employed in my models represents an empirical approach that may give results that do not follow theoretical hypotheses. For example, I included area of open space as a variable. Theoretically, more open space would decrease concentrations, since most open space areas generally have fewer emissions than, for example, the surrounding roads. However, in some of the regression models (see below for full description) this variable gave contradictory results (i.e., a negative coefficient at small buffer lengths and a positive coefficient at large buffer lengths). There could be many reasons for this outcome; one reason is that for many locations in Minneapolis, off-

street trails through parks are located adjacent to other emission sources like freeways or industrial areas. It is possible that area of open space at certain buffer lengths correlates with those emission source more than other candidate variables. This hybrid approach results in models that likely suffer from similar limitations as other LUR models such as potential lack of transferability between geographic areas and thus should be interpreted from a theoretical perspective with caution.

Land use regression model results

As described earlier, my goal was to select 8 LUR models (4 pollutants; 2 times of day) to estimate concentrations for every street segment in Minneapolis. I varied other parameters (i.e., averaging time, measure of distribution at each aggregation location, spatial resolution of measurement aggregation) to inform my choice of base-case models. Since a large number of LUR models were evaluated, I focused on evaluating trends from varying these parameters when choosing final models; this section focuses on trends in model performance when temporal and spatial smoothing is applied to the mobile measurement data. Since I found that my dependent variables (i.e., the aggregated pollutant measurements) were log-normally distributed, I log-transformed the air pollution measurements as a model input; model performance statistics such as error and bias were transformed back to a normal scale for reporting purposes.

Model results by averaging time and measure of distribution

I varied the averaging time of the mobile measurements to explore what impact temporally smoothing the concentration data had on LUR model performance. Since I chose to aggregate measurements in 100m increments the results shown below are based

on that choice. For each pollutant I show results for goodness-of-fit (adjusted R^2), mean absolute error, and mean absolute bias. Absolute error is the absolute difference between model estimates and actual values; absolute bias is the absolute error normalized to the input concentration values (see equations 4.1 and 4.2).

$$absolute\ error = abs(\hat{y} - y) \tag{4.1}$$

$$absolute\ bias = \frac{abs(\hat{y}-y)}{y} \tag{4.2}$$

where $\hat{y}$ is the model predicted value and y is the observed value. When evaluating trends in these statistics for choosing the final models I took into account both the changes in model performance (based on the model metrics above) as well as striving to minimize the time averaging when possible. Since time averaging the mobile measurements also represents spatially smoothing the data, my goal was to avoid time averaging when model performance did not increase greatly with time averaging.

I show results both for measures of central tendencies (i.e., mean and median) and other measures of the distribution (10^{th}, 25^{th}, 75^{th}, 90^{th} percentiles) at each aggregation location to explore how models perform using various estimates of concentrations as inputs. I also show results for morning (n=12 sampling runs) and afternoon (n=30 sampling runs) separately. Figures 4.5-4.8 show results for particle number, black carbon, $PM_{2.5}$, and particle size separately.

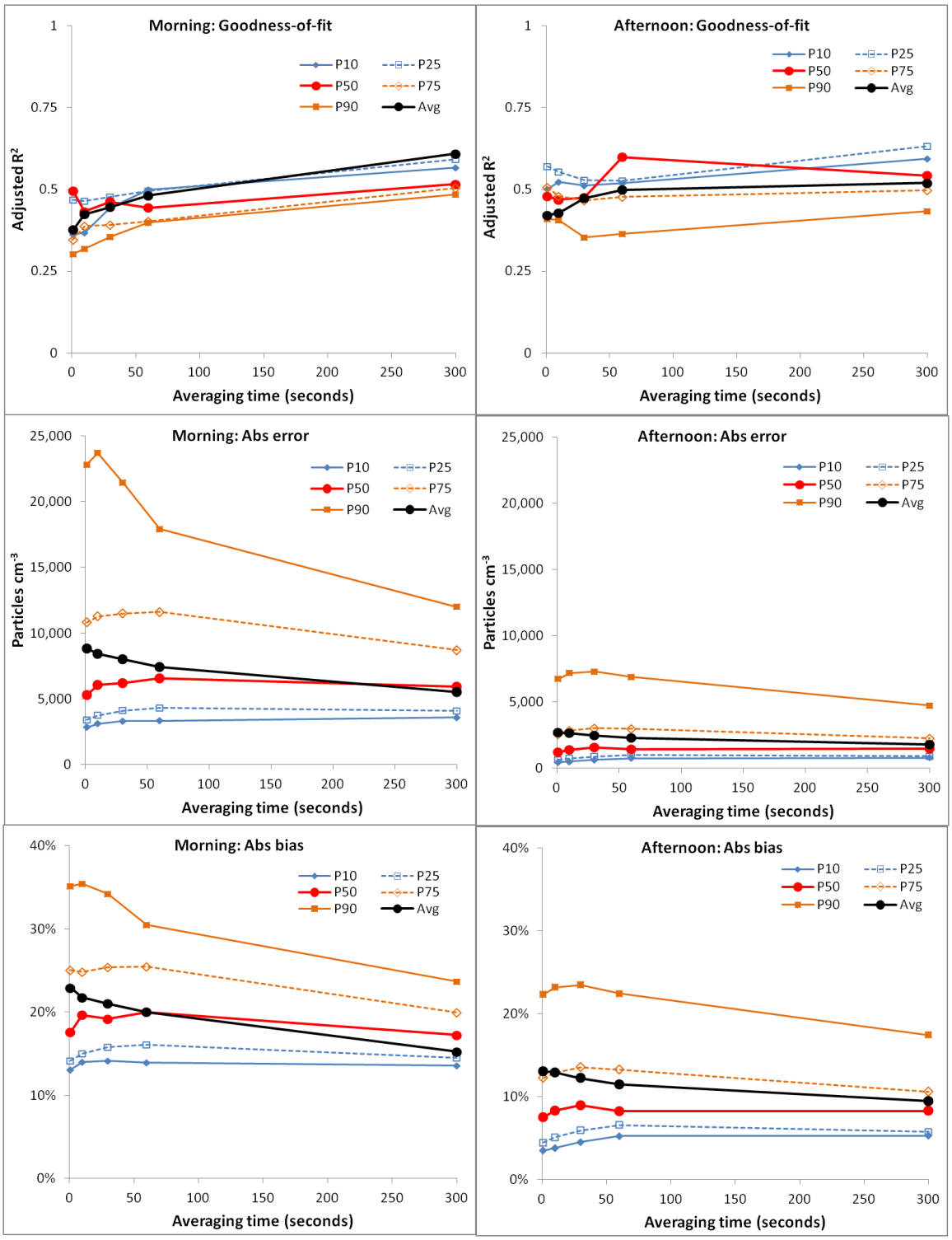

Figure 4.5 Particle number concentration model performance (top panels: goodness-of-fit; middle panels: absolute error; bottom panels: absolute bias) by distribution parameter and averaging time for morning (left panels) and afternoon (right panels) sampling runs.

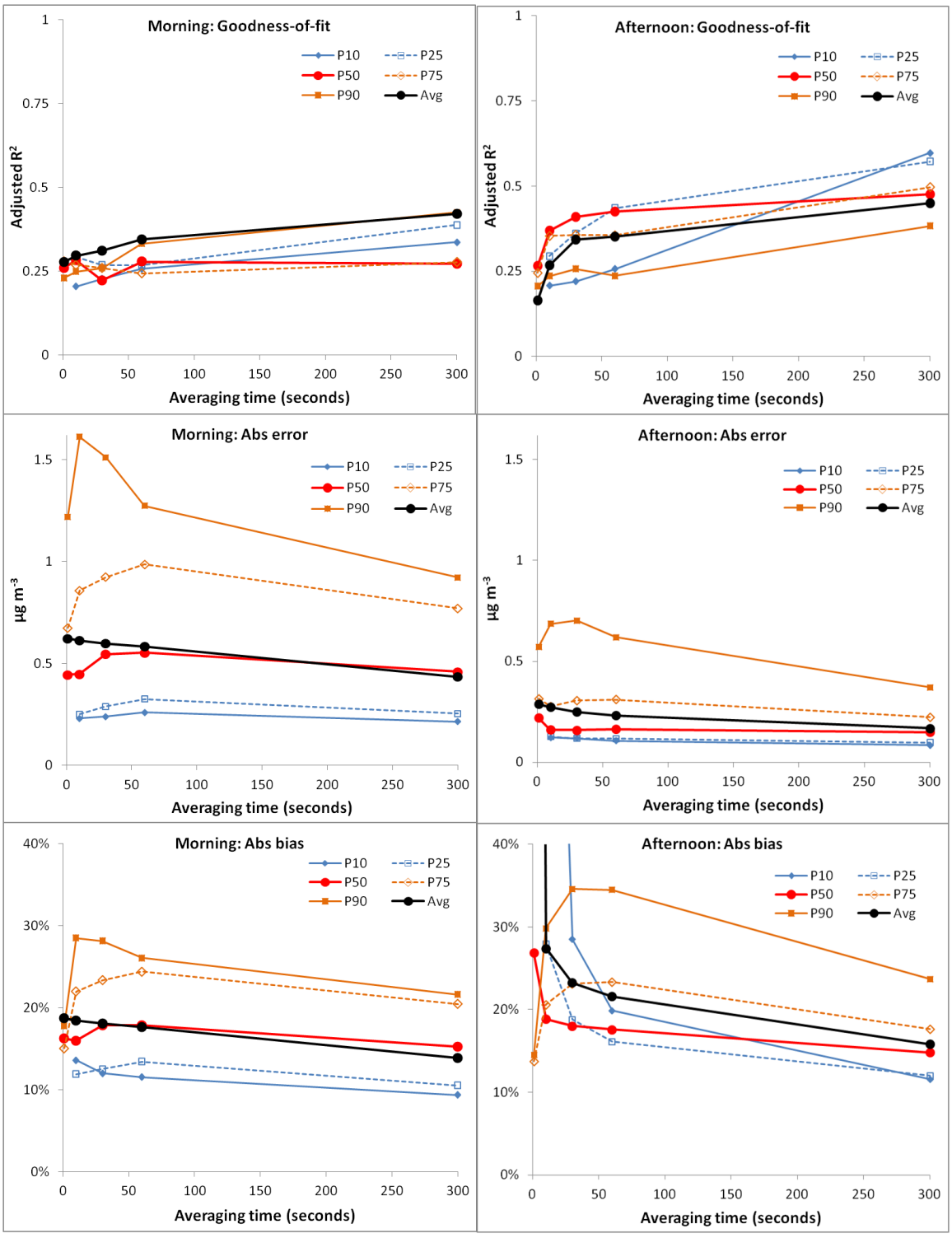

Figure 4.6 Black carbon concentration model performance (top panels: goodness-of-fit; middle panels: absolute error; bottom panels: absolute bias) by distribution parameter and averaging time for morning (left panels) and afternoon (right panels) sampling runs.

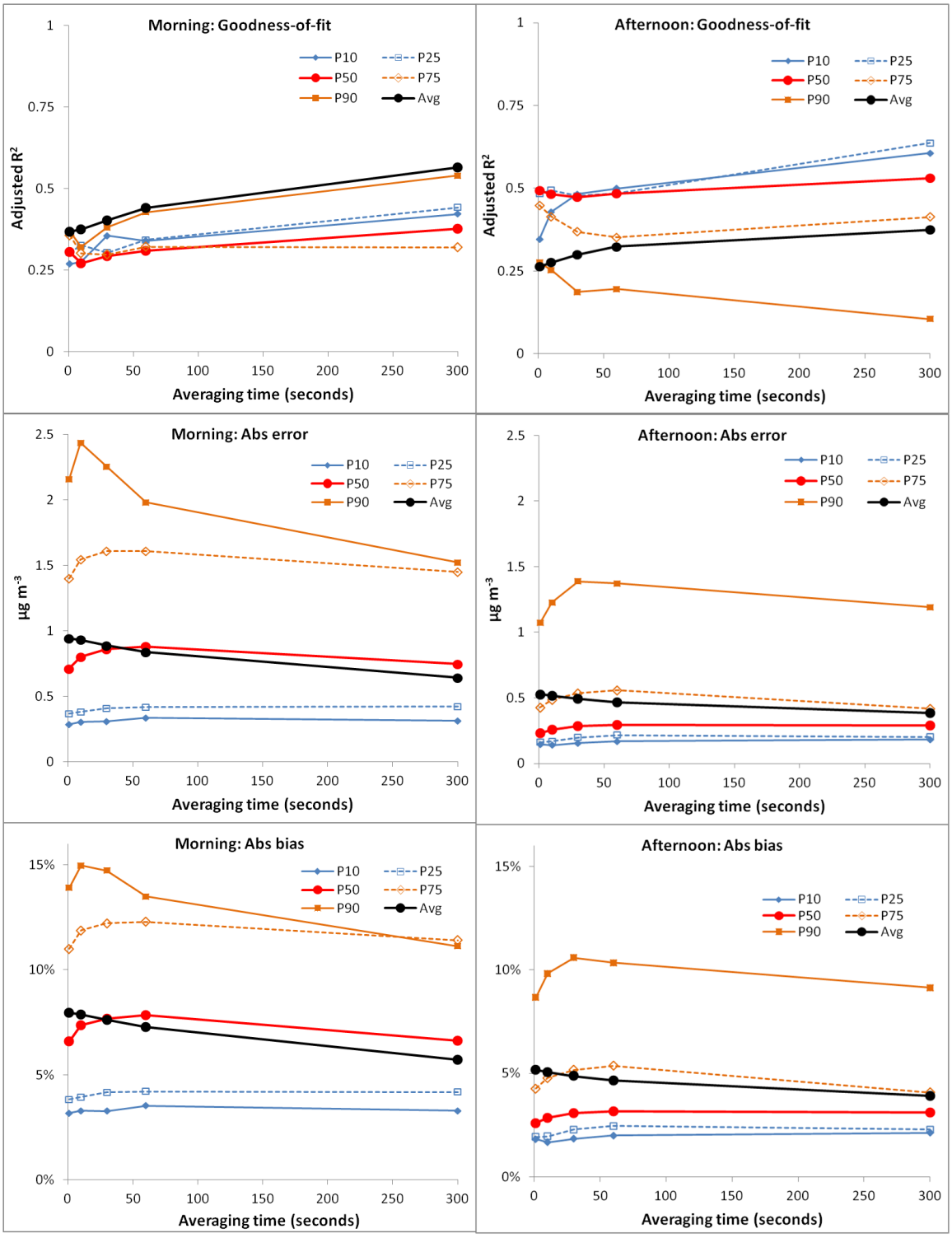

Figure 4.7 $PM_{2.5}$ concentration model performance (top panels: goodness-of-fit; middle panels: absolute error; bottom panels: absolute bias) by distribution parameter and averaging time for morning (left panels) and afternoon (right panels) sampling runs.

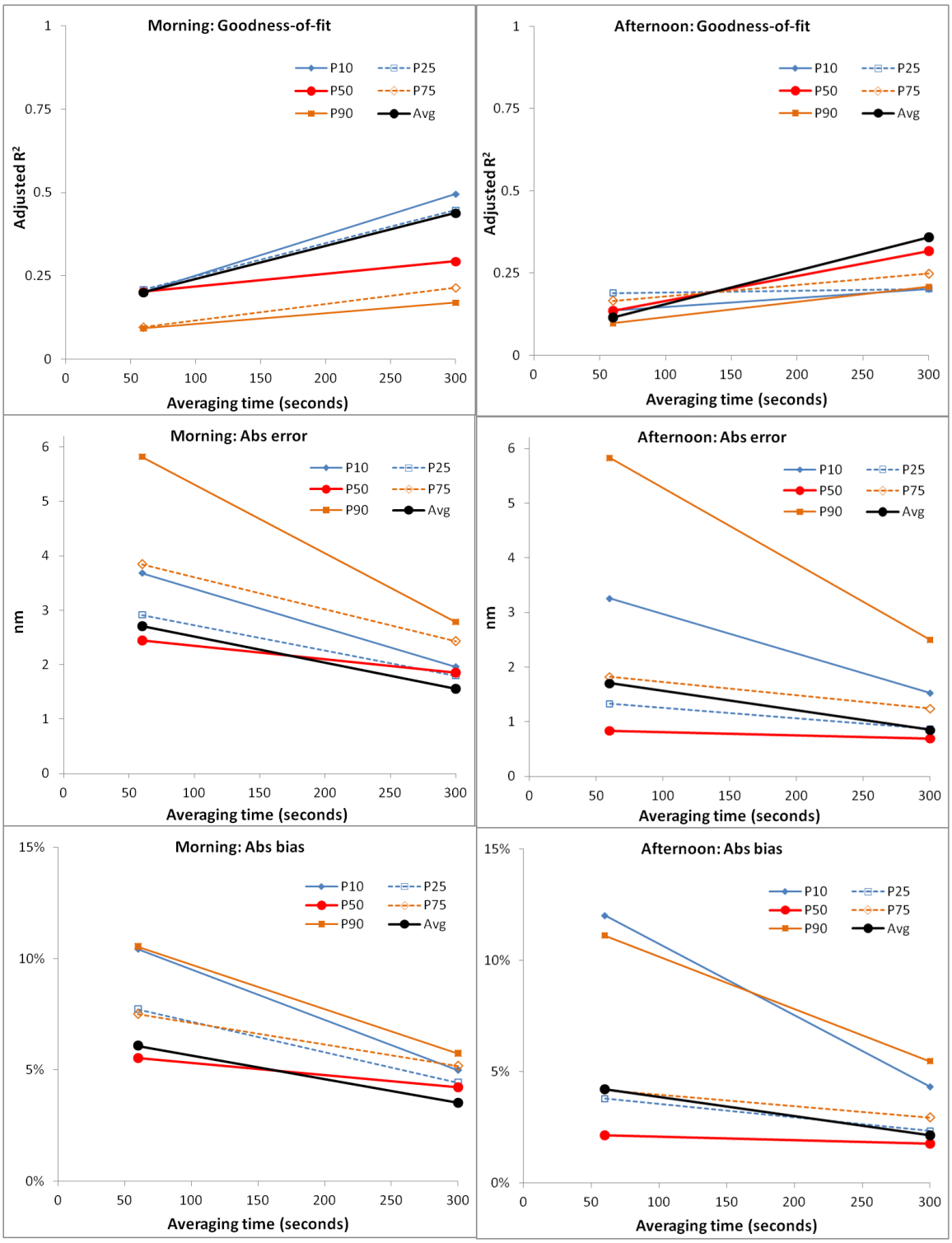

Figure 4.8 Particle size model performance (top panels: goodness-of-fit; middle panels: absolute error; bottom panels: absolute bias) by distribution parameter and averaging time for morning (left panels) and afternoon (right panels) sampling runs.

Model performance improved modestly with longer averaging times. For all measures of particulate air pollution, adjusted R^2 increased slightly with greater time averages; absolute error and bias also decreased slightly. Increasing the averaging time improved model performance most for the models of the upper ends of the measurement distribution (90^{th} and 75^{th} percentile) at aggregation locations and had little effect on the lower ends of the distribution (i.e., 10^{th} and 25^{th} percentile). Since averaging time had only a moderate effect on model performance it is likely best to use models that minimize smoothing (i.e., small averaging times or no averaging times) to minimize spatial smoothing that is inherent to temporally smoothing mobile measurements. For example, my average biking speed was ~10 mph; the longest averaging time shown in the figures above (i.e., 300s) represents averaging values over ~0.8 miles of the sampling route. Since my goal is to model small-scale differences in air pollution it is best not to employ time averaging unless it is necessary to gain sufficient model performance. Furthermore, it is possible that any improvement in model performance (e.g., increased adjusted R^2) from these longer time averages is at least partially due to spatially smoothing the data along the sampling routes, not necessarily better characterizing the spatial patterns in pollutant concentrations.

In general, model performance was best for the lower ends of the distribution (i.e., 10^{th} and 25^{th} percentile) and worst at the upper ends of the distribution (i.e., 75^{th} and 90^{th} percentiles) at each aggregation location. This behavior makes sense since the lower percentile models are essentially modeling baseline or background concentrations (limited spatial variability) while the higher percentile models are modeling relatively

acute-exposure events whose magnitude may depend highly on idiosyncratic attributes (e.g., the specific vehicle in front of you, the distance to that vehicle, etc.). Comparing the two central tendencies investigated (mean and median concentrations), among all pollutants, the models based on median concentrations generally performed better than the models based on mean concentration. In some cases (e.g., for $PM_{2.5}$ and black carbon in the mornings) adjusted R^2 values were higher for the mean model than for the median model; however, in all cases absolute error and bias were either similar or lower for median concentrations.

Model performance was generally better in the afternoons than mornings. This effect could potentially be attributable to differences in the spatial patterns of pollutants during those times of days (e.g., lower background concentrations and spatial variability in the afternoon as compared to the mornings) or could be owing to the fact that there were relatively fewer sampling runs in the mornings (n=12) than in the afternoons (n=30). The smaller number of morning sampling runs may have introduced uncertainty into the spatial estimates of concentrations used for modeling that hindered model performance in mornings relative to afternoons.

Model adjusted R^2 was highest for particle number concentrations (adjusted R^2: ~0.5) and moderate for both $PM_{2.5}$ and black carbon concentrations (adjusted R^2: ~0.3-0.5); adjusted R^2 was lowest for models of particle size (R^2 ~0.25). However, absolute bias was lowest for particle size and $PM_{2.5}$ (~3-8%) and relatively higher for particle number and black carbon (~10-20%). For black carbon it appears that an averaging time of ~60s was beneficial to overall model performance (see Figure 4.6) as that was the

point of diminishing return in improvements in model performance. The effect of averaging time was especially pronounced for the afternoon models; improvements in model performance with averaging time for black carbon is likely due to the noise in the data from the instrumentation used to measure concentrations (i.e., the micro-aethalometer). Real-time measurements from micro-aethalometers are known to have significant noise at small time scales (e.g., 1-30s); it is common to use time averaging to increase the signal to noise ratio from this instrument. As such, this analysis suggests it may be appropriate to apply time averaging of ~60s to the black carbon concentrations to obtain reliable LUR models for extrapolation. For the other measures of particulate air pollution (i.e., particle number, $PM_{2.5}$, particle size), I did not uncover evidence that averaging the 1-second measurements improved the LUR model.

Model results by spatial aggregation

In addition to testing the effect of temporal smoothing of the mobile measurements, I also explored how the choice of aggregating measurements at 100m intervals impacted model performance. To do this I re-aggregated concentration data (as explained above) at half (50m) and double (200m) the distance as the base-case (100m). This exercise shed light on how the amount of spatial smoothing affected the performance metrics of the LUR models. Since my main objective is to develop models of central tendencies at the aggregation locations I present results here for models that used the mean and median concentrations as dependent variables. Similar to the results presented for time averaging, I show adjusted R^2, absolute error, and absolute bias for each pollutant and for morning and afternoon models separately. I summarized results by

both the resolution of spatial aggregation (50m, 100m, 200m) and each time average. By simultaneously illustrating how model results changed for both of these factors I could check for interactions between smoothing the data spatially or temporally. Results are shown in Figures 4.9-4.12.

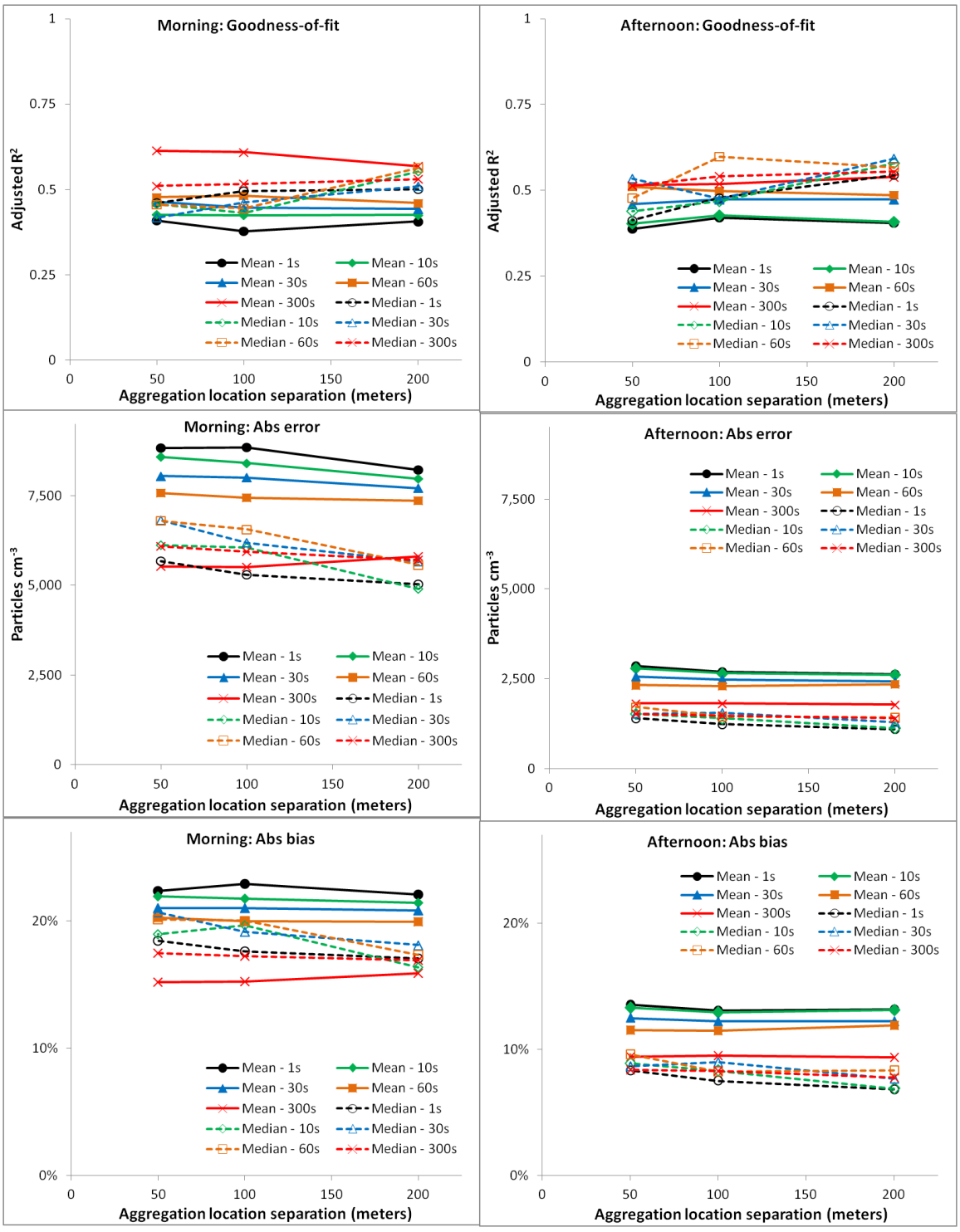

Figure 4.9 Particle number concentration model performance (top panels: goodness-of-fit; middle panels: absolute error; bottom panels: absolute bias) by separation distance of aggregation locations and averaging time for morning (left panels) and afternoon (right panels) sampling runs.

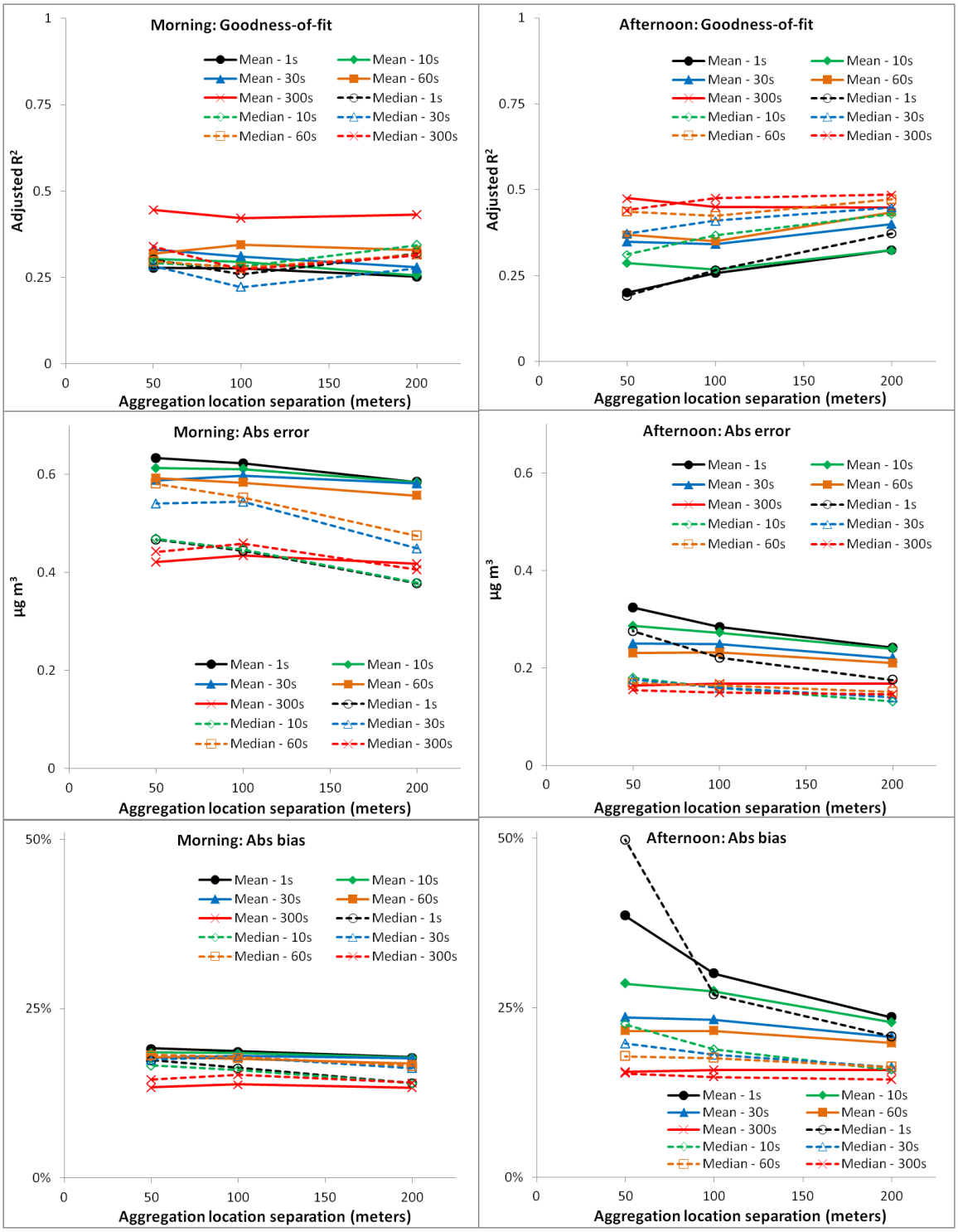

Figure 4.10 Black carbon concentration model performance (top panels: goodness-of-fit; middle panels: absolute error; bottom panels: absolute bias) by separation distance of aggregation locations and averaging time for morning (left panels) and afternoon (right panels) sampling runs.

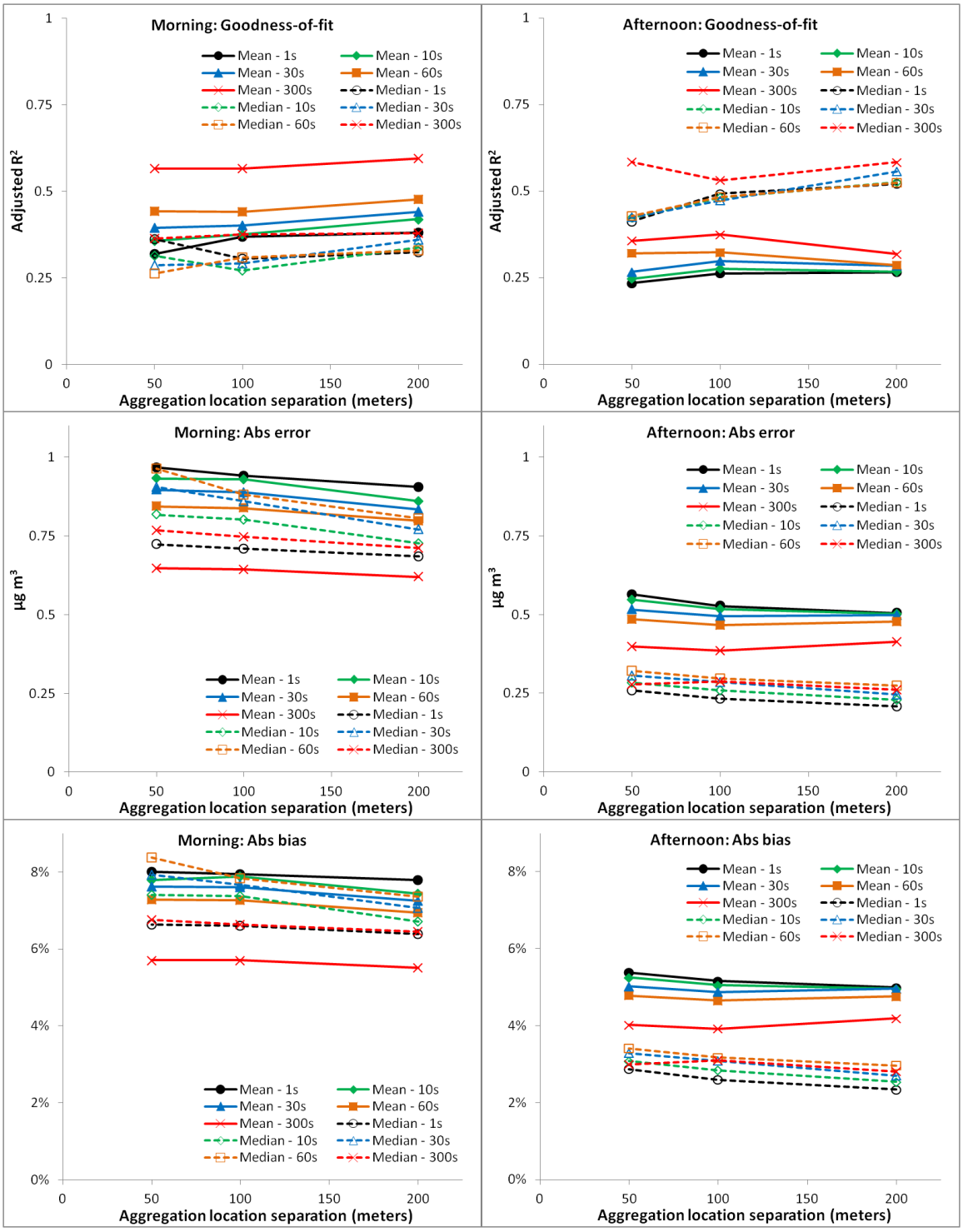

Figure 4.11 $PM_{2.5}$ concentration model performance (top panels: goodness-of-fit; middle panels: absolute error; bottom panels: absolute bias) by separation distance of aggregation locations and averaging time for morning (left panels) and afternoon (right panels) sampling runs.

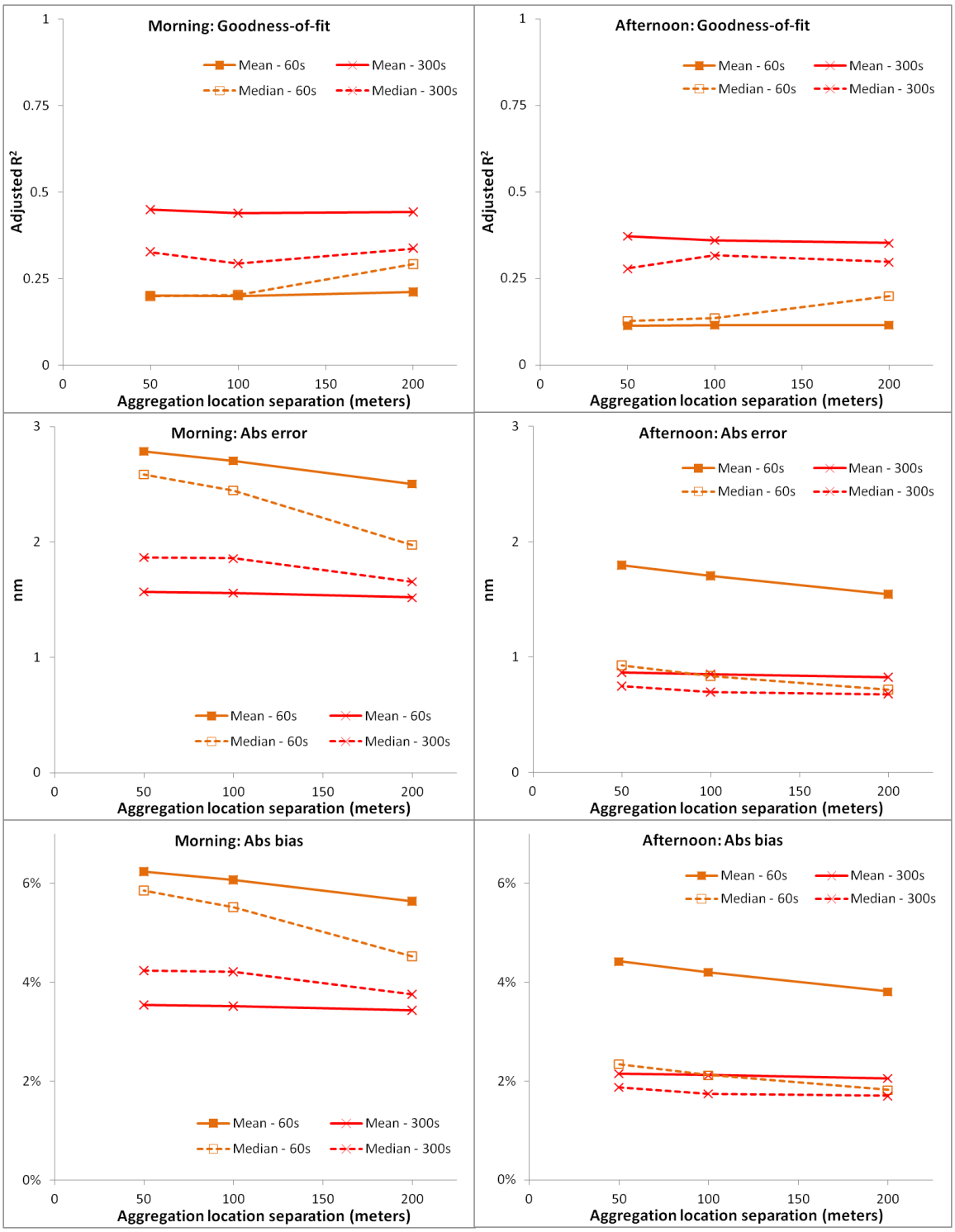

Figure 4.12 Particle size model performance (top panels: goodness-of-fit; middle panels: absolute error; bottom panels: absolute bias) by separation distance of aggregation locations and averaging time for morning (left panels) and afternoon (right panels) sampling runs.

There was little difference in model performance by the spatial resolution of measurement aggregation. All three measures of model performance (adjusted R^2, absolute error, absolute bias) remained fairly consistent for each of the aggregation cases and for each of the pollutants. For most cases, models of median concentrations performed slightly better than models of mean concentrations. There was slight evidence of poor model performance for black carbon concentrations at the 50m aggregation distance for small time averages (i.e., 1s and 10s). This result again is likely attributable to the signal-to-noise ratio from the micro-aethalometer and suggests that LUR models of black carbon concentrations may benefit from slight temporal and spatial smoothing of the mobile measurement data. A useful further analysis would be to test smaller spatial resolutions (e.g., 25m) to explore if model performance remains similar.

In most cases the difference in model performance was greater for changes in time average than for differences in spatial aggregation distance. This finding suggests that there is likely little to be gained from spatial averaging of the data over larger distances. It may also be a result of the fact that time averaging the measurement data is not only smoothing the data temporally but also spatially since the measurements were collected in a mobile fashion. Overall, the results from the two sensitivity analyses (i.e., for time averages and spatial aggregation) suggest that minimal smoothing of the data is necessary for LUR modeling. One notable exception is the measurements of black carbon which may benefit from slight smoothing due to noise in the micro-aethalometer data.

Choice of land use regression models for extrapolation

To estimate particulate air pollution concentrations for the entire City of Minneapolis I chose 8 base-case LUR models (4 pollutants; 2 times of day). I chose models based on both model performance and constraints meant to ensure the concentration estimates are comparable to the bicycle and pedestrian traffic estimates described in Chapter 5. First, I chose models based on the 100m aggregation locations to stay roughly consistent with the bicycle and pedestrian traffic measurements (~1 city block) and to minimize misclassification of measurements across blocks. For particle size I chose models based on the 200m aggregation since the NanoScan's minimum time resolution is 1 minute (a time that corresponds to ~260m traveled along the route at an average speed of 10mph). Since model performance was better with the log-transformed dependent variable I chose all models using log-transformed concentrations. For six of the eight chosen models, using median (rather than mean) concentrations at the aggregation location resulted in preferable model performance. For the other two models ($PM_{2.5}$ and black carbon in mornings) mean concentrations performed best; to stay consistent (and since differences in model performance were small) I chose to use median concentrations in all final models. I strived to use the smallest acceptable time averages to preserve small-scale changes in on-road concentrations that may exist. I chose models with no time averaging for three of the pollutants ($PM_{2.5}$ [1s], particle number [1s], and particle size [60s]). As discussed above, the black carbon models required slight time averaging (60s) to reduce the noise in the measurements from sampling with a micro-aethalometer.

To evaluate my choice of base-case models, I also separately pulled models that performed best for each of the eight model cases (i.e., each pollutant and time of day). To make this comparison I chose models with the highest adjusted R^2. Table 4.3 shows the 8 models chosen for extrapolation; Table 4.4 shows the "best" case models.

Table 4.3 Models chosen to extrapolate central tendency exposure concentrations to the entire City

Model	Spatial Resolution	Log transform	Time average	Aggregation distribution parameter	R^2	Adj R^2	Absolute error	Bias	Absolute bias	Number of independent variables included
$PM_{2.5}$ Morning	100m	Yes	1s	median	0.31	0.30	0.71 μg m^{-3}	0.4%	6.6%	14
$PM_{2.5}$ Afternoon	100m	Yes	1s	median	0.50	0.49	0.23 μg m^{-3}	0.1%	2.6%	12
Particle Number Morning	100m	Yes	1s	median	0.50	0.50	5,290 pt cm^{-3}	2.6%	17.6%	18
Particle Number Afternoon	100m	Yes	1s	median	0.48	0.48	1,230 pt cm^{-3}	0.6%	7.5%	7
Black Carbon Morning	100m	Yes	60s	median	0.29	0.28	0.55 μg m^{-3}	3.0%	17.8%	16
Black Carbon Afternoon	100m	Yes	60s	median	0.43	0.42	0.16 μg m^{-3}	2.6%	17.6%	15
Particle Size Morning	200m	Yes	60s	median	0.30	0.29	1.97 nm	0.2%	4.5%	8
Particle Size Afternoon	200m	Yes	60s	median	0.22	0.20	0.72 nm	0.0%	1.8%	11

Table 4.4 Models of central tendencies with highest adjusted R^2

Model	Spatial Resolution	Log transform	Time average	Aggregation distribution parameter	R^2	Adj R^2	Absolute error	Bias	Absolute bias	Number of independent variables included
$PM_{2.5}$ Morning	200m	Yes	60s	Mean	0.49	0.48	0.80 μg m^{-3}	0.5%	6.9%	13
$PM_{2.5}$ Afternoon	200m	Yes	30s	Median	0.57	0.56	0.25 μg m^{-3}	0.1%	2.7%	14
Particle Number Morning	200m	Yes	60s	Median	0.58	0.56	5,570 pt cm^{-3}	2.4%	17.3%	19
Particle Number Afternoon	100m	Yes	60s	Median	0.61	0.60	1,450 pt cm^{-3}	0.6%	8.2%	26
Black Carbon Morning	100m	Yes	60s	Mean	0.35	0.35	0.58 μg m^{-3}	2.8%	17.6%	14
Black Carbon Afternoon	200m	Yes	60s	Median	0.49	0.47	0.15 μg m^{-3}	2.2%	16.3%	13
Particle Size Morning	200m	Yes	60s	Median	0.30	0.29	1.97 nm	0.2%	4.5%	8
Particle Size Afternoon	200m	Yes	60s	Median	0.22	0.20	0.72 nm	0.03%	1.8%	12

In general, models chosen for extrapolation performed similarly to the models with the highest adjusted R^2. Adjusted R^2 was slightly lower for the extrapolation models than for the "best" models; however, absolute error, bias, and absolute bias were very similar between the two groups of models. In most cases, the "best" models included more spatial (mostly 200m aggregation) and temporal (mostly 60s) smoothing of the data. Since error and bias were mostly similar between the two groups of models it is possible that the higher R^2 values in the "best" group is a result of a reduction in the variability of the model input concentrations from spatial and temporal smoothing; it also could be the result of smoothing noise in the time-series data. The two groups of models included mostly similar numbers of independent variables with the exception of the afternoon particle number concentration model where the "best" model included many more independent variables than the models chosen for extrapolation.

Based on adjusted R^2, error, and bias, models generally performed better for the afternoons than for the mornings. Better model performance in the afternoons could be attributed to the larger number of sampling runs completed in the afternoon (n=30) than in the mornings (n=12); more sampling runs along each road segment likely yielded a better estimate of "typical" concentrations at those points which is what the LUR models attempt to predict (see discussion of this issue above). The uncertainty in estimating typical concentrations from relatively fewer numbers of sampling runs in the morning could be exacerbated by the fact there is more spatial variability in concentrations in the mornings than in the afternoons. Absolute bias was relatively low for all models (1.8-18%) and lower for pollutants with less spatial variability ($PM_{2.5}$ [averaged between

morning and afternoon: 4.6%], particle size [3.2%]) than for the traffic-related pollutants which have high spatial and temporal variability (particle number [12.6%], black carbon [17.7%]). Absolute bias was also lower for afternoon than for morning models.

Tables 4.5-4.12 give details on each model chosen for extrapolation. Since I used log-transformed concentrations as the dependent variable all model coefficients are reported in log space; the percent increase in pollutant concentrations per unit increase in each independent variable are given as a reference to simplify interpretation. For example, the value of 0.88% for traffic intensity in the first table below (Table 4.5) means that an increase in traffic intensity of 1 AADT m^{-2} corresponds to a 0.88% increase in concentration. Final values for the independent variable inclusion criteria (p-value and VIF) are given along with measures of each variable's contribution to the model (partial R^2 and $\beta \times IQR$) for comparison. My model building approach tested VIF and p-values when a variable was added to the model. Those statistics were then re-calculated for the final models (i.e., with all included variables); in one case for the final models (morning particle number model) the VIF for one variable slightly violated the original inclusion criteria (length of freeway; VIF=5.4); this variable also had a relatively small standard error (~8% of the β). Of the 8,183 independent variables selected among all 612 LUR models 161 (~2%) violated the VIF threshold in the final model specification (standard error for βs was typically small); the mean VIF value for the variables which violated the threshold was only slightly above the inclusion criteria (mean VIF for variables above threshold: 5.9). Since the violation of the VIF criteria was minimal, I did not further reduce models but instead stayed consistent with the original inclusion criteria.

Table 4.5 Final morning particle number concentration model

Variable	Buffer length (m)	Units	β (log)	β (% increase)	p-value	Partial R^2	IQR	β × IQR	VIF
Intercept	-	-	12.0	-	<0.01	-	-	-	-
Open space	25	m^2	-7.2E-05	-0.0072%	<0.01	0.15	1,039	-0.172	2.7
Industry	500	m^2	7.7E-07	0.000077%	<0.01	0.25	85,483	0.085	1.6
Traffic intensity	-	AADT m^{-2}	8.7E-03	0.88%	<0.01	0.29	5	0.053	1.3
Major roads	25	m	1.4E-03	0.14%	<0.01	0.33	50	0.106	1.7
Railway	400	m^2	1.3E-06	0.00013%	<0.01	0.35	6,041	0.012	2.2
House density	500	Units m^{-2}	5.0E-05	0.0050%	<0.01	0.37	1,031	0.055	2.1
Freeways	3,000	m	-8.8E-06	-0.00088%	<0.01	0.39	42,969	-0.101	5.4
Retail	75	m^2	1.3E-05	0.0013%	<0.01	0.42	4,630	0.065	1.6
Bus routes	100	m	1.2E-05	0.0012%	<0.01	0.42	1,131	0.015	1.8
Open space	1,500	m^2	-7.7E-08	-0.0000077%	<0.01	0.43	699,430	-0.035	3.2
Local roads	3,000	m	-5.8E-06	-0.00058%	<0.01	0.45	31,643	-0.092	3.4
Open space	5,000	m^2	2.6E-08	0.0000026%	<0.01	0.47	4,587,969	0.102	2.1
Local roads	25	m	-1.1E-03	-0.11%	<0.01	0.47	44	-0.048	1.7
Intersections	2,000	Count	9.9E-04	0.099%	<0.01	0.48	126	0.100	4.7
Elevation	-	m	-1.4E-03	-0.14%	<0.01	0.49	30	-0.036	2.3
Railway	100	m^2	1.7E-05	0.0017%	<0.01	0.49	0	0.000	1.8
Bus stops	100	Count	1.3E-02	1.3%	<0.01	0.50	2	0.023	1.8
Major roads	750	m	-9.0E-06	-0.00090%	<0.01	0.50	5,079	-0.046	3.4

Table 4.6 Final afternoon particle number concentration model

Variable	Buffer length (m)	Units	β (log)	β (% increase)	p-value	Partial R^2	IQR	β × IQR	VIF
Intercept	-	-	9.4	-	<0.01	-	-	-	-
Major roads	200	m	5.0E-05	0.0050%	<0.01	0.25	647	0.087	2.0
Industry	1,500	m^2	9.5E-08	0.000010%	<0.01	0.37	946,282	0.085	1.4
House density	1,000	Units m^{-2}	4.8E-05	0.0048%	<0.01	0.41	779	0.036	1.3
Retail	25	m^2	4.2E-05	0.0042%	<0.01	0.44	487	0.024	1.3
Bus stops	75	Count	1.2E-02	1.26%	<0.01	0.46	2	0.028	1.4
Railway	400	m^2	7.7E-07	0.000077%	<0.01	0.47	6,041	0.005	1.3
Major roads	25	m	7.2E-04	0.072%	<0.01	0.48	50	0.036	1.6

Table 4.7 Final morning black carbon concentration model

Variable	Buffer length (m)	Units	β (log)	β (% increase)	p-value	Partial R^2	IQR	β × IQR	VIF
Intercept	-	-	-0.05	-	<0.01	-	-	-	-
Dist. to major rds.	-	m	-3.5E-04	-0.035%	0.01	0.06	77	-0.071	2.0
Industry	400	m^2	7.0E-07	0.000070%	<0.01	0.10	51,374	0.048	1.7
House density	400	Units m^{-2}	1.1E-04	0.011%	<0.01	0.16	1,175	0.085	2.3
All roads	3,000	m	-2.5E-06	-0.00025%	<0.01	0.18	73,802	-0.080	2.5
Traffic intensity	-	AADT m^{-2}	4.4E-03	0.44%	0.01	0.20	5	0.032	1.7
Bus routes	150	m	6.0E-06	0.00060%	<0.01	0.21	3,287	0.022	1.4
Railway	150	m^2	9.5E-06	0.0010%	<0.01	0.22	0	0.000	1.2
Major roads	25	m	1.5E-03	0.15%	<0.01	0.24	50	0.079	2.2
Local roads	5,000	m	2.1E-06	0.00021%	<0.01	0.24	29,114	0.027	1.9
Open space	1,500	m^2	-3.3E-08	-0.0000033%	<0.01	0.25	699,430	-0.023	1.8
Retail	75	m^2	8.1E-06	0.00081%	<0.01	0.25	4,630	0.027	1.5
Open space	5,000	m^2	2.7E-08	0.0000027%	<0.01	0.25	4,587,969	0.038	2.3
Industry	3,000	m^2	5.0E-08	0.0000050%	<0.01	0.27	3,212,355	0.122	3.9
Freeways	1,000	m	1.0E-05	0.0010%	<0.01	0.28	6,956	0.064	2.3
House density	25	Units m^{-2}	-1.3E-05	-0.0013%	0.01	0.28	1,796	-0.024	1.8
Intersections	300	Count	-4.9E-03	-0.49%	0.01	0.29	7	-0.034	1.8

Table 4.8 Final afternoon black carbon concentration model

Variable	Buffer length (m)	Units	β (log)	β (% increase)	p-value	Partial R^2	IQR	β × IQR	VIF
Intercept	-	-	-0.3	-	<0.01	-	-	-	-
Local roads	1,000	m	-1.5E-05	-0.0015%	<0.01	0.18	11,055	-0.196	1.6
Dist. to major rds.	-	m	-5.1E-04	-0.051%	<0.01	0.23	77	-0.067	1.9
Open space	3,000	m^2	1.8E-08	0.0000018%	<0.01	0.27	1,114,829	0.039	2.2
Industry	1,000	m^2	7.0E-08	0.0000070%	0.05	0.30	404,541	0.071	2.4
Retail	25	m^2	9.1E-05	0.0091%	<0.01	0.32	487	0.040	1.2
Bus routes	75	m	2.7E-05	0.0027%	<0.01	0.34	749	0.021	1.3
Freeways	1,500	m	-1.1E-05	-0.0011%	<0.01	0.36	14,691	-0.078	2.5
Freeways	400	m	4.5E-05	0.0045%	<0.01	0.39	720	0.036	1.6
Open space	5,000	m^2	1.5E-08	0.0000015%	<0.01	0.40	4,587,969	0.063	1.5
Railway	100	m^2	1.8E-05	0.0018%	<0.01	0.40	0	0.000	1.2
House density	50	Units m^{-2}	1.9E-05	0.0019%	<0.01	0.41	1,808	0.020	1.4
Major roads	25	m	1.4E-03	0.14%	<0.01	0.42	50	0.067	2.1
Freeways	5,000	m	1.8E-06	0.00018%	<0.01	0.42	28,460	0.038	1.8
Industry	75	m^2	8.7E-06	0.00087%	<0.01	0.43	6	0.000	1.6
House density	1,000	Units m^{-2}	-4.9E-05	-0.0049%	<0.01	0.43	779	-0.038	2.2

Table 4.9 Final morning $PM_{2.5}$ concentration model

Variable	Buffer length (m)	Units	β (log)	β (% increase)	p-value	Partial R^2	IQR	β × IQR	VIF
Intercept	-	-	1.7	-	<0.01	-	-	-	-
Industry	1,500	m^2	3.5E-08	0.0000035%	<0.01	0.07	946,282	0.049	3.2
House density	1,500	Units m^{-2}	5.0E-05	0.0050%	<0.01	0.17	785	0.048	2.3
Railway	150	m^2	4.6E-06	0.00046%	<0.01	0.19	0	0.000	1.3
Bus stops	100	Count	5.1E-03	0.51%	<0.01	0.21	2	0.014	1.6
HH income	25	Dollars	-6.7E-07	-0.000067%	<0.01	0.22	32,130	-0.018	1.4
Open space	3,000	m^2	1.8E-08	0.0000018%	<0.01	0.25	1,114,829	0.013	2.0
Industry	150	m^2	8.0E-07	0.000080%	0.01	0.26	4,307	0.005	1.6
Retail	25	m^2	1.4E-05	0.0014%	0.02	0.26	487	0.010	1.4
Traffic intensity	-	AADT m^{-2}	2.0E-03	0.20%	<0.01	0.27	5	0.007	1.3
Railway	3,000	m^2	7.3E-08	0.0000073%	<0.01	0.28	625,347	0.025	3.3
Intersections	5,000	Count	1.3E-04	0.013%	<0.01	0.29	174	0.020	2.4
Open space	25	m^2	-2.7E-05	-0.0027%	<0.01	0.30	1,039	-0.016	2.0
Intersections	400	Count	-1.9E-03	-0.19%	<0.01	0.31	13	-0.024	2.1
Major roads	75	m	8.6E-05	0.0086%	<0.01	0.31	258	0.022	1.5

Table 4.10 Final afternoon $PM_{2.5}$ concentration model

Variable	Buffer length (m)	Units	β (log)	β (% increase)	p-value	Partial R^2	IQR	β × IQR	VIF
Intercept	-	-	2.1	-	<0.01	-	-	-	-
Bus stops	200	Count	1.6E-03	0.16%	<0.01	0.23	7	0.025	2.5
Industry	1,000	m^2	2.7E-08	0.0000027%	<0.01	0.34	404,541	0.023	1.8
Railway	400	m^2	4.5E-07	0.000045%	<0.01	0.37	6,041	0.002	1.3
Major roads	50	m	1.1E-04	0.011%	<0.01	0.40	120	0.018	1.4
HH income	500	Dollars	-5.4E-07	-0.000054%	<0.01	0.42	27,550	-0.008	1.6
Bus routes	25	m	2.7E-05	0.0027%	<0.01	0.44	100	0.003	1.6
Retail	150	m^2	8.7E-07	0.000087%	<0.01	0.46	16,179	0.012	1.8
Open space	5,000	m^2	2.5E-09	0.0000003%	<0.01	0.48	4,587,969	0.011	1.2
Population density	500	People m^{-2}	-5.4E-06	-0.00054%	<0.01	0.49	2,591	-0.010	2.4
House density	75	Units m^{-2}	2.7E-06	0.00027%	<0.01	0.49	1,720	0.005	1.4
Intersections	150	Count	-1.7E-03	-0.17%	0.01	0.50	3	-0.005	1.4
Traffic intensity	-	AADT m^{-2}	4.8E-04	0.048%	0.02	0.50	5	0.002	1.2

Table 4.11 Final morning particle size concentration model

Variable	Buffer length (m)	Units	β (log)	β (% increase)	p-value	Partial R^2	IQR	β × IQR	VIF
Intercept	-	-	3.5	-	<0.01	-	-	-	-
HH income	3,000	Dollars	2.9E-06	0.00029%	<0.01	0.12	12,754	0.027	2.2
Freeways	400	m	-1.1E-05	-0.0011%	<0.01	0.21	697	-0.011	1.7
Local roads	3,000	m	9.3E-07	0.000093%	<0.01	0.22	31,306	0.012	1.5
Bus routes	1,000	m	1.6E-07	0.000016%	<0.01	0.24	115,331	0.010	2.0
Retail	100	m^2	-2.4E-06	-0.00024%	<0.01	0.26	7,449	-0.015	1.4
Open space	5,000	m^2	-7.3E-09	-0.00000072%	<0.01	0.29	4,587,232	-0.032	2.1
Industry	300	m^2	-1.6E-07	-0.000016%	0.03	0.29	26,265	-0.005	1.2
Freeways	100	m	-6.4E-05	-0.0064%	0.01	0.30	0	0.000	1.6

Table 4.12 Final afternoon particle size concentration model

Variable	Buffer length (m)	Units	β (log)	β (% increase)	p-value	Partial R^2	IQR	β × IQR	VIF
Intercept	-	-	3.5	-	<0.01	-	-	-	-
Bus routes	5,000	m	-5.1E-08	-0.0000051%	<0.01	0.04	338,166	-0.007	3.1
Intersections	5,000	Count	9.0E-05	0.0090%	<0.01	0.09	174	0.010	3.0
Local roads	3,000	m	-4.3E-07	-0.000043%	<0.01	0.12	31,306	-0.009	2.4
Industry	500	m^2	-4.0E-08	-0.0000040%	0.01	0.13	87,441	-0.003	1.8
House density	1,000	Units m^{-2}	-1.3E-05	-0.0013%	<0.01	0.15	788	-0.006	2.3
Retail	25	m^2	5.3E-06	0.00053%	0.01	0.16	468	0.002	1.1
Local roads	1,000	m	1.2E-06	0.00012%	<0.01	0.17	11,307	0.007	2.5
Railway	500	m^2	1.3E-07	0.000013%	<0.01	0.18	13,532	0.001	1.8
Freeways	2,000	m	4.5E-07	0.000045%	<0.01	0.19	25,204	0.007	2.7
HH income	1,500	Dollars	4.3E-07	0.000043%	<0.01	0.20	18,385	0.004	3.0
Freeways	150	m	-9.6E-06	-0.0010%	0.04	0.21	0	0.000	1.2
HH income	100	Dollars	-1.9E-07	-0.000019%	<0.01	0.22	31,859	-0.006	2.5

In most of the models chosen for extrapolation, a small number of the independent variables accounted for a large proportion of the variance explained by the models. In six of the eight models the first two variables included in the model accounted for over half of the final R^2; in the other two models the first three variables accounted for over half of the R^2. Each subsequent variable added to the model explained much less of the variability in the concentration data.

A unique aspect of my approach to build LUR models is the density of concentration estimates in the study area. This aspect of the measurement data was reflected in the variable selection process as many variables with relatively small buffer sizes were selected in the models. Among the models chosen for extrapolation, 23 variables (24%) were selected at the sub-100m level; the proportion of sub-100m variables was slightly higher for the traffic-related pollutants (black carbon [29%]; particle number [30%]). Among all final models, variables selected at these small buffer lengths included length of major roads (n=6), retail area (n=6), house density (n=3), and bus routes/stops (n=3). The fact that these variables were selected at a small spatial scale suggests that activity centers – here, origins (house density), destinations (retail areas), and busy travel routes (major roads and bus routes/stops) – are important to the small-scale variation in traffic-related pollutants.

Another notable finding is that some variables behaved differently at different buffer lengths. For example, when the open space area variable was selected at a buffer length of 1,500 m or less, the coefficient was always negative (i.e., inverse correlation) as expected. When open space area was selected at a very small buffer size (e.g., 25 m) the

coefficient remained negative and had a larger magnitude than larger buffer sizes. However, when open space area was selected at a buffer length of >1,500 meters, the coefficients were positive. This result is not necessarily intuitive and may be attributable to confounding factors; for example, one explanation may be that many of the off-street trails (where there is a large amount of open space located in close proximity to the trails) are located either in old rail corridors near freeways (i.e., Cedar Lake Trail) or along busy parkways near activity centers (e.g., West River Parkway near downtown Minneapolis or around Lake Calhoun). It could be that the larger buffer sizes are not only picking up the effect of the open space itself but also the surrounding land uses. This finding is one example of how theoretical impacts of LUR models should be interpreted with caution. In the case of open space with a buffer <1,500 m, direct extrapolation of the LUR coefficients would suggest that more open space would yield worse pollution, a finding that I hesitate to hold up as correct. Instead, I believe it is more likely that open space happens to sometimes correlate with higher-emitting land uses.

The models described above provide evidence of environmental justice issues associated with air pollution concentrations in Minneapolis. For example, in both $PM_{2.5}$ models, household income was selected and associated with lower concentrations in high-income areas (and, conversely, higher concentrations in low-income areas). The particle size models also selected household income in both models and two of the three buffer sizes had positive coefficients indicating particle size is slightly larger in high income areas; this result suggests that high income areas are likely located further from emission sources such as high traffic roads. Although these results do not imply causation

between income and concentration, they do indicate that low income areas are located in higher concentration areas and that this relationship is robust to controlling for the other variables included in these models.

Importance of independent variables in models

The results above included two criteria for evaluating independent variables: (1) inclusion in the final models and (2) the magnitude of the coefficient. To supplement the tables of regression statistics shown above, I also created plots that included two additional parameters: (1) $\beta \times IQR$ and (2) the partial R^2 for each independent variable. In addition to the magnitude of the β coefficient in a regression model, it is also important to include information about the range of values for that variable. I calculated the product of the variable coefficient (β) and interquartile range (IQR) to account for both factors. I then plotted $\beta \times IQR$ vs. the partial R^2 for each independent variable, pollutant, and time of day. Variables that are in the upper-right of each plot represent variables that have the most influence on the modeled concentrations (i.e., high $\beta \times IQR$ and high partial R^2). Variables that increased and decreased concentrations are shown in separate data series (circles for increased concentrations [positive beta]; squares for decreased concentrations [negative beta]). Each data point is labeled with the variable selected but without the associated buffer size (since space in each plot was limited). Results are shown in Figures 4.13-4.16.

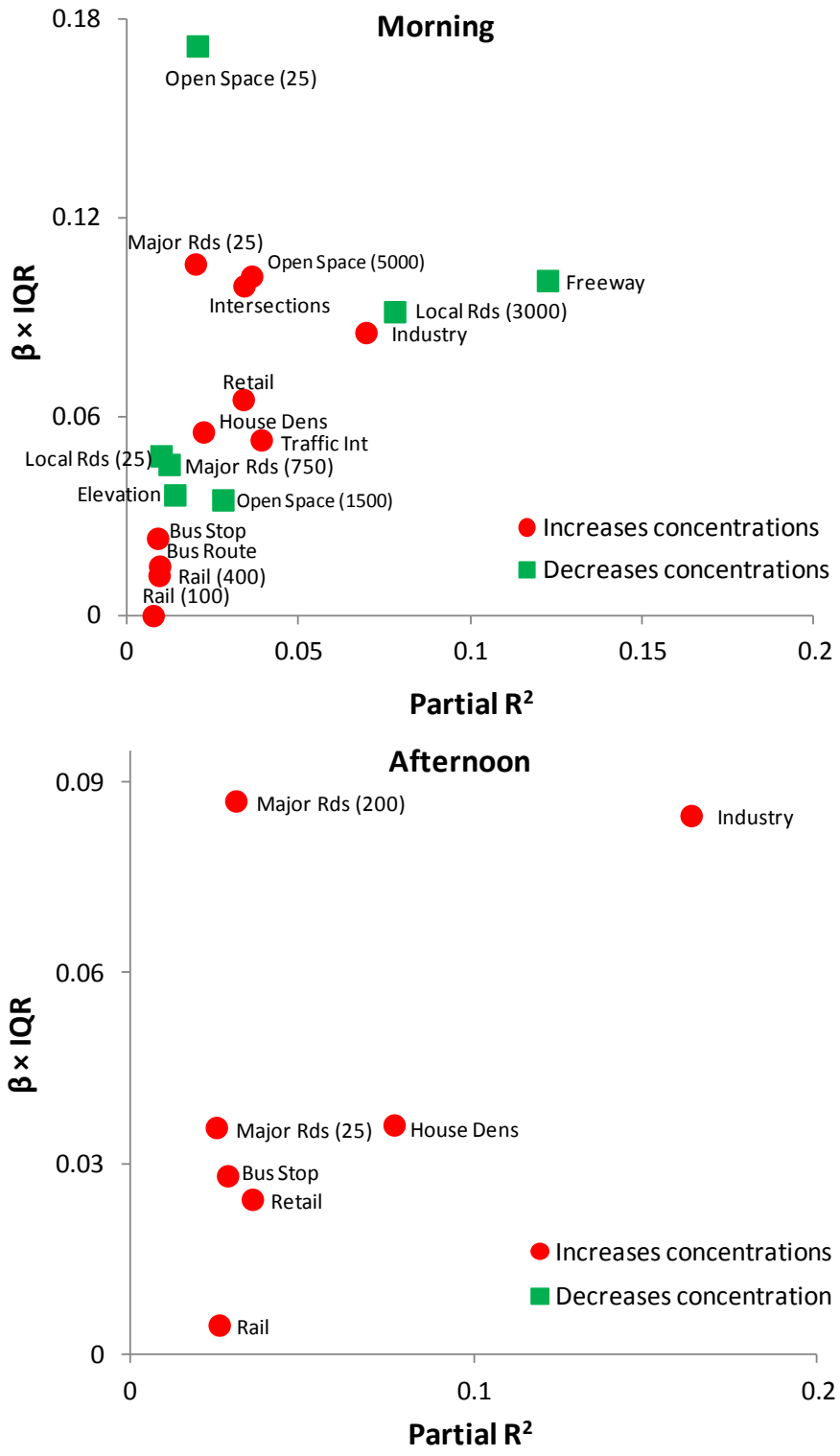

Figure 4.13 Independent variables included in particle number concentration models. Variables with high β×IQR and R^2 added to the model have the most impact on concentrations. Buffer sizes included in label when variable was selected multiple times.

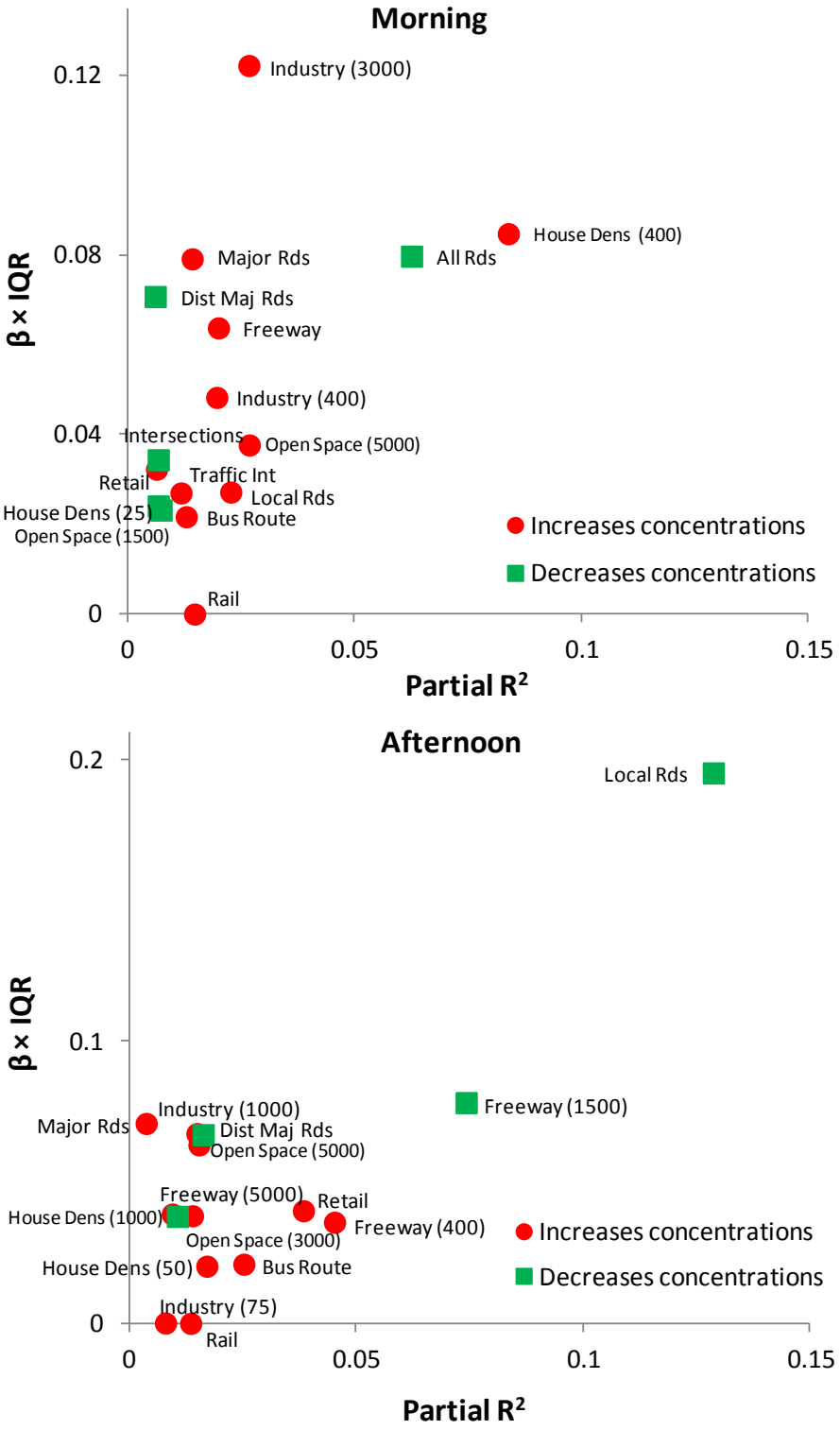

Figure 4.14 Independent variables included in black carbon concentration models. Variables with high β×IQR and R^2 added to the model have the most impact on concentrations. Buffer sizes included in label when variable was selected multiple times.

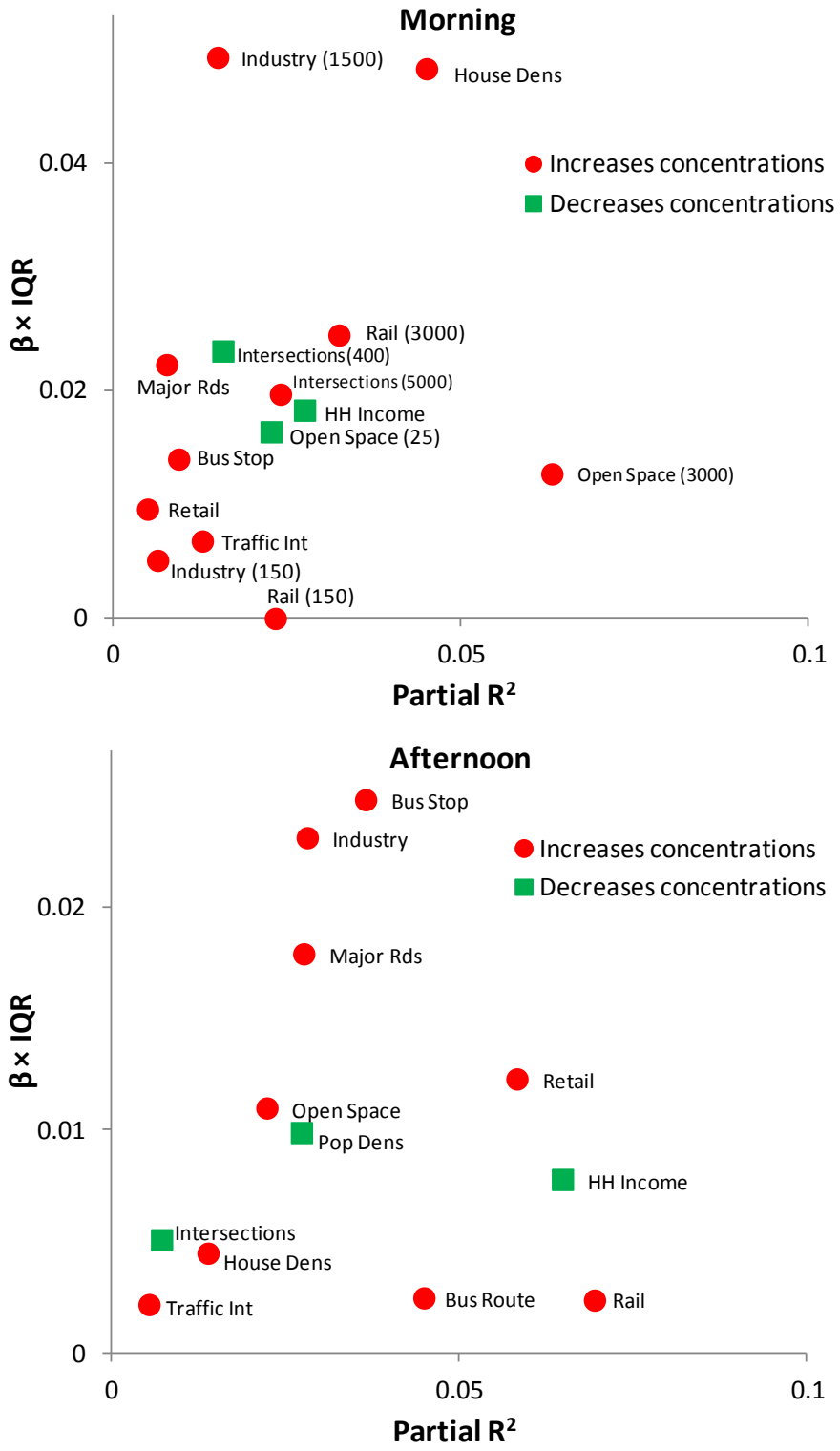

Figure 4.15 Independent variables included in $PM_{2.5}$ concentration models. Variables with high β×IQR and R^2 added to the model have the most impact on concentrations. Buffer sizes included in label when variable was selected multiple times.

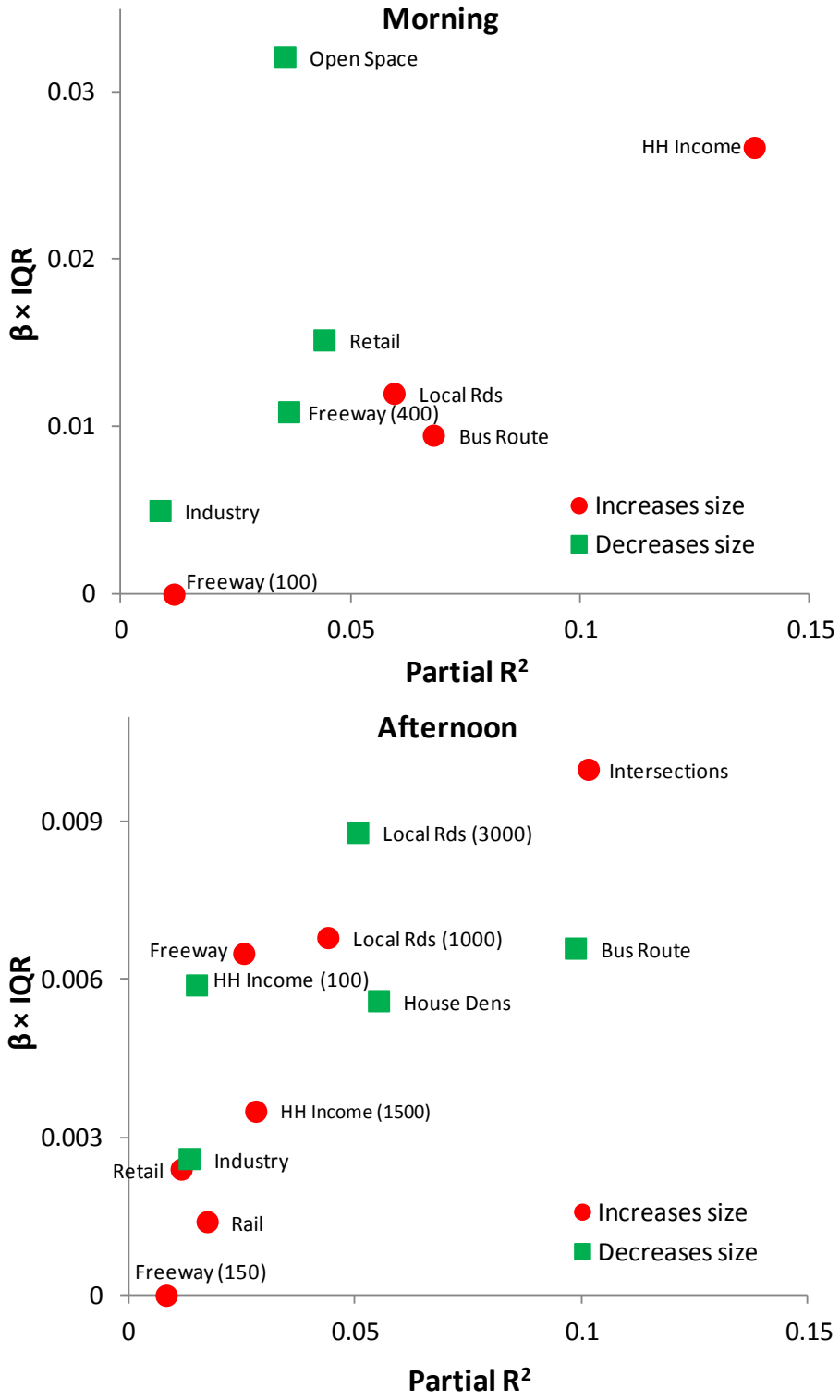

Figure 4.16 Independent variables included in particle size models. Variables with high β×IQR and R^2 added to the model have the most impact on concentrations. Buffer sizes included in label when variable was selected multiple times.

Figures 4.13-4.16 highlight the fact that a relatively small number of variables stand out as important in each model. For each model many variables are clustered near the lower left of the plot (low β×IQR and low partial R^2) with 1-4 variables separated towards the upper right of the plot (high β×IQR and high partial R^2). Variables that were the most important for predicting particulate air pollution among the models were those related to separation from emission sources (e.g., open space area, distance from major roads, length of local [low-traffic] roads) and proximity to and density of emission sources (e.g., industrial area, house density, length of high-traffic roads). Variables that increased and decreased concentrations were included (and important) in all models except for the afternoon particle number model which included only variables that increased concentrations.

Variables that were most important in the models (i.e., located in the upper right of the plots) were usually among the first variables added to the models. These variables likely are responsible for predicting a large portion of the overall trends in particulate concentrations across the City. The variables that were added later in the models adjust estimates for smaller-scale concentration gradients (e.g., distances from major roads) or less frequent emission sources within the City (e.g. close proximity to railways or freeways which occurred less frequently along the sampling route than other variables but were often selected in modeling).

Land use regression model validation

I tested final model performance using three approaches: (1) a random holdout of 1/3 of the measurement data to use as a validation dataset, (2) a systematic hold out of

each sampling route (i.e., using a model built from 2 routes to predict the third), and (3) testing for spatial autocorrelation among model residuals. Results for each approach are presented below.

Random holdout validation

I employed a Monte Carlo-based approach to randomly hold out a subset of the measurement data to use as a validation dataset. I randomly selected 1/3 of the concentration dataset for each model ("test" datasets); then, I re-estimated the LUR models using the remaining 2/3 of the dataset ("build" datasets) and estimated concentrations at the test dataset locations. I compared model estimates and observed concentrations by correlation and report validation R^2 values for those comparisons. I repeated this process 100 times for each model. Boxplots of the results from this Monte Carlo validation approach are shown in Figure 4.17.

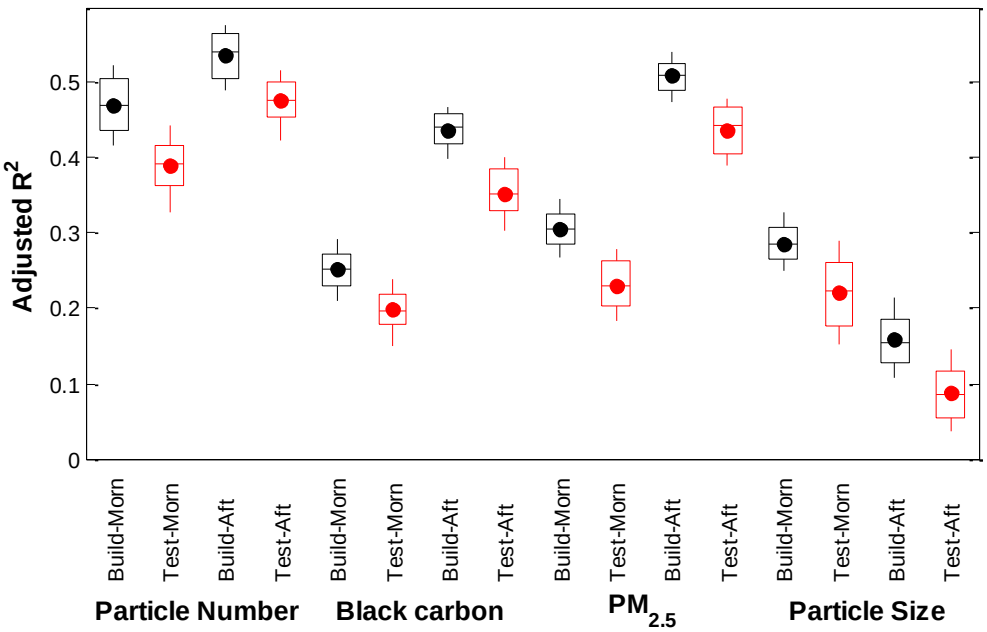

Figure 4.17 Model validation R^2 for the 1/3 random holdout Monte Carlo-based analysis.

In general, validation R^2 values were slightly lower than for the full models (average gap between model-building and model-testing R^2, among values in Figure 4.16, is 0.07), suggesting that the goodness-of-fit statistics reported for the final models may be slightly overestimated. This issue is especially important when using the models for extrapolation to locations without measurements. The difference between model building and validation R^2 was similar among pollutants and time of day; variability of the R^2 values among the Monte Carlo runs was also similar. Variability among Monte Carlo runs suggests model estimates may be impacted by choice of measurement locations used to build the final LUR models.

Systematic validation by sampling route

To further test the results of the LUR models I applied a more rigorous, systematic validation approach. Specifically, instead of randomly holding out 1/3 of the measurement data, I held out data from 1 of the sampling routes and re-estimated LUR models using the other 2 routes. Then, I estimated concentrations for the route that was not included in model building and compared to the measured concentration estimates. This process was repeated for each sampling route and each model; I generated four scatterplots for comparison – three plots of predicted vs. observed concentrations for the systematic holdout approach for each route and a fourth plot for the full model. Each plot shows a best fit line (solid line) with R^2 and a hypothetical 1:1 line representing perfect model performance (dashed line). Scatterplots are shown in Figures 4.18-4.25.

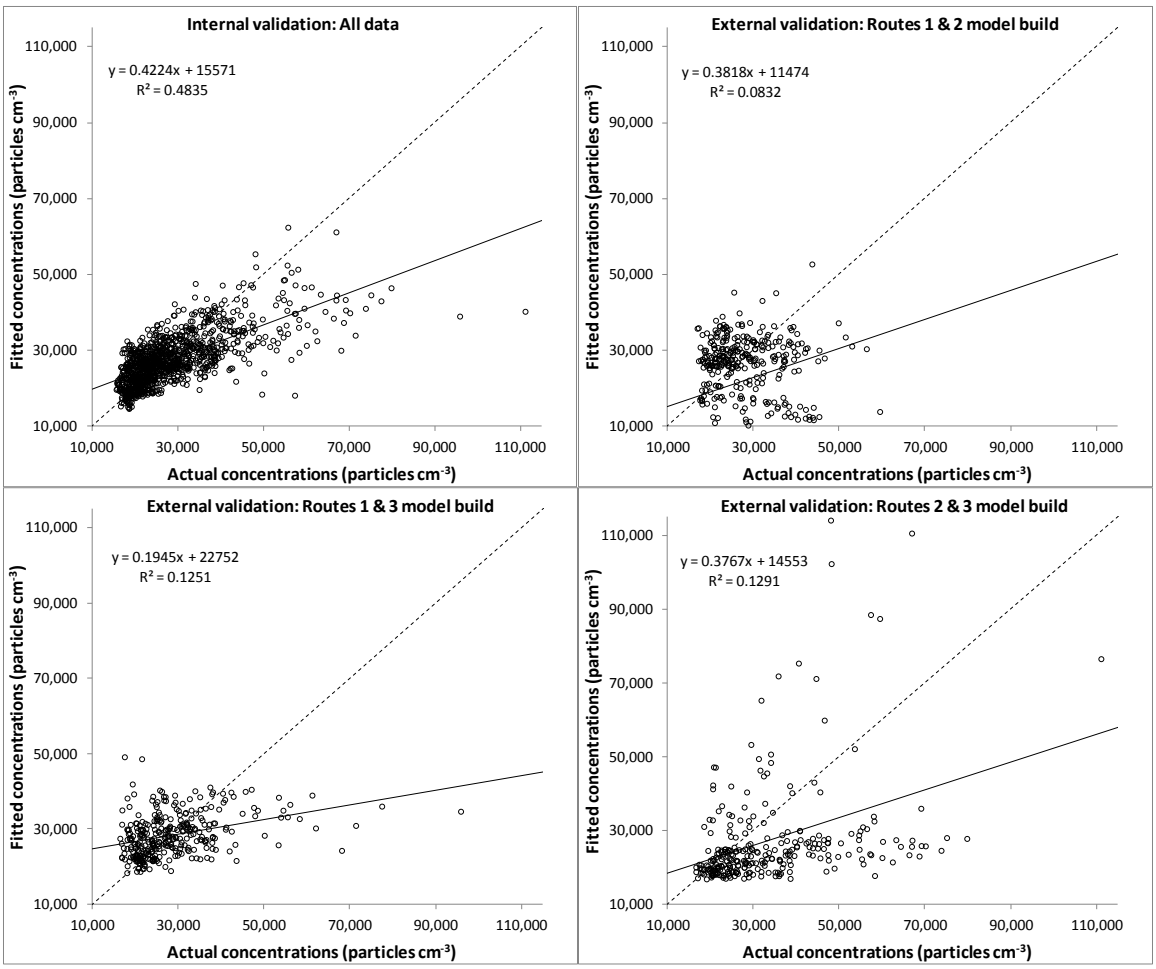

Figure 4.18 Morning particle number concentration sampling runs: Actual vs. predicted for the full model (upper left) and three systematic validation cases which involved building models using two routes and predicting concentrations from the third route (route 3 test dataset [upper right], route 2 test dataset [lower left], route 3 test dataset [lower right]).

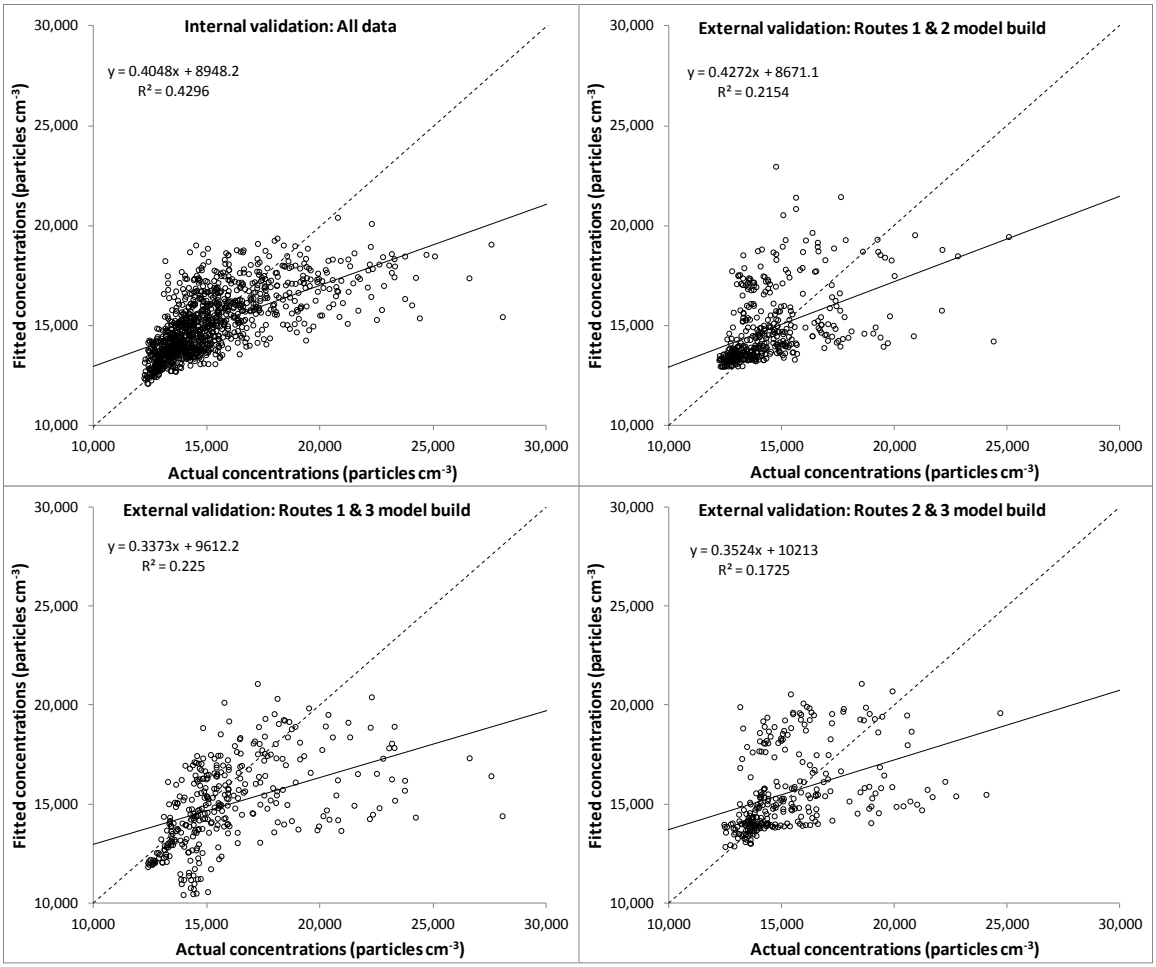

Figure 4.19 Afternoon particle number concentration sampling runs: Actual vs. predicted for the full model (upper left) and three systematic validation cases which involved building models using two routes and predicting concentrations from the third route (route 3 test dataset [upper right], route 2 test dataset [lower left], route 3 test dataset [lower right]).

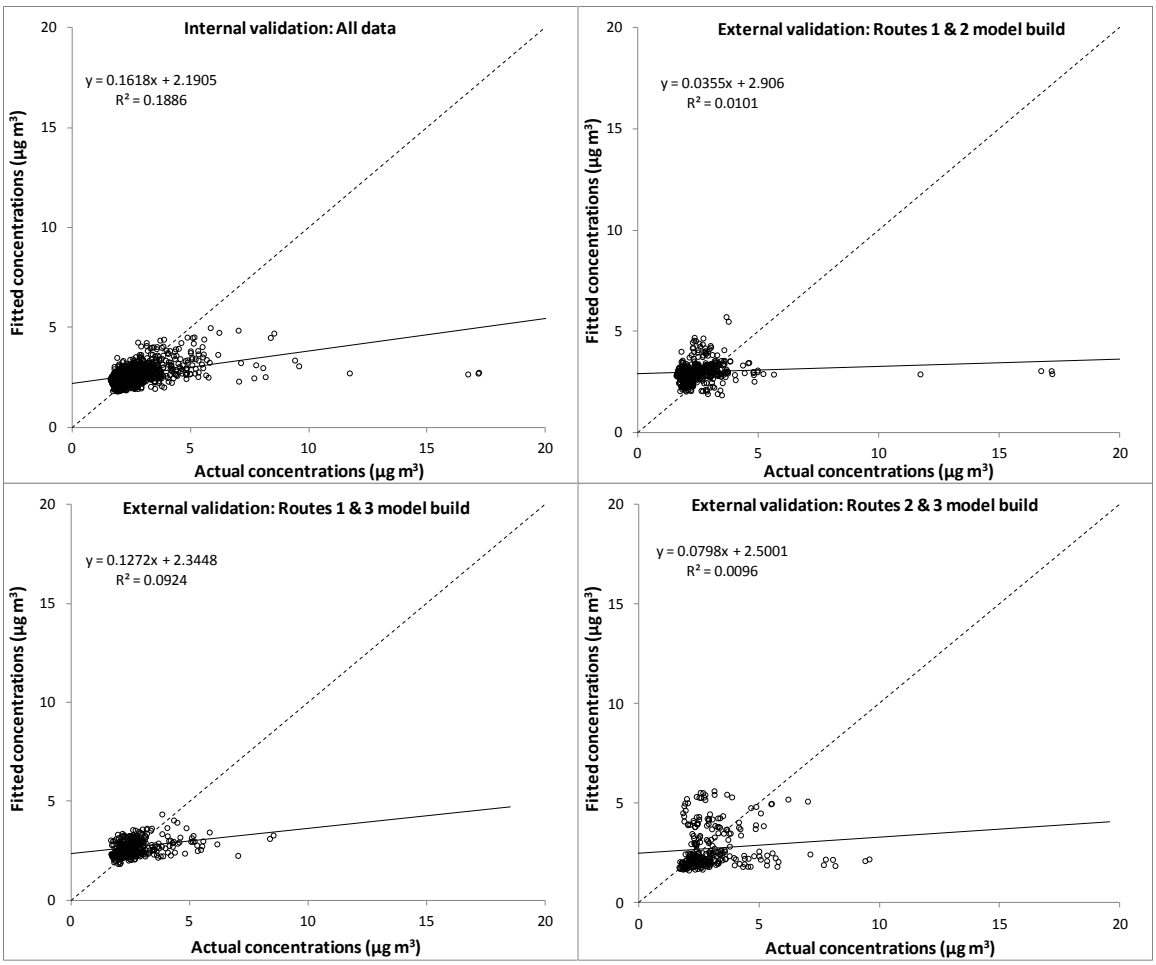

Figure 4.20 Morning black carbon concentration sampling runs: Actual vs. predicted for the full model (upper left) and three systematic validation cases which involved building models using two routes and predicting concentrations from the third route (route 3 test dataset [upper right], route 2 test dataset [lower left], route 3 test dataset [lower right]).

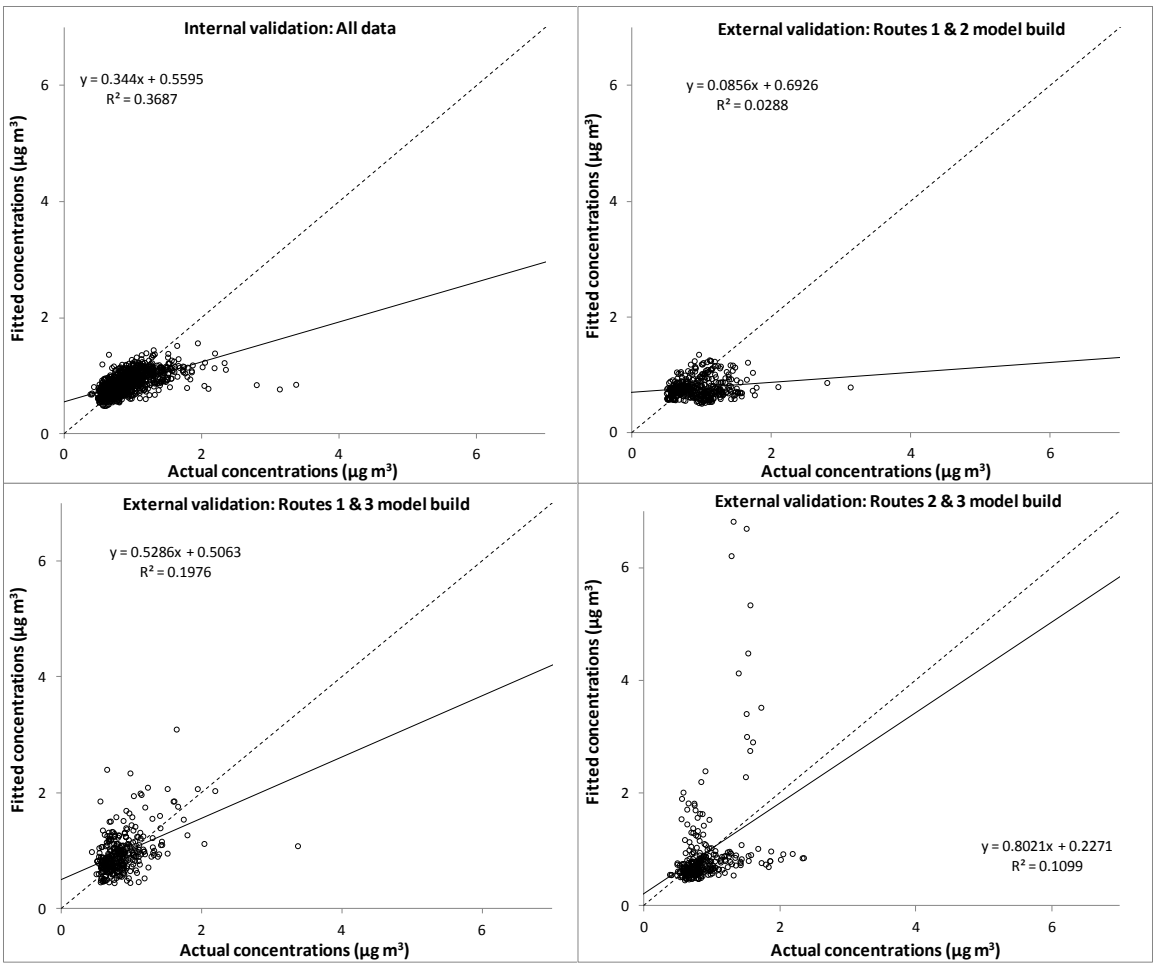

Figure 4.21 Afternoon black carbon concentration sampling runs: Actual vs. predicted for the full model (upper left) and three systematic validation cases which involved building models using two routes and predicting concentrations from the third route (route 3 test dataset [upper right], route 2 test dataset [lower left], route 3 test dataset [lower right]).

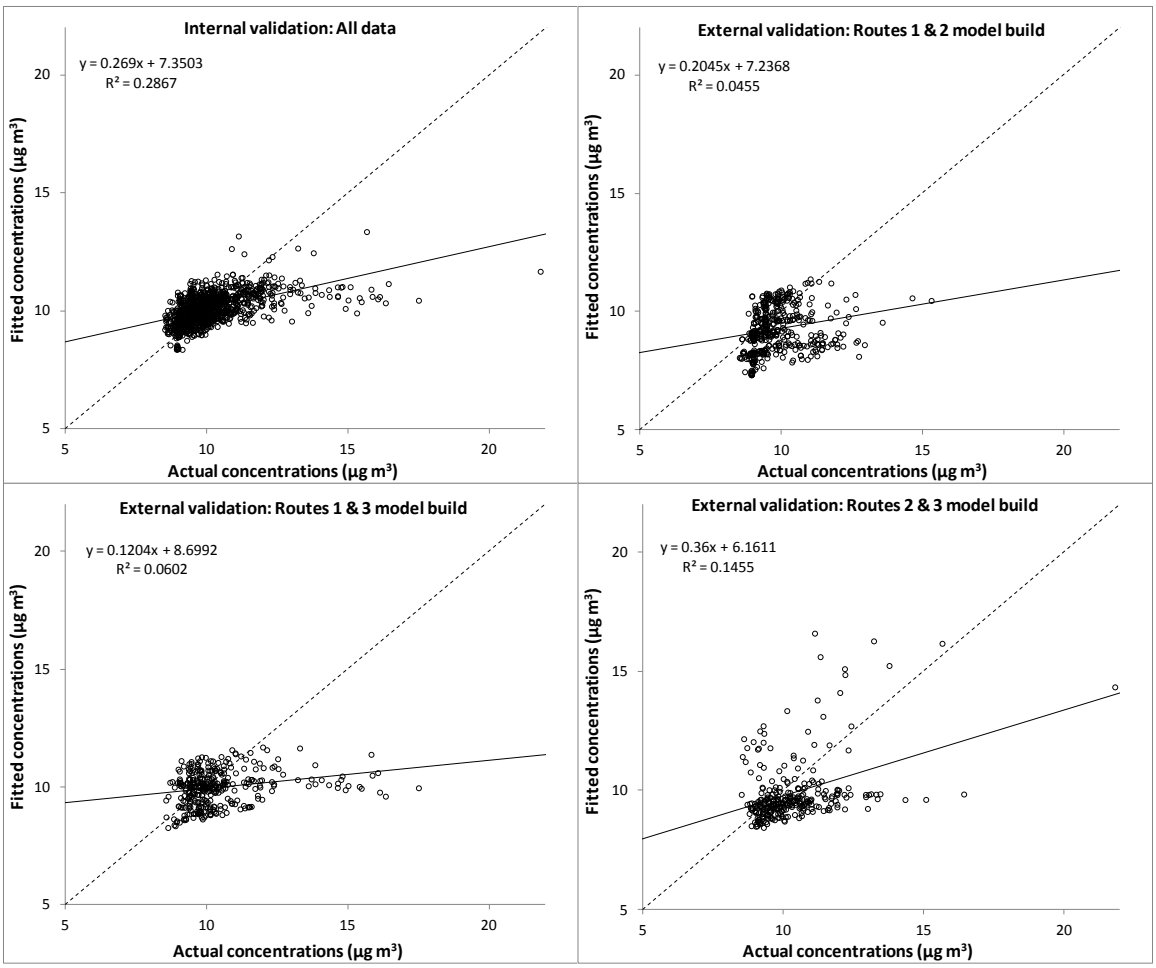

Figure 4.22 Morning $PM_{2.5}$ concentration sampling runs: Actual vs. predicted for the full model (upper left) and three systematic validation cases which involved building models using two routes and predicting concentrations from the third route (route 3 test dataset [upper right], route 2 test dataset [lower left], route 3 test dataset [lower right]).

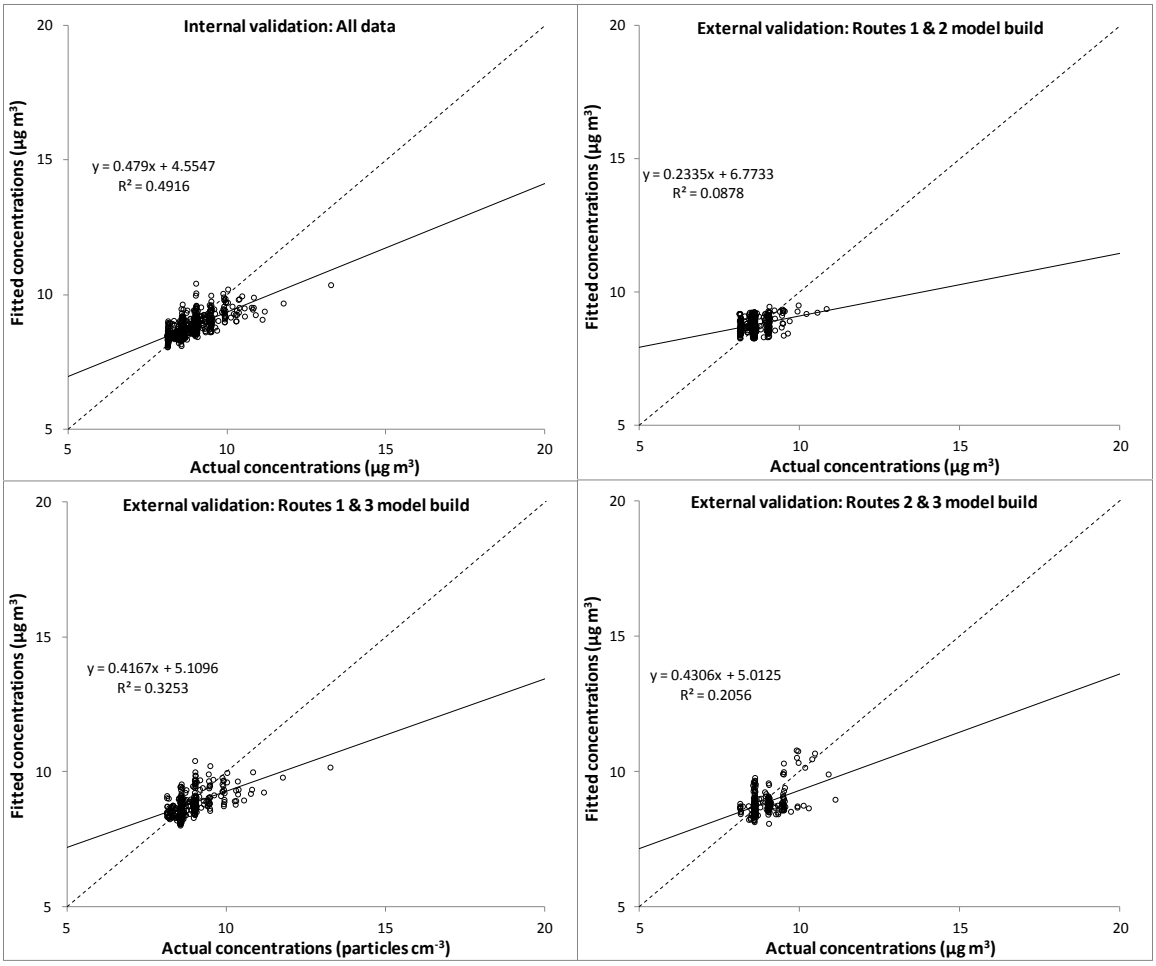

Figure 4.23 Afternoon $PM_{2.5}$ concentration sampling runs: Actual vs. predicted for the full model (upper left) and three systematic validation cases which involved building models using two routes and predicting concentrations from the third route (route 3 test dataset [upper right], route 2 test dataset [lower left], route 3 test dataset [lower right]).

Note: The actual (x-axis) concentrations are mostly aligned at specific intervals in Figure 4.24. This is partly a result of the precision of the DustTrak (1 µg/m^3) and that there was low variability in concentration values at each aggregation location; median values were typically calculated from a small number of concentration values. Morning $PM_{2.5}$ results did not show this pattern because the underwrite function was highly non-linear (i.e., adding scatter to the concentration estimates); for the afternoon, underwrite estimates were mostly flat (i.e., linear and similar concentrations before and after runs).

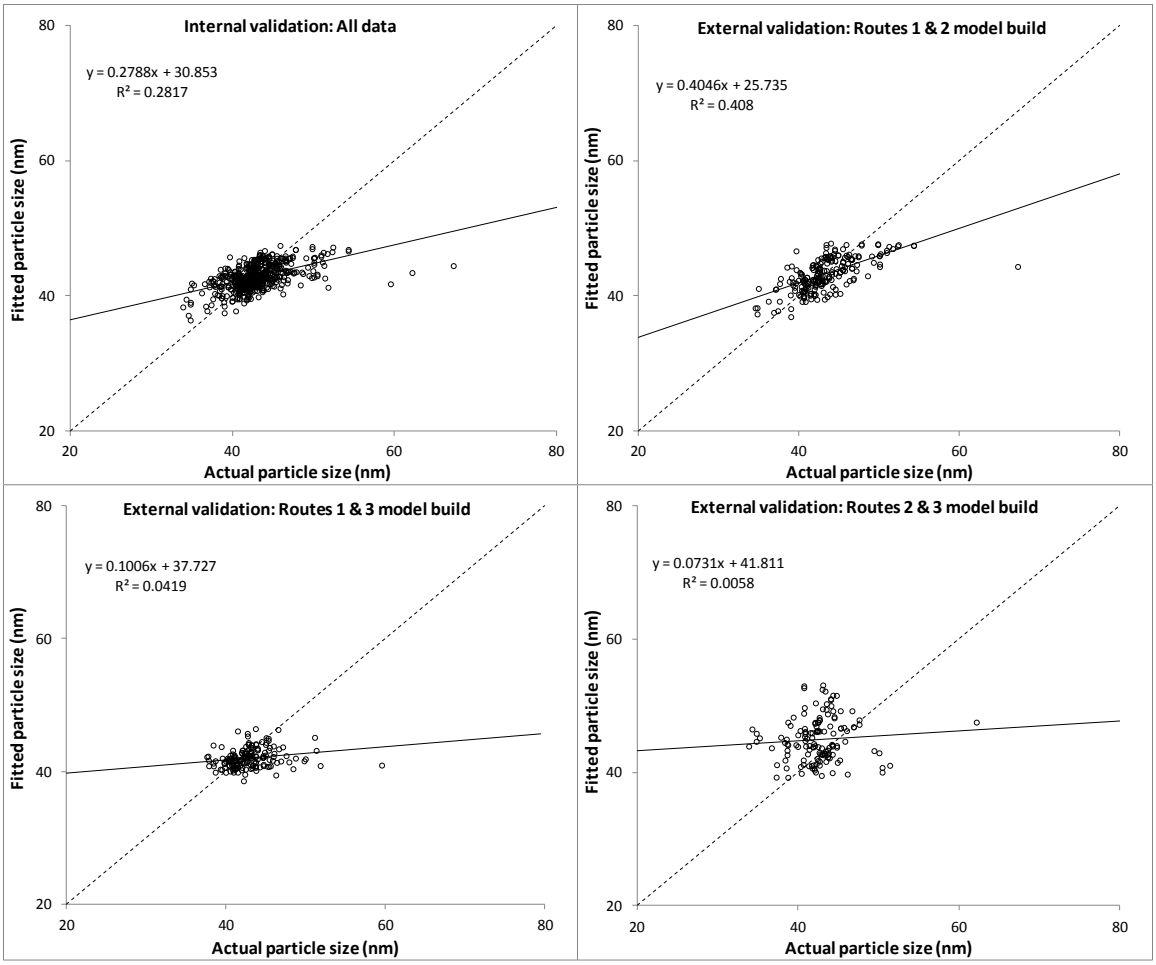

Figure 4.24 Morning geometric mean particle size sampling runs: Actual vs. predicted for the full model (upper left) and three systematic validation cases which involved building models using two routes and predicting concentrations from the third route (route 3 test dataset [upper right], route 2 test dataset [lower left], route 3 test dataset [lower right]).

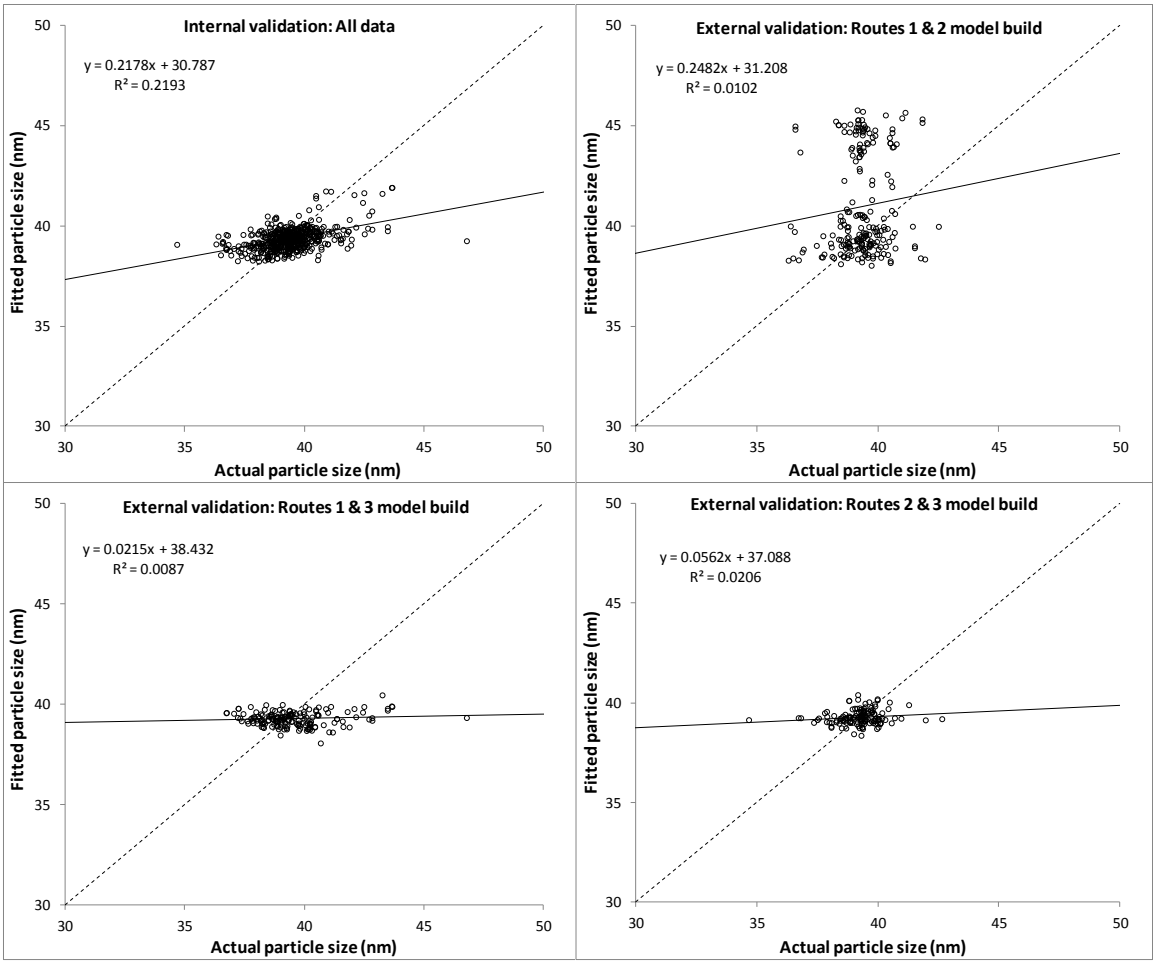

Figure 4.25 Afternoon geometric mean particle size sampling runs: Actual vs. predicted for the full model (upper left) and three systematic validation cases which involved building models using two routes and predicting concentrations from the third route (route 3 test dataset [upper right], route 2 test dataset [lower left], route 3 test dataset [lower right]).

Models were not robust to the systematic validation approach. R^2 values were low for predicted vs. observed concentrations for nearly all validation models; in many cases the predicted vs. observed concentrations did not appear to be well correlated. This finding is perhaps because of how the sampling routes were chosen. I strived to span the variable space for many predictor variables when designing the sampling routes; namely,

road type (as a proxy for traffic intensity), industrial land use, open space area, and various quadrants of the City. Since my study design required completing sampling routes in 2 hour periods, I was not able to balance spanning all of these factors within each individual sampling run; instead, my goal was to span the variable space for these predictor variables among all sampling routes. Thus, this validation approach may be an overly lofty criterion for an acceptable model based on my data collection method. For example, route 3 was disproportionately on off-street trails through parks and on mostly local roads; thus, concentrations were typically lower on that route than on routes 1 and 2. Because of that difference, one would not expect the models built using routes 1 and 2 to accurately predict concentrations on route 3. As another example, route 2 was concentrated mostly in downtown Minneapolis, which typically had higher concentrations than the other two routes. Furthermore, there was high variability in what types of land use dominated on each sampling route. For example, route 2 had disproportionately high retail area, length of major road, and traffic intensity since that route was mostly located downtown; route 1 had the lowest retail area, length of major roads, and traffic intensity but had significantly more industrial area than the other two routes. Figure 4.26 and 4.27 shows the distribution of concentrations at aggregation locations for the LUR models and select land use and road characteristics for each sampling route to illustrate these differences. In general, variability for land uses was larger than for concentrations among the sampling routes; variability in concentrations was larger in the mornings than in the afternoons.

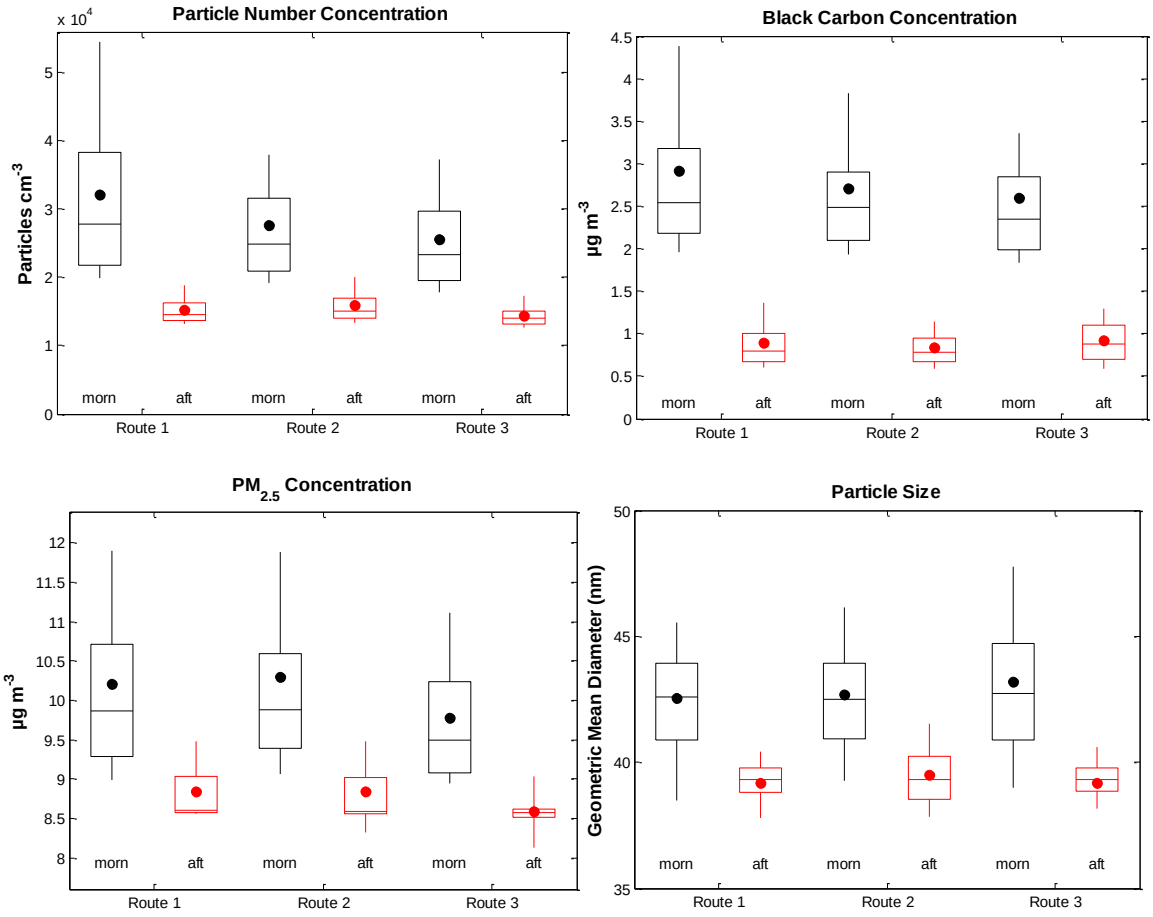

Figure 4.26 Concentrations at aggregation locations used for LUR modeling (100m resolution) by sampling route.

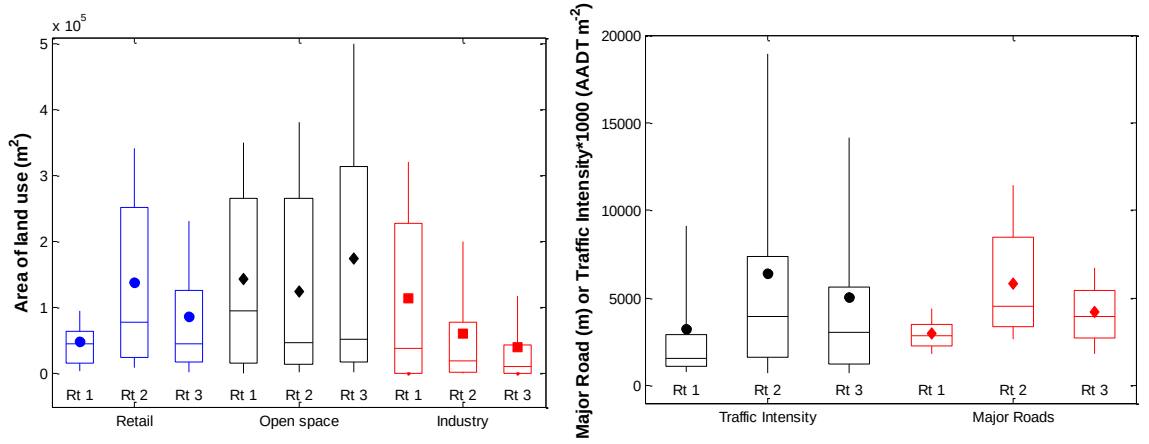

Figure 4.27 Distribution of select land use variables (500m buffer) at the aggregation locations used for LUR modeling (100m) by sampling route.

Scatterplots of predicted vs. observed concentrations for the full models (see Figures 4.18-4.25) suggest that the final LUR models likely underestimate higher (and more infrequent) concentrations. (This behavior was exacerbated when the dependent variable [i.e., pollutant concentration] was not log-transformed.) Therefore, my extrapolated estimates of concentrations may be a conservative estimate of the spatial variability of particulate concentrations. One reason for this behavior may be that the range in concentrations was relatively small (and concentrations were generally low) for many of the models (e.g., black carbon and $PM_{2.5}$ models) making it difficult to build models that accurately estimate the relatively fewer higher concentrations. Using this approach in a study area where there are more observations with high concentrations may help better specify the models. Alternatively, greater attention to obtaining independent variables corresponding to high-concentration conditions might improve the model in the future. Another issue may be the lack of data specific to traffic patterns during rush-hours (see discussion of spatial autocorrelation of model residuals in the next section); areas where concentrations were underestimated were most frequently places where there was heavy congestion (typically on arterial roads near on/off ramps to freeways) during rush-hour. Future modeling may wish to seek out real-time traffic data, or other real-time data that may correlate with emissions, to improve the model's ability to predict high-concentration episodes. Models of particle size showed an especially dampened estimate of the variability in the observed values; this finding is perhaps an effect of the time averaging (60s) inherent to the instrument used to collect particle size measurements

(NanoScan) and spatial averaging used to aggregate measurements (200m aggregation location separation).

Assessing spatial autocorrelation

I explored spatial autocorrelation among model residuals to assess overall model fit as well as any patterns in locations where model estimates were poor. A common metric used to assess spatial autocorrelation in LUR modeling and other contexts is Moran's I. Moran's I tests for correlation between a value and other observations in close geographic proximity to that value. It is a global statistic giving one value for an entire dataset; Moran's I ranges from -1 to 1 with -1 representing perfect dispersion (i.e., perfect anti-correlation), 0 representing a random distribution, and 1 representing a high degree of clustering (i.e., perfect correlation). I tested LUR model residuals using Moran's I to assess model fit. A perfect model with no autocorrelation in residuals would give a Moran's I near 0. I varied the input parameters for Moran's I including how the weights matrix is calculated (inverse distance, inverse distance squared, or all points in a fixed distance) as well as the search radius for calculating the parameter (all calculations were performed in ArcGIS 10.1). Results for each model are in Table 4.13.

Table 4.13 Global Moran's I for LUR model residuals

	Inverse distance				**Inverse distance squared**				**Fixed distance**			
	100m	**250m**	**500m**	**1,000m**	**100m**	**250m**	**500m**	**1,000m**	**100m**	**250m**	**500m**	**1,000m**
PN morning	0.44	0.32	0.23	0.16	0.38	0.34	0.30	0.28	0.47	0.29	0.16	0.10
PN afternoon	0.59	0.55	0.41	0.23	0.94	0.84	0.75	0.67	0.53	0.50	0.29	0.06
BC morning	0.61	0.35	0.22	0.13	0.61	0.48	0.41	0.37	0.50	0.23	0.09	0.03
BC afternoon	0.53	0.39	0.27	0.15	0.42	0.38	0.34	0.30	0.56	0.34	0.18	0.03
$PM_{2.5}$ morning	0.33	0.23	0.17	0.09	0.24	0.21	0.19	0.17	0.37	0.21	0.12	0.03
$PM_{2.5}$ afternoon	0.54	0.46	0.33	0.18	0.76	0.67	0.60	0.53	0.49	0.41	0.22	0.03
Size morning	-	0.19	0.09	0.05	-	0.17	0.12	0.10	-	0.21	0.07	0.01
Size afternoon	-	0.14	0.08	0.03	-	0.13	0.10	0.07	-	0.16	0.06	-0.01

In general, the model residuals showed moderate spatial autocorrelation. Typically, the residuals for the afternoon models had higher spatial autocorrelation than mornings. As the search radius increased, Moran's I decreased; that result suggests that spatial autocorrelation is mostly an issue at small geographic scales. Here, the 100m distance represents a strict test of spatial autocorrelation since that distance represents testing against the nearest neighbor (i.e., I aggregated measurements at 100m distances), the 250m search radius represents testing against ~5 neighbors, and the 500 meter search radius ~10 neighbors. ESRI suggests setting the search radius to include at least 8 neighbors (ESRI, 2014). Previous LUR models typically strive for values of Moran's I that are nearer to zero than reported here; a difficulty in comparing spatial autocorrelation in my sample vs. previous LUR models is that my concentration estimates are separated by short distances and are likely influenced by similar emission sources (e.g., passing vehicles) and thus any one location along the sampling routes that is underestimated by the model likely also has neighbors that are underestimated. Other differences in my work relative to other LURs include the inclusion of mobile monitoring, and the far larger number of individual measurements in my sample relative to a typical LUR (though for much shorter averaging time in my case).

To explore the local patterns of spatial autocorrelation, I used a Local Indicator of Spatial Analysis (LISA) developed by Anselin (1995) to assess the spatial patterns of the spatially autocorrelated model residuals. I used a LISA in ArcGIS called Anselin Local Moran's I. This statistic is similar to the Global Moran's I but instead the statistic is calculated for each observation individually. LISA separates the variable of interest (i.e.,

model residuals) into 5 groups: (1) clusters of high values (in this case high residuals are model underestimates), (2) clusters of low values (model overestimates), (3) low value spatial outliers (low value near cluster of high values), (4) high value spatial outliers (high values near a cluster of low values, and (5) values that were not clustered or outliers. I mapped values that were classified as either clusters or spatial outliers to assess where model estimates were poor. Maps for the traffic-related pollutants (particle number, black carbon) are shown in Figure 4.28; maps for the area source pollutants ($PM_{2.5}$, particle size) are shown in Figure 4.29.

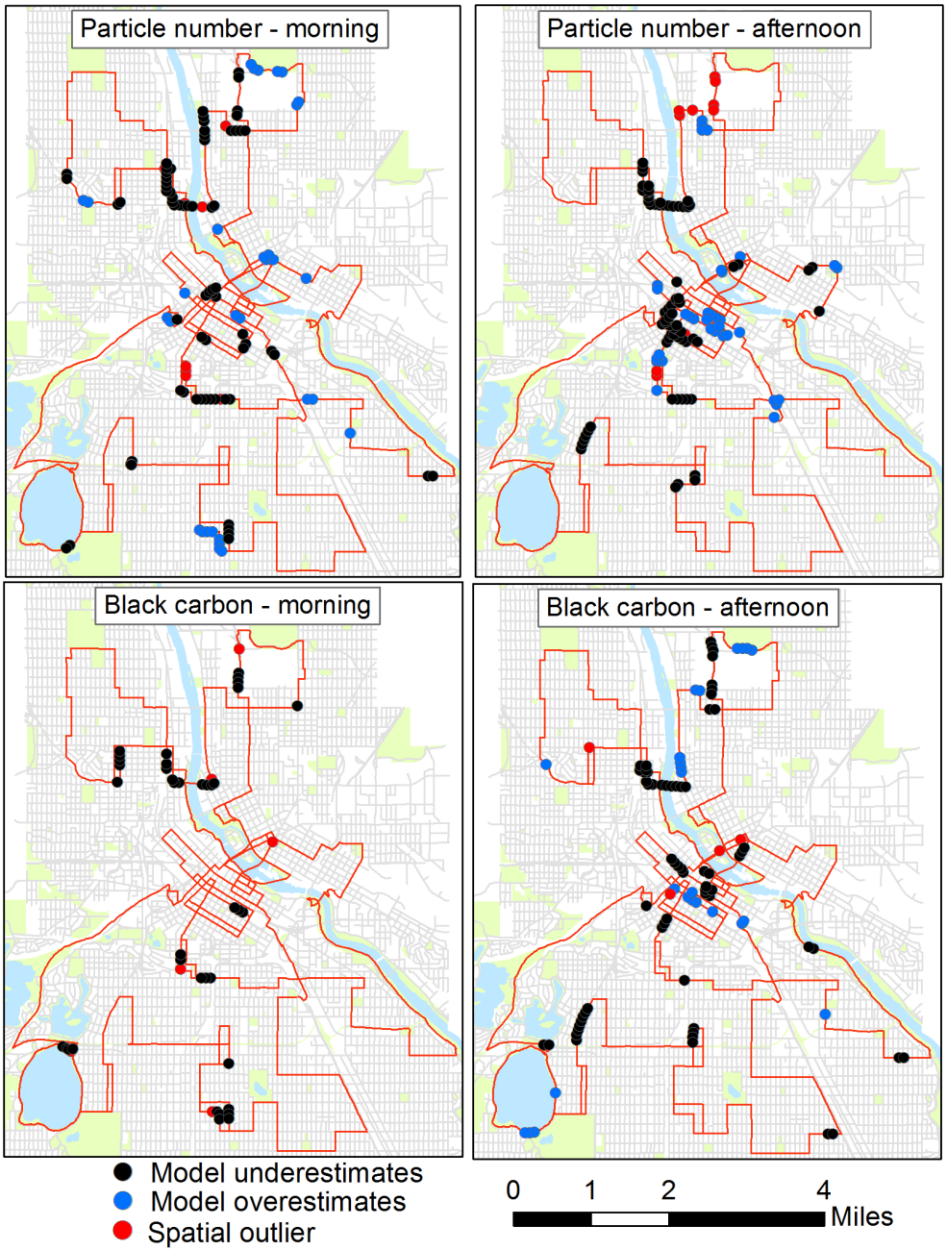

Figure 4.28 Outliers and clusters of model over/underestimates identified by LISA (Anselin Local Moran's I) analysis for the traffic-related pollutants. Locations shown for outliers where models over and underestimate concentrations.

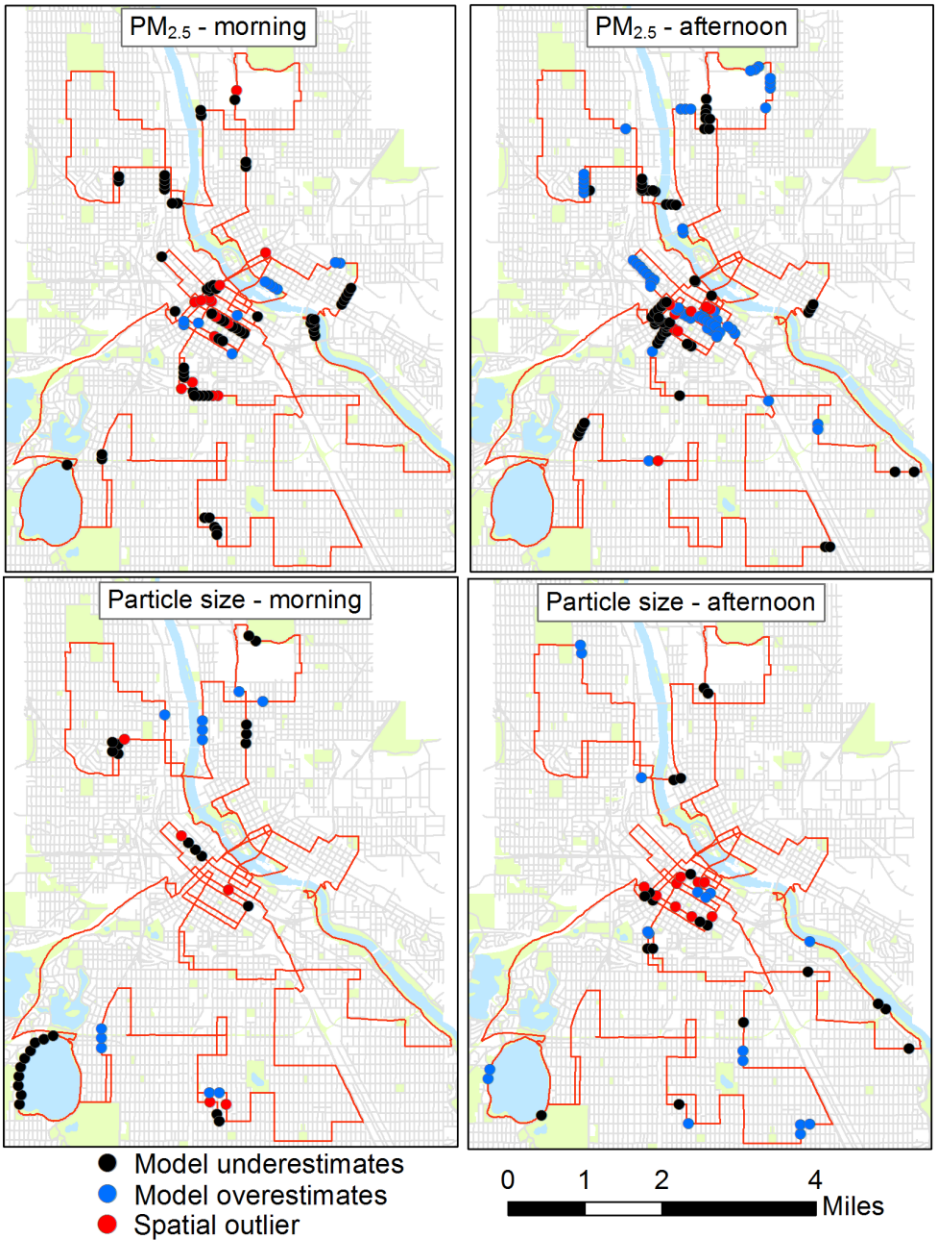

Figure 4.29 Outliers clusters of model over/underestimates identified by LISA (Anselin Local Moran's I) analysis for the area-scale pollutants. Locations shown for outliers where models over and underestimate concentrations.

For the LISA analysis, most values were not classified as clusters or outliers (see Table 4.14); among the values classified as clusters (~10%), most were locations where the model underestimated concentrations. There were observable patterns in the

clustering of model under/over estimates; specifically, the model tended to underestimate concentrations in areas where high levels of congestion occur during rush-hour. Areas commonly underestimated among all models were: (1) various streets in downtown Minneapolis, (2) portions of Franklin Ave near the I-35W on/off ramps, (3) the Broadway Ave. bridge and Washington Ave. near the I-94 on/off ramps, and (4) various heavy-traffic arterial streets. During sampling runs these locations were typically heavily congested; sometimes I was unable to pass through the congestion by bicycle (with the trailer) and thus was forced to wait in idling traffic for long periods of time. Examples from the video footage are shown in Figure 4.30.

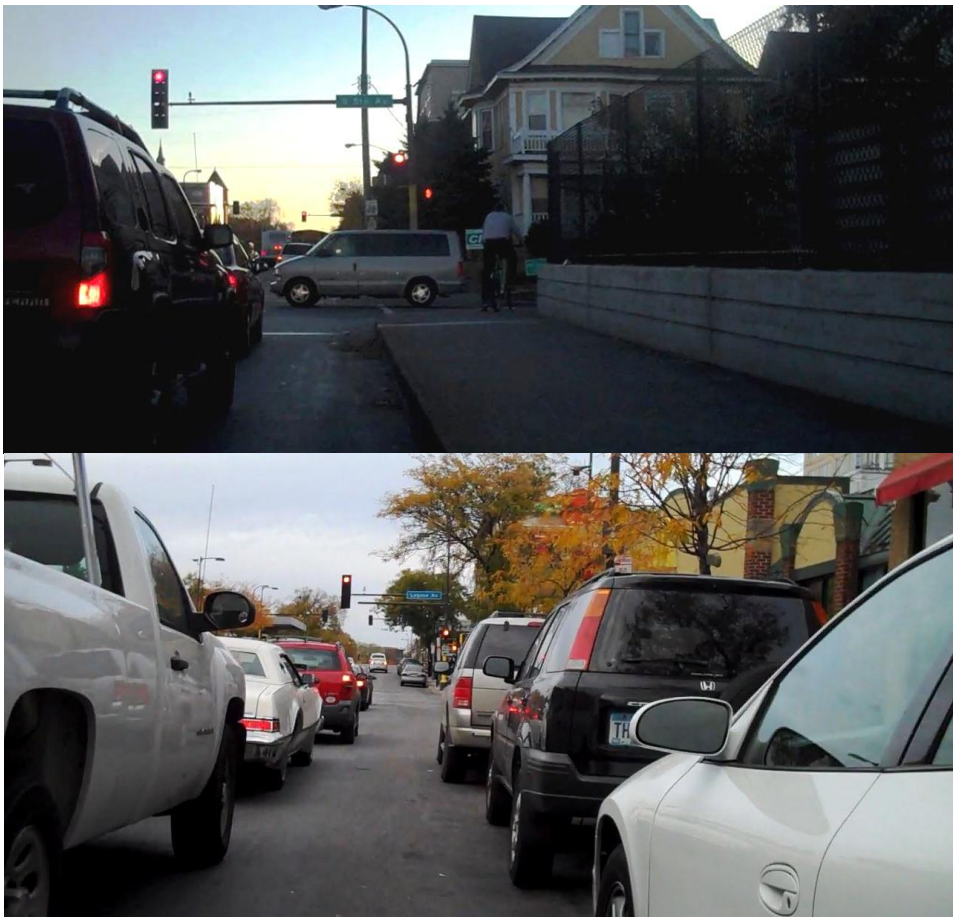

Figure 4.30 Example of congested locations where models underestimate concentrations (Franklin Ave. above I-35W [top]; Hennepin Ave in South Minneapolis [bottom]).

It is likely that my models do not estimate concentrations well in the congested areas because spatial information on congestion was not available to use as a predictor variable in the LUR models. I used a metric derived by the Minnesota Pollution Control Agency (MPCA) that quantifies traffic intensity; however, that metric was calculated using annual average daily traffic (AADT) estimates. AADT does not capture hourly patterns in traffic or congestion on small stretches of road; it instead captures variability in traffic by road segment for average daily totals. Another issue that may impact model estimates in these areas is that I have not included variables in the LUR models that account for traffic mix (i.e., truck vs. passenger-vehicle). Spatial estimates of truck traffic were not available for the entire City; Minnesota Department of Transportation does estimate truck traffic for a select few roads in the City (mostly state aid highways) but since my goal was to estimate models based on data that was available for the entire City (i.e., to extrapolate estimates), I did not include those estimates in my models. In general, better spatial information about motor vehicle patterns would likely improve LUR model performance for on-road concentrations, especially for models (like those presented here) that aim to estimate concentrations during specific times of day. Proportions of aggregation locations classified as clusters of model over/under estimates and outliers are shown in Table 4.14.

Table 4.14 Aggregation location (LUR model inputs) classified as clusters of over/underestimates or outliers by LISA

	Cluster		Spatial outlier	Not significant
	Model underestimate	Model overestimate		
PN morning	6.4%	2.8%	0.7%	90.1%
PN afternoon	6.4%	3.3%	0.9%	89.4%
BC morning	3.5%	0.0%	0.5%	95.9%
BC afternoon	6.0%	2.2%	0.4%	91.5%
$PM_{2.5}$ morning	5.3%	1.0%	1.3%	92.4%
$PM_{2.5}$ afternoon	5.1%	5.1%	0.7%	89.0%
Size morning	4.5%	2.0%	0.9%	92.5%
Size afternoon	3.5%	3.1%	1.6%	91.8%

Comparison to other LUR studies using mobile measurements

There are a limited number of studies that use mobile measurements to develop LUR models (I summarized only studies with mobile measurements, not rotating fixed-sites). Very few of the studies design measurement campaigns with the goal of model building to extrapolate estimates. In Table 4.15, I have summarized these studies by pollutant and model performance. Only 3 studies designed measurements with the goal of extrapolation, and all were for woodsmoke (two in Vancouver, Canada; one in upstate New York). Most studies in Table 4.15 collected measurements using motor vehicles and many focused (at least partly) on freeways. Many of the studies included real-time traffic estimates as predictor variables for the time of measurement collection; in most cases this approach precludes the possibility of extrapolating estimates to locations without automated counters. In general my models performed similarly (by model R^2) to the other studies. Only my models used mobile measurements to estimate particle size and black carbon concentration; similarly, they were also the only models to extrapolate estimates other than $PM_{2.5}$ from mobile measurements.

Table 4.15 Summary of other studies using mobile measurements to develop LUR models

Study	Pollutants	Location	Mode	Geographic scale	For extrapolation	Regression	Model R^2	Notes
This study	PNC BC $PM_{2.5}$ Particle size	Minneapolis, MN	Bicycle	Urban area	Yes	Linear	Adj-R^2: Morning (afternoon) PNC: 0.50 (0.48) BC: 0.28 (0.42) $PM_{2.5}$: 0.3 (0.49) Size: 0.29 (0.20)	Did not use real-time traffic inputs; goal of models is for extrapolation.
Patton et al. (2014)	PNC	Somerville, MA	Recreational vehicle	Neighborhood (near freeway)	No	Linear	0.38-0.47 (cross validated [CV])	Short sampling route near freeway. Included real-time traffic counts.
Larson et al. (2007)	Particle light absorption coefficient	Vancouver, BC	Motor vehicle	Urban area	Yes	Linear	0.64	Measurements at night (winter). Model for emissions from woodsmoke.
Larson et al. (2009)	Particle light absorption coefficient	Vancouver, BC	Motor vehicle	Urban area	Yes	Linear	0.56 (CV)	Same as Larson et al. (2007) but summertime measurements.
Su et al. (2011)	$PM_{2.5}$ (woodsmoke)	Upstate New York	Motor vehicle	Seven counties	Yes	Linear	0.58	Combined fixed-site and mobile monitoring. Sampling at night for woodsmoke.
Zwak et al. (2011)	PNC $PM_{2.5}$	Brooklyn, NY	Pedestrian	Neighborhood	No	GAM	PNC: 0.32 $PM_{2.5}$: 0.85	Walked neighborhood routes. Used real-time traffic counts.
Li et al. (2014)	PNC $PM_{2.5}$ NO_x PB-PAH	Los Angeles, CA	Hybrid vehicle	Urban area	No	Linear GAM	PNC: 0.45 $PM_{2.5}$: 0.51 NO_x: 0.37 PB-PAH: 0.41	Good spatial coverage. Used real-time traffic data. Modest improvement for GAM models (R^2 increased 0.5-0.1)
Aggarwal et al. (2012)	PNC	Minneapolis, MN	Motor vehicle	Urban area	No	Linear	0.77 (adj-R^2)	Freeways only; used real-time traffic data.

Chapter conclusions

This chapter described an approach for developing LUR models using mobile measurements of particulate air pollution. I developed n=1,224 LUR models, of which n=612 are reported above. Many of the models were developed to test whether certain parameters such as averaging time and method of spatial aggregation have an impact on model performance. I chose final models for extrapolation based on trends observed during the analyses described above and to ensure final models would be comparable to the estimates of bicycle and pedestrian traffic described in the following chapter. I explored final model performance using random and systematic hold-outs of the input data as well as exploring trends in spatial autocorrelation. Below are main findings from this chapter.

Methodological findings

1. LUR models with no time averaging (i.e., 1s measurements [60s for the NanoScan]) performed similarly to those with slight time averaging (i.e., 10-300s). Measurements for black carbon (from the micro-aethalometer) required slight smoothing (60s).
2. Model performance for central tendencies of the measurements at each aggregation location was similar for various spatial resolutions. The ability to estimate distributional parameters (i.e., 10^{th} and 90^{th} percentiles) was diminished as spatial resolution increased because the number of measurements per aggregation location decreased.

3. LUR models were somewhat robust to validation using a random holdout of measurement locations (mean decrease in model R^2 between model-building and model-testing: 0.07) but not robust to a systematic validation performed by alternately holding out each sampling route (mean decrease in R^2: 0.20). Models typically underestimated the highest observed concentrations.
4. Spatial autocorrelation was present for model residuals in clusters along the sampling route. Locations that were spatially autocorrelated were usually places where models underestimated concentrations; these areas were typically congested with vehicle traffic during sampling. Better information on the spatial patterns of traffic at specific times of day (to use as a predictor variable) would likely improve model performance.
5. Future studies that use mobile measurements to estimate LUR models should explore how the frequency of sampling a route and the number of days sampled can impact model performance. The only modest goodness-of-fit statistics reported here (morning [afternoon] adjusted R^2 were 0.50 [0.48] for particle number, 0.28 [0.42] for black carbon, 0.30 [0.49] for $PM_{2.5}$, and 0.29 [0.20] for particle size) may partially be a result of uncertainty of the concentration estimates at each aggregation location. This uncertainty could be reduced by completing more sampling runs (I collected 25 [62] hours of morning [afternoon] on-road and 12 [30] hours of reference site measurements; 886 total miles cycled). Similarly, applying this approach in a more polluted study area may yield more insight into model performance at higher concentrations.

6. Aggregating measurements at a smaller spatial resolution (e.g., 25m) would be helpful to determine if models perform similarly with smaller amounts of data per aggregation location.

Empirical findings

1. LUR models had modest goodness-of-fit and performed best for particle number concentration (morning [afternoon] adjusted R^2: 0.5 [0.48]) followed by $PM_{2.5}$ (adj-R^2: 0.3 [0.49]) and black carbon (adj-R^2: 0.28 [0.42]). Models performed worst for particle size (adj-R^2: 0.29 [0.2]).
2. Independent variables that were frequently selected among the LUR models were those related to separation from emission sources (e.g., open space area, distance from major roads, length of local [low-traffic] roads) and proximity to and density of emission sources (e.g., industrial area, house density, length of high-traffic roads).
3. Industrial area was selected in all of the final LUR models (at buffer distances of 75-3,000 meters). Chapter 3 presents regression results that suggest industrial area and truck traffic are correlated and that trucks are important predictors of on-road concentrations. More spatial information on truck traffic may help improve LUR model performance.
4. Areas that demonstrated strong spatial autocorrelation for model residuals were located on roads with high congestion near entrances and exits to freeways. Since hourly estimates of congestion are not readily available (spatial patterns of congestion are also not available) this variable is difficult to capture in LUR

models and is likely (at least partly) responsible for the model underestimates at high concentrations. Future studies should strive to acquire real-time estimates of traffic data to better explain hourly spatial patterns of air pollution concentrations.

5. Models for $PM_{2.5}$ and particle size suggest that lower income households are located in more polluted areas (higher $PM_{2.5}$ concentrations, lower particle size) corroborating other findings of environmental injustice in previous studies.

Chapter 5 Comparing spatial patterns of particulate air pollution and non-motorized traffic in Minneapolis, MN

One potential use of the air pollution measurements and models described in the previous chapters is that the results from those analyses can be used to make estimates of particulate air pollution concentrations at locations in Minneapolis where measurements don't exist. Estimates of concentrations potentially have practical uses for policy-makers, planners, researchers, and the general public. The concentration estimates may be used in exposure assessment, building low-exposure bicycle and pedestrian transportation networks, identifying concentration hot-spots, or identifying areas of environmental injustice. Developing models that are capable of estimating the spatial patterns of pollutant concentrations are an important contributor to planning for healthy, clean cities.

In this chapter I outline an example application of the LUR models developed in Chapter 4. Specifically, I compare the spatial patterns of particulate air pollution, bicycle traffic volumes, and pedestrian traffic volumes in Minneapolis to explore patterns of population level exposure during non-motorized travel. Below, I first explain how I extrapolated estimates of particulate air pollution concentrations to the entire City. Then, I describe how I developed statistical models to estimate bicycle and pedestrian traffic volumes for all streets in Minneapolis using volunteer-based counts of bicycles and pedestrians from 2007-2010. Finally, I compare the spatial patterns of non-motorized traffic with the patterns of particulate air pollution and discuss the implications for urban planning.

Estimating particulate concentrations for all locations in Minneapolis

Using the eight LURs from Chapter 4 (four pollutant attributes, two times-of-day), I estimated concentrations on all street segments in Minneapolis, MN. Street segments were defined as the road between any two intersections. I estimated concentrations at the midpoint of each street segment to match the estimates of bicycle and pedestrian traffic volumes (also by street segment) described below. This procedure resulted in 12,369 point estimates of on-road particulate concentrations across the City (median road segment length: 120 meters). A slightly different approach was used to estimate concentrations for off-street trails. Since the trail network is much less extensive than the road network defining a trail segment as the distance between two intersections resulted in long segments of trail. Instead, I chose to make estimates of concentrations at 100 meter intervals along the trail network to match the spatial resolution of the LUR models. This approach resulted in estimates of air pollution at 1,235 trail locations. Combining with the on-road estimates yields a total of 13,569 point estimates.

Using the base-case models described in Chapter 4 required calculating 69 of the candidate buffer variables and 3 of the point variables at every extrapolation location. I used the same methods for calculating buffer variables as described in Chapter 4; calculating the buffer variables required significant processing time (each variable took ~24 hours to calculate on a single computer). Once all independent variables were calculated, I applied the 8 base-case regression equations to estimate concentrations; results were then transformed back to a normal concentration scale (dependent variable inputs were log-transformed; see Chapter 4). Figures 5.1-5.4 show maps of estimated

concentrations for each model. Color ramps to classify concentrations are shown on an absolute scale; however, the scale is different between mornings and afternoons so spatial patterns were visible during both times of day. (Concentrations were typically higher in the mornings.)

Particle number concentrations (Figure 5.1) followed similar patterns in mornings as in afternoons; however, estimated concentrations (and variability in concentrations) were higher in the mornings than in the afternoons. Elevated concentrations were mostly in areas near activity centers (e.g., downtown Minneapolis and portions of South Minneapolis) and along industrial corridors and railway areas in North and Northeast Minneapolis. Smaller-scale areas of elevated concentrations were generally on or near major roads. Concentrations were lowest in areas away from downtown with low density of major roads. An interesting shift in the spatial patterns between morning and afternoon rush-hour is that areas with the highest concentrations seemed to be near or on freeways in the mornings (e.g., just southwest of downtown near the I-94 and I-35W interchange) and higher on major roads feeding onto freeways in the afternoon (e.g., in downtown Minneapolis or major roads in surrounding neighborhoods). Since I do not have measurements where the elevated concentrations are located in the morning, I have no way to check if this shift is real or an artifact of the extrapolation procedure.

Black carbon concentrations (Figure 5.2) mostly followed similar spatial patterns to those observed for particle number concentrations. Concentrations were high near activity centers in downtown and South Minneapolis, near industrial areas, and along or near major roads. In general the black carbon concentrations seemed to be more localized

(i.e., decrease rapidly from major roads or activity centers) than particle number concentrations. One area where the model results were higher than expected is around Lake Calhoun and Lake Harriet in South Minneapolis for the afternoon rush-hour. The first variable selected in that model (see Figure 4.13) is the length of local roads (a proxy for areas with few emissions; negative coefficient) within 1,000 meters; the third variable selected was amount of open space within 3,000 meters (positive coefficient; see Chapter 4 for a discussion of potential confounders with open space at large buffers). Since the lakes take up much of the area around the high concentration areas the open space predictor variable has a high value in this area and the local road variable is likely small. Since this area type is unique in Minneapolis it is likely that this area is misrepresented in the model and the corresponding concentration estimates could be overestimates.

General patterns of $PM_{2.5}$ concentrations (Figure 5.3) were similar to patterns for black carbon and particle number concentrations. Downtown and industrial areas in North and Northeast Minneapolis showed mostly elevated concentrations (along with portions of South Minneapolis in the morning). Small-scale variability of $PM_{2.5}$ concentrations was notably lower than for particle number and black carbon concentrations; especially, in the afternoon where most of the estimates fall within a ~1 $\mu g/m^3$ range. The highest $PM_{2.5}$ concentrations in the afternoon were estimated along Marquette Ave. and 2nd Ave. where the density of both bus routes and bus stops are high. Estimated concentrations were lowest in Southwest Minneapolis where emission density is relatively low and median household incomes are highest.

Spatial patterns of particle size were the most spatially smoothed among the four measures of particulate air pollution. This relatively smooth surface could be (1) a real pattern for average particle size in the City or (2) an artifact of the measurement instrument used (the NanoScan needs 60s to complete a particle size distribution scan) or the slightly higher degree of spatial smoothing that was applied during measurement aggregation (i.e., 200m aggregation instead of 100m). The spatial patterns follow intuition in that smaller mean particle sizes are mostly where the other models show the highest concentrations (and thus likely the most fresh emissions) in the City. For example, the smallest particle sizes for both mornings and afternoons seem to be near the freeways (i.e., I-94 and I-35W) as well as in downtown Minneapolis. Since it is expected there would be smaller mean particle size near emission sources and larger particle sizes at greater distances from emission sources the inverted pattern shown in Figure 5.4 is plausible for this measure of particulate air pollution.

Among the four measured parameters of particulate air pollution, the traffic-related pollutants (particle number and black carbon concentrations) demonstrated the most spatial variability. Concentrations of those two pollutants not only varied across the City but also on small-spatial scales (e.g., as distance from a major road increased). Spatial variability in $PM_{2.5}$ concentrations was small (especially in the afternoon); the larger-scale gradients (i.e., downtown to outer lying neighborhoods) were consistent with the other pollutants. Particle size also demonstrated more regional or larger-scale changes than local, small-scale changes and was mostly a function of distance from emission

sources. (Model estimates along a transect across the City are presented later in this chapter to highlight these patterns.)

Spatial variability in estimated concentrations was generally larger in mornings than in afternoons for all four measures of particulate air pollution. Differences between mornings and afternoons were most pronounced for particle number (morning [afternoon] difference between 90^{th} and 10^{th} percentile: 16,200 [3,500] particles cm^{-3}), particle size (7.6 [2.0] nm) and $PM_{2.5}$ (2.3 [0.6] $\mu g\ m^{-3}$). Morning [afternoon] differences in the spatial variability for black carbon concentrations (0.99 [0.37] $\mu g\ m^{-3}$) were still several-fold, though in amounts lower than for the other pollutants. These spatial patterns imply that choices made about where active travel occurs in the morning may be more important than choices made during the afternoon.

To summarize comments above, the spatial patterns of concentrations shown in Figures 5.1-5.4 seem to follow the expected patterns. Namely, concentrations tend to be elevated in areas where there are dense networks of major roads in conjunction with activity centers (downtown Minneapolis, portions of South Minneapolis), near significant emission sources (industrial and railway areas), and lower in areas that are farther from traffic sources (open space and on local roads). Although there are differences in the magnitude of spatial variability and the overall level of estimated concentrations for pollutant the overall results seem to track each other fairly well and generally follow intuition. There are a number of white spaces in the maps shown below; these are locations where there are no roads (or where road density is low). For example, lakes, rivers, parks, or railways among others.

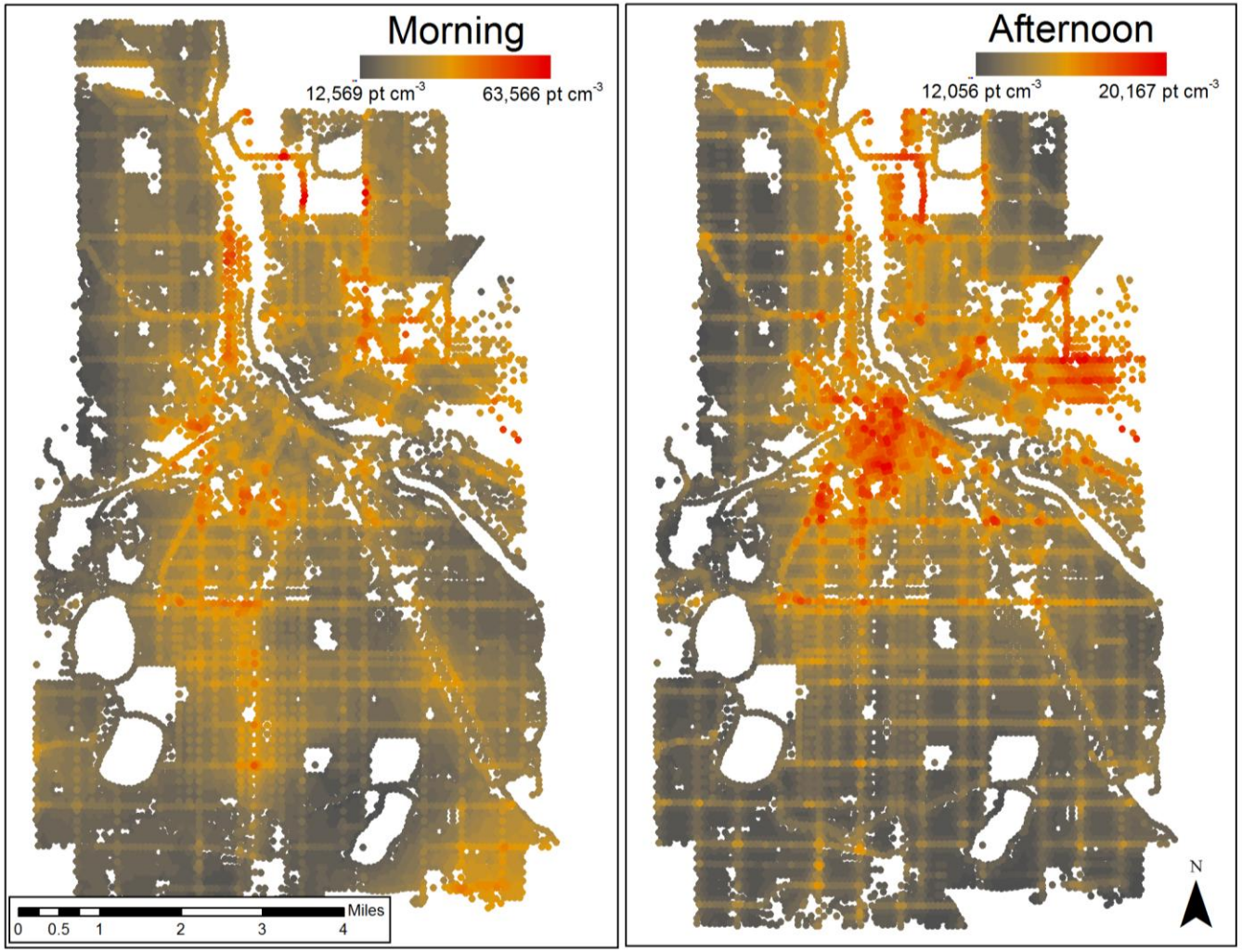

Figure 5.1 Particle number concentration for street segments in Minneapolis, MN. Note: Separate scales for mornings and afternoons.

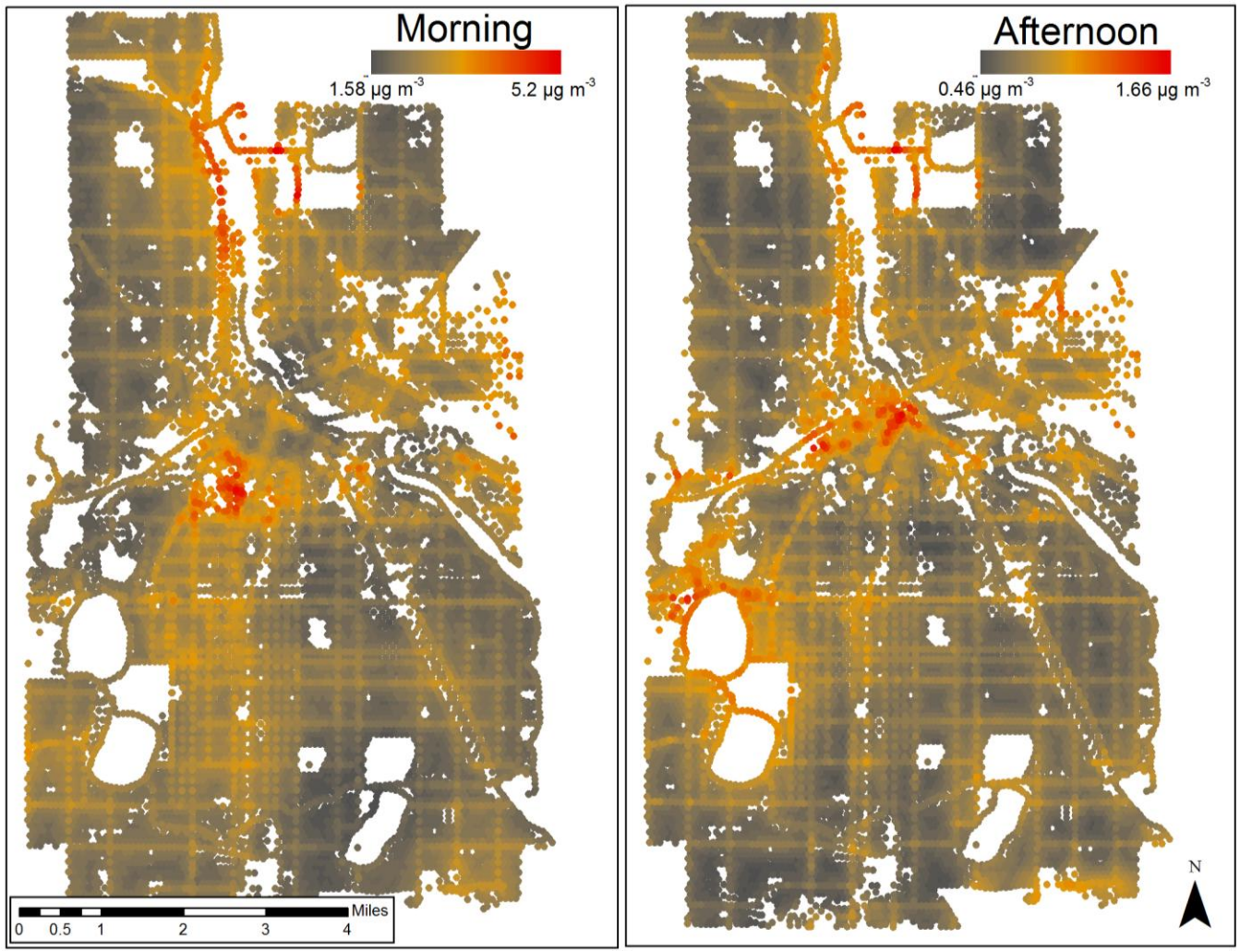

Figure 5.2 Black carbon concentration for all street segments in Minneapolis, MN. Note: Separate scales for mornings and afternoons.

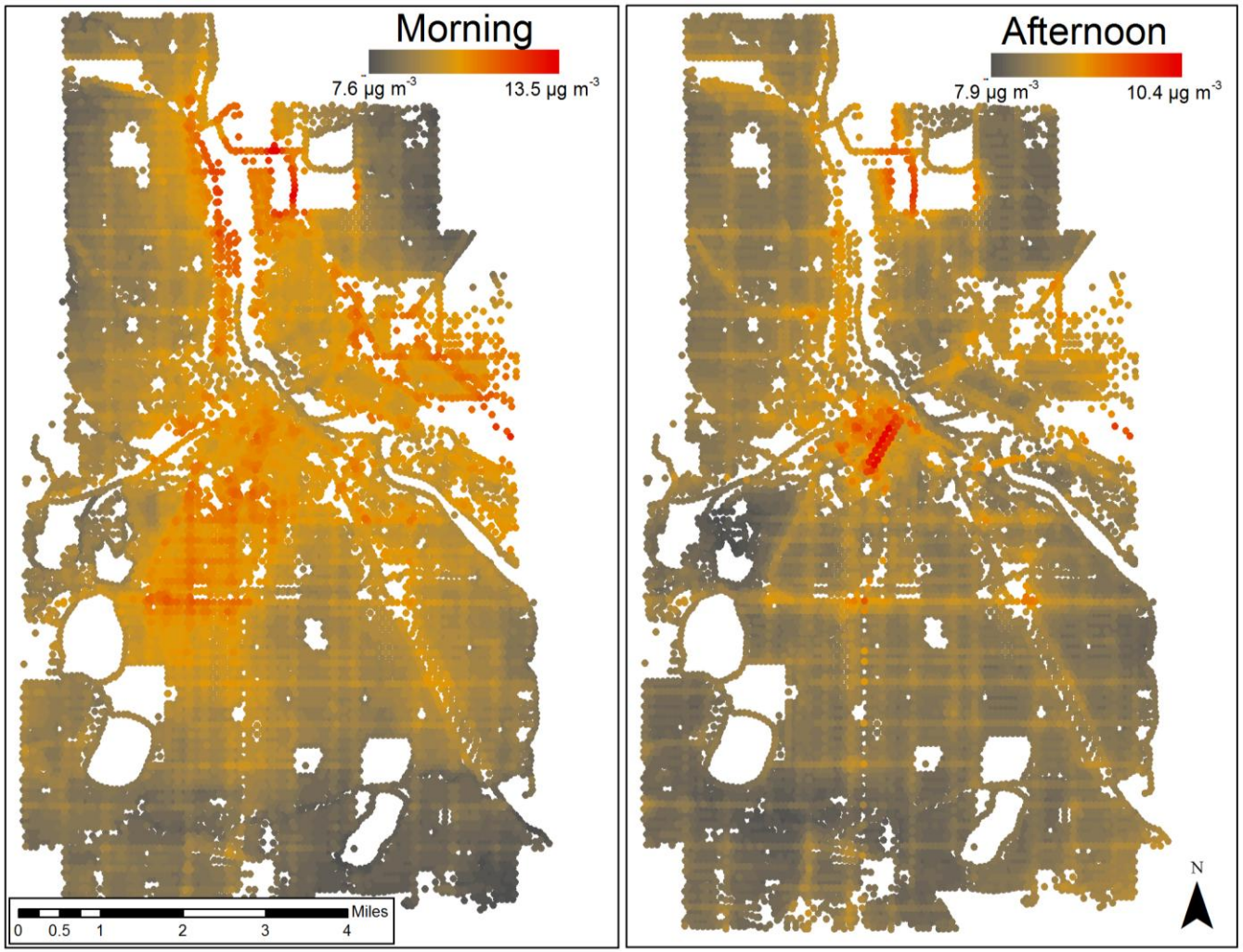

Figure 5.3 $PM_{2.5}$ concentration for all street segments in Minneapolis, MN. Note: Separate scales for mornings and afternoons.

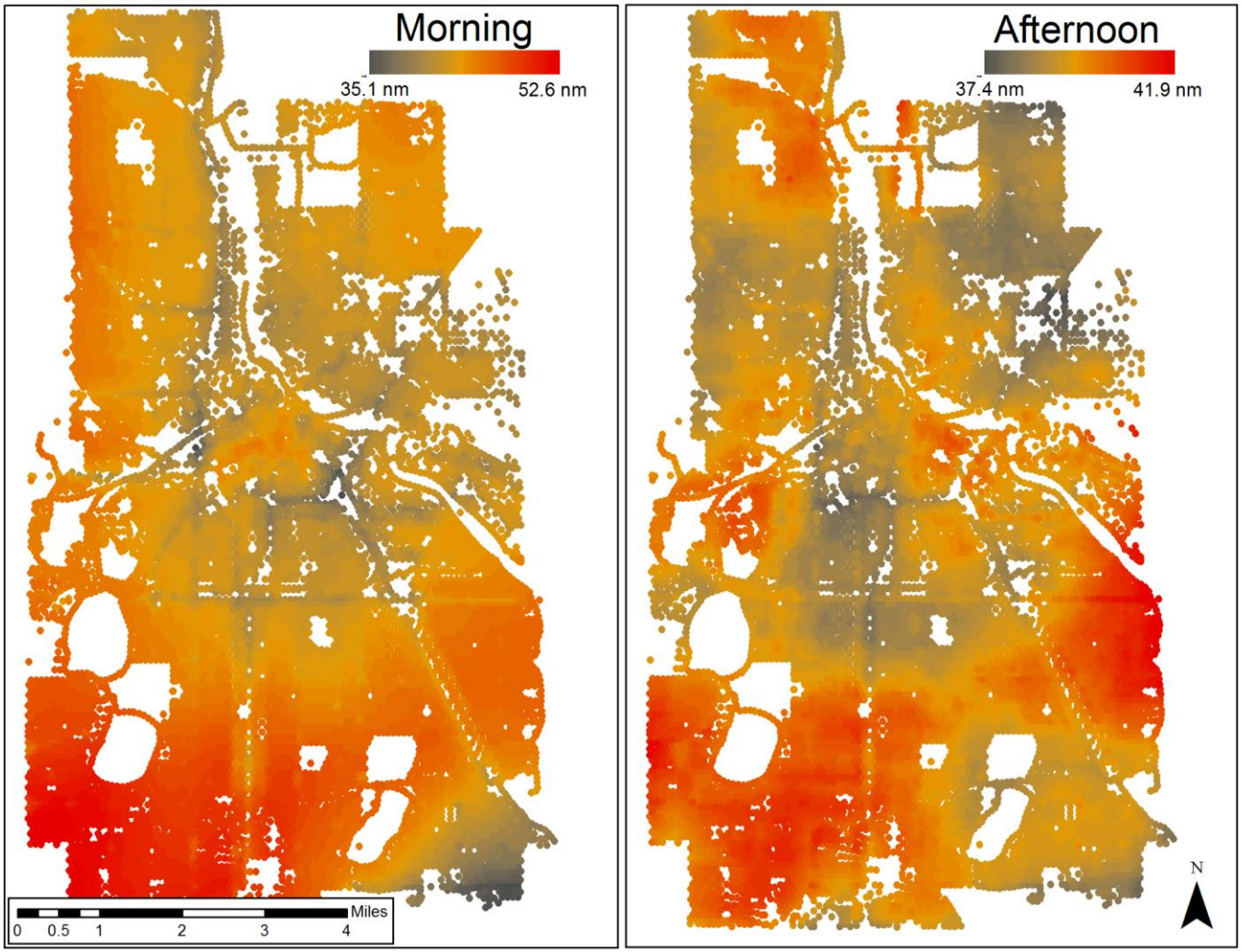

Figure 5.4 Geometric mean particle size for street segments in Minneapolis, MN. Note: Separate scales for mornings and afternoons.

I extracted model estimates along a transect of the City to compare the spatial variability among pollutants. I chose a transect that begins and ends in residential neighborhoods and passes through areas of high emission density such as downtown Minneapolis. As noted above, particle number and black carbon showed more spatial variability than $PM_{2.5}$ and particle size. In general, spatial variability was higher in the mornings than in the afternoons; differences in spatial variability between mornings and afternoons were also largest for particle number and black carbon. Furthermore, the traffic-related pollutants (particle number and black carbon) seemed to track fairly well. Figure 5.5 shows the transect overlaid on model estimates of particle number concentrations in the afternoon; Figure 5.6 shows concentrations as a function of distance along the transect.

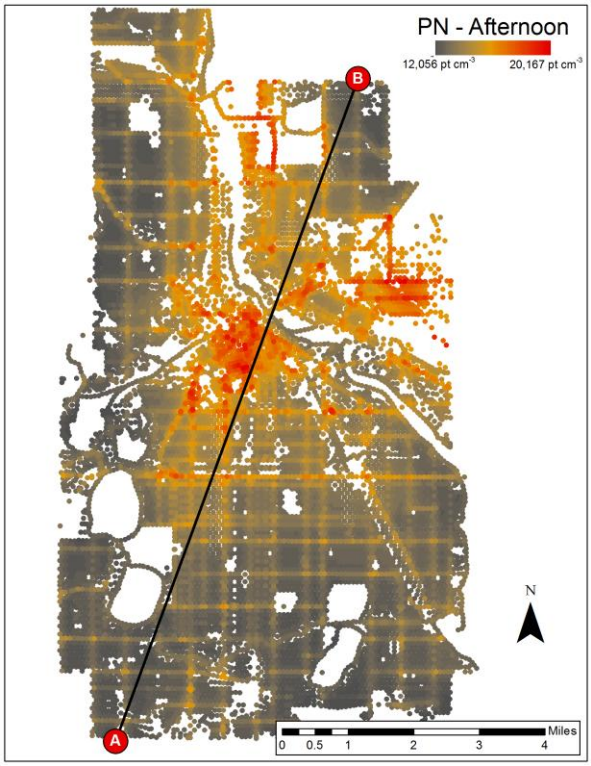

Figure 5.5 Transect used to show degree of spatial smoothing of model concentration estimates (particle number concentration is shown as an example).

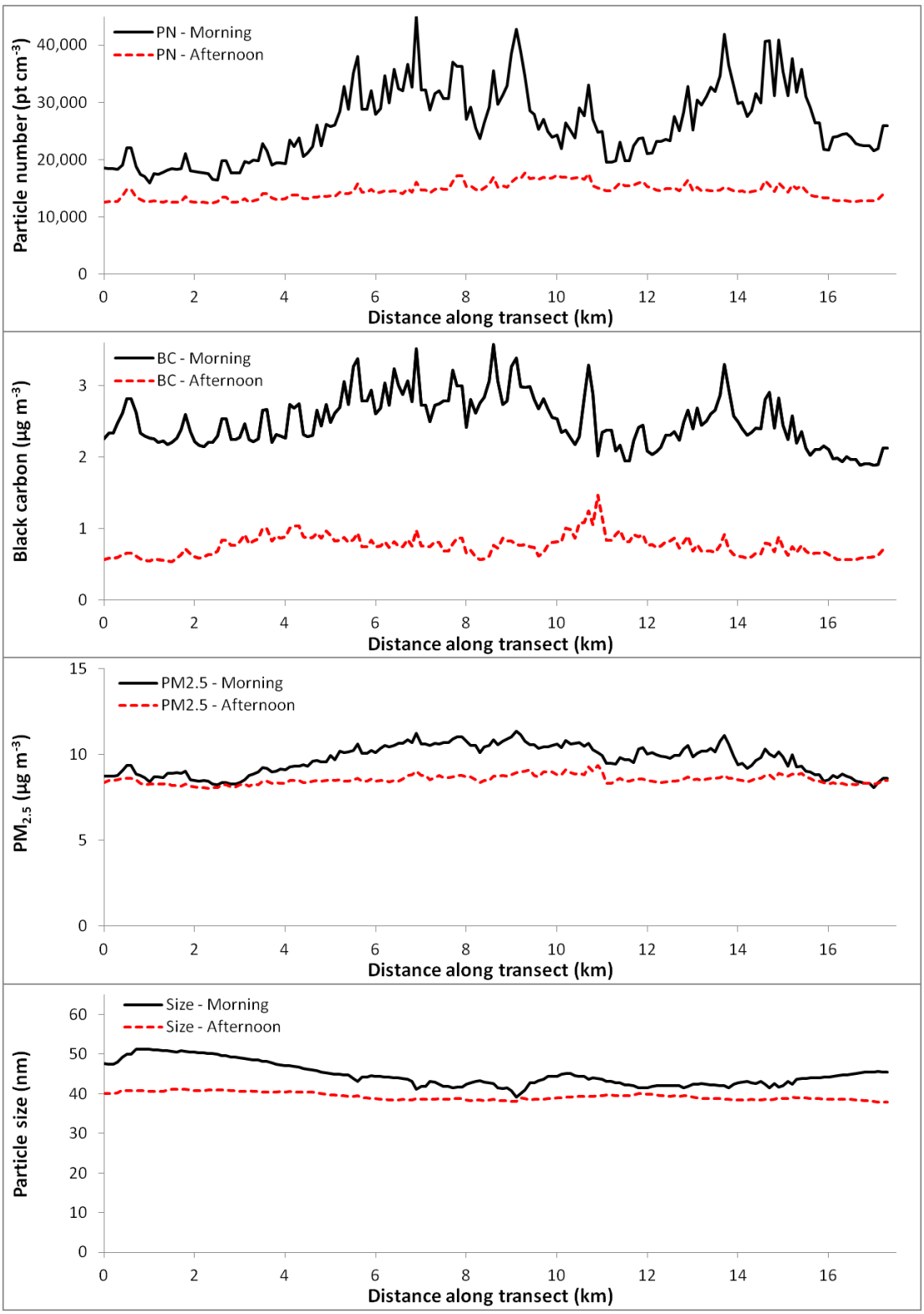

Figure 5.6 Particulate concentrations as a function of distance along the transect shown in Figure 5.5.

Statistical models of bicycle and pedestrian traffic volumes in Minneapolis

In the following section I build on an approach for estimating bicycle and pedestrian traffic on all roads and trails in Minneapolis, MN (Hankey et al., 2012). The approach involves using volunteer-based counts of cyclists and pedestrians to develop statistical models of traffic volumes using land use, demographic, and weather related variables; those statistical models can then be used to estimate bicycle and pedestrian traffic volumes on roads without counts. My main objective is to use the estimates of bicycle and pedestrian traffic to compare to the estimates of particulate air pollution described above. Combining estimates of non-motorized traffic and particulate concentrations allows for exploration of how the spatial patterns of both factors influence exposure. In this section I present a summary of the counts (2007-2010) of cyclists (n=436 counts) and pedestrians (n=431 counts) in the City of Minneapolis and present models that (1) explore correlates of pedestrian and bicycle traffic volumes, (2) estimate non-motorized traffic in locations without counts, and (3) test for trends in non-motorized traffic over time. I developed scaling factors for adjusting peak-hour counts to 12-hour "daily" counts as inputs for two types of regression models (ordinary least squares and negative binomial) used to estimate 12-hour bicycle and pedestrian traffic volumes for the entire City.

Description of non-motorized traffic counts used to estimate models

The City of Minneapolis Department of Public Works (DPW) and Transit for Livable Communities (TLC), a nonprofit organization selected by Congress to oversee the $21.5 million Non-Motorized Transportation Pilot Project, provided electronic

spreadsheet files of 436 counts of cyclists and pedestrians at 259 locations in Minneapolis during 2007-2010. Counts (completed by staff working with volunteers) were taken at varying times and for various durations. Most observations (330) were two-hour counts completed during the 4pm-6pm peak-hour period; forty-three observations were 12-hour counts (6:30am-6:30pm). All counts were taken on weekdays in September of each year. A small number of the counts were censored: (1) counts that were not completed in September (monthly counts occur at 10 of the locations), and (2) counts collected within 1 kilometer of the University of Minnesota campus (these counts had abnormally high bicycle and pedestrian volumes).

Bicycle and pedestrian counts were conducted according to DPW and TLC protocols (DPW, 2011) that were adapted from the National Bicycle and Pedestrian Documentation Project (Jones, 2009). A screen line was defined at each count location (located somewhere on the mid-block portion of each street or sidewalk segment). All pedestrians and cyclists passing that screen line were counted regardless of direction of travel.

The count locations were not chosen specifically for modeling spatial patterns of traffic; they were chosen purposefully because of interest in particular locations and were not chosen to be representative of street types, traffic flows in the city, neighborhoods, or range of weather extremes. Specifically, TLC and DPW chose locations where there were planned infrastructure improvements or where high non-motorized traffic volumes were expected. Although type of infrastructure or the presence of a bus line were not systematically considered in the choice of locations, the dataset included the full range of

street types in the city, a mix of on-street and off-street bicycle facilities, and locations with and without bus lines. Of the 259 locations, 59% were on arterials or collectors, 24% were local streets, and the remainder (16%) were off-street trails (i.e., multi-use, paved trails [15%]) or principal arterials (1%). There were bicycle facilities (separate lanes, shared lanes or "sharrows," or off-street facilities) at 27% of all locations (12% of the locations were roads with on-street facilities). Fifty-three percent of all locations were on a street with at least one bus route. The count locations are shown in Figure 5.7.

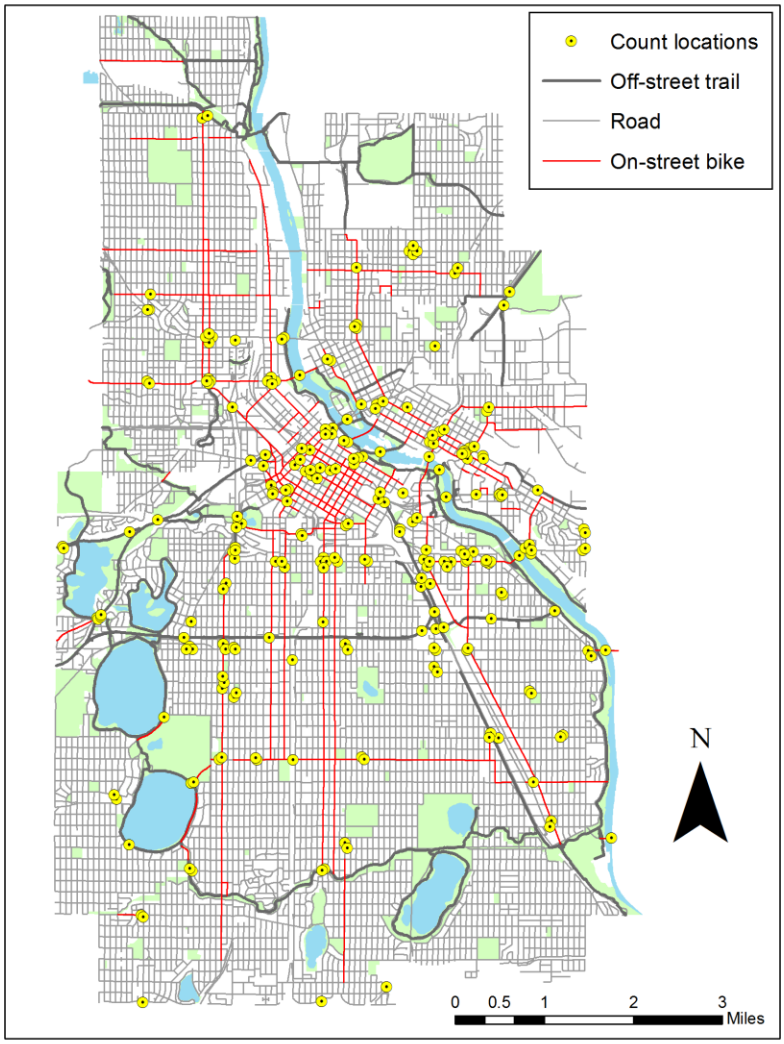

Figure 5.7 Non-motorized count locations used by the City of Minneapolis and Transit for Livable Communities.

Most of the traffic counts were collected during peak-hour (4-6pm); approximately 14% of the counts were for varying duration and at various times of day. I used the 43 counts with 12-hour observations to develop scaling factors for normalizing hourly counts to 12-hour counts. For example, the mean proportion of 12-hour bicycle traffic during the 7am-8am hour was 7.5% (see Table 5.1). The scaling factor for estimating 12-hour traffic for any counts taken during this hour was 1/0.075, or 13.3. These scaling factors were used to normalize all counts from different time periods to a common time period (i.e., 12-hour) for purposes of modeling. Correlation between predicted and actual counts using the scaling method was high ($R^2 \geq 0.89$). A limitation of this method (which is standard practice in estimation of vehicular average annual daily traffic [AADT] volumes) is that these scaling factors reflect average relationships between peak-hour and 12-hour volumes and do not fully reflect the daily variability in traffic volumes. Time of day proportions and scaling factors for bicycle and pedestrian traffic are presented in Table 5.1. Peak-hour traffic for both bicycles and pedestrians occurs between 5pm and 6pm. However, the mid-day hours account for a larger proportion of traffic for pedestrians (8.7-9.7%) than for cyclists (5.2-7.2%).

Table 5.1 Scaling factors derived from 12-hour counts to normalize all hourly traffic counts (adapted from Hankey et al. [2012])

Hour of day	Bicycle			Pedestrian		
	Percent of 12-hour count (95% CI)	Scale factor (95% CI)	Correlation R^2	Percent of 12-hour count (95% CI)	Scale factor (95% CI)	Correlation R^2
7-8am	7.5% (6.5-8.6%)	13.2 (11.6-15.4)	0.88	6.9% (5.8-8.0%)	14.5 (12.5-17.2)	0.91
8-9am	9.3% (8.2-10.5%)	10.7 (9.5-12.2)	0.9	5.3% (4.4-6.2%)	18.7 (16.0-22.6)	0.96
9-10am	7.8% (6.6-8.9%)	12.9 (11.2-15.2)	0.89	6.1% (5.3-6.9%)	16.4 (14.5-18.9)	0.97
10-11am	6.4% (5.5-7.3%)	15.6 (13.8-18.1)	0.89	5.9% (5.0-6.9%)	16.8 (14.4-20.1)	0.96
11-noon	5.9% (4.9-6.9%)	16.9 (14.5-20.3)	0.87	9.2% (7.9-10.4%)	10.9 (9.6-12.7)	0.99
noon-1pm	5.2% (4.3-6.1%)	19.1 (16.3-23.0)	0.77	9.7% (8.3-11.1%)	10.3 (9.0-12.1)	0.99
1-2pm	7.2% (5.8-8.5%)	14.0 (11.8-17.2)	0.88	8.7% (7.6-9.9%)	11.5 (10.1-13.2)	0.99
2-3pm	7.5% (6.6-8.4%)	13.3 (11.8-15.1)	0.84	8.8% (6.9-10.7%)	11.4 (9.3-14.5)	0.98
3-4pm	9.3% (8.2-10.3%)	10.8 (9.7-12.1)	0.9	7.8% (7.0-8.6%)	12.8 (11.6-14.3)	0.98
4-5pm	12.0% (11.0-12.9%)	8.4 (7.7-9.1)	0.93	10.4% (9.3-11.5%)	9.6 (8.7-10.8)	0.97
5-6pm	12.6% (11.2-14.0%)	7.9 (7.1-8.9)	0.89	12.3% (10.9-13.6%)	8.2 (7.4-9.2)	0.996

The time of day patterns derived from the 12-hour volunteer-based (manual) counts were compared to an automated bicycle counter (inductive loop detector) on the Midtown Greenway (an off-street trail) to compare time of day patterns from an automated counter and volunteer-based counts. This comparison suggests that time of day patterns for bicycles track well between the two data sets (loop detector and manual counts); both datasets show morning and afternoon peaks with similar magnitudes. The Midtown Greenway has a slightly larger afternoon peak which may be due to elevated recreational uses during that period of the day on off-street trails. Time of day patterns for pedestrians did not track well with either of the bicycle count patterns. Pedestrian traffic

seems to increase consistently throughout the day with three peaks: morning, noon-hour, and afternoon highlighting the need to use mode specific scaling factors.

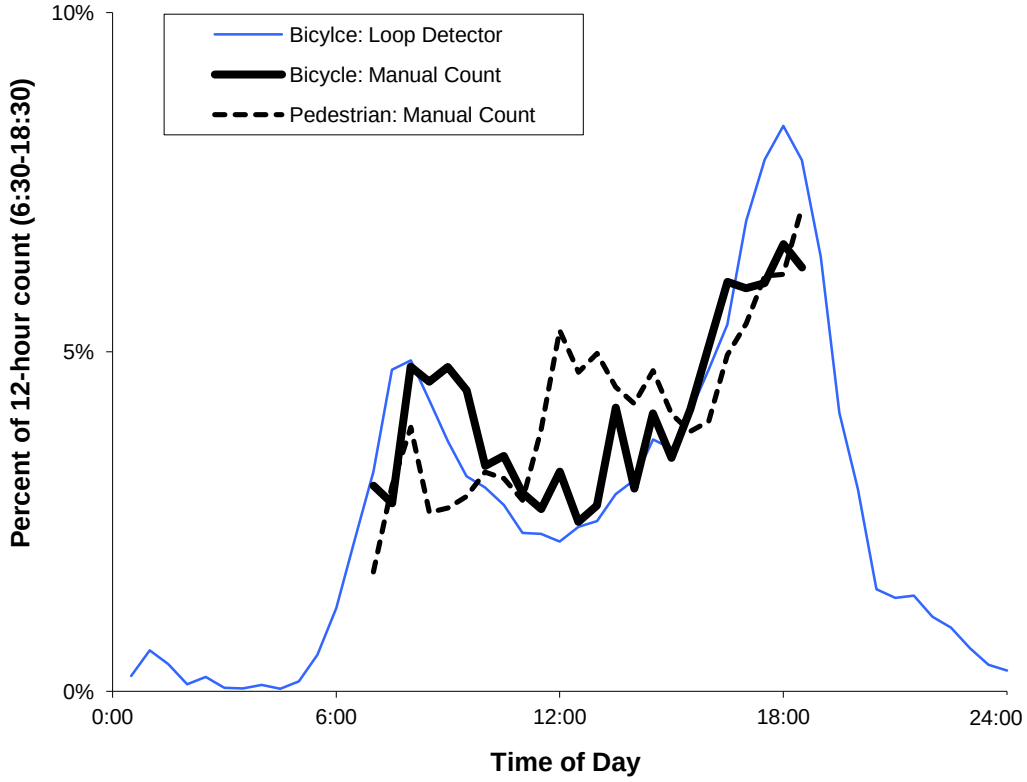

Figure 5.8 Time of day patterns for the volunteer-based (manual) on-street count dataset as compared to an automated bicycle counter on an off-street trail.

Using the scaling factors in Table 5.1, counts from all times of day were scaled to 12-hour counts to use as a common time period for modeling. Descriptive statistics for the estimated 12-hour bicycle and pedestrian counts are presented by facility and road type in Table 5.2. Bicycle traffic is highest on off-street facilities, followed by arterials, collectors, and local streets. Mean 12-hour pedestrian counts also are lowest on local streets. On average, pedestrian counts are higher on collectors than on arterials, although

this relationship does not hold if median traffic is used as the indicator. Overall, mean pedestrian counts were 35% higher than bicycle counts.

Table 5.2 Descriptive statistics of adjusted counts used as inputs for regression modeling (adapted from Hankey et al. [2012])

Bicycles	**Principal arterial**		**Minor arterial**		**Collector**		**Local**		**All streets**		**Off-street trail**
	Bike facility		Bike facility		Bike facility		Bike facility		Bike facility		
	Yes	No	Yes	No	Yes	No	Yes	No	Yes	No	
Observations	none	8	45	155	13	44	12	70	70	277	89
Max	none	262	1,909	1,331	396	1,701	964	822	1,909	1,701	2,840
Mean	none	184	547	371	163	326	395	182	450	310	912
Median	none	214	405	232	171	201	396	136	370	208	818
Min	none	12	122	4	41	21	71	0	41	0	16
Mean hourly	none	15	46	31	14	27	33	15	38	26	76
Pedestrians	**Principal arterial**		**Minor arterial**		**Collector**		**Local**		**All streets**		**Off-street trail**
Observations	8		195		57		82		342		89
Max	150		5,502		13,424		1,476		13,424		3,150
Mean	70		736		1,184		291		688		340
Median	64		579		323		196		376		133
Min	18		13		4		0		0		0
Mean hourly	6		61		99		24		57		28

Estimated 12-hour bicycle counts ranged from zero on a street without bicycle facilities to a high of ~2,800 on an off-street facility. Across all 259 locations, the mean 12-hour bicycle count (for 436 observations) was 456 per 12-hour day or ~38 cyclists per hour on average (but ranging from ~24 cyclists per hour in the lowest-travel hour [noon-1pm] to ~57 cyclists per hour in the highest-travel hour [4 pm-6 pm]). Mean hourly bicycle counts on off-street facilities (76/hour) and streets with bicycle lanes (38/hour) were 193% and 45% higher, respectively, than mean hourly traffic on streets without facilities (26/hour). Pedestrian traffic was, on average, 96% higher on streets with a bus line (71/hour) than on streets without (30/hour), and this relationship held for all street

functional types except principal arterials, where there was not enough data to explore this relationship (8 total locations; 1 principal arterial with a bus line).

Excluding off-street facilities (and principal arterials where bicycle traffic ostensibly is prohibited), bicycle volumes are associated with street functional class: they are highest on arterials, followed by collectors, and then local streets. For most street types, bicycle counts are higher on streets with bicycle facilities than on streets without facilities. Descriptive statistics of the estimated counts do not show a positive impact for bicycle facilities on collector streets, however, results obtained when controlling for other factors (i.e., in a regression model) suggest this may be the result of my sample (see Table 5.4 and the discussion of my regression models below). The relative differences in bicycle volumes between roads with and without bicycle facilities are larger for local streets (117%) than for arterials (47%).

Methods for developing regression models

Past studies have used both ordinary least squares (OLS; Haynes and Andrezejewski, 2010; Jones, 2010; Lindsey et al., 2006) and negative binomial (Cao et al., 2006) regression models to describe and estimate non-motorized traffic. Although it is generally known that OLS modeling is not the best approach for traffic counts relatively few studies have compared the implications of model choice for estimating traffic volumes that can be used in planning practices (Kim and Susilo, 2011). Negative binomial regression was originally developed for datasets for non-normal datasets that were restricted to nonzero integer values; negative binomial regression is similar to a Poisson regression except that it better handles datasets that are highly skewed such as

the count dataset evaluated here. In this chapter I present results using both OLS and negative binomial regression methods as a comparison.

Bicycle and pedestrian regression models were estimated separately using the independent variables in Table 5.3 (using OLS and negative binomial regression routines in STATA © and an extension, SPost [Long and Freese, 2005]). Street functional types (both with and without bicycle facilities) were modeled using dummy variables. In both the bicycle and pedestrian traffic models, local streets with no facilities are the suppressed case as they are expected to have the lowest non-motorized traffic (this modeling choice was made by stratifying the counts by street type [see Table 5.2]). Interpretations of significance for other street types are made relative to traffic on local streets without bicycle facilities. The year of the count was included as a level variable to test for trends over time and daily weather variables were included to control for any differences in weather conditions during the count days. The remaining variables all were related to other attributes of the count location (e.g., neighborhood socio-demographic and built environment characteristics).

Table 5.3 Independent variables in statistical models of bicycle and pedestrian traffic (adapted from Hankey et al. [2012])

Continuous variable	Description	Mean (standard deviation)	Units/notes
Socio-demographic (SES) variables			
Pct_nonwhite[a]	Percentage of neighborhood residents that are non-white	0.33 (0.25)	Areal unit: Census block group
Pct_under5_over65[a]	Percentage of neighborhood residents over the age of 65 or under the age of 5	0.15 (0.08)	Areal unit: Census block group
Pct_4yrdegree[a]	Percentage of neighborhood residents with a college education	0.39 (0.20)	Areal unit: Census block group
MedianHHInc[a]	Median household income	39 (19)	Areal unit: Census block group; Variable unit: Thousands of dollars
Crime[b]	Number of violent crimes per year	50 (57)	Areal unit: City neighborhood
Built environment variables			
PopDens[a]	Population density	3,299 (2,652)	Areal unit: Census block group; Variable unit: Persons km^{-2}
LUMix[c]	Measure of mixing of land uses	0.56 (0.20)	Areal unit: Census block group; Index (range: 0-1) with 1 indicating high mixing and 0 low mixing
Water_dist	Distance from nearest body of water	2.9 (2.1)	Variable unit: Kilometers
CBD_dist	Distance from the central business district (CBD)	1.3 (1.8)	Variable unit: Kilometers
Employment[d]	Number of jobs accessible by transit	30,215 (26,773)	Areal unit: Census block group; Number of jobs within a 30 minute transit ride (< 3 transfers)
Weather and temporal variables			
Tmax[e]	Recorded daily high temperature	23 (3.6)	Variable unit: Degrees Celsius
Precip[e]	Recorded precipitation	0.2 (0.8)	Variable unit: Centimeters
Categorical variable	**Description**	**Frequency**	**Notes**
Road and facility variables			
Principal[f]	Principal arterial street	8	Designed for 15,000-100,000 ADT and 40-50 mph
Arterial[f]	Arterial street	200	Designed for 5,000-30,000 ADT and 35-45 mph
Collector[f]	Collector street	57	Designed for 1,000-15,000 ADT and 30-40 mph
Local[f]	Local street	82	Designed for less than 1,000 ADT and 30 mph
BusRoute[g]	Presence of one or more bus routes	227	
OnStreet[f]	On-street bicycle facility	70	Bike lane or shared space
Offstreet[f]	Off-street trail	89	Bicycle or pedestrian trails separate from roads
Temporal variables			
Year	Level variable indicating year count occurred	N/A	Base case: Year-2007

[a]US Census (2000); [b]City of Minneapolis crime statistics (http://www.minneapolismn.gov/police/crime-statistics/); [c]Land use data: Metropolitan Council (2005); [d]Fan et al. (2012); [e]University of Minnesota Climatology Working Group (climate.umn.edu); [f]City of Minneapolis Department of Public Works; [g]MetroTransit schedules (www.datafinder.org).

Results of non-motorized traffic models and extrapolated spatial patterns

Bicycle and pedestrian traffic were modeled separately; Table 5.4 presents results for two types of regression models for each mode: (1) ordinary least squares and (2) negative binomial. Negative binomial regression has been argued to better approximate traffic for non-motorized modes (Cao et al., 2006; Kim and Susilo, 2011).

Table 5.4 Regression results for models of bicycle and pedestrian traffic (adapted from Hankey et al. [2012])[a]

	Bicycle Models			**Pedestrian Models**		
	OLS	*Negative binomial*		*OLS*	*Negative binomial*	
	β	*β*	*Marginal*	*β*	*β*	*Marginal*
Constant	-20.9	4.77 ***	-	789 *	5.57 ***	-
Socio-demographic variables						
Pct_nonwhite	190 *	0.514 **	67%	-29.8	0.743 **	110%
Pct_under5_over65	462 *	0.640	90%	32.5	-0.919	-60%
Pct_4yrdegree	689 ***	1.35 ***	285%	372	1.39 ***	302%
MedianHHInc	-4.10 ***	-0.00890 ***	-0.89%	2.08	0.00376	-0.38%
Crime	-0.153	-0.000791	-0.079%	2.95 **	0.00237	-0.24%
Built environment variables						
PopDens	-0.00762	-0.0000254	-0.0025%	-0.0353 *	0.0000140	0.0014%
LUMix	12.9	0.613 ***	85%	-920 ***	-0.532 *	-41%
Water_dist	17.6	0.0560 *	5.8%	-21.6	-0.116 ***	-11%
CBD_dist	-55.2 ***	-0.196 ***	-18%	-40.3	-0.151 ***	-14%
Employment	0.00110	0.00000461 *	0.00046%	0.0162 ***	0.00000516	0.00052%
Weather and temporal variables						
Tmax	-2.65	-0.015	-1.5%	-26.0 *	-0.0124	-1.2%
Precip	-54.3 **	-0.163 ***	-15%	-128 **	-0.150 **	-14%
Road and facility variables						
Principal	-116	-0.275	-24%	66.4	-0.823 **	-56%
Arterial	141 ***	0.396 ***	49%	392 **	0.774 ***	117%
Collector	3.28	0.098	10%	611 ***	0.853 ***	135%
Local	(base case)					
BusRoute	N/A			100	0.211	24%
OnStreet	98.8 *	0.317 ***	37%	N/A		
Offstreet	691 ***	1.46 ***	332%	254 *	0.190	21%
Temporal variables						
Year	61.6 ***	0.0453 ***	4.6%	-5.95	0.000970	0.097%
Goodness-of-fit						
	Adj R^2	*Cox-Snell* R^2		*Adj* R^2	*Cox-Snell* R^2	
	0.38	0.48		0.30	0.42	

[a] *** denotes p-value <0.01; ** denotes p-value < 0.05; * denotes p-value < 0.10.

Overall, goodness-of-fit was better for bicycle traffic (OLS: adj. $R^2 = 0.38$; Negative binomial: Cox-Snell Pseudo $R^2 = 0.48$) than for pedestrian traffic (OLS: adj. $R^2 = 0.30$; Negative binomial: Cox-Snell Pseudo $R^2 = 0.42$). More independent variables were significant for the bicycle model than for the pedestrian model. There were more significant variables in the negative binomial models than in the OLS models for both bicycles and pedestrians. For most statistically significant variables, the direction of effect (i.e., increasing or decreasing traffic) was the same for pedestrians and bicycles.

Neighborhood design and urban form play a role in explaining bicycle traffic. Bicycle facilities have a significant impact on bicycle traffic and this effect is much larger for off-street (332% increase) than for on-street (37% increase) facilities. Furthermore, a one-unit increase of land use mix (entropy index of four land use types) increased bicycle traffic by 85% and traffic decreased 18% per kilometer in distance from the central business district (CBD). Certain neighborhood socio-demographic characteristics (i.e., percent non-white, percent with a college degree, and median household income), precipitation, and arterial roads had significant effects on bicycle traffic. Lastly, the models suggest that overall bicycle traffic is increasing 4.6% per year ($p<0.01$; see Table 5.4).

Road classification, proximity to amenities, and activity centers are important explanatory variables for pedestrian traffic. Roads typically associated with destinations or retail corridors (arterial and collectors) significantly increased pedestrian traffic. Additionally, pedestrian volumes are larger near the CBD (15% decrease per kilometer from the CBD) and bodies of water (11% decrease per kilometer from the nearest body of

water). Neighborhood socio-demographics (i.e., percent non-white and percent with a college degree) and precipitation also are correlated with pedestrian traffic. Unlike for bicycle traffic, there was no evidence that pedestrian traffic is increasing over time.

I used the results of the regression models to estimate 12-hour non-motorized traffic counts for all street segments in the City of Minneapolis. I chose to use the negative binomial regressions for extrapolation since (1) the input data better fits the specification for that regression type (i.e., nonnegative integers) and (2) extrapolated values using OLS regression included a large number of locations with negative values for predicted bike and pedestrian counts (40 [42]% of extrapolated locations for bicycles [pedestrians]).

For each independent variable, values were obtained for every street segment (excluding freeways and on-ramps) based on and geographic location (i.e., block group of segment location) and attributes specific to each segment (e.g., street classification, presence of a bike facility, etc.). For model predictions employed here, I assumed a temperature of 25ºC and no precipitation. Since counts are from September, these results should be interpreted as typical traffic volumes during non-precipitation days in September only (see Figure 5.9). As expected, given the relative significance of variables in both the bicycle and pedestrian models, the maps reflect the importance of street functional class (i.e., higher levels of traffic on arterials and collectors) and measures of the built environment (e.g., higher levels of traffic in the downtown area and areas of higher land use mix). These maps also highlight a few key differences between bicycle and pedestrian traffic, namely: (1) off-street trails seem to have larger relative volumes

for cyclists than for pedestrians and (2) pedestrian traffic is more tightly clustered around retail corridors and activity centers (e.g., near the CBD and along major transportation corridors) than bicycle traffic.

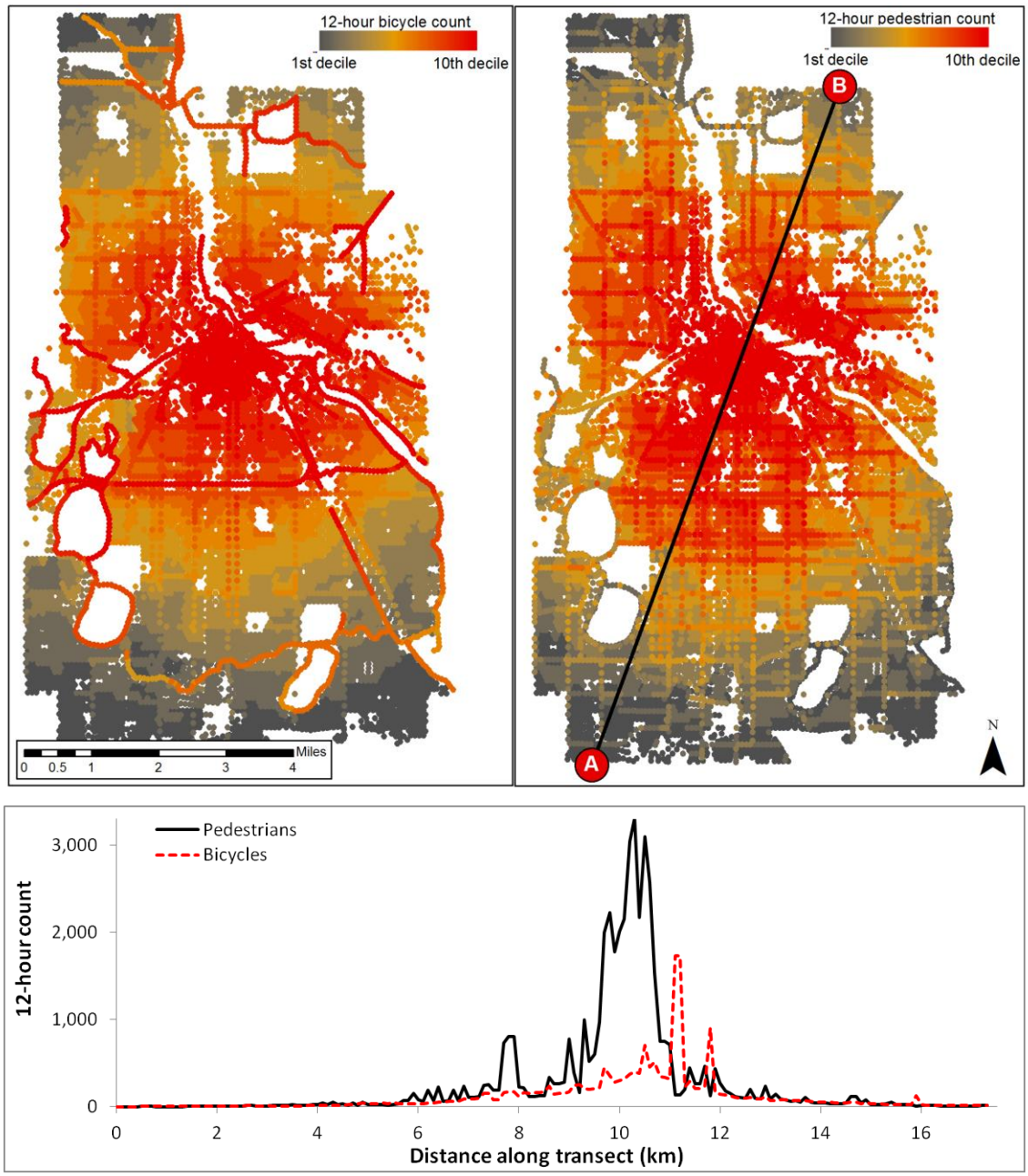

Figure 5.9 Estimated 12-hour (6:30am – 6:30pm) bicycle and pedestrian traffic volumes in Minneapolis, MN (shown by decile). Model estimates along the transect are shown in the bottom panel.

The regression models described here include data for counts during 2007-2010. To test the predictive power of the models I re-estimated the negative binomial models for counts during 2007-2009 and predicted 12-hour bicycle and pedestrian counts at 85 locations (46 new and 39 previously sampled locations) where counts were collected in 2010. I compared predicted counts from the regression models to the year-2010 counts (12-hour estimates based on the scaling factors). Although this validation procedure involves comparison of two estimates (i.e., the regression model predictions vs. the 12-hour counts estimated [using scaling factors] from observed peak-hour counts), the procedure yields useful information about model performance in this context.

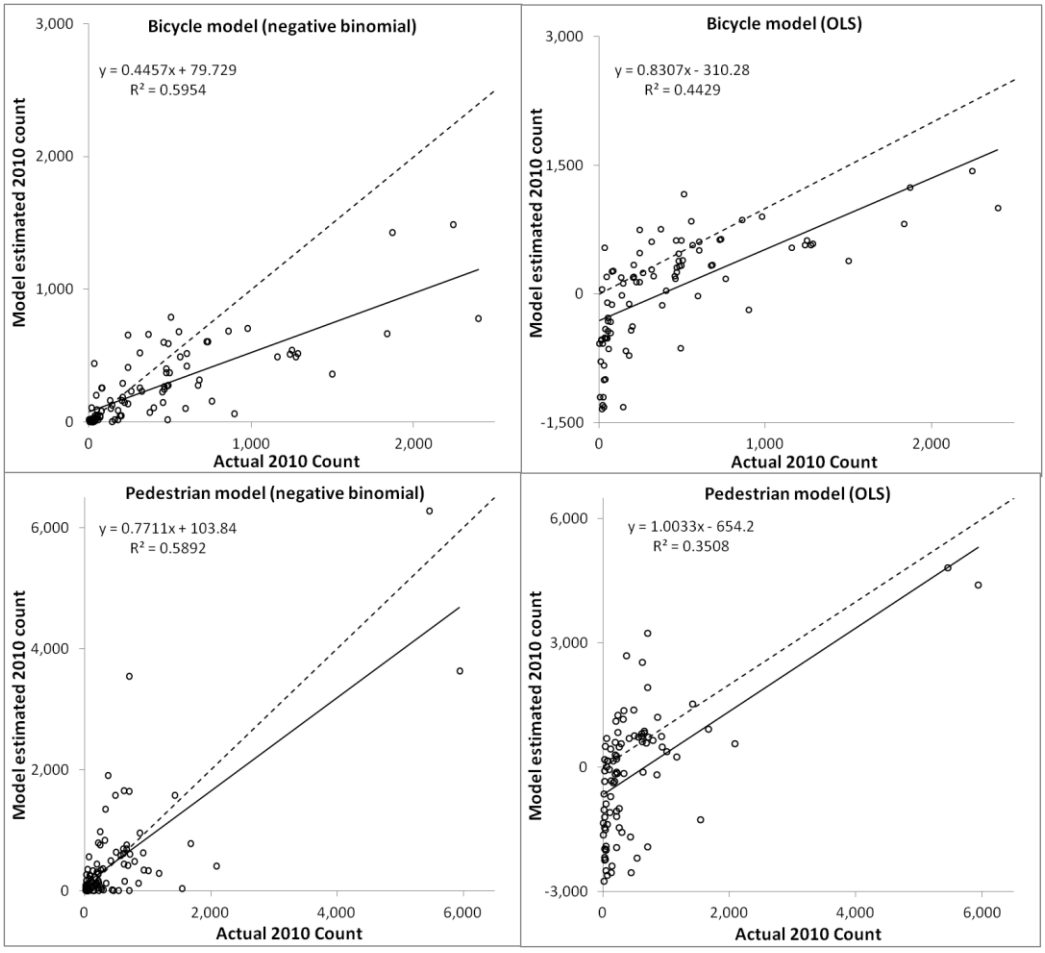

Figure 5.10 Scatterplot of model predicted vs. estimated 12-hour counts for year-2010.

Figure 5.10 shows that the negative binomial models generally do a reasonable job (R^2: 0.59) of estimating overall trends in non-motorized traffic. A challenge with this approach to validation is that there is variability in traffic volumes both among locations and within locations across days (and years). For example, at some locations (where there are multiple years of data to compare) peak-hour counts differ by as much as a factor of 2 between years. Given the sample sizes available in this dataset (i.e., most locations have 2 or less counts over the study period), it is difficult to capture this within-location variability in the models described above. As more data becomes available it may be possible to build models that better explain between-location and within-location variability.

Comparison of spatial patterns of air pollution and non-motorized traffic

A key outcome of the models developed in this dissertation (i.e., models of non-motorized traffic and particulate air pollution) is the capability to explore the within-city spatial patterns of two important health determinants: (1) rates of active travel and (2) concentrations of particulate air pollution. Describing the ways these two factors interact may give planners better insight on how to design clean, healthy cities. A limited number of studies have explored interactions between neighborhood "walkability" (i.e., the likelihood a resident will walk based on characteristics in that neighborhood) and ambient air pollution concentrations (Marshall et al., 2009; Frank et al., 2005). My models offer unique insight to nuances of this topic in two distinct ways. First, my estimates of non-motorized traffic describe where people are actually located while biking or walking rather than estimating the likelihood someone will walk or bike based on their home

location (as is the case for "walkability" metrics). Second, my LUR-based estimates of particulate air pollution concentrations are able to pick up small-scale changes in concentrations that a sparsely distributed regulatory monitor network cannot. By comparing the spatial patterns of the estimates from these models I am able to assess population-level exposure (i.e., for estimates of all walkers and bikers) and explore factors of the built environment that may impact these exposures.

In the following section I present two analyses to explore interactions among estimates from my models: (1) a mapping exercise to identify different characteristic areas in Minneapolis that may be of interest to planners (e.g., "healthy" [high active travel; low air pollution] or "unhealthy" [low active travel; high air pollution] neighborhoods) and (2) exploring how certain aspects of the built environment (e.g., street characteristics, population density, land use mix) and socio-economic metrics (e.g., household income, proportion of non-white residents) are correlated with both health determinants. I then discuss how analyses that account for both factors (i.e., non-motorized transport and air pollution estimates) simultaneously can be useful to planners and policy-makers interested in designing clean, healthy cities and neighborhoods.

For these analyses I compare morning and afternoon rush-hour concentrations to 12-hour volumes of bicycle and pedestrian traffic. Since the dataset I used to estimate bike and pedestrian volumes included mostly counts in the afternoon the spatial patterns of non-motorized traffic likely better describe afternoon than morning spatial patterns. I could have scaled 12-hour counts to specific time periods (i.e., 7-9am and 4-6pm) using the scaling factors described above (Table 5.1); however, I chose not to do this since the

same factor would be applied to all locations and thus the spatial patterns would not change for each time period (the absolute values of the estimated traffic volumes would merely shift). Better information on time of day patterns at the on-street count locations would allow for analyzing patterns in this way.

Mapping categories of exposure

A core motivation for combining outputs from these models is to explore patterns of population-level rather than individual-level exposure during active travel. For example, if one is only interested in individual-level exposure (e.g., when choosing a cycling route or estimating exposure for survey participants during travel) then a concentration surface is sufficient information. However, a key question for planning healthy neighborhoods is how exposure patterns change at a population-level. For example, an area with moderate concentrations but high levels of active travel may be more important for population-level exposure than an area with high concentrations but is used by cyclists or pedestrians infrequently.

I mapped four types of areas that may be of interest to planners who aim to reduce population-level exposure to air pollution during active travel (and improving the health outcomes of neighborhoods overall [Table 5.5]). The area definitions in Table 5.5 are meant to capture places in Minneapolis that are health promoting (i.e., "healthy" areas), detrimental to health (i.e., "unhealthy"), and places that do well in one category but need to shift the other health determinant (either decreasing particulate concentrations ["high exposure"] or increasing active travel ["opportunity"]) to switch those neighborhoods to the "healthy" category. To define these four areas I stratified all roads by estimates of

particulate concentration and non-motorized traffic and pulled areas that performed in the highest or lowest quartile for each parameter. I then mapped areas that met the criteria specified in Table 5.5 for each mode (i.e., biking and walking) and each type of particulate concentration (i.e., particle number, black carbon, $PM_{2.5}$). Maps for each pollutant are shown in Figures 5.11-5.13; definitions and brief descriptions of each area type are shown in Table 5.5.

Table 5.5 Definitions of areas defined by spatial patterns of non-motorized travel and particulate concentrations

Area type	**Active travel**	**Air pollution**	**Description**	**Percentage of roads in area type (morning [afternoon])**		
				Particle number	Black carbon	$PM_{2.5}$
Healthy	Highest quartile	Lowest quartile	Areas with maximum health benefits. High active travel; low concentrations.	Bike: 3% [1%] Ped: 0.7% [0.1%]	Bike: 3% [2%] Ped: 3% [3%]	Bike: 1% [2%] Ped: 0.03% [1%]
High exposure	Highest quartile	Highest quartile	Areas where population-level exposure is high. High active travel; high concentrations.	Bike: 11% [14%] Ped: 12% [15%]	Bike: 7% [11%] Ped: 11% [11%]	Bike: 13% [13%] Ped: 15% [13%]
Opportunity	Lowest quartile	Lowest quartile	Areas that could benefit most from increased active travel. Low active travel; low concentrations.	Bike: 12% [13%] Ped: 12% [13%]	Bike: 7% [9%] Ped: 8% [9%]	Bike: 17% [13%] Ped: 17% [12%]
Unhealthy	Lowest quartile	Highest quartile	Areas that provide little health benefits. Low active travel; high concentrations.	Bike: 2% [0.8%] Ped: 3% [1%]	Bike: 1% [3%] Ped: 3% [3%]	Bike: 0.1% [2%] Ped: 0.8% [3%]
All other areas	-	-	Areas not classified in one of the four categories above.	Bike: 72% [71%] Ped: 72% [71%]	Bike: 82% [75%] Ped: 75% [74%]	Bike: 69% [70%] Ped: 67% [71%]

[a] Percentages are based on aggregated classification (see Figure 5.14).

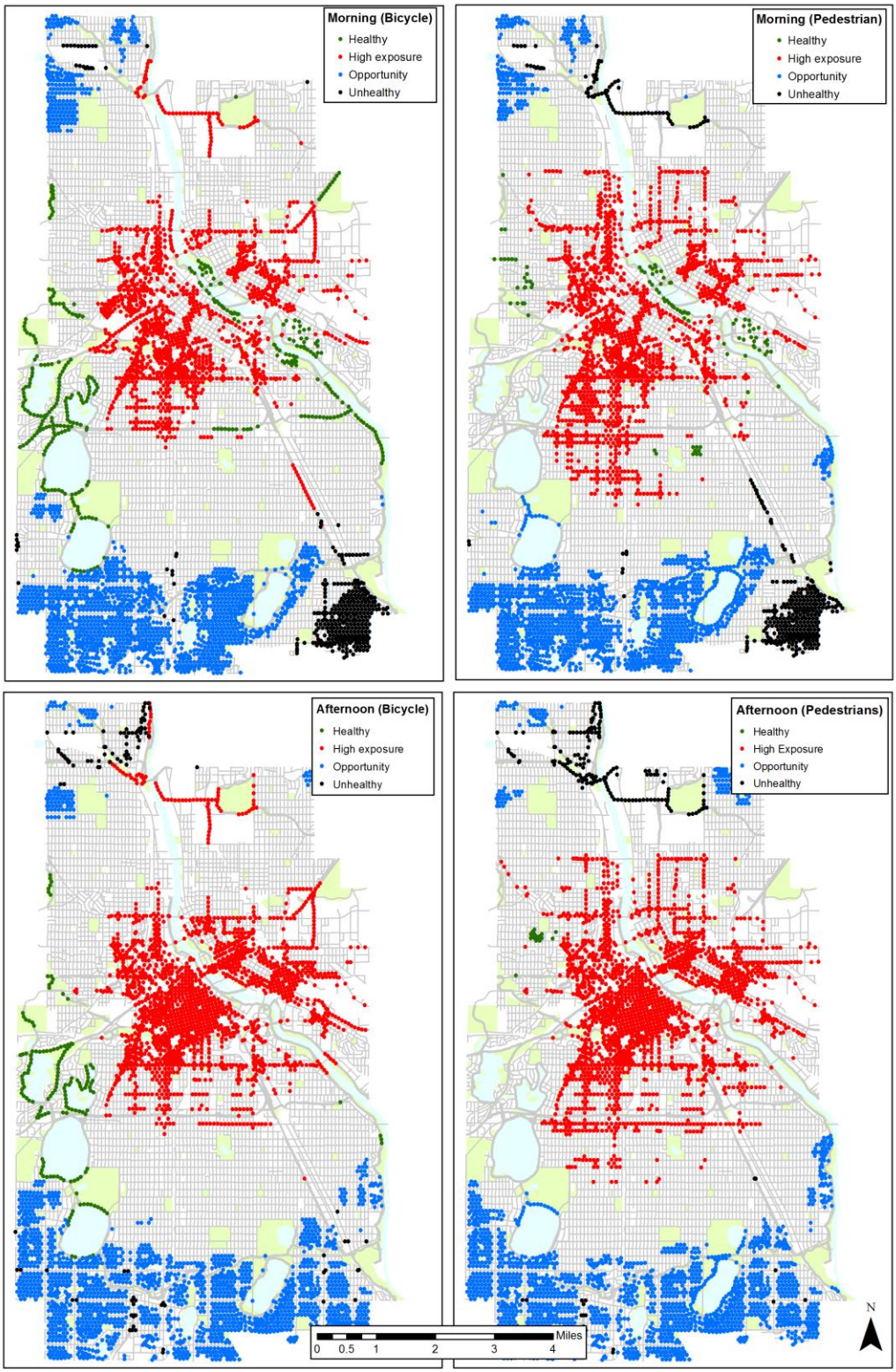

Figure 5.11 Neighborhoods identified by overlays of bicycle and pedestrian traffic and particle number concentration. Area types shown in the legends are defined in Table 5.5.

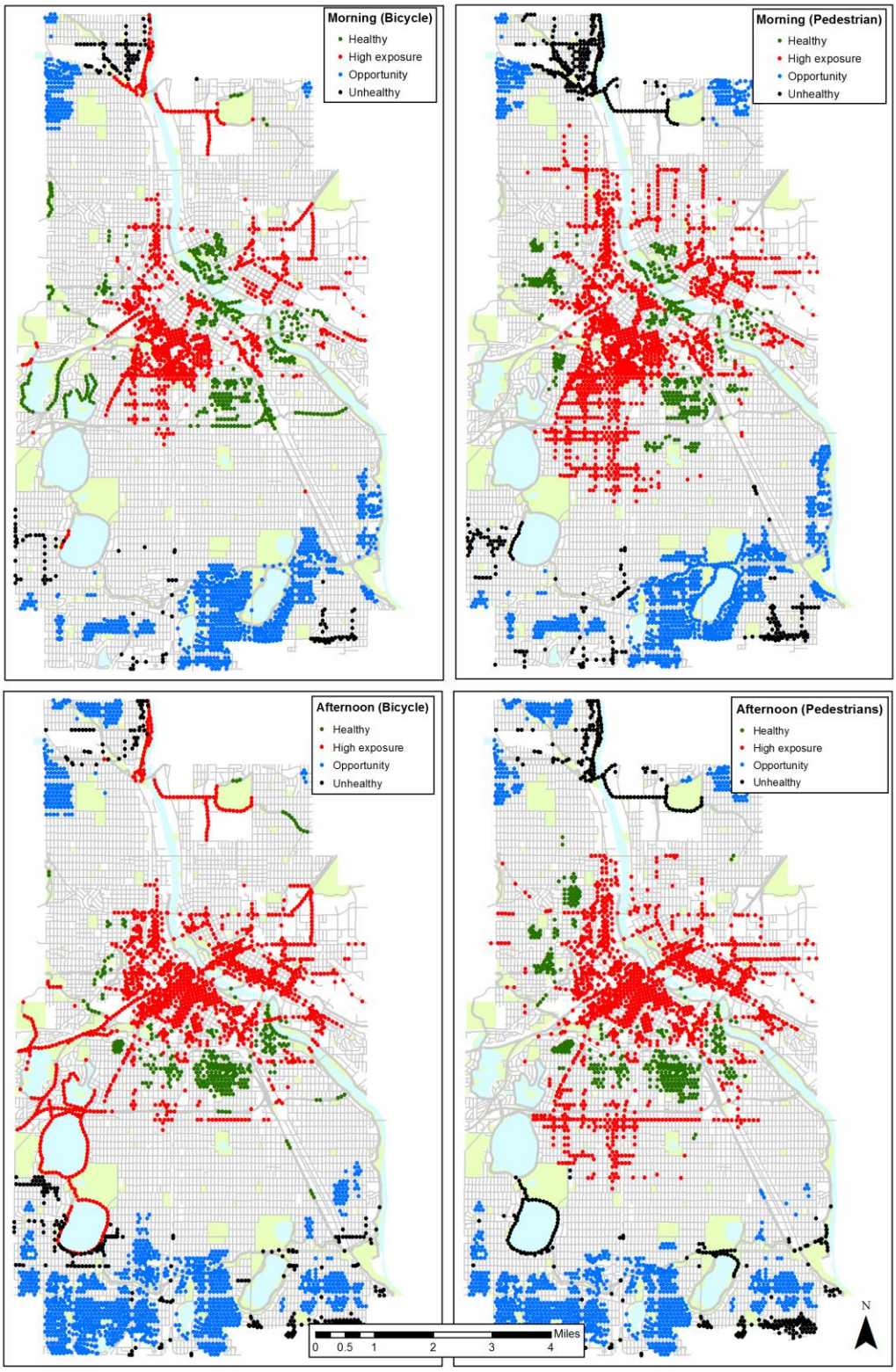

Figure 5.12 Neighborhoods identified by overlays of bicycle and pedestrian traffic and black carbon concentration. Area types shown in the legends are defined in Table 5.5.

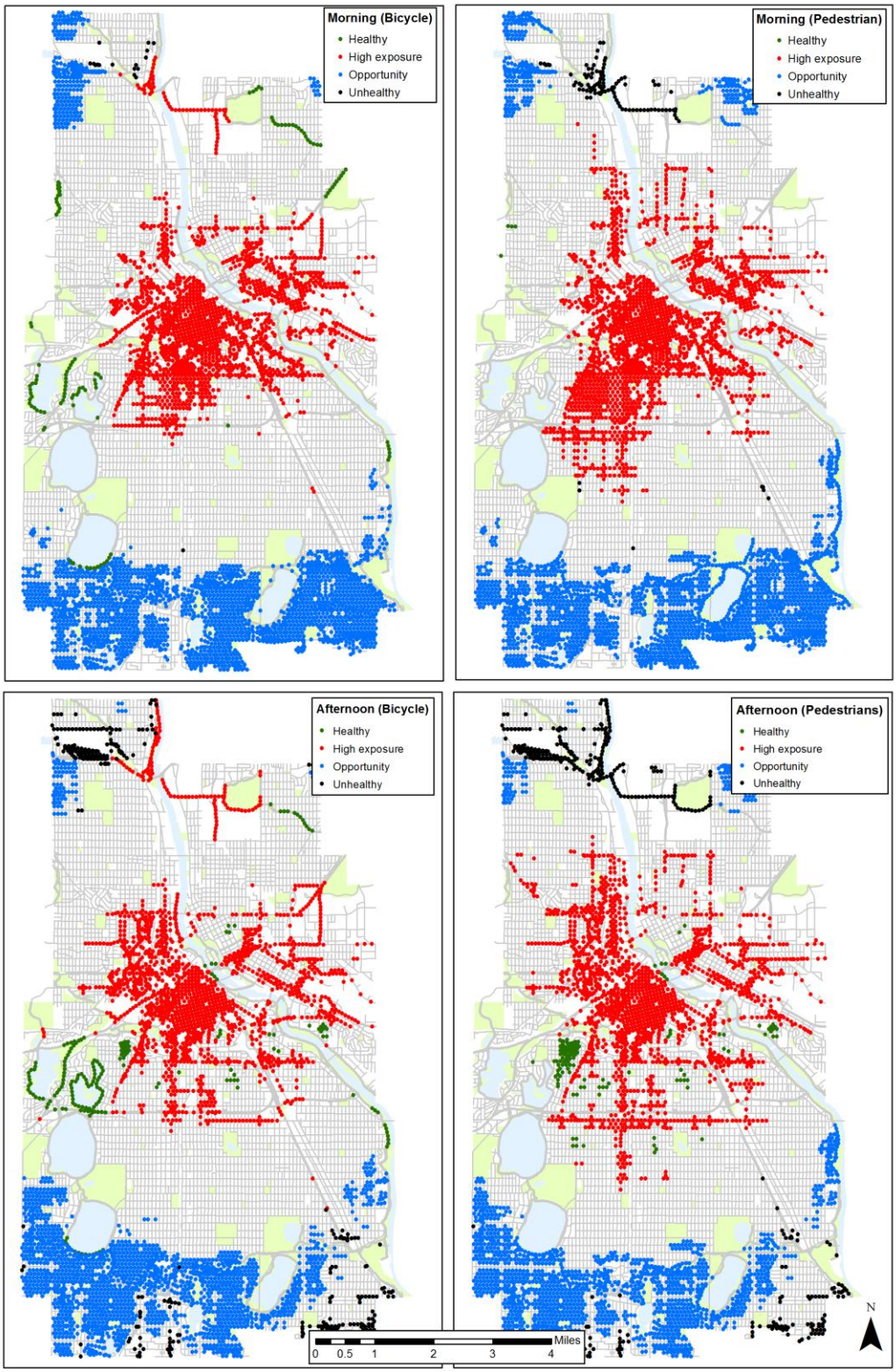

Figure 5.13 Neighborhoods identified by overlays of bicycle and pedestrian traffic and $PM_{2.5}$ concentration. Area types shown in the legends are defined in Table 5.5.

Figures 5.11-5.13 identify the four area types described in Table 5.5 for each pollutant, mode, and time of day. Some patterns are broadly consistent among these factors but there also exist nuanced differences among the different pollutants. Below I describe trends for each pollutant separately and then discuss patterns that are common among the various measures of particulate air pollution.

Particle number concentration: During morning rush-hour there are two areas that are classified as healthy for both cyclists and pedestrians: (1) the "Mills district" near the Mississippi River, downtown Minneapolis, and the Stone Arch Bridge and (2) the main campus of the University of Minnesota. For cyclists there are also a number of off-street trails classified as healthy including West River Parkway along the Mississippi River and around the Chain of Lakes (specifically, Cedar Lake and Lake of the Isles). Areas classified as high exposure were mostly in or near downtown Minneapolis and were mostly confined to high traffic roads (arterials and collectors). Areas of opportunity were located primarily in the southern part of the City and confined mostly to local roads. Unhealthy areas were located in the Southeast corner of the City (near the airport) and on some major roads or intersections of major roads in South Minneapolis. There were also small sections of North Minneapolis that were classified as unhealthy; mostly along St. Anthony Parkway for pedestrians.

During the afternoon rush-hour neighborhoods were mostly classified in a similar pattern as for morning rush-hour with a few exceptions. Most notably, areas classified as healthy shrank or nearly disappeared; trails around the Chain of Lakes remained as areas classified as healthy for bicycles. Areas classified as high exposure spread more

homogenously across downtown and the St. Anthony Main district. Also, areas classified as unhealthy in South Minneapolis were not present in the afternoon.

Black carbon concentration: Among all pollutants, black carbon had the most area classified as healthy. In general these areas were located just outside of downtown Minneapolis and away from major roads. Large swaths of the Seward neighborhood, University of Minnesota, and areas along the Mississippi river accounted for most of the areas classified as healthy; smaller pockets of the Kenwood neighborhood and North Minneapolis were also classified as healthy. High exposure areas were mostly in or near downtown and were more clustered around major roads than for particle number concentrations. Opportunity areas were mostly in southern Minneapolis (with small areas in northern Minneapolis) and covered a smaller amount of area than for particle number. Unhealthy areas were located sporadically through the southern and northern parts of the City; the unhealthy areas around Lake Calhoun are likely a result of the artifact of extrapolating the afternoon black carbon LUR model (discussed above).

Similar to particle number concentrations, the amount of area classified as healthy was reduced in the afternoon. Neighborhoods around the Mississippi River and the University of Minnesota campus were no longer classified as healthy; the Seward and Kenwood neighborhoods (along with other relatively smaller pockets of neighborhoods near downtown) remained classified as healthy. High exposure areas became more abundant throughout downtown and the St. Anthony Main district. Opportunity areas grew slightly in size and shifted west; the amount and location of unhealthy neighborhoods remained fairly consistent by time of day.

$PM_{2.5}$ concentrations: Among the four measures of particulate air pollution the smallest amount area was classified as healthy for $PM_{2.5}$ concentrations; during morning rush-hour healthy areas were confined to a limited number of trails for cyclists around Lake of the Isles and Cedar Lake. High exposure areas were mostly around downtown and throughout the Uptown neighborhood. High exposure areas were more homogenous for $PM_{2.5}$ than for particle number and black carbon and included roads across functional class. Similar to particle number and black carbon, a large portion of southern Minneapolis was classified as an area of opportunity and small portions of St. Anthony Parkway were classified as unhealthy. The main shift between morning and afternoon rush-hours was that areas classified as healthy grew modestly in size to include more of the Kenwood and Chain of Lakes neighborhoods as well as pocket neighborhoods near downtown Minneapolis; other categories remained relatively consistent by time of day.

Aggregate spatial patterns: To explore spatial patterns that are common among all three pollutants, I created a map that combines area classifications for each pollutant. I selected roads that were classified as a certain area type for any two of the pollutants (e.g., if a road was "healthy" for two of the three pollutants that road was classified as "healthy"). This approach resulted in similar spatial trends to the trends observed for individual pollutants. Namely, the fewest number of roads were classified as healthy (1%) and unhealthy (1%); many roads were classified as high exposure (12%) and opportunity areas (12%). Healthy neighborhoods were mostly located near, but just outside, of downtown; for bicycles, healthy areas also included off-street trails near lakes of parkways. Figure 5.14 shows the map with aggregated spatial trends.

An important aspect of this analysis is that ~74% of roads did not fall into any of the 4 categories defined in Table 5.5. I chose to highlight areas that do especially well (or poor) for each factor (i.e., active travel or air pollution); however areas that were not classified as one of the 4 categories may be important since they include places where moderate shifts in one factor may push those neighborhoods into one of the highlighted groups. For example, there may be a road that has low particulate concentrations but moderate rates of active travel; if levels of active travel are increased on that road, it would shift to the "healthy" category. Conversely, there may be areas where concentrations are high and rates of active travel are moderate; if levels of active travel decrease, then those areas would shift to the "unhealthy" category. Furthermore, many of the areas that are unclassified are residential neighborhoods. As such these areas may require different strategies to shift activities; for example, it is likely that many activities in residential areas are primarily recreational in nature, while many of the activities in downtown (where exposure is high) are utilitarian trips. This nuance may be important for encouraging activities that are overall health protective.

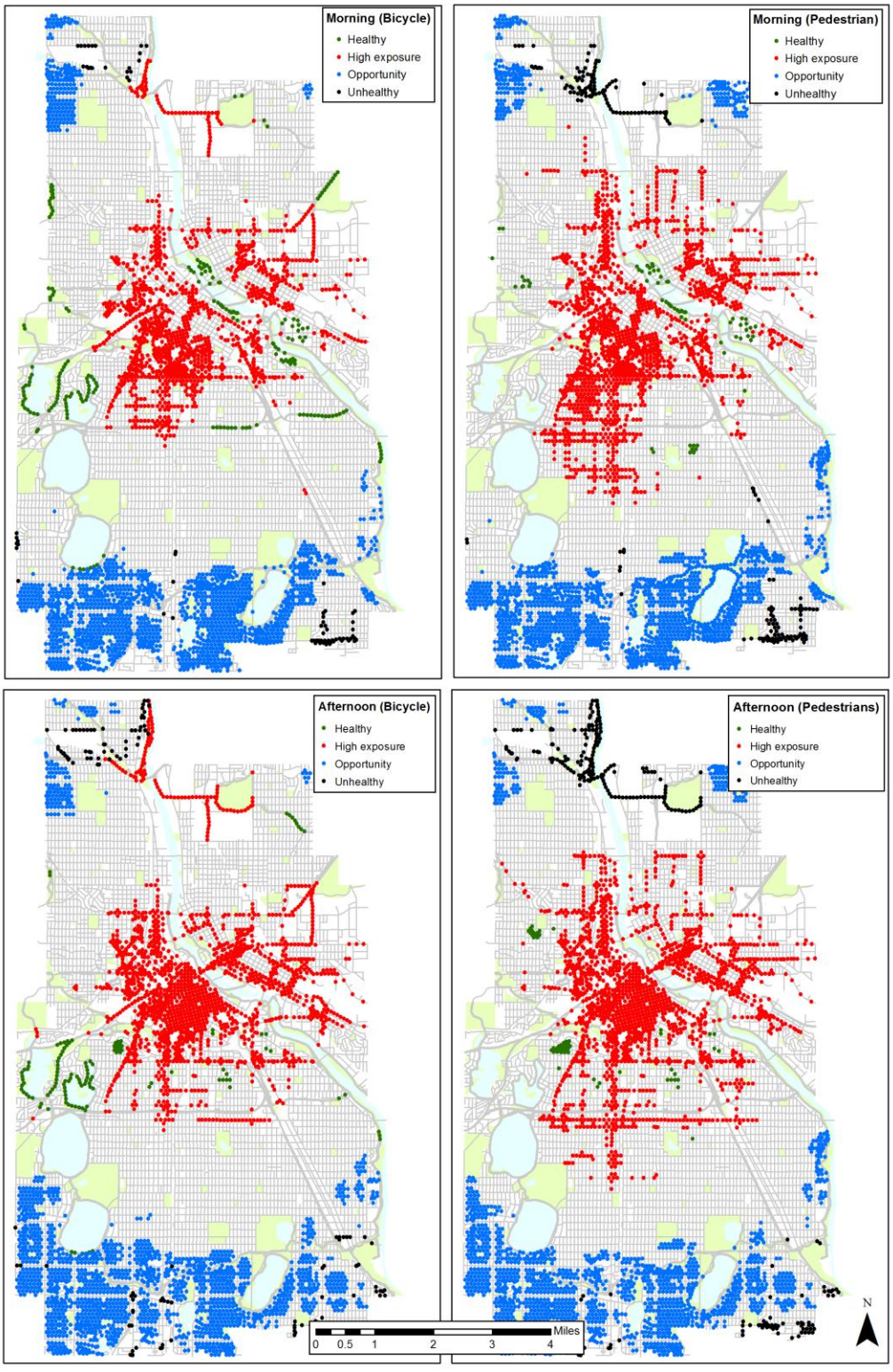

Figure 5.14 Neighborhood types among all pollutants. Roads were classified in area types if they met criteria for two of three pollutants.

Exposure and the built environment

Another way to assess best practices for planning for healthy cities is to explore how non-motorized traffic and particulate air pollution are correlated with certain aspects of the built environment. In this section I summarize my model results by characteristics of streets, the built environment, and neighborhood demographics to explore how urban design and environmental justice issues may be impacted by the spatial patterns of these two factors. I focus mainly on commonly cited strategies for improving "walkability" (i.e., increasing population density and land use mix), metrics frequently used to assess environmental injustice (i.e., household income and proportion of non-white residents), and patterns by street functional class.

I designed my air pollution sampling routes to sample approximately equally on roads for each street functional class, based on the assumption that traffic and emissions are associated with street classification. Similarly, as highlighted by the statistical models of non-motorized traffic, pedestrian and bicycle traffic volumes are also correlated with street functional class. In Figure 5.15 I summarized model estimates (n=13,569) for both non-motorized traffic and particulate concentrations by road type; I show median values for the distribution of estimates classified as each road type.

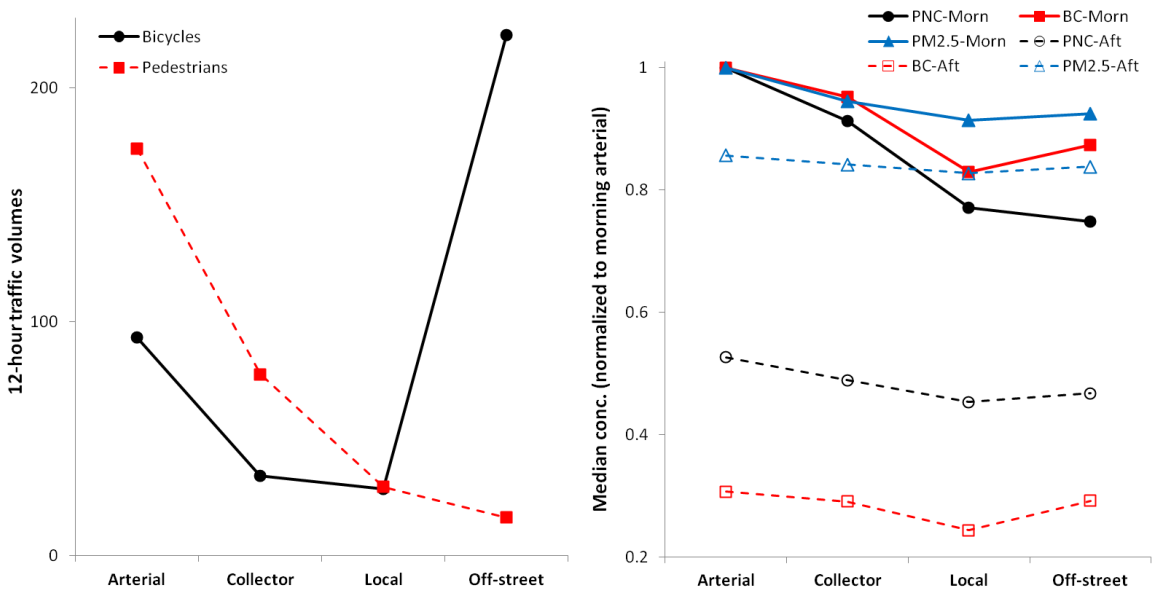

Figure 5.15 Median non-motorized traffic volumes and LUR concentration estimates by road type. Concentrations normalized to morning, arterial values.

Median pedestrian traffic volumes were highest on arterials, decreased with functional class, and were lowest on off-street trails; bicycle traffic volumes also decreased with street functional class with the exception of the largest volumes occurring on off-street trails. Median modeled concentrations by road type mostly followed the expected pattern, i.e., decreasing concentrations on lower-traffic roads. Particle number and black carbon concentrations had the largest difference in concentrations between low- and high-traffic roads (23 [14]% reduction for morning [afternoon] particle number and 17 [21]% for black carbon between arterial and local roads). Smaller changes were modeled for $PM_{2.5}$ concentrations and particle size, however, the direction of change for each ($PM_{2.5}$ decreases [particle size increases] with functional class) followed the expected direction.

For all concentrations (except for particle number in the mornings) median concentrations were slightly higher on off-street trails than on local roads. This effect is

potentially due to the location of many off-street trails, for example, those that are located along or near busy principal arterials (Hiawatha Trail), along freeways (Cedar Lake Trail), or near railways (University Avenue Trail). Another potential explanation is that the models may overestimate concentrations on some off-street trails. For example, this may be the case for the afternoon black carbon model. In that model (see Figure 5.2) elevated concentrations were estimated around Lake Calhoun and Lake Harriet (where there is a significant amount of off-street trail); the afternoon black carbon model included a variable for open space at 3,000 and 5,000 meters. As discussed in Chapter 4 the overestimates in that area could potentially be explained by much of the open space on the sampling route being co-located with emission sources (i.e., Cedar Lake Trail in close proximity to freight rail and freeways); since the lakes and parks around Lake Calhoun and Lake Harriet account for a large area of open space, the estimates for the off-street trails for that model could be overestimated.

The clear implication for exposure from Figure 5.15 is that most cycling and walking occurs on high-traffic roads that are the most polluted (with the exception of bike traffic on off-street trails). This finding makes sense since most utilitarian cyclists and pedestrians are using infrastructure to get to destinations and high-traffic roads are often designed to provide the most efficient access to destinations. However, it may be possible to make small shifts in the transportation network to slightly change traffic patterns of non-motorized traffic and reduce exposure to air pollution. For example, Minneapolis is currently building a network of bicycle boulevards. Bicycle boulevards are local roads (typically in close proximity and parallel to major retail corridors) that are designated

bikeways with traffic calming measures (e.g., speed bumps, bump outs, one-way vehicle traffic, etc.) that discourage vehicle traffic (but do not prohibit it) while encouraging bicycle traffic. One question that arises is what impact shifting non-motorized traffic from major roads to adjacent local roads may have on exposure. To shed light on this question I summarized model estimates for non-motorized traffic volumes and particulate concentrations by major roads and local roads at specific distances from the nearest major road; Figure 5.16 shows the gradients for both as distance from a major road increases.

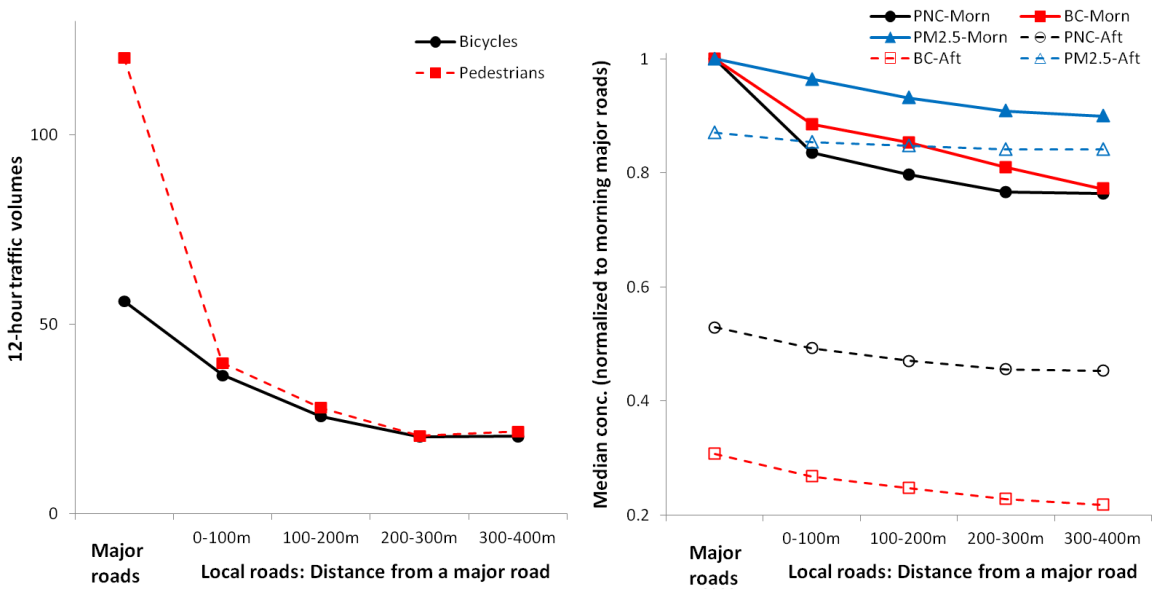

Figure 5.16 Median non-motorized traffic volumes and LUR concentration estimates by distance from a major road. Concentrations normalized to morning, major roads values.

Bicycle and pedestrian traffic is highest on major roads and decreased steadily as the distance from a major road increased; the decrease for pedestrian traffic was more pronounced than for bicycle traffic. As expected, modeled concentrations decrease as the distance from a major road increase. This effect was more pronounced for particle number and black carbon concentrations than for $PM_{2.5}$ and particle size. The median block size in Minneapolis is ~120 meters which is located in the second bin for local

roads in Figure 5.16 (100-200 meters). Therefore, for the bicycle boulevard example described above, shifting traffic over one block corresponds to an estimated average decrease in morning [afternoon] exposure concentrations of 21 [12]% for particle number, 15 [20]% for black carbon, 7 [3]% for $PM_{2.5}$. Consistent with the decreasing pollutant concentrations particle size increased 2 [0.2]% (not shown in figure).

Shifting traffic to adjacent streets will likely be a more realistic planning goal for cyclists than for pedestrians. People travel to get to destinations and most destinations are located along major transportation corridors. The statistical models of non-motorized traffic volumes highlighted that bicycle traffic is higher on off-street trails and on-street bicycle facilities all else being equal; the models did not find evidence that pedestrian traffic was higher on off-street trails. That result is consistent with evidence (Hood et al., 2011) that cyclists may be willing to travel slightly longer distances to use safer, designated facilities (e.g., bicycle boulevard) and thus planners may be able to design bicycle networks that are complimentary to the vehicle network but separate cyclists from emissions. It is possible that this type of strategy may also reduce other risk factors such as traffic accidents.

Strategies other than shifting traffic to adjacent streets may be needed for pedestrians. In situations where exposure to air pollution is higher than acceptable for pedestrians, strategies that remove the pollution from the pedestrians may be required. For example, density of bus stops and bus routes were statistically significant in many of the LUR models used to extrapolate concentration estimates to the City; it may be desirable to reduce bus traffic or number of stops along a corridor with high pedestrian

traffic but instead locate those stops and routes in close proximity to the pedestrian corridor. An example of this type of strategy is currently being executed on Nicollet Mall in downtown Minneapolis. Nicollet mall had some of the highest pedestrian counts in the dataset used to estimate the non-motorized traffic volumes; in the past Nicollet mall has also been a major bus corridor. Approximately 2 years ago the Marq2 project was completed which effectively moved much of the bus traffic on Nicollet Mall to two adjacent (parallel) streets; subsequently, the remaining buses have been mostly replaced by a small number of hybrid electric buses in the MetroTransit fleet. Currently, plans are in the design phase for an electrified streetcar that would partially run down Nicollet Mall; if this plan proceeds it would represent an eventual transition from a heavily trafficked diesel bus corridor to one that has only electrified transit. This is an example of one strategy to remove emission sources that are in close proximity to large populations of pedestrians.

Two commonly cited land use planning goals in US cities are to increase population density and land use mix. Although evidence is mixed on the real impact of increasing these two land use characteristics, planners commonly point to decreased automobile travel, mode shifting to biking and walking, and increased transit use as a result from policies that encourage density and land use mix. I stratified my model estimates of non-motorized traffic volumes and particulate concentrations by both of these land use factors to explore whether there is any association for increased active travel or changes in particulate concentrations from the spatial patterns of these factors across the City.

Population density and land use mix were calculated based on the data reported in Table 5.3 (and used for estimating the statistical models of non-motorized traffic). Both attributes were calculated at the block group level. Land use mix was calculated using the entropy index used by Frank et al. (2004) where a score of 1 represents perfect mixing and a score of 0 represents only 1 type of land use; the entropy index measures the degree to which land uses are heterogeneously distributed within a neighborhood according to the formula below:

$$LUMix = \frac{-\sum(p_i \times \ln(p_i))}{\ln(k)} \quad (5.1)$$

Where p_i is the proportion of area of land use type i in the block group and k is the number of land use categories. I used four types of land use to calculate this index: (1) residential, (2) commercial and office, (3) social and institutional, and (4) park or recreational. Results of the model estimates stratified by land use mix and population density are shown in Figure 5.17.

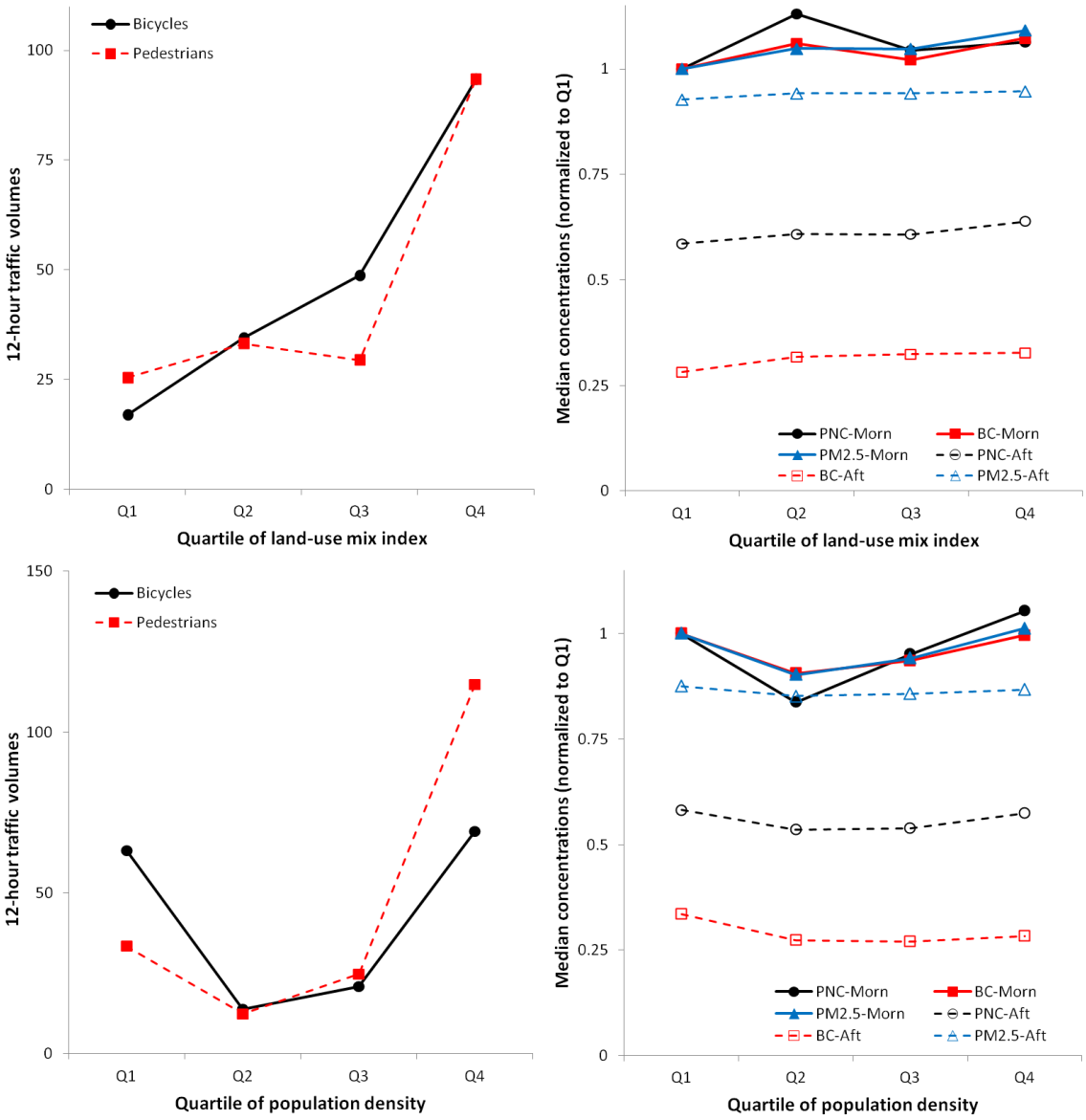

Figure 5.17 Median non-motorized traffic volumes and LUR concentration estimates by quartile of land use mix and population density.

Land use mix was associated with increased non-motorized traffic. Bicycle and pedestrian traffic volumes were nearly 4 times higher in areas that were in the highest vs. the lowest quartile of the land use mix index. Particulate concentrations were mostly unchanged by degree of land use mix, with only a slight increase in black carbon concentrations with increasing land use mix. These patterns suggest that while land use

mix is correlated with increased rates of active travel it may not impact air pollution concentrations at the same time. It is likely that the location in the City of these areas with high land use mix plays a larger role than the land use itself; for example, being located near a freeway, downtown, or in a residential neighborhood is probably a more significant factor in determining the exposure concentration than the degree of land use mix. As such, a planning goal may be to increase pocket areas of high land use mix at the neighborhood level to increase rates of active travel while mitigating exposure to air pollution. This may be an ideal strategy in areas such as the "opportunity" areas defined and mapped in the previous section.

Trends in non-motorized traffic volumes and particulate concentrations were less clear for population density. Bicycle and pedestrian traffic was highest in the densest areas (highest quartile) but second highest in the least dense areas; traffic volumes seemed to generally increase from quartile 2 to 4. This could potentially be the result of certain high use areas being located in low density areas, for example, in downtown Minneapolis (low number of residents), high-use off-street trails in residential areas (e.g., Cedar Lake Trail), and around parks and lakes (i.e., along the Mississippi River or the Chain of Lakes). Population density may be an indicator of generating non-motorized traffic but it does not appear to be well correlated with where people walk and bike. Trends in particulate concentrations were also mixed; it appears there may be a slight increase in concentrations from quartiles 2 to 4 but concentrations in most quartiles were slightly lower than in the first quartile. This suggests that on a neighborhood scale,

population density is not well correlated with either particulate concentrations or non-motorized traffic volumes.

To explore any possible interaction between land use mix and population density I used bivariate analysis to evaluate both factors simultaneously. Figure 5.18 shows trends in active travel and particulate concentrations buy quartile of population density (x-axis) and quartile of land use mix (separate data series for each quartile). In general, rates of active travel increased as both population density and land use mix increased; however, other patterns that also emerge. For example, areas with the lowest quartile of both land use mix and population density had the lowest traffic volumes; conversely, areas in the highest quartile of both factors had the highest traffic volumes. Results were mixed for neighborhoods that had moderate amounts of mixing and density. For both bicycles and pedestrians, when land use mix is high (i.e., for the highest quartile), population density was correlated with traffic volumes. Particulate concentrations were mostly unchanged regardless of amount of density and land use mix; concentrations increased very slightly at higher population densities for the mornings. Although not causal, these results suggest that a health-promoting urban planning strategy may be to locate pockets of land use that are dense and well mixed in areas that are removed from emission sources but close to residential areas (i.e., people). This type of strategy may have the potential to encourage active travel while minimizing exposure to particulate air pollution.

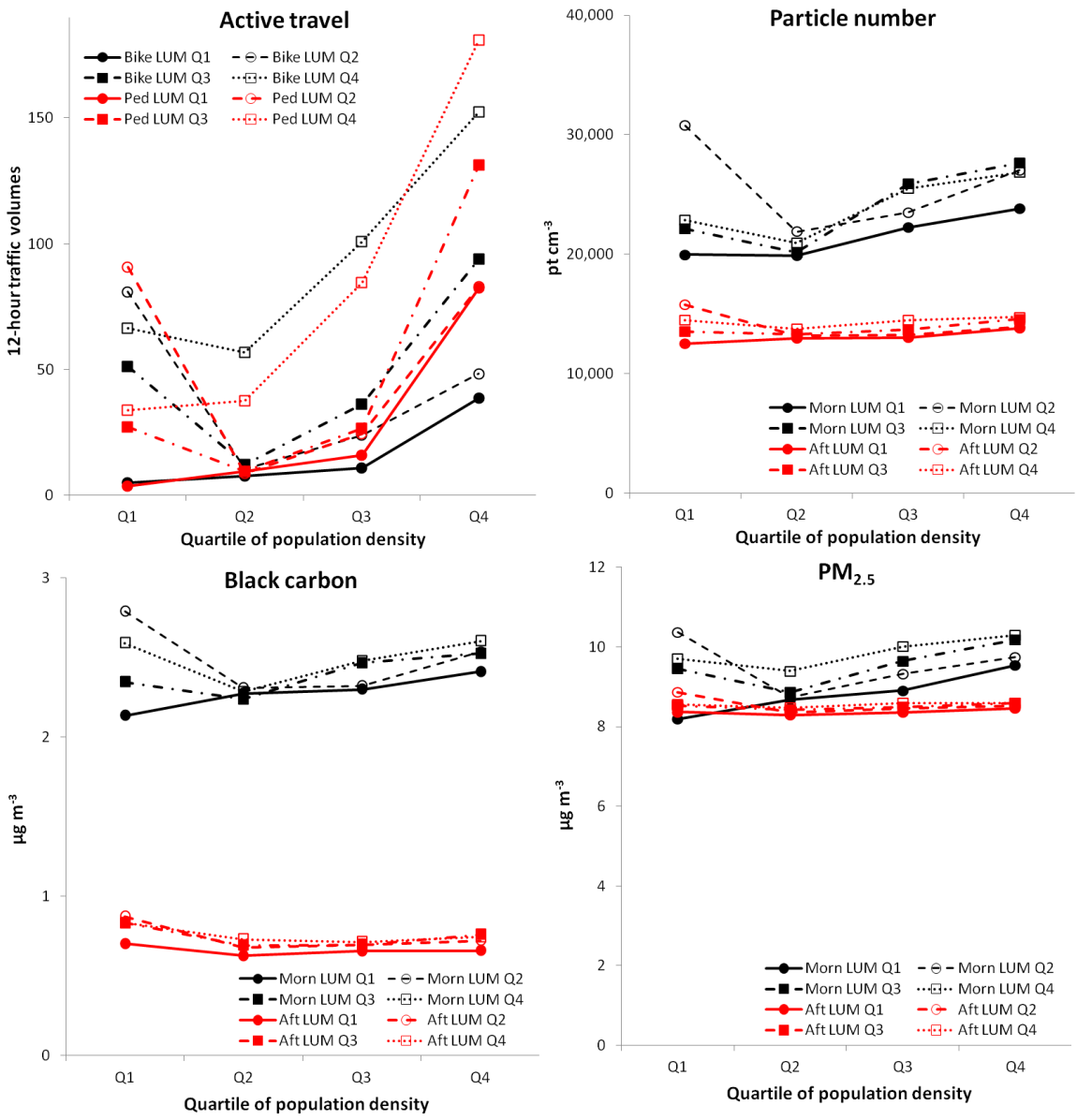

Figure 5.18 Rates of active travel and particulate concentrations by population density and land use mix (x-axis is by quartile of population density; lines represent quartiles of land use mix).

Another important aspect of planning for healthy cities is ensuring access to health promoting neighborhoods is distributed equitably among the population. In the environmental justice literature two metrics commonly used to explore equity issues for

exposure to environmental hazards are household income and race (Brooks and Sethi, 1997; Clark et al., 2014; Schweitzer and Zhou, 2010; Miranda et al., 2011). Following those studies I stratified my model estimates by median household income and proportion of non-white residents (calculated at the block group level; Figure 5.19).

Bicycle and pedestrian traffic was highest in low-income block groups and areas with the highest proportions of non-whites. Since traffic count information does not yield information on where pedestrians and bicyclists live, it is not possible to infer whether active travel within a certain area can be attributed primarily to residents in that neighborhood or primarily people from outside the neighborhood. Likely both cases exist, for example, downtown Minneapolis has a low household median income and high proportion of non-whites but a low resident population in general, yet the highest recorded counts were in downtown Minneapolis. That result is consistent with the hypothesis that most cyclists and pedestrians in downtown Minneapolis were not residents but rather at those locations for other purposes (likely, employment); it is also possible that more localized neighborhood traffic away from downtown may be primarily due to local residents. Regardless, for this dataset, non-motorized traffic levels seem to be associated with lower household income and higher proportions of non-white residents.

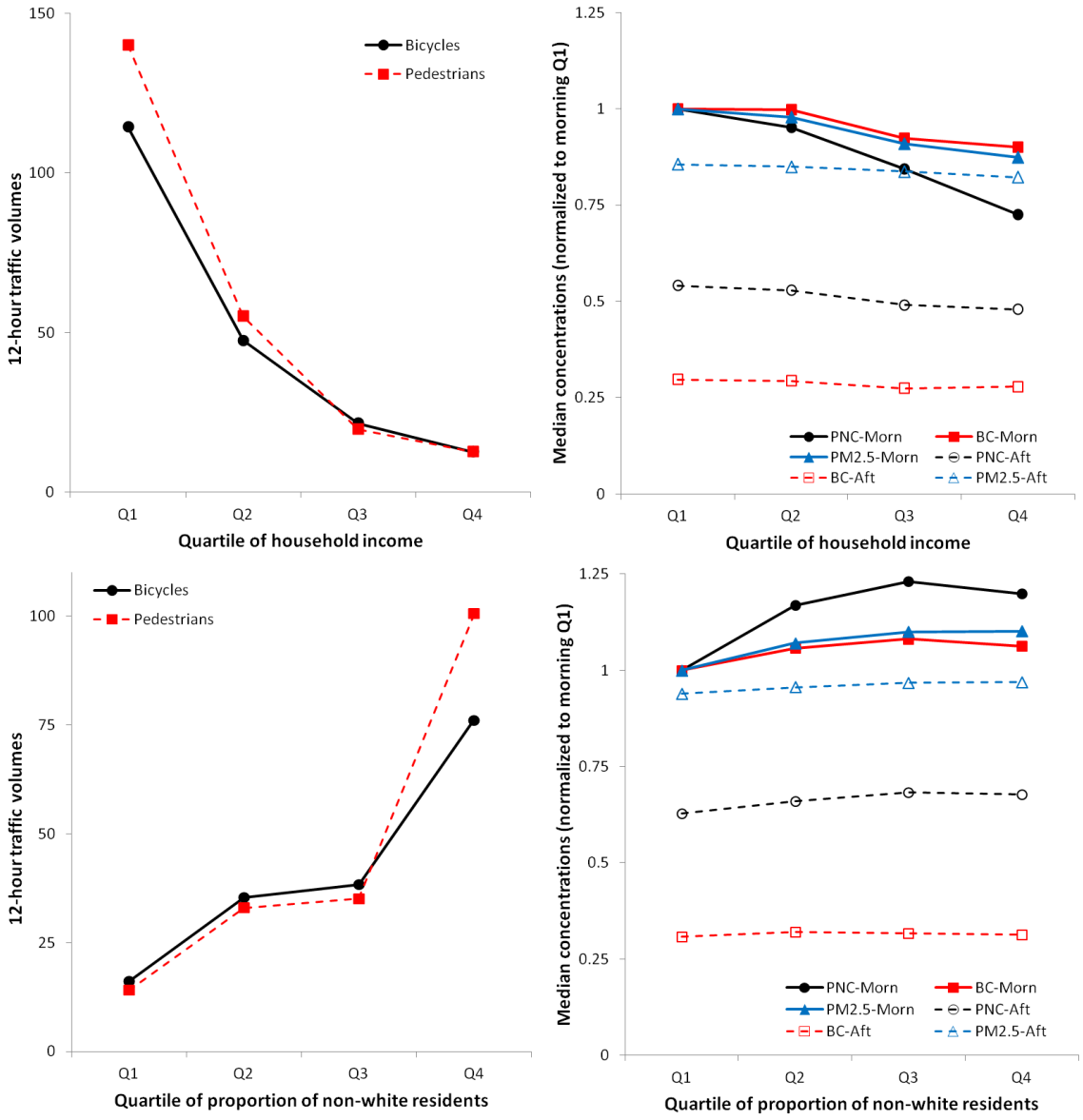

Figure 5.19 Median non-motorized traffic volumes and LUR concentration estimates by quartile of median neighborhood household income and proportion of non-white residents.

Particulate concentrations decreased with higher household income and lower proportions of non-white residents. That result is consistent with results of previous studies of environmental injustice for ambient air pollution (Clark et al., 2014; Hajat et

al., 2013; Marshall et al., 2014; Miranda et al., 2011). The differences in concentrations between high- and low-income areas as well as between high and low proportions of non-white residents were largest for particle number concentrations. There was also a fairly strong trend (not shown in Figures 5.19 and 5.20) for smaller particle sizes in low-income, non-white areas, which is consistent with those locations being located nearer to fresh combustion emissions. These trends in particulate concentrations coupled with the increased volumes of bicycle and pedestrian traffic suggest that a large portion of the air pollution exposure burden while walking and biking is likely occurring in low-income, non-white neighborhoods.

To explore any interaction between these two metrics I plotted (Figure 5.20) rates of active travel and particulate concentration by quartile of household income (x-axis) and quartile of non-white residents (separate data series). In general, rates of active travel decreased as income increased. Active travel was higher in neighborhoods with more non-white residents; however, this difference was largest in low-income neighborhoods and diminished in high-income areas. Particulate concentrations were lowest in areas of high income; in some cases (e.g., black carbon in mornings), concentrations were also elevated in areas with higher proportions of non-whites. The trends shown in Figure 5.20 suggest that rates of active travel are high in low-income, non-white communities and that concentrations are also slightly higher in those areas.

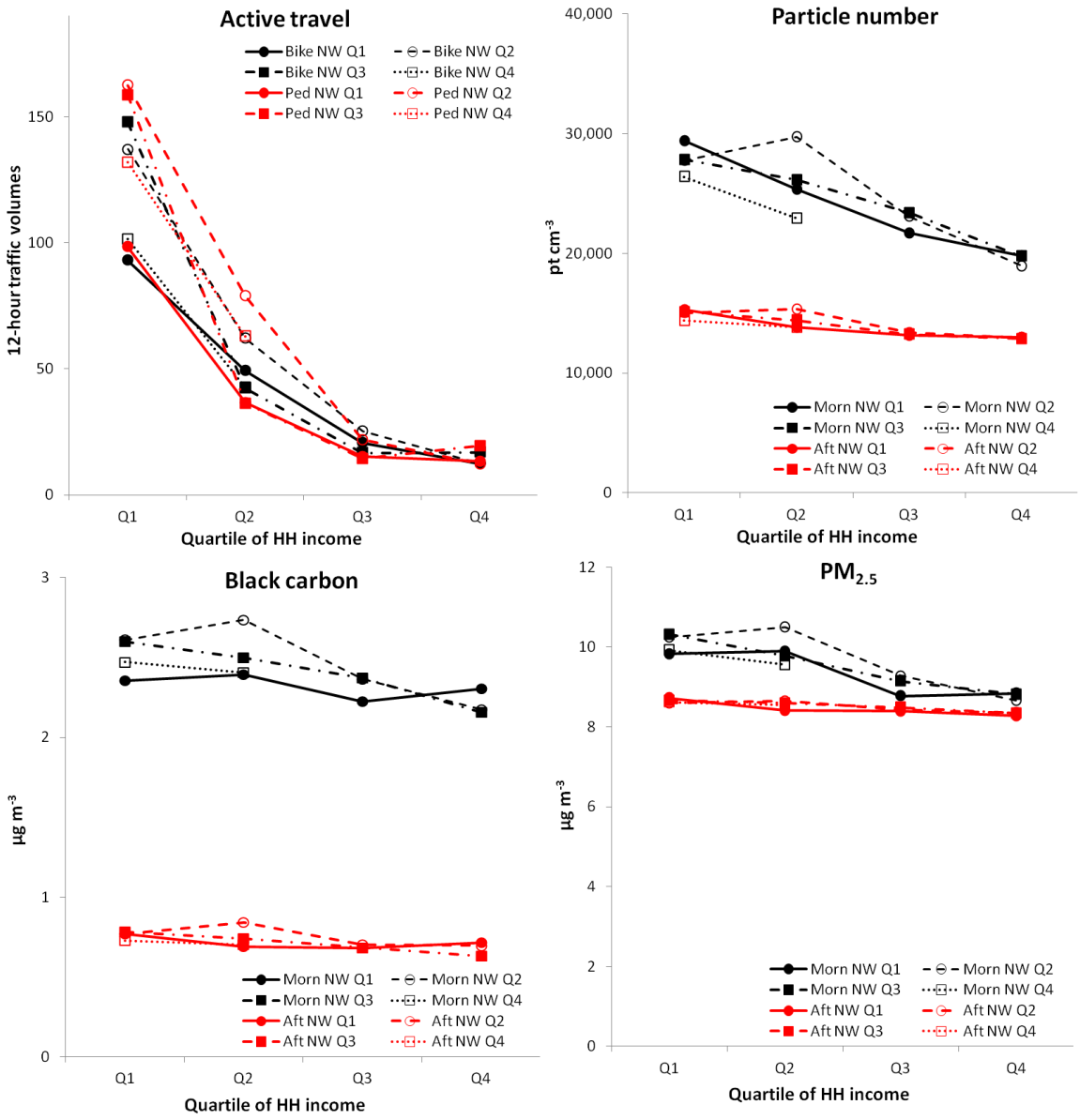

Figure 5.20 Neighborhood-level rates of active travel and particulate concentrations by household income and proportion of non-white residents (x-axis is by quartile of income; lines represent quartiles of proportion of non-white residents). Note: Third and fourth quartiles of income are not shown for the highest quartile of proportion of non-whites since those samples sizes were very small.

Chapter conclusions

This chapter described spatial patterns of particulate air pollution in Minneapolis, MN derived from estimates of concentrations from the LUR models presented in Chapter 4. I compared spatial patterns of particulate air pollution to patterns of non-motorized traffic estimated by statistical models of volunteer-based counts. Key results from this comparison are listed below:

1. Estimates of pollutant concentration generally follow intuitive spatial patterns, with higher concentrations on-roadway and near downtown. Concentrations as well as spatial variability were higher in the mornings than in afternoons. There were small shifts in concentration "hot-spots" between mornings and afternoons.
2. Spatial patterns of non-motorized traffic can be described using short-duration counts. While longer-term counts would improve estimation accuracy general trends were modeled using extrapolations of peak-hour volunteer-based counts.
3. Combining spatial information about particulate air pollution and non-motorized traffic allowed for identification of characteristic neighborhood types. Relatively few neighborhoods were classified as "healthy" (1%; high active travel; low air pollution); most neighborhoods are either "high exposure" (12%; high active travel; high air pollution) or "opportunity" areas (12%; low active travel; low air pollution). Identifying neighborhoods in these categories highlighted areas where changing one factor (active travel rates or

air pollution exposure) would push those neighborhoods into the “healthy” category.

4. Patterns of active travel and air pollution exposure by street functional class suggest shifts in to the transportation network that may reduce exposure (i.e., moving bikers away from pollution and moving pollution away from pedestrians).
5. Land use mix was associated with increased active travel and did not seem to influence particulate concentrations; no discernible pattern was observed between population density and either factor.
6. Based on the model estimates described here, the highest rates of active travel are in neighborhoods with low-income and a high proportions of non-whites. Air pollution concentrations too are highest in those neighborhoods.

Chapter 6 Conclusions

This dissertation describes the collection and use of data from mobile, on-road measurements of particulate air pollution concentrations to explore patterns of exposure during active travel. In this final chapter I summarize core conclusions from the analyses presented above. My conclusions include both methodological findings (i.e., how best to collect, adjust, and model my data) as well as empirical findings (i.e., what I learned about how exposure occurs during active travel). I summarize these two sets of conclusions separately and discuss how future research may improve our understanding of this topic.

Methodological findings

I developed a sampling platform that allowed for real-time, mobile measurements of on-road particulate concentrations. I made modest modifications to commercially available products to develop the platform; specifically, (1) I added a padded mounting baseboard (to minimize vibrations) and an elevated air intake to the bicycle trailer and (2) I made slight hardware modifications to the air pollution devices to disable a tilt alarm and better keep batteries in place during sampling runs.

An important aspect of how I chose sampling routes included choosing roads from all street functional classes and a variety of land uses. While those goals remain important in future mobile sampling campaigns, my analyses indicate taking additional factors into account may be helpful. For example, industrial area was significant in all 8 of the final land use regression (LUR) models I used for extrapolation and was also correlated with truck traffic (regressions based on video-based traffic counts). Where

information on truck traffic volumes is available stratifying sampling routes by both industrial area and level of truck traffic may shed light on which factor is more correlated with on-road concentrations. Additionally, where information on actual traffic counts for the time periods of interest are available it may be helpful to systematically sample for all traffic levels rather than use street classification as a proxy.

I controlled for day-to-day differences in background concentrations across sampling days by using underwrite functions. This approach better characterized non-linear changes in background concentrations than linear interpolation or simply averaging reference measurements before and after sampling runs. Using the underwrite functions better characterized parameters such as the proportion of exposure due to in-traffic emissions (φ) and allowed for analysis of the how background vs. on-road concentrations are correlated with parameters such as particle size. A key outcome of using the underwrite functions was the development of a dataset that was adjusted for day-to-day variability in background concentrations to use in analyses of the spatial patterns of the measured pollutants.

I modeled spatial patterns of particulate concentrations using LUR. I developed a method to use mobile measurements of particulate concentrations rather than fixed-site, long-term measurements. I found that the scale of spatial aggregation (i.e., 50-200m) of the air pollution measurements had little impact on model performance; however, increasing spatial resolution (i.e., aggregating measurements at smaller distance) reduced the ability to model parameters other than central tendencies at each aggregation location. In general, minimal time averaging of the mobile measurements was needed to build

LUR models; an exception was for black carbon which required slight (i.e., 60s) temporal smoothing to reduce noise in the measurement data. Since the number of aggregation locations used for the final models was large (n~1,100) I was able to perform both systematic and random model validation for larger subsets of the data than for typical models. Models were mostly robust to a random 1/3 hold-out of the input data; models were not robust to a systematic hold-out of each sampling route. Future sampling campaigns should better design sampling routes to vary all emission parameters (i.e., traffic measures, land uses) within each route and not only among all routes if systematic validation is desired. Finally, I found that model residuals were spatially autocorrelated for ~10% of the aggregation locations. At these locations models mostly underestimated concentrations; I hypothesize that the reason for the underestimates is heavy congestion at those locations that is not represented in the GIS-based independent variables in my models. When modeling for specific times of day, future studies should try to also include variables that capture traffic patterns specifically for those times of day.

Empirical findings

I found that traffic emissions were a significant component of exposure during active travel. For example, I calculated the share of concentrations attributable to on-road sources (φ) in mornings [afternoons] for each pollutant: particle number 59% [41%], black carbon 45% [54%], and $PM_{2.5}$ 31% [24%]. Particle number and black carbon concentrations were the most correlated pollutants for my on-road measurements (1 [30] minute time average R^2: 0.39 [0.61]). All between-pollutant correlations increased with averaging time. Particle size was correlated with particle number (inverse correlation)

and black carbon (direct correlation) concentration. When I separated concentrations into a background and on-road component, background concentrations better explained particle size.

Motor-vehicle traffic in close proximity to my bicycle during sampling was correlated with increased concentrations. I used the video footage from the camera mounted on my handlebars to estimate traffic counts at a randomly selected set of locations along the sampling route. Regression using separate counts of trucks, buses, and passenger vehicles suggest that all vehicle types are correlated with increased short-duration spikes in concentrations but that trucks are correlated with the largest magnitude of increased concentrations. For example, a truck in the video frame was correlated with a 30,600 pt/cc [1.6 $\mu g/m^3$] increase in particle number [black carbon] concentration compared to a 2,300 pt/cc [0.26 $\mu g/m^3$] increase for buses and a 240 pt/cc [0.02 $\mu g/m^3$] increase for passenger-vehicles. These findings suggest traffic in general is important for exposure but also that infrequent events such as a passing truck can be important (and quantifiable) for acute exposure events.

The LUR models I developed using the mobile measurements suggest land use can partly explain local variation in particulate concentrations. A number of variables were commonly selected in the LUR models including those related to separation from emission sources (e.g., open space area, distance from major roads, length of local [low-traffic] roads) and proximity to and density of emission sources (e.g., industrial area, house density, length of high-traffic roads). One variable that was selected in all final LUR models here was industrial area. It is possible that emissions within the industrial

areas are responsible for increased emissions leading to increased concentrations; however, it is also plausible that industrial area is simply a proxy for increased truck traffic. I found via the video footage that high counts of trucks were more likely to be in industrial areas.

The LUR models presented in Chapter 4 had modest goodness-of-fit. Morning [afternoon] adjusted R^2 were 0.50 [0.48] for particle number, 0.28 [0.42] for black carbon, 0.30 [0.49] for $PM_{2.5}$, and 0.29 [0.20] for particle size. This is at least partly owing to the fact that most models underestimated concentrations at locations where measured concentrations were highest. Inspection of spatial autocorrelation among model residuals revealed that locations where the models performed poorly were mostly on busy arterials near on/off ramps to freeways. These locations were heavily congested during sampling (i.e., stop and go traffic); furthermore, the level of congestion is exacerbated at these locations during rush-hours (when I sampled). These traffic patterns were not captured in my GIS variables and could be a reason for the model underestimates. As such, my estimates of pollutant concentrations in Minneapolis are likely conservative for some locations.

Spatial patterns of particulate concentrations generally followed intuitive patterns (i.e., elevated concentrations were near activity centers and major roads). Spatial variability and the absolute value of concentrations were higher in the mornings than in the afternoons. Particle size was smallest near freeways and downtown Minneapolis and largest in the outlying neighborhoods. Small-scale shifts in concentration hot-spots were apparent from the estimated concentration surfaces during morning and afternoon rush-

hour. For example, in the mornings hot-spots were mostly located near freeways (e.g., I-94 and I-35W interchange) but shifted slightly to major roads on the municipal network (e.g., downtown Minneapolis) in the afternoon.

In Chapter 5 I outlined a sample application of the LUR models developed in Chapter 4. Specifically, I used GIS to overlay the LUR output and estimates of bicycle and pedestrian traffic volumes (from statistical models based on peak-hour counts) to identify areas that were classified as "healthy" (high rates of active travel, low particulate concentrations) and "high exposure" (high rates of active travel, high particulate concentrations). I found that few areas in Minneapolis were classified as "healthy" and identified areas where shifting one health determinant (e.g. increasing active travel or reducing concentrations) would shift neighborhoods to the "healthy" category.

Comparing concentrations with non-motorized traffic volumes allowed for exploration of population-level patterns of exposure. In Chapter 5 I highlighted how small changes to the transportation network potentially could improve population-level exposure. For example, shifting bicycle traffic from major roads to adjacent, parallel local roads would reduce morning [afternoon] exposure concentrations by an estimated 21% [12%] for particle number, 15% [20%] for black carbon, and 7% [3%] for $PM_{2.5}$. I also explored how both non-motorized traffic and particulate concentrations were associated with traditional planning goals, i.e., increasing land use mix and population density. Greater land use mix was associated with increased non-motorized traffic and did not seem to impact median concentrations; population density did not seem to be correlated strongly with either factor. These findings suggest increasing pocket areas of

land use mix in areas where there are low concentrations (i.e., residential neighborhoods) may be a health promoting planning strategy. More work is needed to confirm what land use planning strategies will yield the most health promoting neighborhoods for these risk factors. Lastly, I found that low income and non-white neighborhoods were associated with elevated levels of active travel and higher levels of particulate air pollution suggesting the burden of exposure during active travel is high in those neighborhoods.

Potential future areas of research

This dissertation offers evidence that spatial patterns of exposure to air pollution during active travel are important to building health promoting cities. However, there are many areas of research that can improve our understanding of how best to assess exposure and better plan for active travel. I briefly discuss some of these issues as they relate to what I have learned from my measurements.

First, my LUR models were developed for very specific time periods (i.e., 7-9am and 4-6pm during late summer/early fall). Key questions remain on how or whether short-duration estimates of concentrations can be scaled to longer-term (e.g., annual-average) concentration estimates. One can imagine a monitoring system that consists of carefully selected long-term measurement sites which could be used to scale short-duration measurements (either from mobile or temporary fixed-site measurements) to long-term averages. A little studied area is what uncertainty exists with this type of approach and what number of mobile-monitoring measurements would be needed at a short-duration site to reliably scale to long-term averages. For example, I completed 10 sampling runs per route in the afternoon and 4 per route in the morning; presumably,

when aggregating those measurements spatially the afternoon results would give closer to "typical" concentrations at those locations for that time period than the morning (since more sampling runs were completed in the afternoon). However, I have no way to relate those concentrations to annual-averages or seasonal patterns at those locations. More research into how coupling fixed-site reference networks and short-duration measurements (mobile or otherwise) would help a great deal in reducing the cost of assessing spatial patterns of air pollution.

Merging temporal and spatial aspects of LUR modeling would be a worthwhile goal for explaining exposure patterns. A limitation to modeling spatiotemporal patterns of pollutant concentrations is the necessary input data used to predict concentrations. For example, I used mainly GIS based variables in my LUR models (as is typical for most LUR modeling). I hypothesized that my models underestimated higher concentrations due to the lack of temporally resolved input data; in this case information about congestion during rush-hour that was not captured in the annual-average based traffic intensity raster developed by the Minnesota Pollution Control Agency. As such, work is needed to generate input data to LUR modeling that reflects the spatiotemporal nature of emission sources such as motor-vehicle traffic patterns.

Similarly, more information on the exposure population of interest (cyclists and pedestrians) would greatly aid in assessing exposure. I used a limited set of peak-hour bicycle and pedestrian counts to estimate non-motorized traffic volumes. If more counts such as these were designed systematically to capture spatial and temporal variability in traffic patterns, population-level exposure analyses like those described in Chapter 5

would be more robust. Two areas of research that are beginning to address this issue are (1) design of systematic bicycle and pedestrian counting programs (modeled after those of motor-vehicles) with the aim of estimating traffic volumes and (2) description of time-activity patterns using mobile phone apps. These two approaches are complementary in that one aims to describe flows of traffic (i.e., count programs) and the other personal exposure patterns (i.e., time-activity patterns); both are critical to our understanding of how populations are exposed to air pollution.

Lastly, more work is needed to inform planners and policy-makers on best practices for making healthy places and cities. For example, my models suggest that strategies such as moving bicycle traffic to local roads (e.g., bicycle boulevards) would reduce exposure. This type of strategy makes sense since cyclists seem to prefer facilities (i.e., statistical models show increased traffic on roads with bike facilities) meaning city planners could simultaneously promote active travel while reducing exposure. Another approach may be increasing land use mix in pocketed areas (i.e., residential neighborhoods) to increase active travel where exposures are low. However, my results are based purely on statistical models; other, case-specific studies (such as intervention studies) are needed to confirm and extend these ideas. A final thought is that when implementing these strategies it is important to ensure that access to health promoting places are distributed in equitable ways. My model results suggest that the highest burden of exposure during active travel occurs in low-income, non-white neighborhoods. More research is warranted on not only how urban populations are exposed but how those patterns are distributed among the population.

I would like to close this dissertation by saying that I have enjoyed working on this topic! My hope is that this work contributes not only to our knowledge of how and where people are exposed to air pollution but how we plan for healthy, clean cities. More work is needed to that end and hopefully this moves us ever so slightly down that path.

Bibliography

Abernathy, R.C., Allen, R.W., McKendry, I.G., Brauer, M., 2013. A land use regression model for ultrafine particles in Vancouver, Canada. Environmental Science and Technology, 47(10), 5217-5225.

Adams, J., 2010. Prevalence and socio-demographic correlates of "active transport" in the UK: analysis of the UK time use survey 2005. Preventive Medicine, 50(4), 199-203.

Aggarwal, S., Jain, R., Marshall, J.D., 2012. Real-time prediction of size-resolved ultrafine particulate matter on freeways. Environmental Science and Technology, 46(4), 2234-2241.

Akita, Y., "LUR Tools: ArcGIS Toolbox for Land Use Regression (LUR) Model." Available: http://www.unc.edu/~akita/lurtools/ [2 June 2014].

Andersen, L.B., Schnohr, P., Schroll, M., Hein, H.O., 2000. All-cause mortality associated with physical activity during leisure time, work, sports, and cycling to work. Archive of Internal Medicine, 160(11), 1621-1628.

Anselin, L., 1995. Local Indicators of Spatial Association – LISA. Geographical Analysis, 27(2), 93-115.

Apte, J.S., Kirchstetter, T.W., Reich, A.H., Deshpande, S.J., Kaushik, G., et al., 2011. Concentrations of fine, ultrafine, and black carbon particles in auto-rickshaws in New Dehli, India. Atmospheric Environment, 45(26), 4470-4480.

Atten, C. Van, Brauer, M., Funk, T., Gilbert, N.L., Graham, L., 2005. Assessing population exposures to motor vehicle exhaust. Reviews on Environmental Health. 20(3), 195-214.

Aultman-Hall, L., Lane, D., Lambert, R., 2009. Assessing impact of weather and season on pedestrian traffic volumes. Transportation Research Record, 2140, 35-43.

Barton, J., Pretty, J., 2010. What is the best dose of nature and green exercise for improving mental heatlh? A multi-study analysis. Environmental Science and Technology. 44(1), 3947-3955.

Bechle, M.J., Millet, D.B., Marshall, J.D., 2011. Effects of income and urban form on urban NO_2: global evidence from satellites. Environmental Science and Technology, 45(11), 4914-4919.

Beckerman, B.S., Jerrett, M., Serre, M., Martin, R.V., Lee, S.J., et al., 2013. A hybrid approach to estimating national scale spatiotemporal variability of PM2.5 in the contiguous United States. Environmental Science and Technology, 47(13), 7233-7241.

Beelen, R., Hoek, G., Fischer, P., van den Brandt, P.A., Brunekreef, B., 2007. Estimated long-term outdoor air pollution concentrations in a cohort study. Atmospheric Environment, 41(7), 1343-1358.

Beelen, R., Hoek, G., van den Brandt, P.A., Goldbohm, A., Fischer, P., et al., 2008. Long-term effects of traffic-related air pollution on mortality in a Dutch cohort (NLCS-AIR study). Environmental Health Perspectives, 116(2), 196-202.

Beelen, R., Hoek, G., Vienneau, D., Eeftens, M., Dimakopoulou, K., et al., 2013. Development of NO2 and NOx land use regression models for estimating air pollution exposure in 36 study areas in Europe – the ESCAPE project. Atmospheric Environment, 72, 10-23.

Bell, M.L., Davis, D.L., Fletcher, T., 2004. A retrospective assessment of mortality from the London smog episode of 1952: the role of influenza and pollution. Environmental Health Perspectives, 112(1), 6-8.

Bell, M.L., Dominici, F., Samet, J.M., 2005. A meta-analysis of time-series studies of ozone and mortality with comparison to the national morbidity, mortality, and air pollution study, Epidemiology, 16(4), 436-445.

Bell, M.L., McDermott, A., Zeger, S.L., Samet, J.M., Dominici, F., 2004. Ozone and short-term mortality in 95 US urban communities, 1987-2000. Journal of the American Medical Association, 292(19), 2372-2378.

Behnam, J., and Patel, B.G., 1977. A method for estimating pedestrian volume in a central business district. Transportation Research Record, 629, 22-26.

Bigazzi, A.Y., Figliozzi, M.A., 204. Review of urban bicyclists' intake and uptake of traffic-related air pollution. Transport Reviews, 34(2), 21-245.

Borriello, G., Chalmers, M., LaMarca A., Nixon, P., 2005. Delivering real-world ubiquitous location systems. Communications of the ACM, 48(3), 36-41.

Both, A.F., Balakrishnan, A., Joseph, B., Marshall, J.D., 2011. Spatiotemporal aspects of real-time PM2.5: low- and middle-income neighborhoods in Bangalore, India. Environmental Science and Technology, 45(13), 5629-5636.

Brauer, M., Hoek, G., van Vliet, P., Meliefste, K., Fischer, P., 2003. Estimating long-term average particulate air pollution concentrations: application of traffic indicators and geographic information systems. Epidemiology. 14(2), 228-239.

Brauer, M., Lencar, C., Tamburic, L., Koehoorn, M., Demers, P., et al., 2008. A cohort study of traffic-related air pollution impacts on birth outcomes. Environmental Health Perspectives, 116(12), 519.

Briggs, D., 2005. The role of GIS: coping with space (and time) in air pollution exposure assessment. Journal of Toxicology and Environmental Health Part A, 68(13-14), 1243-1261.

Briggs, D.J., de Hoogh, C., Gulliver, J., Wills, J., Elliott, P., 2000. A regression-based method for mapping traffic-related air pollution: application and testing in four contrasting urban environments. Science of the Total Environment, 253(1-3), 151-167.

Briggs, D.J., de Hoogh, K., Morris, C., Gulliver, J., 2008. Effects of travel mode on exposures to particulate air pollution. Environment International, 34(1), 12-22.

Brooks, N., Sethi, R., The distribution of pollution: community characteristics and exposure to air toxics. Journal of Environmental Economic Management, 32(2), 233-250.

Brugge, D., Durant, J.L., Rioux, C., 2007. Near-highway pollutants in motor vehicle exhaust: a review of epidemiologic evidence of cardiac and pulmonary health risks. Environmental Health, 6(23), 1-12.

Brunekreef, B., Holgate, S.T., 2002. Air pollution and health. The Lancet, 360 (9341), 1233-1242.

Cao, X., Handy, S., Mokhtarian, P., 2006. The influences of the built environment and residential self-selection on pedestrian behavior: evidence from Austin, TX. Transportation, 33(1), 1-20.

Carr, D., von Ehrenstein, O., Weiland, S., Wagner, C., Wellie, O., 2002. Modeling annual benzene, toluene, NO_2, and soot concentrations on the basis of road traffic characteristics. Environmental Research, 90(2), 111-118.

CDC (Centers for Disease Control and Prevention), 2012. "CDC's Healthy Communities Program: Program Overview." Available: http://www.cdc.gov/healthycommunitiesprogram/overview/index.htm [1 May 2012].

Chakrabarti, B., Fine, P.M., Delfino, R., Sioutas, C., 2004. Performance evaluation of the active-flow personal DataRAM PM2.5 mass monitor (Thermo Anderson pDR-1200) designed for continuous personal exposure measurements. Atmospheric Environment, 38(20), 3329-3340.

Chauhan, A.J., Inskip, H.M., Linaker, C.H., Smith, S., Schreiber, J., et al., 2003. Personal exposure to nitrogen dioxide (NO2) and the severity of virus-induced asthma in children. The Lancet, 361(9373), 1939-1944.

City of Minneapolis. Crime Statistics and Reports. Available: www.minneapolismn.gov/police/crime-statistics [8 May 2010].

Clark, L.P., Millet, D.B., Marshall, J.D., 2011. Air quality and urban form in the US urban areas: evidence from regulatory monitors. Environmental Science and Technology, 45(16), 7028-7035.

Clark, L.P., Millet, D.B., Marshall, J.D., 2014. National patterns in environmental injustice and inequality: outdoor NO_2 air pollution in the United States. PLoS ONE, 9(4), e94431.

Cohen, M.A., Adar, S.D., Allen, R.W., Avol, E., Curl, C.L., 2009. Approach to estimating participant pollutant exposures in the multi-ethnic study of Atherosclerosis and air pollution (MESA Air). Environmental Science and Technology. 43(13), 4687-4693.

Correia, A.W., Pope, C.A., Dockery, D.W., Wang, Y., Ezzati, M., et al., 2013. Effect of air pollution control on life expectancy in the United States: an analysis of 545 counties for the period from 2000 to 2007. Epidemiology, 24(1), 23-31.

Crouse, D.L., Peters, P.A., van Donkelaar, A., Goldberg, M.S., Villeneuve, P.J., et al., 2012. Risk of nonaccidental and cardiovascular mortality in relation to long-term exposure to low concentrations of fine particulate matter: a Canadian national-level cohort study. Environmental Health Perspectives, 120(5), 708-714.

Cyrys, J., Hochadel, M., Gehring, U., Hoek, G., Diegmann, V., et al., 2005. GIS-based estimation of exposure to particulate matter and NO_2 in an urban area: stochastic versus dispersion modeling. Environmental Health Perspectives, 113(8), 987-992.

Daniels, M.J., Dominici, F., Samet, J.M., Zeger, S.L., 2000. Estimating particulate matter-mortality dose-response curves and threshold levels: an analysis of daily time-series for the 20 largest US cities. American Journal of Epidemiology, 152(5), 397-406.

de Hartog, J.J., Boogaard, H., Nijland, H., Hoek, G., 2010. Do the health benefits of cycling outweigh the risks. Environmental Health Perspectives, 118(8), 1109-1116.

de Hoogh, K., Wang, M., Adam, M., Badaloni, C., Beelen, R., et al., 2013. Development of land use regression models for particle composition in twenty study areas in Europe. Environmental Science and Technology, 47(11), 5778-5786.

Dill, J., 2009. Bicycling for transportation and health: the role of infrastructure. Journal of Public Health Policy, 30, S95-S110.

Dockery, D.W., Pope, C.A., Xu, X., Spengler, J.D., Ware, J.H., et al., 1993. An association between air pollution and mortality in six US cities. The New England Journal of Medicine, 329(24), 1753-1759.

Dominici, F., Peng, R.D., Bell, M.L., Pham, L., McDermott, A., et al., 2006. Fine particulate air pollution and hospital admission for cardiovascular and respiratory diseases. Journal of the American Medical Association, 295(10), 1127-1134.

Dons, E., Int Panis, L., Van Poppel, M., Theunis, J., Wets, G., 2012. Personal exposure to black carbon in transport microenvironments. Atmospheric Environment, 55, 392-398.

Dons, E., Int Panis, L., Van Poppel, M., Theunis, J., Willems, H., et al., 2011. Impact of time-activity patterns on personal exposure to black carbon. Atmospheric Environment, 45(21), 3594-3602.

DPW (Department of Public Works, City of Minneapolis), 2011. "Non-Motorized Traffic Counts Operations and Estimation Methodology." City of Minneapolis. Available: http://www.minneapolismn.gov/www/groups/public/@publicworks/documents/images/wcms1p-085492.pdf [10 May 2010].

Eeftens, M., Beelen, R., de Hoogh, K., Bellander, T., Cesaroni, G., et al., 2012. Development of land use regression models for PM(2.5), PM(2.5) absorbance, PM(10)

and PM(coarse) in 20 European study areas; results of the ESCAPE project. Environmental Science and Technology, 46(20), 11195-11205.
EPA (Environmental Protection Agency), 2013. "National Ambient Air Quality Standards for Particulate Matter." Federal Register, 78(10), [EPA-HQ-OAR-2007-0492; FRL-9761-8].
Esaway, M.E., Lim, C., Sayed, T., Mosa, A.I., 2013. Development of daily adjustment factors for bicycle traffic. Journal of Transportation Engineering, 139(8), 859-871.
ESRI (Environmental Systems Research Institute), 2014. "How spatial autocorrelation (Global Moran's I) works." Available: http://resources.arcgis.com/en/help/main/10.1/index.html#//005p0000000t000000 [15 July 2014].
Ewing, R., Cervero, R., 2001. Travel and the built environment. Transportation Research Record, 1780, 87-114.
Fan, Y., Guthrie, A., Levinson, D., 2012. Impact of light rail implementation on labor market accessibility: A transportation equity perspective. Journal of Transport and Land Use, 5(3), 28-39.
FHWA (Federal Highway Administration), 1998. "Transportation and Global Climate Change: A Review and Analysis of the Literature." US Department of Transportation. Report No: DOT-T-97-03.
Frank, L.D., Andresen, M.A., Schmid, T.L., 2004. Obesity relationships with community design, physical activity, and time spent in cars. American Journal of Preventive Medicine, 27(2), 87-96.
Frank, L.D., Engelke, P., 2005. Multiple impacts of the built environment on public health: walkable places and exposure to air pollution. International Regional Science Review, 28(2), 193-216.
Friedman, M.S., Powell, K.E., Hutwagner, L., Graham, L.M., Teague, W.G., 2001. Impact of changes in transportation and commuting behaviors during the 1996 summer Olympic games in Atlanta on air quality and childhood asthma. Journal of the American Medical Association, 285(7), 897-905.
Fruin, S., Westerdahl, D., Sax, T., Sioutas, C., Fine, P.M., 2008. Measurements and predictors of on-road ultrafine particle concentrations and associated pollutants in Los Angeles. Atmospheric Environment, 42(2), 207-219.
Fruin, S., Winer, A.M., Rodes, C.E., 2004. Black carbon concentrations in California vehicles and estimation of in-vehicle diesel exhaust particulate matter exposure. Atmospheric Environment, 38(25), 4123-4133.
Gauderman, W.J., Vora, H., McConnell, R., Berhane, K., Gilliland, F., et al., 2007. Effect of exposure to traffic on lung development from 10 to 18 years of age: a cohort study. The Lancet. 369(9561), 571-577.

Gilbert, N., Woodhouse, S., Stieb, D., Brook, J., 2003. Ambient nitrogen dioxide and distance from a major highway. Science of the Total Environment, 312(1-3), 43-46.
Grabow, M.L., Spak, S.N., Holloway, T., Stone Jr., B., Mednick, A.C., Patz, J.A., 2011. Air quality and exercise-related health benefits from reduced car travel in the Midwestern United States. Environmental Health Perspectives, 120(1), 68-76.
Gulliver, J., de Hoogh, K., Hansell, A., Vienneau, D., 2013. Development and back-extrapolation of NO2 land use regression models for historic exposure assessment in Great Britain. Environmental Science and Technology, 47(14), 7804-7811.
Gulliver, J., Morris, C., Lee, K., Vienneau, D., Briggs, D., et al., 2011. Land use regression modeling to estimate historic (1962-1991) concentrations of black smoke and sulfur dioxide for Great Britain. Environmental Science and Technology, 45(8), 3526-3532.
Guo, J., Bhat, C., Copperman, R., 2007. Effect of the built environment on motorized and non-motorized trip making: substitutive, complementary, or synergistic? Transportation Research Record, 2010(1), 1-11.
Hajat, A., Diez-Roux, A.V., Adar, S.D., Auchincloss, A.H., Lovasi, G.S., et al. 2013. Air pollution and individual and neighborhood socioeconomic status: evidence from the multi-ethnic study of atherosclerosis (MESA). Environmental Health Perspectives, 121(11-12), 1325-1333.
Hamer, M., Chida, Y., 2008. Active commuting and cardiovascular risk: a meta-analytic review. Preventive Medicine, 46(1), 9-13.
Handy, S., 2005. Smart growth and the transportation-land use connection: what does the research tell us? International Regional Science Review, 28(2), 146-167.
Handy, S., McCann, B., Bailey, L., Ernst, M., McRee, L., et al., 2009. The Regional Response to Federal Funding for Bicycle and Pedestrian Projects. Institute of Transportation Studies, University of California Davis.
Hankey, S., Lindsey, G., Wang, X., Borah, J., Hoff, K., et al., 2012. Estimating use of non-motorized infrastructure: Models of bicycle and pedestrian traffic in Minneapolis, MN. Landscape and Urban Planning, 107(3), 307-316.
Hankey, S., Marshall, J., Brauer, M., 2012. Health impacts of the built environment: within-urban variability in physical inactivity, air pollution, and ischemic heart disease mortality. Environmental Health Perspectives, 120(2), 247-253.
Harrison, R.M., Jones, A.M., 2005. Multisite study of particle number concentrations in urban air. Environmental Science and Technology, 39(16), 6063-6070.
Hatzopoulou, M., Weichenthal, S., Dugum, H., Pickett, G., Miranda-Moreno, L., et al., 2013. The impact of traffic volume, composition, and road geometry on personal air pollution exposures among cyclists in Montreal, Canada. Journal of Exposure Science and Environmental Epidemiology, 23(1), 46-51.

Haynes, M., and S. Andrzejewski, 2010. “GIS Based Bicycle and Pedestrian Demand Forecasting Techniques.” Fehr & Peers. TMIP Webinar. Available: http://tmiponline.org/Clearinghouse/Items/20100429_-_GIS-based_Bicycle_and_Pedestrian_Demand_Forecasting_and_Traffic_Count_Programs.aspx [4 April 2011].

HEI (Health Effects Institute), 2009. “Traffic-Related Air Pollution: A Critical Review of the Literature on Emissions, Exposure, and Health Effects.” Special Report #17, Available: http://pubs.healtheffects.org/view.php?id=334 [9 September 2010].

Henderson, S., Beckerman, B., Jerrett, M., Brauer, M., 2007. Application of land use regression to estimate long-term concentrations of traffic-related nitrogen oxides and fine particulate matter. Environmental Science and Technology, 41(7), 2422-2428.

Hoek, G., Beelen, R., de Hoogh, K., Vienneau, D., Gulliver, J., et al., 2008. A review of land-use regression models to assess spatial variation of outdoor air pollution. Atmospheric Environment, 42(33), 7561-7578.

Hoek, G., Beelen, R., Kos, G., Dijkema, M., Van Der Zee, S., et al., 2011. Land use regression model for ultrafine particles in Amsterdam. Environmental Science and Technology, 45(2), 622-628.

Hoek, G., Brunekreef, B., Fischer, P., van Wijnen, J., 2001. The association between air pollution and heart failure, arrhythmia, embolism, thrombosis, and other cardiovascular causes of death in a time series study. Epidemiology, 12(3), 355-357.

Hoek, G., Brunekreef, B., Goldbohm, S., Fischer, P., Van den Brandt, P.A., 2002. Association between mortality and indicators of traffic-related air pollution in the Netherlands: a cohort study. The Lancet, 360 (9341), 1203-1209.

Hong, A.E., Bae, C., 2012. Exposure of bicyclists to air pollution in Seattle, Washington: Hybrid analysis using personal monitoring and land use regression. Transportation Research Record, 2270, 59-66.

Hood, J., Sall, E., Charlton, B., 2011. A GPS-based bicycle route choice model for San Francisco, California. Transportation Letters: International Journal of Transportation Research, 3(1), 63-75.

Hu, S., Fruin, S., Kozawa, K., Mara, S., Paulson, S.E., et al., 2009. A wide area of air pollutant impact downwind of a freeway during pre-sunrise hours. Atmospheric Environment, 43(16), 2541-2549.

HUD (Department of Housing and Urban Development), 2012. “Partnership for Sustainable Communities: An Interagency Partnership HUD-DOT-EPA.” Available: http://www.sustainablecommunities.gov [1 May 2012].

Hunter, W., and Huang, H.F., 1995. User counts on bicycle lanes and multiuse trails in the United States. Transportation Research Record, 1502, 45-57.

Hystad, P., Setton, E., Cervantes-Larios, A., Poplawski, K., Deschenes, S., et al., 2011. Canada wide land-use regression models created from fixed site monitors and

validated with independent city-specific measurements. Epidemiology, 22(1), S214-S215.
Iacono, M., Krizek, K., El-Geneidy, A., 2010. Measuring non-motorized accessibility: issues, alternatives, and execution. Journal of Transport Geography, 18(1), 133-140.
Int Panis, L., de Geus, B., Vandenbulcke, G., Willems, H., Degraeuwe, B., et al., 2010. Exposure to particulate matter in traffic: a comparison of cyclists and car passengers. Atmospheric Environment, 44(19), 2263-2270.
Jerrett, M., Arain, M.A., Kanaroglou, B., Beckerman, D., Crouse, D., et al., 2007. Modeling the intraurban variability of ambient traffic pollution in Toronto, Canada. Journal of Toxicology and Environmental Health Part A, 70(3-4), 200-212.
Jerrett, M., Arain, A., Kanaroglou, P., Beckerman, B., Potoglou, D., 2005. A review and evaluation of intraurban air pollution exposure models. Journal of Exposure Analysis and Environmental Epidemiology, 15(2), 185-204.
Jerrett, M., Burnett, R.T., Ma, R., Pope, C.A., Krewski, D., Newbold, K.B., et al., 2005. Spatial analysis of air pollution and mortality in Los Angeles. Epidemiology, 16(6), 727-736.
Jerrett, M., Burnett, R.T., Pope, C.A., Ito, K., Thurston, G., et al., 2009. Long-term ozone exposure and mortality. The New England Journal of Medicine, 360(11), 1085-1095.
Jerrett, M., Finkelstein, M.M., Brook, J.R., Arain, M.A., Kanaroglou, P., 2009. A cohort study of traffic-related air pollution and mortality in Toronto, Ontario, Canada. 117(5), 772-777.
Jones, M., 2009. "National Bicycle and Pedestrian Documentation Project." Presented at Transportation Research Board, Washington, D.C. Available: http://bikepeddocumentation.org/downloads/ [10 August 2014].
Jones, M., Ryan, S., Donlon, J., Ledbetter, L., Ragland, D.R., Arnold, L., 2010. "Seamless Travel: Measuring Bicycle and Pedestrian Activity in San Diego County and Its Relationship to Land Use, Transportation, Safety, and Facility Type." UC Berkeley Safe Transportation Research & Education Center. UC Berkeley, Caltrans Task Order 6117.
Karnaroglou, P.S., Jerrett, M., Morrison, J., Beckerman, B., Arain, M.A., et al., 2005. Establishing an air pollution monitoring network for intra-urban population exposure assessment: a location-allocation approach. Atmospheric Environment, 39(13), 2399-2409.
Kashima, S., Yorifuji, T., Tsuda, T., Doi, H., 2009. Application of land use regression to regulatory air quality data in Japan. Science of the Total Environment, 407(8), 3055-3062.
Kim, N., Susilo, Y., 2011. Comparison of pedestrian trip generation models. Journal of Advanced Transportation, 47(4), 399-412.

Kirchstetter, T.W., Novakov, T., 2007. Controlled generation of black carbon particles from a diffusion flame and applications in evaluating black carbon measurement methods. Atmospheric Environment, 41(9), 1874-1888.

Knibbs, L.D., Cole-Hunter, T., Morawska, L., 2011. A review of commuter exposure to ultrafine particles and its health effects. Atmospheric Environment, 45(16), 2611-2622.

Krewski, D., Jerrett, M., Burnett, R.T., Ma, R., Hughes, E., et al., 2009. "Extended follow-up and spatial analysis of the American Cancer Society study linking particulate air pollution and mortality." Health Effects Institute. Research Report 140. Boston, MA.

Krizek, K.J., 2007. Estimating the economic benefits of bicycling and bicycle facilities: an interpretive review and proposed methods. Essays on Transport Economics, Springer Publishing, 219-248.

Krizek, K.J., Barnes, G., Thompson, K., 2009. Analyzing the effect of bicycle facilities on commute mode share over time. Journal of Urban Planning and Development, 135(2), 66-73.

Kumar, N., 2009. An optimal spatial sampling design for intra-urban population exposure assessment. Atmospheric Environment, 43(5), 1153.

Laden, F., Neas, L.M., Dockery, D.W., Schwartz, J., 2000. Association of fine particulate matter from different sources with daily mortality in six US cities. Environmental Health Perspectives, 108(10), 941-947.

Laden, F., Schwartz, J., Speizer, F.E., Dockery, D.W., 2006. Reduction in fine particulate air pollution and mortality: extended follow-up of the Harvard Six Cities study. American Journal of Respiratory and Critical Care Medicine, 173(6), 667-672.

Lankford, J., Lankford, S., Grybovych, O., Bowles, B., Fleming, K., et al., 2011. "Economic and health benefits of bicycling in Iowa." Prepared for the Iowa Bicycle Coalition. Sustainable Tourism and Environmental Program, University of Northern Iowa, Cedar Falls, Iowa. Available: http://www.uni.edu/step/reports/economic_health_benefits_of_bicycling.pdf [15 June 2014].

Larson, T., Henderson, S.B., Brauer, M., 2009. Mobile monitoring of particle light absorption coefficient in an urban area as a basis for land use regression. Environmental Science and Technology, 43(13), 4672-4678.

Larson, T., Su, J., Baribeau, A., Buzzelli, M., Setton, E., et al., 2007. A spatial model of urban winter woodsmoke concentrations. Environmental Science and Technology, 41(7), 2429-2436.

Leyden, K.M., 2003. Social capital and the built environment: the importance of walkable neighborhoods. American Journal of Public Health, 93(9), 1546-1551.

Li, L., Wu, J., Hudda, N., Sioutas, C., Fruin, S.A., Delfino, R.J., 2013. Modeling the concentrations of on-road air pollutants in Southern California. Environmental Science and Technology, 47(16), 9291-9299.

Lightowlers, C., Nelson, T., Setton, E., Keller, C.P., 2008. Determining the spatial scale for analyzing mobile measurements of air pollution. Atmospheric Environment, 42(23), 5933-5937.

Lindsey, G., Han, Y., Wilson, J., Yang, J., 2006. Neighborhood correlates of urban trail traffic. Journal of Physical Activity and Health, 1(S1), S134-S152.

Lindsey, G., Wilson, J., Rubchinskaya, E., Yang, J., Alexa, C., 2008. Urban form, trail characteristics, and trail use: implications for design. Journal of Urban Design, 13(1), 107-132.

Lindsey, G., Wilson, J., Rubchinskaya, E., Yang, J., Han, Y., 2007. Estimating urban trail traffic: methods for existing and proposed trails. Landscape and Urban Planning, 81(4), 299-315.

Long, J.S., Freese, J., 2005. Regression Models for Categorical Dependent Variables Using Stata (2nd ed.). College Station, TX. Stata Press.

Lund, H., 2002. Pedestrian environments and sense of community. Journal of Planning Education Research, 21(3), 301-312.

Marshall, J.D., Brauer, M., Frank, L.D., 2009. Healthy neighborhoods: walkability and air pollution. Environmental Health Perspectives, 117(11), 1752-1759.

Marshall, J.D., Nethery, E., Brauer, M., 2008. Within-urban variability in ambient air pollution: comparison of estimation methods. Atmospheric Environment, 42(6), 1359-1369.

Marshall, J.D., Riley, W.J., McKone, T.E., Nazaroff, W.W., 2003. Intake fraction of primary pollutants: motor vehicle emissions in the South Coast Air Basin. Atmospheric Environment, 37(24), 3455-3468.

Marshall, J.D., Swor, K.R., Nguyen, N., 2014. Prioritizing environmental justice and equality: diesel emissions in Southern California. Environmental Science and Technology, 48(7), 4063-4068.

McCreanor, J., Cullinan, P., Nieuwenhuijsen, M.J., Stewart-Evans, J., Malliarou, E., et al., 2007. Respiratory effects of exposure to diesel traffic in persons with asthma. New England Journal of Medicine, 357(23), 2348-2358.

McMurry, P.H., Zhang, X., Lee, Q.T., 1996. Issues in aerosol measurement for optical assessments. Journal of Geophysical Research, 101(D14), 19188-19197.

McNeill, L.H., Kreuter, M.W., Subramanian, S.V., 2006. Social environment and physical activity: a review of concepts and evidence. Social Science Medicine, 63(4), 1011-1022.

Metropolitan Council, 2005. Land Use Data and Maps. Available: http://www.metrocouncil.org/Reports/publications.htm [24 May 2010].

MetroTransit. Bus Routes and Schedules. Available: www.datafinder.org [20 May 2010].
Miller, K.A., Siscovick, D.S., Sheppard, L., Shepherd, K., Sullivan, J.H., et al., 2007. Long-term exposure to air pollution and incidence of cardiovascular events in women. New England Journal of Medicine, 356(5), 447.
Minnesota Climatology Working Group. Historic Temperature and Precipitation Data. Available: climate.umn.edu [20 May 2010].
Miranda, M.L., Edwards, S.E., Keating, M.H., Paul, C.J., 2011. Making the environmental justice grade: the relative burden of air pollution exposure in the United States. International Journal of Environmental Research and Public Health, 8(6), 1755-1771.
Miranda-Moreno, L.F., Nosal, T., Schneider, R.J., and Proulx, F., 2013. Classification of bicycle traffic patterns in five North American Cities. Paper prepared for presentation at the 92nd Annual Meeting of the Transportation Research Board.
Mott, J.A., Wolfe, M.I., Alverson, C.J., Macdonald, S.C., Bailey, C.R., et al., 2002. National vehicle emissions policies and practices and declining US carbon monoxide-related mortality. Journal of the American Medical Association, 288(8), 988-995.
Nafstad, P., Haheim, L.L., Wisloff, T., Gram, F., Oftedal, B., et al., 2004. Urban air pollution and mortality in a cohort of Norwegian men. Environmental Health Perspectives, 112(5), 610-615.
Nemery, B., Hoet, P.H.M., Nemmar, A., 2001. The Meuse Valley fog of 1930: an air pollution disaster. The Lancet, 357(9257), 704-708.
Nordback, K., Marshall, W.E., Janson, B.N., and Stolz, E., 2013. Errors in estimating annual average daily bicyclists from short-term counts. Paper prepared for presentation at the 92nd Annual Meeting of the Transportation Research Board.
Novotny, E.V., Bechle, M.J., Millet, D.B., Marshall, J.D., 2011. National satellite-based land-use regression: NO2 in the United States. Environmental Science and Technology, 45(10), 4407-4414.
Patton, A.P., Collins, C., Naumova, E.N., Zamore, W., Brugge, D., Durant, J.L., 2014. An hourly regression model for ultrafine particles in a near-highway urban area. Environmental Science and Technology, 48(6), 3272-3280.
Peters, A., von Klot, S., Heier, M., Trentinaglia, I., Hormann, A., 2004. Exposure to traffic and the onset of myocardial infarction, 351(17), 1721-1730.
Politis, M., Pilinis, C., Lekkas, T.D., 2008. Ultrafine Particles (UFP) and Health Effects. Dangerous. Like no other PM? Review and Analysis. Global Nest Journal, 10(3), 439-452.
Pope, C.A., Burnett, R.T., Krewski, D., Jerrett, M., Shi, Y., et al., 2009a. Cardiovascular mortality and exposure to airborne fine particulate matter and cigarette smoke. Circulation, 120(11), 941-948.

Pope, C.A., Burnett, R.T., Thun, M.J., Calle, E.E., Krewski, D., et al., 2002. Lung cancer, cardiopulmonary mortality, and long-term exposure to fine particulate air pollution. Journal of the American Medical Association, 287(9), 1132-1141.

Pope, C.A., Burnett, R.T., Thurston, G.D., Thun, M.J., Calle, E.E., et al., 2004. Cardiovascular mortality and long-term exposure to particulate air pollution: epidemiological evidence of general pathophysiological pathways of disease. Circulation, 109(1), 71-77.

Pope, C.A., Dockery, D.W., 2006. Health effects of fine particulate air pollution: lines that connect. Journal of Air and Waste Management Association, 56(6), 709-742.

Pope, C.A., Ezzati, M., Dockery, D.W., 2009b. Fine-particulate air pollution and life expectancy in the United States. The New England Journal of Medicine, 360(4), 376-386.

Pope, C.A., Muhlestein, J.B., May, H.T., Renlund, D.G., Anderson, J.L., et al., 2006. Ischemic heart disease events triggered by short-term exposure to fine particulate air pollution. Circulation, 114(23), 2443-2448.

Porter, C., Suhrbier, J., 1999. Forecasting bicycle and pedestrian travel: state of the practice and research needs. Transportation Research Record, 1674, 4-101.

Pushkarev, B., and Zupan, J.B., 1971. Pedestrian travel demand. Highway Research Record, 377, 37-53.

Puustinen, A., Hameri, K., Pekkanen, J., Kulmala, M., de Hartog, J., et al., 2007. Spatial variation of particle number and mass over four European cities. Atmospheric Environment, 41(31), 6622-6636.

Quiros, D.C., Lee, E.S., Wang, R., Zhu, Y., 2013. Ultrafine particle exposures while walking, cycling, and driving along an urban residential roadway. Atmospheric Environment, 73, 185-194.

Ramachandran, G., Adgate, J.L., Pratt, G.C., Sexton, K., 2003. Characterizing indoor and outdoor 15 minute average PM2.5 concentrations in urban neighborhoods. Aerosol Science and Technology, 37(1), 33-45.

Reyes, J.M., Serre, M.L., 2014. An LUR/BME framework to estimate $PM_{2.5}$ explained by on road mobile and stationary sources. Environmental Science and Technology, 48(3), 1736-1744.

Reynolds, K., Wolch, J., Byrne, J., Chou, C., Feng, G., Weaver, S., Jerrett, M., 2007. Trail characteristics as correlates of urban trail use. American Journal of Health Promotion, 21(4 Suppl), 335-345.

Ripamonti, G., Jarvi, L., Molgaard, B., Hussein, T., Nordbo, A., et al., 2013. The effect of local sources on aerosol particle number size distribution concentrations and fluxes in Helsinki, Finland. Tellus B, 65, 19786.

Ritz, B., Yu, F., Fruin, S., Chapa, G., Shaw, G.M., et a., 2002. Ambient air pollution and risk of birth defects in Southern California. American Journal of Epidemiology, 155(1), 17-25.

Rojas-Rueda, D., de Nazelle, A., Tainio, M., Nieuwenhuijsen, M.J., 2011. The health risks and benefits of cycling in urban environments compared with car use: health impact assessment study. British Medical Journal, 343, d4521.

Rose, N., Cowie, C., Gillett, R., Marks, G.B., 2011. Validation of a spatiotemporal land use regression model incorporating fixed site monitors. Environmental Science and Technology, 45(1), 294-299.

Rosenlund, M., Forastiere, F., Stafoggia, M., Porta, D., Perucci, M., et al., 2008. Comparison of regression models with land-use and emissions data to predict the spatial distribution of traffic-related air pollution in Rome. Journal of Exposure Science and Environmental Epidemiology, 18(2), 192-199.

Ross, Z., Jerrett, M., Ito, K., Tempalski, B., Thurston, G.D., 2007. A land use regression for predicting fine particulate matter concentrations in the New York City region. Atmospheric Environment, 41(11), 2255-2269.

Ruidavets, J.B., Cournot, M., Cassadou, S., Giroux, M., Meybeck, et al., 2005. Ozone air pollution is associated with acute myocardial infarction. Circulation, 111(5), 563-569.

Ryan, P.H., LeMasters, G.K., 2007. A review of land-use regression models for characterizing intraurban air pollution exposure. Inhalation Toxicology, 19(Suppl 1), 127-133.

Sahsuvaroglu, T., Arain, A., Kanaroglou, P., Finkelstein, N., Newbold, B., et al., 2006. A land use regression model for predicting ambient concentrations of nitrogen dioxide in Hamilton Ontario, Canada. Journal of Air and Waste Management Association, 56(10), 1059-1069.

Sampson, P.D., Richards, M., Szpiro, A.A., Bergen, S., Sheppard, L., et al., 2013. A regionalized national universal kriging model using partial least squares regression for estimating annual PM2.5 concentrations in epidemiology. Atmospheric Environment, 75, 383-392.

Saraswat, A., Apte, J.S., Kandlikar, M., Brauer, M., Henderson, S.B., Marshall, J.D., 2013. Spatiotemporal land use regression models of fine, ultrafine, and black carbon particulate matter in New Delhi, India. Environmental Science and Technology, 47(22), 12903-12911.

Schwartz, J., Laden, F., Zanobetti, A., 2002. The concentration-response relation between PM2.5 and daily deaths. Environmental Health Perspectives, 110(10), 1025-1029.

Schweitzer, L., Zhou, J., 2010. Neighborhood air quality, respiratory health, and vulnerable populations in compact and sprawled regions. Journal of the American Planning Association, 76(3), 363-371.

Snyder, L.P., 1994. The death-dealing smog over Donora, Pennsylvania: industrial air pollution, public health policy, and the politics of expertise, 1948-1949. Environmental History Review, 18(1), 117-139.

Stieb, D.M., Judek, S., Burnett, R.T., 2002. Meta-analysis of time-series studies of air pollution and mortality: effects of gases and particles and the influence of cause of death, age, and season. Journal of Air and Waste Management Association, 52(4), 470-484.

Strak, M., Boogaard, H., Meliefste, K., Oldenwening, M., Zuurbier, M., et al., 2010. Respiratory health effects of ultrafine and fine particle exposure in cyclists. Occupational and Environmental Medicine, 67(2), 118-124.

Stone, B., 2008. Urban sprawl and air quality in large US cities. Journal of Environmental Management, 86(4), 688-698.

Sugiyama, T., Leslie, E., Giles-Corti, B., Owen, N., 2008. Associations of neighborhood greenness with physical and mental health: do walking, social coherence and local social interaction explain the relationships? Journal of Epidemiology and Community Health, 62(5), e9.

Su, J.G., Allen, G., Miller, P.J., Brauer, M., 2013. Spatial modeling of residential woodsmoke across a non-urban upstate New York region. Air Quality and Atmospheric Health, 6(1), 85-94.

Su, J.G., Jerrett, M., Beckerman, B.A., 2009. A distance-decay variable selection strategy for land use regression modeling of ambient air pollution exposures. Science of the Total Environment, 407(12), 3890-3898.

Unger, J., 1995. Sedentary lifestyle as a risk factor for self-reported poor physical and mental health. American Journal of Health Promotion, 10(1), 15-17.

US Census Bureau, 2000. American Factfinder. Available: www.census.gov [10 May 2010].

Van Poppel, M., Peters, J., Bleux, N., 2013. Methodology for setup and data processing of mobile air quality measurements to assess the spatial variability of concentrations in urban environments. Environmental Pollution, 183, 224-233.

Vienneau, D., de Hoogh, K., Bechle, M.J., Beelen, R., Donkelaar, A., Martin, R.V., Millet, D.B., Hoek, G., Marshall, J.D., 2013. Western European land use regression incorporating satellite- and ground-based measurements of NO2 and PM10. Environmental Science and Technology, 47(23), 13555-13564.

Vinzents, P.S., Moller, P., Sorensen, M., Knudsen, L.E., et al., 2005. Personal exposure to ultrafine particles and oxidative DNA damage. Environmental Health Perspectives, 113(11), 1485-1490.

Wang, Y., Hopke, P.K., Utell, M.J., Urban-scale seasonal and spatial variability of ultrafine particle number concentrations. Water, Air, and Soil Pollution, 223(5), 2223-2235.

Watson, J.G., and Chow, J.C., 2001. Estimating middle-, neighborhood-, and urban-scale contributions to elemental carbon in Mexico City with a rapid response aethalometer. Journal of the Air and Waste Management Association, 51(11), 1522-1528.

Weichenthal, S., Kulka, R., Dubeau, A., Martin, C., Wang, D., et al., 2011. Traffic-related air pollution and acute changes in heart rate variability and respiratory function in urban cyclists. Environmental Health Perspectives, 119(10), 1373-1378.

Weigand, L., 2008. A Review of the Literature: The Economic Benefits of Bicycling. Initiative for Bicycle and Pedestrian Innovation. Center for Transportation Studies, Portland State University. Portland, Oregon.

Westerdahl, D., Fruin, S., Sax, T., Fine, P.M., Sioutas, C., 2005. Mobile platform measurements of ultrafine particles and associated pollutant concentrations on freeways and residential streets in Los Angeles. Atmospheric Environment, 39(20), 3597-3610.

WHO (World Health Organization), 2009. Global Health Risks: Mortality and Burden of Disease Attributable to Selected Major Risks. Available: http://www.who.int/healthinfo/global_bur den_disease/GlobalHealthRisks_report_ful l.pdf [10 May 2010].

Wilhelm, M., Ritz, B., 2002. Residential proximity to traffic and adverse birth outcomes in Los Angeles County, California, 1994-1996. Environmental Health Perspectives, 111(2), 207-216.

Wilker, E.H., Baccarelli, A., Suh, H., Vokonas, P., Wright, R.O., Schwartz, J., 2010. Black carbon exposures, blood pressure, and interactions with single nucleotide polymorphisms in microRNA processing genes. Environmental Health Perspectives, 118(7), 943-948.

Woodcock, J., Edwards, P., Tonne, C., Armstrong, B.G., Ashiru, O., et al., 2009. Public health benefits of strategies to reduce greenhouse-gas emissions: urban land transport. The Lancet, 374(9705), 1930-1943.

Zhang, K., Wexler, A., Zhu, Y., Hinds, W., et al., 2002. Evolution of particle number distribution near roadways. Part II: the 'road-to-ambient' process. Atmospheric Environment, 38(38), 6655-6665.

Zhou, Y., Levy, J.I., 2007. Factors influencing the spatial extent of mobile source air pollution impacts: a meta-analysis. BMC Public Health, 7, 89-100.

Zhu, Y., Hinds, W., Kim, S., Shen, S., Sioutas, C., 2002a. Study of ultrafine particles near a major highway with heavy-duty diesel traffic. Atmospheric Environment, 36(27), 4323-4335.

Zhu, Y., Hinds, W., Kim, S., Sioutas, C., 2002b. Concentration and size distribution of ultrafine particles near a major highway. Journal of the Air and Waste Management Association, 52(9), 1032-1042.

Zuurbier, M., Hoek, G., Oldenwening, M., Lenters, V., Meliefste, K., et al., 2010. Commuters' exposure to particulate matter air pollution is affected by mode of transport, fuel type, and route. Environmental Health Perspectives, 118(6), 783-789.
Zwak, L.M., Paciorek, C.J., Spengler, J.D., Levy, J.I., Modeling spatial patterns of traffic-related air pollutants in complex urban terrain. Environmental Health Perspectives, 119(6), 852-859.